Molecular tools to unravel the mechanism of action of *M. tuberculosis* phenotypic hits

Alice Ruth Moorey

A thesis submitted to the University of Birmingham for the degree of

DOCTOR OF PHILOSOPHY

School of Biosciences

College of Life and Environmental Sciences

University of Birmingham

November 2021

Abstract

Until early 2020, tuberculosis (TB) was the deadliest disease caused by a single infectious agent. While Covid-19 has since gained the morbid accolade of the most lethal pathogen, TB remains a major threat to global health. The increasing rate of multi drug resistant (MDR) and extensively drug resistant (XDR) TB has led to the indisputable need for new anti-TB drugs. The primary aim of this research has been to investigate hits from drug screening programmes and, through the application of microbiological and molecular techniques, elucidate their targets. With a focus on re-examining existing therapeutics in the context of TB drug discovery, we tested three distinct groups of drugs to explore their activity against *Mycobacterium tuberculosis* (*Mtb*): BM212 series inhibitors of the transporter protein MmpL3; human diacylglycerol transferase (DGAT1) inhibitors and human kinase inhibitors. Inhibitors of MmpL3 are notoriously structurally diverse, and it is not uncommon for them to have alternative targets. Using chemoproteomic profiling the BM212 series of inhibitors were screened for alternative protein targets, revealing the binding of BM212 analogue compounds to the transcriptional regulator EthR2, which was confirmed using an *in vitro* tryptophan fluorescence assay. In the second chapter, we have explored the anti-TB activity of human DGAT1 inhibitors. *Mtb* is able to utilise host triacylglycerol as a source of energy and carbon and can store large amounts of TAG as intracellular lipid inclusion bodies (ILIs). Preliminary research showed that inhibiting host DGAT1 reduces TB infection in macrophages; we have demonstrated the activity of DGAT1 inhibitors against *Mtb* H37Rv and *M. bovis* BCG *in vitro*. Using a combination of whole cell assays, lipid profiling, and biochemical assays, we have observed the inhibition of bacterial triacylglycerol synthases by a DGAT1 inhibitor and have identified Tgs3 as the DGAT1 inhibitor protein target. Finally, we have selected phenotypic hits from a screen of human kinase inhibitors for their activity against *Mtb* and through the sequencing of spontaneous resistant mutants have identified a number of potential targets in *Mtb.*

Contents

List of Figures

List of Tables

List of Equations

List of Abbreviations

μL	Microlitre
μM	Micromolar
ADC	Albumin, Dextrose, Catalase
AG	Arabinogalactan
Ara	Arabinose
ATP	Adenosine Triphosphate
BCG	Bacillus Calmette-Guérin
BSA	Bovine Serum Albumin
CCL	Clarified Cell Lysate
CFU	Colony Forming Unit
CMN	*Corynebacterium-Mycobacterium-Nocardia*
CoA	Coenzyme A
d	Doublet (Chemical Synthesis)
DAG	Diacylglycerol
DAT	Diacyltrehalose
DGAT	Diacylglycerol Acyltransferase
DMSO	Dimethyl Sulfoxide
DNA	Deoxyribonucleic Acid
DOT	Directly Observed Treatment
DPA	Decaprenylphosphoryl-β-D-Arabinofuranose
EMB	Ethambutol
ETA	Ethionamide
EV	Empty Vector
f	Furanose
F	Fluorescence Emission
FAMEs	Fatty Acid Methyl Esters
FAS	Fatty Acid Synthase
FDA	Food and Drug Administration

FFA	Free Fatty Acid
FIC	Fractional Inhibitory Concentration
FMA	Free Mycolic Acid
g	Gram
Gal	Galactose
GlcNAC	N-Acetylglucosamine
GMM	Glucose Monomycolate
GSK	Glaxo Smith Kline
HIV	Human Immunodeficiency Virus
HPLC	High Pressure Liquid Chromatography
HTS	High Throughput Screening
Hz	Herz
ILI	Intracellular Lipid Inclusion
InDel	Insertion/Deletion
INH	Isoniazid
IPTG	Isopropyl β-D-1-Thiogalactopyranoside
J	coupling constant
Kan	Kanamycin
kb	kilobase
K_D	Dissociation Constant
kDa	Kilodalton
LAM	Lipoarabinomannan
LB	Luria-Bertani
LM	Lipomannan
M	Molar
MA	Mycolic Acid
mA	Milliamp
MAG	Monoacylglycerol
mAGP	Mycolyl-Arabinogalactan-Peptidoglycan
MAMEs	Mycolic Acid Methyl Esters

MDR	Multi Drug-Resistant
Man	Mannose
mg	Milligram
MIC	Minimum Inhibitory Concentration
mL	Millilitre
mM	Millimolar
MMG	Monomycoloyl Glycerols
MOM	Mycobacterial Outer Membrane
MPA	Molybdophosphoric Acid
Mtb	*Mycobacterium tuberculosis*
MTBC	*M. tuberculosis* complex
MurNAc	N-acetylmuramic acid
MurNGlyc	N-glycolmuramic acid
NADH	Nicotinamide Adenine Dinucleotide
NBD	Nitro-Benzoxadiazol
NMR	Nuclear Magnetic Resonance
OADC	Oleic Acid, Albumin, Dextrose, Catalase
OD	Optical Density
P	Phospholipid
PAGE	Polyacrylamide Gel Electophoresis
PBP	Penicillin Binding Protein
PBS	Phosphate-Buffered Saline
PCR	Polymerase Chain Reaction
PDIM	Phenolphthiocerol Dimycocerosate
PGL	Peptidoglycan
PGL	Phenolic Glycolipid
PI	Phosphatidylinositol
PIM	Phosphatidylinositol Mannosides
PK / PD	Pharmacokinetics / Pharmacodynamics
ppm	Parts Per Million

PZA	Pyrazinamide
q	Quartet (Chemical Synthesis)
RIF	Rifampicin
RR-TB	Rifampicin Resistant Tuberculosis
s	Singlet (Chemical Synthesis)
SAR	Structure Activity Relationship
SDS	Sodium Dodecyl Sulfate
SNP	Single Nucleotide Polymorphism
t	Triplet (Chemical Synthesis)
TAG	Triacylglycerol
TB	Tuberculosis
TBAH	Tetrabutylammonium Hydroxide
TBS	Tris-Buffered Saline
TBS-T	Tris-Buffered Saline with Tween
TDM	Trehalose Dimycolate
TGS	Triacylglycerol Synthase
TLC	Thin Layer Chromatography
TMM	Trehalose Monomycolate
v	Volume
V	Volt
VOT	Video Observed Treatment
w	Weight
WGS	Whole Genome Sequencing
WHO	World Health Organization
WT	Wild Type
XDR	Extensively Drug Resistant
δ	Chemical Shift (Chemical Synthesis)
Δ	Difference (or Deletion when used in plasmid names)

Declaration

The work presented in this thesis has been carried out under the supervision of Prof Gurdyal S. Besra and Dr Luke J. Alderwick in the School of Biosciences at the University of Birmingham, UK, B15 2TT during the period September 2017 to November 2021. The work in this thesis is original except where acknowledged by reference. This work has resulted in one first author publication. This publication may have similarities to Chapter 1. These similar sections included in my thesis are my original work with no significant contribution to the text by Professor Gurdyal S. Besra or Dr. Luke J. Alderwick. No part of the work is being, or has been submitted for a degree, diploma or any other qualification at any other University.

Professor Gurdyal S. Besra

Published work associated with this thesis

Moorey AR, Cabanillas A, Batt SM, Ghidelli-Disse S, Urones B, Sanz O, Lelievre J, Bantscheff M, Cox LR, Besra GS. The multi-target aspect of an MmpL3 inhibitor: The BM212 series of compounds bind EthR2, a transcriptional regulator of ethionamide activation. Cell Surf. 2021 Nov 23;7:100068. doi: 10.1016/j.tcsw.2021.100068.

University of Birmingham Research Archive

e-Theses Repository

Acknowledgements

I would like to extend my sincere gratitude to everyone who has made this thesis possible. Firstly, my supervisor, Professor Gurdyal S. Besra FMedSci FRS, for guiding me and sharing his wealth of knowledge and expertise. Thank you to those who enabled this research through funding and collaboration: The Medical Research Council who provided funding; GlaxoSmithKline for their funding and collaboration; and Dr Reynolds (University of Alabama) and Dr Brown (Newcastle University) for their collaboration in the screening of BR compounds. I would like to thank Alejandro Cabanillas (chemical synthesis) and Sonja Ghidelli-Disse (chemical proteomics) for experiments performed in Chaper 2. In addition, Lluis Ballell for the preliminary screening of DGAT inhibitors and data reported in Section 3.2.1. I would particularly like to thank Dr Apoorva Batt, Dr Luke Alderwick and Dr Patrick Moynihan for their commitment to making the TB labs a welcoming, collaborative research environment, and Dr Jess Blair and Sue Knight who are jointly responsible for supporting me through multiple lockdowns.

I am especially grateful for the help of Dr Katherine Abrahams and Dr Sarah Batt for their patience, mentorship and, most importantly their friendship over the past four years, and to Nat, Sid, Albel and Ian who have helped me so many times. To everyone in the TB labs, past and present, thank you. I could not have achieved this without you. Special thanks go to fellow Besra PhD student Chris, who offered encouragement and fun every day, and the wonderful Alice and Anja who offered kindness and cocktails when I needed them the most.

I could not have finished this thesis without the support of my Mum and Dad who have experienced the highs and lows of my PhD with me, and Hannah, Andy and Eliza who have provided entertainment, encouragement and even accommodation. Finally, to George and

Rosie, your unwavering love and support has kept me going through failed experiments, hours of thesis writing and a global pandemic, I can't thank you enough.

This thesis is dedicated to Professor David E. Minnikin, who laid down the

fundamental principles of the Mycobacterial cell wall, without whom

much of this research would not have been possible.

Chapter 1

General Introduction

1. General Introduction

1.1.　　　Origins of a Deadly Disease

Tuberculosis (TB) remains one of the most challenging threats to global health. Over 130 years after Robert Koch first presented his Nobel prize winning discovery of the causative pathogen of TB, *Mycobacterium tuberculosis* (Aufrecht, 1882), the infection is responsible for over 1.4 million deaths and over 7.1 million new cases per year (WHO, 2020). Koch is quoted as saying "If the importance of a disease for mankind is measured by the number of fatalities it causes, then TB must be considered much more important than those most feared infectious diseases, plague, cholera and the like" (Frith, 2014). Indeed, *M. tuberculosis,* has even been described as the world's most successful pathogen due to its prevalence, virulence and endurance (Hingley-Wilson *et al.*, 2003).

The *Mycobacterium* genus is believed to have originated millions of years ago (Hayman, 1984; Hershkovitz *et al*., 2008). Its history has been pieced together over several decades of research, with evidence gathered from geographic distribution (Hayman, 1984), molecular genetics (Gutierrez *et al*., 2005) and detection of ancient mycobacterial lipid biomarkers (Minnikin *et al.,* 2015). Estimates suggest that an *M. tuberculosis* ancestor was present among early hominids in East Africa and that it coevolved with its human host (Daniel, 2006; Gutierrez *et al*., 2005), while other mycobacterial species, including *Mycobacterium ulcerans,* are thought to date back to a similar time (Hayman, 1984). It is believed that modern pathogenic mycobacterial species share a common ancestor from 35,000-15,000 years ago (Daniel, 2006; Gutierrez *et al*., 2005). Lipid

biomarkers of TB infections have been detected in Neolithic bone samples from the Eastern Mediterranean dating back 9,000 years (Hershkovitz *et al*., 2008). DNA evidence of TB infections has also been found in Egyptian mummies (Ziskind *et al.,* 2007; Donoghue *et al.*, 2010).

Early descriptions of TB infections (known at the time as Phthisis, meaning to decay) can be found in the works of Ancient Greek physicians, rhetoricians and philosophers. Hippocrates wrote on the characteristic lesions of the lung (Frith, 2014; Hippocrates, 1849), while Soranus of Ephesus described "a latent fever… accompanied by much coughing… with the discharge of sanious sputa." (Fisch *et al*., 1952; Karamanou *et al*., 2012). At the turn of the 18th century the infectious nature of TB was described, and again in 1720 by the English physician Benjamin Marten in his "A new theory of consumption" (Barberis *et al*., 2017; Doetsch, 1978). While physicians strove to treat the scourge that was consumption and debated its cause, the public began to romanticise the "white plague", so called due to the pallid complexions of sufferers. The pale ethereal look inspired intrigue, prompting Lord Byron to remark "I should like, I think, to die of consumption" (Daniel, 2006; Rene *et al*., 1953). By this time consumption was believed to have infected between 70 - 90% of the population of Europe and North America (Pezzella, 2019), and was ultimately responsible for the deaths of many 19th century literary greats, including John Keats, Robert Louis Stevenson and the Brontë sisters (Frith, 2014).

The 19th century brought scientific advances which led to the discovery of the tubercle bacillus. In 1865, French surgeon Jean-Antoine Villemin demonstrated that inoculating

a rabbit with purulent liquid from the corpse of a person who had died of TB led to extensive infection in the lungs of rabbits (Daniel, 2006). Shortly after, in 1882, Robert Koch isolated the tubercle bacillus for the first time and presented his discovery to the Society of Physiology in Berlin (Barberis *et al*., 2017). From the mid-19th century onwards, numerous discoveries and observations led to a growing understanding of TB infections and paved the way for modern medical treatments and management of the disease. One of the most remarkable advancements was the development of the Bacille Calmette-Guérin (BCG) vaccine in the 1920s which made use of a strain of *Mycobacterium bovis,* the causative agent of bovine TB, attenuated by serial passage in the laboratory of Albert Calmette at the Pasteur Institute (Calmette, 1928; Daniel, 2005). By the mid-20th century, radiographic chest screening which had been introduced during World War I had become an effective method of detecting signs of TB, and was widely carried out among both military and civilian populations throughout Europe (Haygood *et al.*, 1992; Daniel, 2006). The application of new scientific techniques to TB research in the early 20th century culminated in the discovery of the first bactericidal agent, Streptomycin, for the treatment of TB (Schatz *et al*., 1944). The discovery of Streptomycin was rapidly followed by the development of other anti-TB drugs such as Isoniazid (INH) in 1952, and rifamycin 5 years after that, both of which formed part of a public health campaign to control and treat TB (Robitzek, 1952; Maggi, 1965; Maggi 1966; Daniel, 2006).

1.2.   Epidemiology

Until 2020, the World Health Organisation (WHO) had consistently listed TB as the most deadly disease caused by a single pathogen worldwide (Vinet *et al*., 2011; WHO, 2015) and it remains the 13th leading cause of death (WHO, 2014). COVID-19 has overtaken TB as the leading infectious disease and the global pandemic has caused a lag in diagnosis of TB which is likely to affect future patient outcomes (WHO, 2015). This is expected to have the biggest impact in low income countries who rely on international aid for the management of such diseases. TB manifests itself as a 'biological expression of inequality' (Dobson, 2015). The influence of socioeconomic status on TB incidence rates is striking: 98% of TB cases occur in low to middle income countries (WHO, 2014). According to 2021 statistics, an alarming 43% of global TB cases were reported in South-East Asia, 25% in Africa and a mere 2.3% in Europe (WHO, 2021) (Figure 1). Even within the UK, rates of TB transmission are disproportionately high in low socioeconomic populations, such as prison inmates and homeless communities (PHE, 2020). Several national and global strategies for tackling TB exist, describing targets for reducing mortalities through education, improved access to treatment and the development of new chemotherapeutics (PHE, 2020). While many countries are achieving a continued reduction in TB incidence, rates of TB in England remain higher than those of the United States of America, and for the first time in 9 years the number of TB notifications in England has risen (PHE, 2020; WHO, 2015).
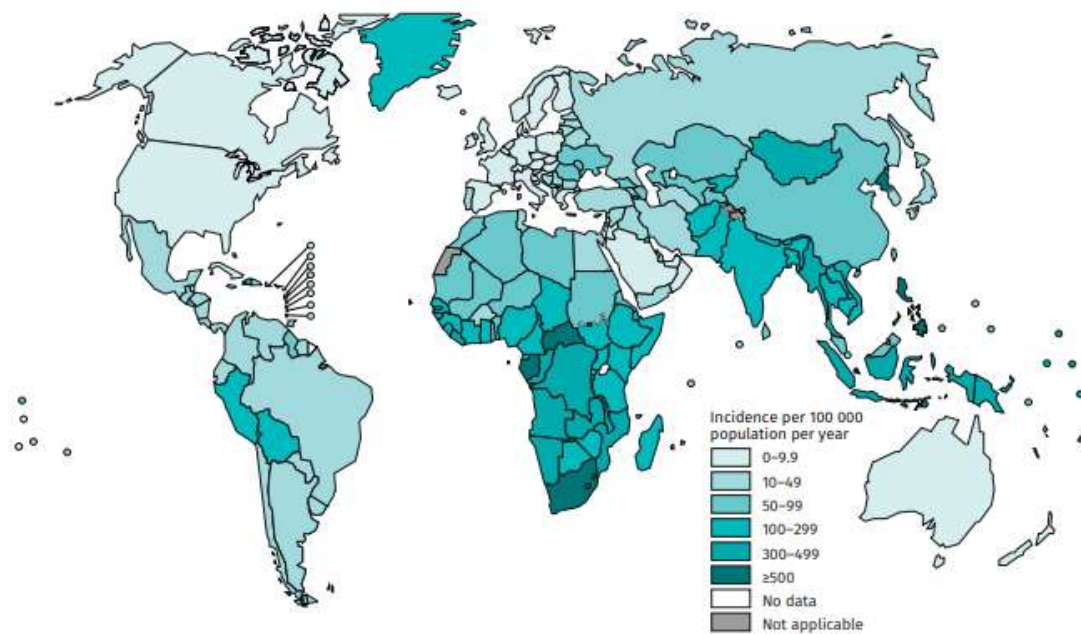
Figure 1. Estimated global incidence rates of TB from the WHO TB report 2021 (WHO, 2021a). Incidence rates are shown by region with lighter colour indicating lower incidence.

1.3.   Clinical Features

M. tuberculosis is transmitted by airborne droplets expelled from the airways of individuals infected with pulmonary or laryngeal TB (Turner *et al.*, 2015). In susceptible individuals, inhalation of droplet nuclei can lead to either an active or latent, non-contagious form of the disease. Once the bacilli have entered the host's lungs, an immune response is triggered. Macrophages target the invading pathogen and phagocytose them in an attempt to either kill cells or inhibit growth which, in some healthy patients is sufficient to protect against infection. In latent TB infections, *Mtb* cells are able to withstand this immune response, but reach a stalemate with the host's defences. Immune cells (primarily T lymphocytes, and a smaller proportion of B lymphocytes, neutrophils and dendritic cells) are recruited to assist the infected

macrophages through the release of cytokines (de Martino *et al.*, 2019; O'Garra *et al.*, 2013). These cells accumulate around the macrophage, containing the infection, but are unable to eradicate the pathogen from the host (Guirado *et al.*, 2013). Under favourable conditions, the bacteria are able to proliferate and spread from the granuloma, causing the host to become infectious. In 90% of cases, infection remains latent with the host experiencing no symptoms (Lin *et al.*, 2010); this ability of the bacteria to colonise a host undetected, causing a sub-clinical infection plays a key role in the success of the pathogen (Lillebaek *et al.*, 2003).

Patients at highest risk of developing an active TB infection are those whose immune systems are compromised, such as post-transplant patients taking immunosuppressant drugs, or HIV positive patients. TB can have particularly severe effects in patients suffering from HIV, as treatment with antibiotics for TB can increase their risk of developing TB-associated immune reconstitution inflammatory syndrome (IRIS). As many as 35% of deaths in HIV-positive patients are caused by co-infection with TB (Lawn *et al.*, 2006).

Mtb is not alone in causing infection in mammals: of the many *Mycobacterium* species, four are responsible for mammalian tubercular infections. *M. tuberculosis, M. bovis, Mycobacterium africanum* and *Mycobacterium microti* form the *M. tuberculosis* complex (MTBC) (De La Rua-Domenech, 2006). While the latter three mostly infect animals, they can all be transmitted to humans, most commonly to those who work closely with animals (Thoen *et al.*, 2008; Sunder *et al.*, 2009).

1.3.1. Mycobacteria Taxonomy

M. tuberculosis is one of over 190 species in the genus *Mycobcacterium,* in the phylum *Actinobacteria,* alongside a diverse range of predominantly Gram-positive bacteria (Tortoli, 2019). While a number of significant human pathogens are taxonomically ranked within this phylum (*M. tuberculosis* and *M. leprae*), a large proportion of *Actinobacteria* are soil dwelling bacteria of critical importance to agriculture due to their role in the decomposition of organic matter and the nitrogen fixing abilities of certain species (Abdelgawad *et al*., 2020; Boonkerd, 1998). For a long time, the extensive, fungus-like mycelia of species in the order *Actinomycetales* isolated from soil led to the belief that they were in fact fungi. Within *Actinomycetales,* the *Corynebacterium-Mycobacterium-Nocardia* (CMN) branch of bacteria are grouped together due to their unusual cell envelope consisting of a layer of mycolic acids (Ventura *et al*., 2007).

Recently, whole genome sequence-based phylogeny has revealed that the genus *Mycobacterium* could be split into five distinct groups: *Mycolicibacterium, Mycolicibacter, Mycolicibacillus, Mycobacterioides* and *Mycobacterium* (Gupta *et al.*, 2018; Meehan *et al.*, 2021). These groups were defined by their average amino acid identity, conserved signature indels and conserved signature proteins (Gupta *et al.*, 2018; Meehan *et al.*, 2021). This thesis exclusively revers to *Mycobacterium* as a genus and does not use the proposed new classification.

A characteristic feature of many *Actinobacteria* species is the high guanine and cytosine (GC) content in their DNA, resulting in a biased amino acid content, with alanine being the most over represented amino acid in high GC-content bacteria (Bohlin *et al*., 2013).

Genomic base variation has a considerable effect on proteins, and can lead to distinct families of proteins, for example *M tuberculosis* express families of glycine-rich proteins, such as the PE-PGRSs (Pro-Glu Polymorphic CG- Repeating Sequence) which are thought to be associated with an ESX-5 secretion system (Abdallah *et al*., 2008; Bohlin *et al*., 2013; Cole *et al*., 1998; Espitia *et al*., 1999).

The genus *Mycobacterium* consists of both obligate and opportunistic pathogens, as well as non-pathogenic species. It can broadly be split into two main groups; the non-tuberculous mycobacteria, such as *Mycobacterium abscessus* and *Mycobacterium avium* which, as opportunistic pathogens, can cause infection in immunocompromised patients (Faria *et al*., 2015; To *et al*., 2020), and the *M. tuberculosis* complex (MTC) which are a group of pathogens which cause TB in humans, such as *M. tuberculosis* and *M. bovis* (Pallavi Sinha *et al*., 2016). Mycobacteria can also be differentiated into two groups based on their growth in media; fast-growing species, such as *Mycobacterium smegmatis* and *M. abscessus*, which will grow to a visible density in liquid medium in under 7 days, and slow-growing species, such as *M. tuberculosis* and *M. bovis* which require longer than 7 days to reach a visible density (Grange, 1996; Chung Jong Kim *et al*., 2013).

The slow-growing nature of *M. tuberculosis*, and the severity of human infections it causes, classifies it a Hazard Group 3 organism. There are a number of different mycobacterial models which can be used more safely and with easier manipulation in the laboratory. Perhaps the most familiar of these is *M. bovis* BCG (bacillus Calmette–Guérin), a slow-growing Hazard Group 2 organism which is genomically very similar to

Mtb (Cole *et al*., 1998; Mahairas *et al*., 1996). *M. bovis* BCG is an attenuated strain, meaning it has reduced virulence and therefore does not cause severe infection, but maintains many other characteristics of the parent strain, such as the ability to induce a host immune response and is used in the only current licensed vaccine against TB, known as the BCG vaccine. In the case of *M. bovis* BCG, this was achieved by multiple laboratory passages of *M. bovis* isolated from a cow, grown on slices of potato cooked in beef bile and glycerol (Lobo *et al*., 2021; Oharan, 2012). Fast-growing mycobacterial species, such as *M. smegmatis* and *M. marinum* are also used as models for *M. tuberculosis* as they are both faster growing and are easier to genetically manipulate. *M. marinum* is particularly useful for *in vivo* studies using zebrafish, as it causes granulomas similar to the characteristic granulomas in human TB infections (Shiloh *et al*., 2010; Tobin *et al*., 2008). *Corynebacterium glutamicum* is popular as a model organism for investigating cell wall biosynthesis; it shares much of its basic cell wall architecture and its lipid characteristics with *M. tuberculosis*, in particular its cell wall mycolates, whilst being able to tolerate deletion of some of the genes which are essential in *M. tuberculosis* (Seidel, *et al*., 2007).

1.4. The Mycobacterial Cell Wall

One of the most distinctive features of the *Mycobacterium* genus is their mycolated waxy outer membrane, which is partially responsible for the success of *M. tuberculosis* as a pathogen. The orientation of mycolic acids, bound to the cell wall which creates an impermeable lipid barrier, giving the cell resistance to many of the broad-spectrum antibiotics used today, making TB infections in humans hard to treat. Species of

mycobacteria with a high content of mycolic acids are described as acid-fast due to the ability of mycolic acids to bind carbol fuchsin, the stain that is retained in the Ziehl-Neelsen acid-fastness test (Wanger *et al.*, 2017).

The characteristic cell wall of *Mycobacterium* species can be described in three main structural parts termed the mycolyl-arabinogalactan-peptidoglycan (mAGP) complex: a layer of peptidoglycan (PG), arabinogalactan (AG) and mycolic acids (Figure 2). Like many other bacterial species, the peptidoglycan layer contributes to the structure and rigidity of the cell, as well as the osmotic balance (Vollmer *et al.*, 2008).

A GlcNAc-L-Rha linker unit, synthesized by the transferases WecA (Rv1302) and WbbL (Rv3265c) (McNeil *et al.*, 1990; Mills *et al.*, 2004; Jin *et al.*, 2010), covalently binds AG to the *N*-glycolmuramic acid (MurNGlyc) residues of PG. The synthesis of AG begins with the polymerisation of galactofuranose (Gal$f$) residues by two galactofuranosyltransferases, until a chain length of approximately 30 residues has been reached (Kremer *et al.*, 2001; Rose *et al.*, 2006; Belánová *et al.*, 2008).

Arabinofuranose (Ara$f$) residues are then added forming highly branched chains with mycolic acids attached at the termini (Alderwick *et al.*, 2005, 2006; Birch *et al.*, 2008; McNeil *et al.*, 1987; Škovierová *et al.*, 2009). Mycolic acids are long-chain fatty acids which form the outer layer of the mAGP complex. Two systems, FAS-I and FAS-II are involved in the synthesis and extension of mycolic acids, resulting in chain lengths of C_{70-90} (Jun Liu *et al.*, 1996).
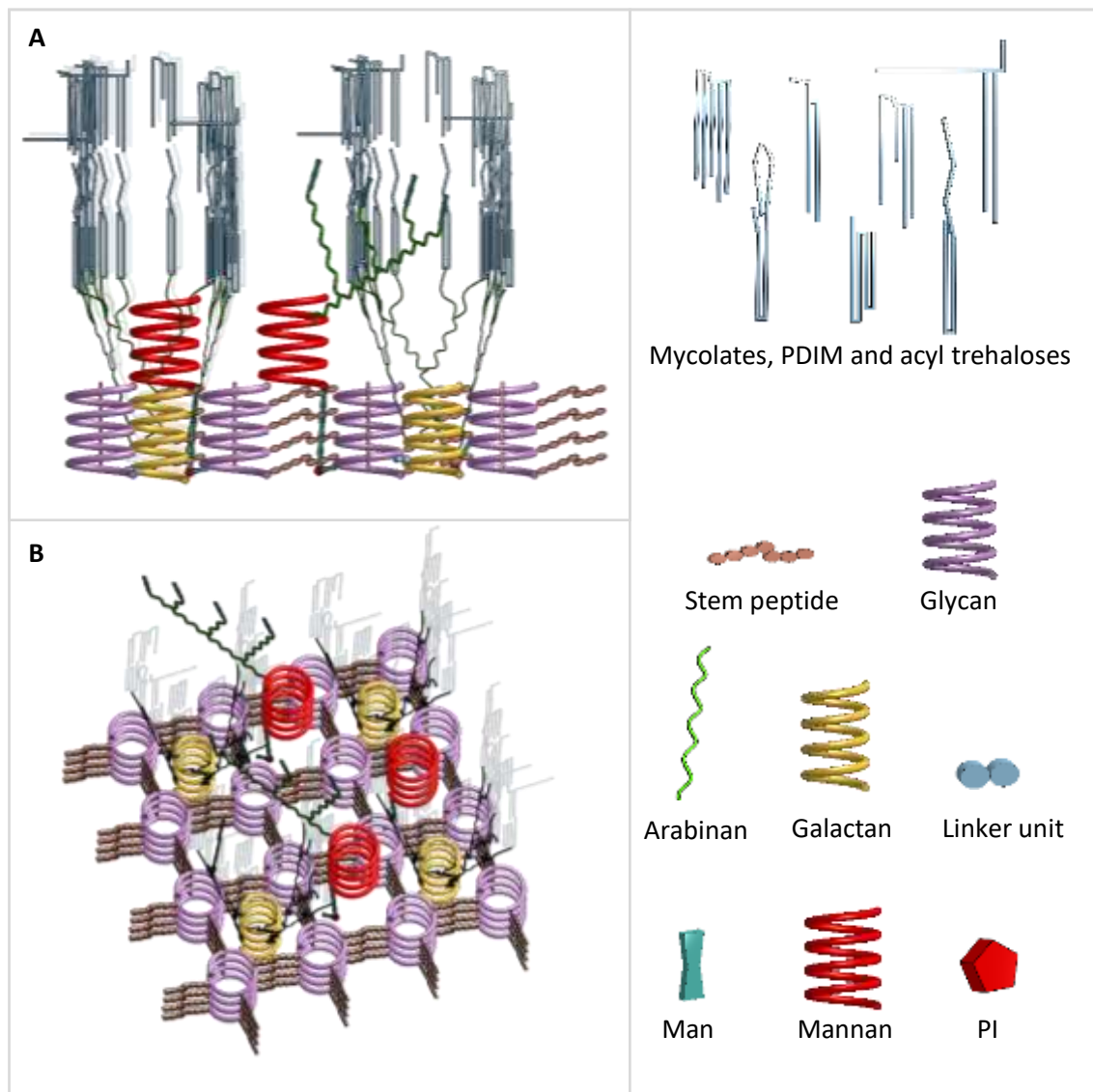
Figure 2. Overview of the Mtb cell wall featuring a peptidoglycan lattice structure with pores through which other molecules protrude. A – side view of the mAGP structure, **B** – top down view of mAGP. Figure produced using Onshape® software.

1.4.1. Peptidoglycan Structure

Peptidoglycan (PG) or murein is found in both Gram-positive and Gram-negative bacteria and is a vital cell wall component. It is important for providing shape and rigidity to the cell, as well as withstanding the hydrostatic (or turgor) pressure which pushes the plasma membrane against the cell wall (Vollmer *et al.*, 2008). PG is integral to the overall

structure of the mycobacterial cell wall, as it acts as a point of attachment for other cell wall components (Brennan *et al.,* 1995). The structure of PG is diverse across different bacterial species. PG is formed from a conserved glycan backbone consisting of alternating chains of GlcNAc and MurNAc residues of varying lengths bound by β(1→4) glycosidic bonds, with chains cross-linked to form a lattice of peptide side chains. It is these trans-peptide bridges which contribute to the diversity of PG (Rogers *et al.*, 1980; Brennan *et al.*, 1995). In *Mtb* the peptide linking strands are of the A1γ type, meaning they have an L-alanyl-γ-D-isoglutamyl-*meso*-diaminopimelyl-D-alanine structure (Schleifer et al., 1972; Brennan et al., 1995) and form (1→4) *meso*-diaminopimelic acid – D-alanine (*m*-DAP - Ala) or (1→3) *meso*-diaminopimelic acid – *meso*-diaminopimelic acid (*m*-DAP - *m*-DAP) linkages with adjacent strands to create the mesh structure characteristic of PG. Mycobacterial species possess a greater overall number of peptide cross-linkages (Matsuhashi, 1966; Vollmer *et al.*, 2004) as well as a higher proportion of (1→3) *m*-DAP – *m*-DAP linkages compared to (1→4) *m*-DAP - Ala linkages than other prokaryotes (Pradeep Kumar *et al*., 2012; Lavollay *et al*., 2008). The strength of mycobacterial peptidoglycan is thought to be further improved by the oxidation of *N*-acetylmuramic acid (MurNAc) to *N*-glycolmuramic acid (MurNGlyc), a structural modification seen in the glycan backbone (Petit *et al.*, 1969; Mahapatra *et al.*, 2005).

The organisation of PG within the cell wall is uncertain, although there is a strong case for the scaffold model of PG orientation (Figure 3), in which short chains of PG form a porous matrix, perpendicular to the plasma membrane, through which other cell wall components, such as the galactan core of AG can pierce (Besra *et al*., 1995, 1997; Dmitriev et al., 1999, 2000, 2003; Meroueh et al., 2006; Minnikin et al., 2002; Rastogi et

al., 1991). This is in contrast to the prior assumption that PG lay parallel to the plasma membrane, with AG and other structures protruding perpendicularly.

Stem peptide (PG)   Glycan (PG)
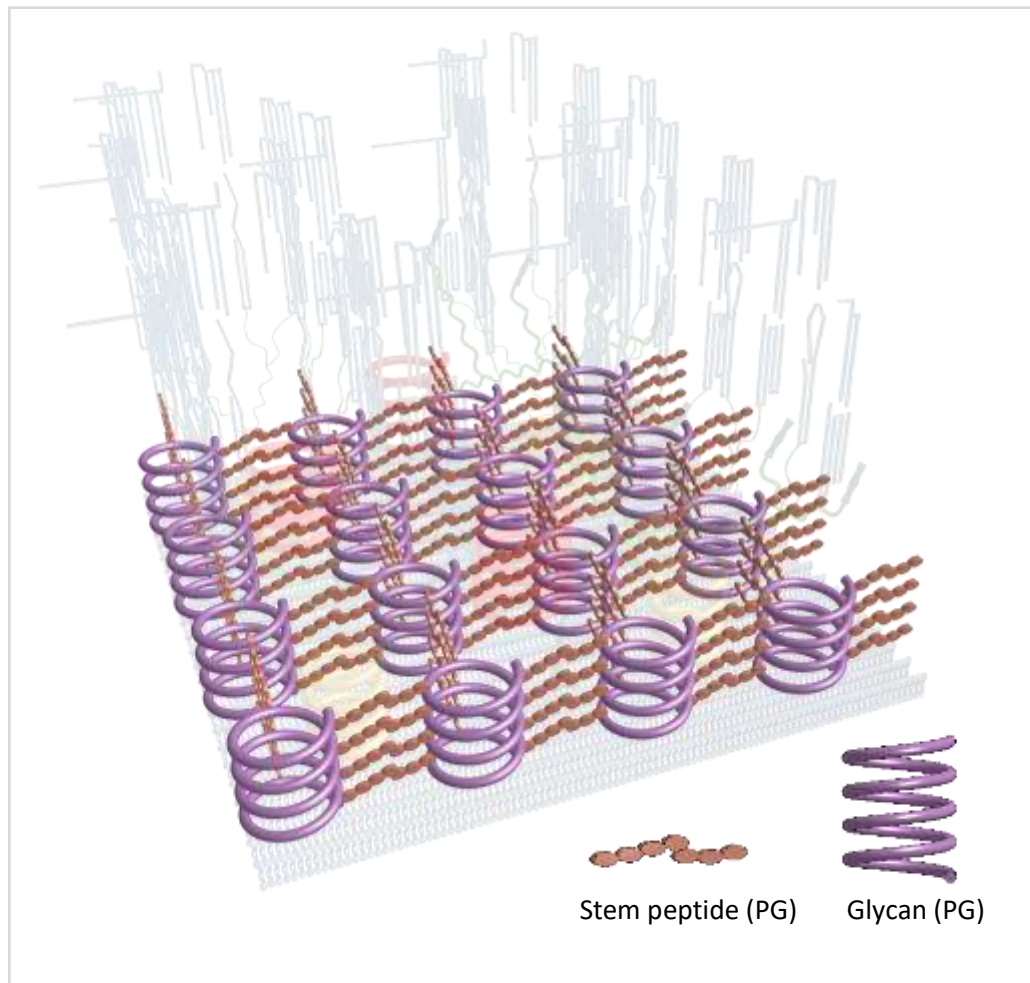
Figure 3. Structure of peptidoglycan in the scaffold formation, showing a lattice-like structure forming pores within the peptidoglycan which protrudes perpendicular to the inner cell membrane (Dmitriev 1999, 2000). Arabinogalactan and other molecules are situated within the peptidoglycan pores and the relative position of other cell wall components can be seen faintly. Figure produced using Onshape® software.

1.4.2. Synthesis of Peptidoglycan

Synthesis of peptidoglycan (Figure 4) starts with the acetyltransferase activity of GlmU (Rv1018c), which transfers the acetyl group of acetyl-CoA to glucosamine-1-phosphate (GlcN-1-P), forming *N*-acetylglucosamine-1-phosphate (GlcNAc-1-P) (Zhang *et al*., 2009). The addition of uridine-5'-monophosphate from UTP, again by GlmU, results in UDP-

GlcNAc (Jagtap *et al.*, 2012; Zhang *et al.*, 2009). From this point onwards, PG synthesis within the cytoplasm is dominated by a group of Mur ligases (MurA-F) (Barreteau *et al.*, 2008), at least four of which (MurC-F) are ATP-dependent (Munshi *et al.*, 2013). MurA (Rv1315) begins by transferring enoylpyruvate to UDP-GlcNAc from phosphoenoylpyruvate, yielding UDP-enoylpyruvyl-GlcNAc (De Smet *et al.*, 1999; Xu *et al.*, 2014) which is subsequently reduced by MurB (Rv0482) to UDP-MurNAc, in a reaction that is reliant on NADPH as a cofactor (Benson *et al.*, 1993; Eniyan *et al.*, 2018). The UDP-N-acetylmuramic acid hydroxylase, NamH, then hydroxylates the UDP-MurNAc molecule, forming UDP-MurGlyc (Mahapatra, *et al.*, 2005; Raymond *et al.*, 2005). At this point, MurC-MurF work sequentially to ligate amino acids together to form the penta-peptide side chain, also known as Park's Nucleotide (Chen *et al.*, 2016; Kurosu *et al.*, 2007; Munshi *et al.*, 2013). MurC (Rv2152c) introduces the first amino acid, L-alanine, followed by MurD (Rv2155c) and MurE (Rv2158c) which add D-*iso*glutamate and *meso*-diaminopimelate, respectively (Basavannacharya *et al.*, 2010; Basavannacharya *et al.*, 2010; Munshi *et al.*, 2013). MurF (Rv2157c) attaches the final di-peptide, D-alanine-D-alanine, which are ligated by Ddl (Rv2981c) prior to their addition to the penta-peptide chain (Bruning *et al.*, 2011; Munshi *et al.*, 2013). The product, UDP-MurNAc/Glyc-L-Ala-D-*iso*Glu-*m*-DAP-D-Ala-D-Ala, is attached to the inner membrane by MurX (Rv2156c) which translocates the pentapeptide to decaprenyl phosphate (C_{50}-P), forming the PG precursor, Lipid I (Chen *et al.*, 2016; Kurosu *et al.*, 2007). The addition of a β(1→4) linked GlcNAc onto MurNAc/Glyc of Lipid I by MurG (Rv2153c) results in Lipid II, concluding the intracellular synthesis of PG (Mengin-Lecreulx *et al.*, 1991).

There has been uncertainty surrounding the enzyme responsible for the translocation of Lipid II from the inner membrane to the periplasm, with two enzymes, FtsW (Rv2154c), and MurJ (Rv3910) being proposed as Lipid II translocases (Kumar *et al.*, 2019; Leclercq *et al.*, 2017; Mohammadi *et al.*, 2011; Ruiz, 2008, 2015; Sham *et al.*, 2014). Recent evidence from native mass spectroscopy and the crystal structure of MurJ identifies MurJ as the flippase most likely to be involved in Lipid II translocation (Bolla *et al.*, 2018; Kuk *et al.*, 2017, 2019; Zheng *et al.*, 2018). FtsW is thought instead to act as a PG glycosyltransferase (Emami *et al.*, 2017; Meeske *et al.*, 2016; Taguchi *et al.*, 2019).

Now situated on the periplasmic side of the membrane, the monofunctional and bifunctional (PonA1, PonA2 and PonA3) class A penicillin binding proteins (PBPs) polymerise PG (Sauvage *et al.*, 2008). The two domains of bifunctional PBPs, the transglycolase and transpeptidase domains, have important roles in linking the building blocks of PG. The transglycolase domain is implicated in the linking of Lipid II to the existing glycan chains of periplasmic PG, while the formation of *m*-DAP and D-Ala (3→4) cross-links in adjacent peptide chains is catalysed by the transpeptidase domain which cleaves a single D-Ala terminal residue (Kieser et al., 2015; Patru et al., 2010; Pandey et al., 2018). The monofunctional PBPs introduce the (3→3) linkages between tetrapeptide chains characteristic of mycobacteria (Pandey *et al.*, 2018). These linkages account for approximately 80% of the linkages in mycobacteria (Kumar *et al.*, 2012; Lavollay *et al.*, 2008), and are formed when the two terminal D-Ala residues are removed from the peptide chain by monofunctional PBPs, and by L,D-transpeptidases (LDTs), respectively (Goffin *et al.*, 2002; Laponogov *et al.*, 2009; Pandey *et al.*, 2018). The LDTs then form

($3\rightarrow3$) linkages between the terminal *m*-DAP residues of adjacent tetrapeptide chains,

concluding the synthesis of peptidoglycan (Laponogov *et al.*, 2009).
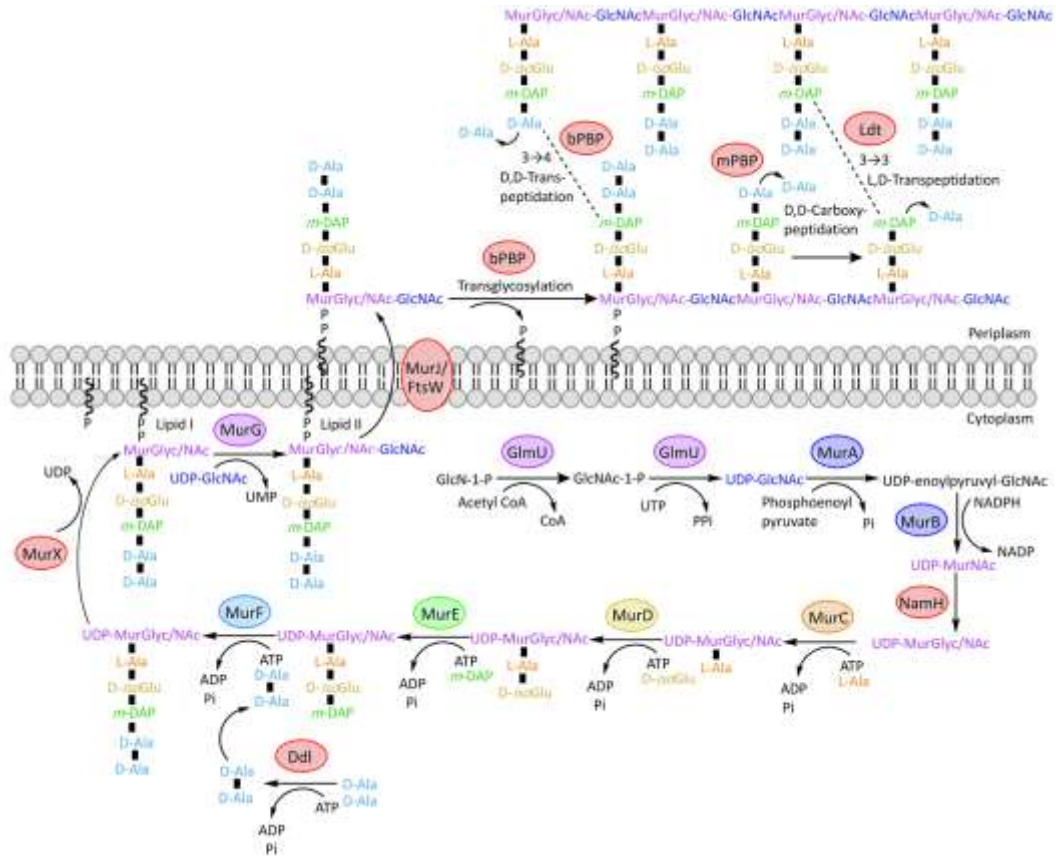
Figure 4. The synthesis of peptidoglycan. A group of Mur ligases are responsible for the majority of PG synthesis carried out in the cytoplasm, before a flipase transfers the PG precursor Lipid II to the periplasm where a group of penicillin binding proteins continue the synthesis. Adapted from Batt *et al.*, 2020.

1.4.3. Arabinogalactan Structure

Arabinogalactan (AG) is the branched structure which, in mycobacteria, is bound to 10-

12% of the muramic acid residues of PG, forming an anchor upon which the mycolic

acids are attached (Figure 5). The galactan portion of the AG heteropolysaccharide is

formed of 30 β-D-galactofuranose (Gal*f*) residues arranged in a chain of alternating

β($1\rightarrow5$) and β($1\rightarrow6$) linkages (Daffe *et al.*, 1990). Diverging from the β($1\rightarrow6$) linked 8th,

10th and 12th Gal*f* residues of the linear galactan chain, bound by a α($1\rightarrow5$) link, is the

highly branched arabinan component, consisting of α(1→5) linked Ara$f$ residues, interspersed with α(1→3) linkages where chains branch (Daffe *et al*., 1990). An unusual feature of AG is that all the arabinose and galactose residues are present in the form of furanose (*f*) rings (McNeil *et al*., 1987). The arabinan chains are terminated by a hexa-arabinofuranose (Araf_6) motif, the terminal two Ara$f$ residues of which serve as a tethering point for mycolic acids.
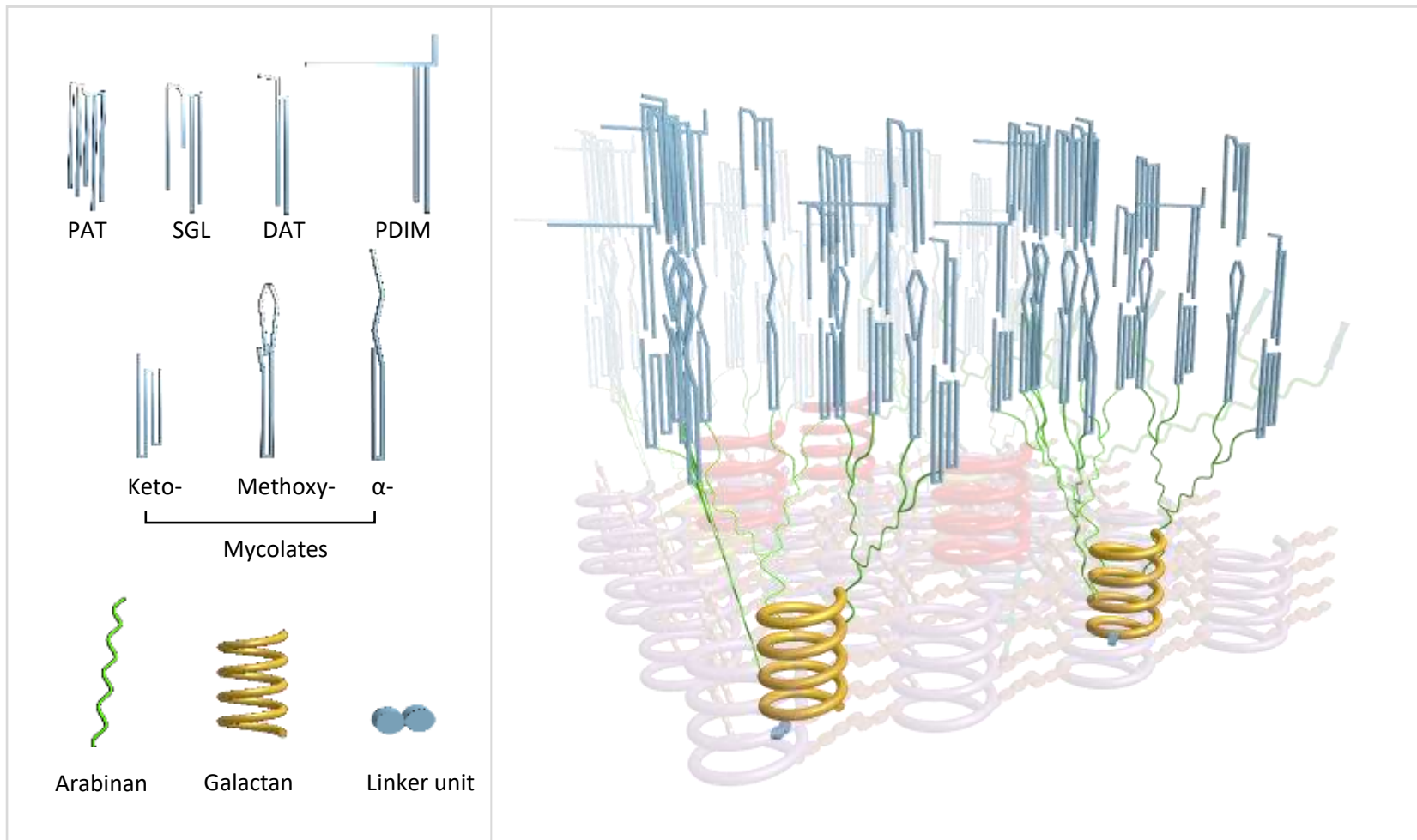
Figure 5. The structure and position of arabinogalactan (AG). AG is seen in yellow and green, nestled amounts the pores of PG and bound by a linker unit. The termini of the branched arabinan chains are decorated with mycolic acids. Additionally, PAT, SGL, DAT and PDIM are arranged around the mycolic acids. Figure produced using Onshape® software.

1.4.4. Synthesis of Arabinogalactan

The synthesis of arabinogalactan begins on the cytoplasmic side of the cell membrane (Figure 6). The formation of a linker unit which eventually acts as the anchor, binding AG to PG, is the first committed step in AG synthesis (Lechevalier *et al.*, 1970; McNeil *et al.*, 1987; Daffe *et al.*, 1990). There are two transferases – WecA (Rv1302), a GlcNAc-1-P transferase (Jin *et al*., 2010), and WbbL (Rv3265c), a rhamnosyltransferase (McNeil *et al.*, 1990; Mills *et al.*, 2004), involved in the synthesis of the linker unit, α-L-rhamnopyranoside-(1→3)-α-D-GlcNAc(1→P). WecA transfers GlcNAc-1-P from UDP-GlcNAC to decaprenylphosphate, forming C_{50}-P-P-GlcNAc, then WbbL transfers L-rhamnose at position-3 of GlcNAC. The decaprenylphosphate acts as the inner membrane anchor, leaving the Rha-GlcNAc component exposed, thus allowing for the addition of two Gal*f* residues by the bifunctional galactofuranosyl transferase, GlfT1 (Rv3782) (Kremer, *et al.*, 2001; Mikušová *et al.*, 2006; Rose *et al.*, 2006; Alderwick *et al.*, 2008; Belánová *et al.*, 2008). GlfT1 transfers a single Gal*f* residue to the rhamnose with a β(1→4) linkage, and then adds the second Gal*f* residue by a β(1→5) glycosidic bond to the first Gal*f* residue (Alderwick *et al*., 2008; Belánová *et al*., 2008; Mikušová *et al*., 2006). From this point, the galactan chain is formed by sequential polymerisation of alternating β(1→6) and β(1→5) linked Gal*f* residues, by GlfT2 (Rv3808c) (Kremer *et al*., 2001; Rose *et al*., 2006). Polymerisation continues until the galactan chain reaches a length of approximately 30 residues, resulting in the formation of a C_{50}-P-P-N-acetylglucosamine-L-rhamnose-galactofuranose$_{30}$ intermediate subunit. The subsequent steps of AG synthesis then take place in the periplasm after the galactose

domain is transported across the membrane, possibly by Rv3782 or Rv3783, which are part of an ABC transporter system (Dianišková *et al.*, 2011).

Arabinosylation of the galactan domain relies upon the arabinan donor decaprenylphosphoryl-β-D-arabinofuranose (DPA), which is synthesized in the cytoplasm (Wolucka *et al.*, 1994). Briefly, DPA synthesis begins with PrsA (Rv1017c) which transfers a pyrophosphate to ribose-5-phosphate to form 5-phosphoribose-1-diphosphate (pRpp) (Alderwick, *et al.*, 2011), whose terminal phosphate is then replaced with decaprenylphosphate (C_{50}-P) by UbiA (Rv3806c), forming DPPR which is anchored in the cell membrane (Alderwick *et al.*, 2005; Huang *et al.*, 2005, 2008). Dephosphorylation of DPPR by Rv3807c produces DPR, which is then epimerized to DPA via an intermediate, DPX, by DprE1 (Rv3790) and DprE2 (Rv3791) (Mikušová *et al.*, 2005). DPA is then transported to the periplasmic face of the cytoplasmic membrane by an unknown transporter.

Multiple arabinofuranosyl transferases are involved in the synthesis of the intricately branched arabinan domain (Alderwick *et al.*, 2005; Birch *et al.*, 2008; Escuyer *et al.*, 2001; Škovierová *et al.*, 2009). The first Ara*f* residues are transferred by AftA (Rv3792) via α(1→5) links to the 8th, 10th and 12th Gal*f* residues of the galactan chain (Alderwick *et al.*, 2006). Elongation of these initial arabinose branches with α(1→5) linkages is thought to be performed by EmbA (Rv3794) and EmbB (Rv3795) which form a dimer (EmbAB), although they also have a role in the later stages of AG synthesis, which has led to their elongation activity being contested (Alderwick *et al.*, 2005; Khasnobis *et al.*, 2006; Zhang *et al.*, 2020). It is possible that they have a dual function. AftC (Rv2673) and

AftD (Rv0236c) are the transferases responsible for introducing α(1→3) linked branches, increasing the complexity of the arabinan domain (Birch *et al*., 2008; Škovierová *et al*., 2009). The terminal arabinose α(1→3) branch point is introduced by EmbAB (Zhang et al., 2020), followed by the formation of the hexa-Ara*f* motif which caps the nonreducing end of the arabinose chain, catalysed by AftB (Rv3805c) (Seidel *et al*., 2007). The addition of D-GalN residues or succinyl residues to the C-2 position of the final 3,5-branched Ara*f* residue by Rv3779 and an unknown transferase respectively, is the penultimate step in AG synthesis. D-GalN residues are added when the arabinose strands are mycolated, while succinyl residues are added to un-mycolated strands (Bhamidi *et al*., 2008; Draper *et al*., 1997; Lee *et al*., 2006; Peng *et al*., 2012; Škovierová *et al*., 2010). Finally, the AG macromolecule is ligated to a MurNGlyc residue of PG by Lcp1 (Harrison *et al*., 2016).
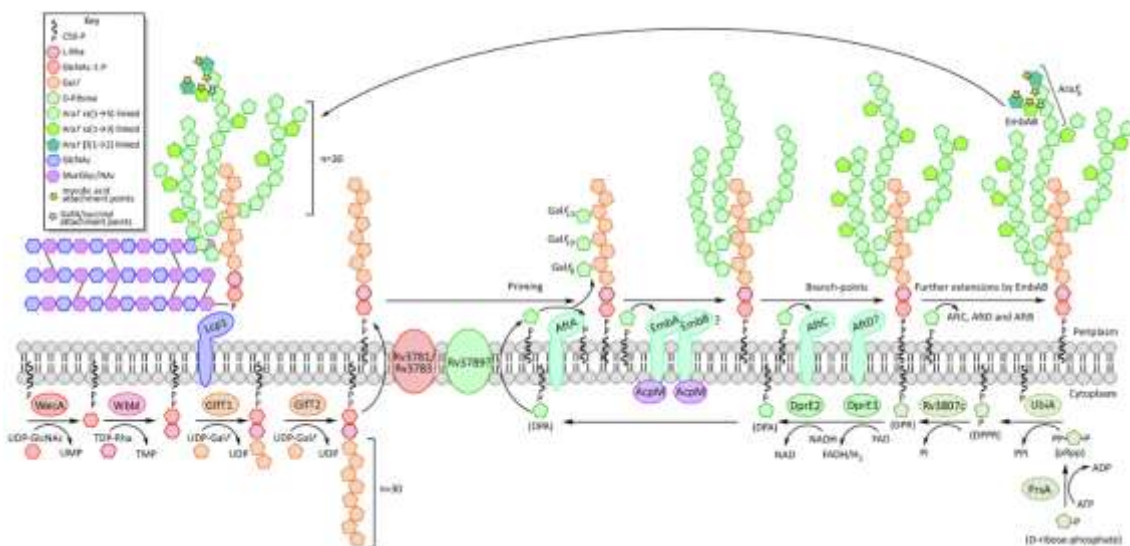
Figure 6. The synthesis of arabinogalactan. Synthesis begins in the cytoplasm with the formation of a linker unit which acts as an anchor for the galactan chain which is elongated by a pair of galactofuranosyl transferases and is decorated with highly branched arabinose chains. Adapted from Batt *et al*., 2020.

1.4.5. Structure of Mycolic Acids

Mycolic acids are C_{70-90} α-alkyl-β-hydroxy fatty acids which form an essential portion of the mAGP complex. They are found tightly packed into the characteristic hydrophobic, impermeable mycobacterial outer membrane (MOM) inner leaflet (Bhatt *et al*., 2005; Brown *et al*., 2007), covalently bound to the terminal arabinan residues of AG (McNeil *et al*., 1991). In addition to the cell wall-bound mycolic acids of the inner leaflet, the outer MOM leaflet contains extractable mycolates in the form of trehalose esters and other lipids. Mycolic acids fold into different conformations depending on their structure and they can be divided into three main groups: α-, keto- and methoxy-mycolates (Figure 7) (Groenewald *et al*., 2014; Villeneuve *et al*., 2005, 2007, 2013). Esters of mycolic acids exist in a number of forms in mycobacteria. The relative amounts of trehalose dimycolates (TDMs), trehalose monomycolates (TMMs) and glucose monomycolates (GMMs) are variable and, as such these esters are thought not to have a major structural role (Bacon *et al*., 2014; Kremer *et al*., 2014; Moody *et al*., 1997). The related monomycoloyl glycerols (MMGs), are thought to have a strong immunomodulatory role, with the ability to stimulate human dendritic cells (Andersen *et al*., 2009). MMGs are present in consistent proportions which may suggest a structural involvement (Minnikin *et al*., 2015).

Additional components argued to be involved in the composition of the outer leaflet of the MOM are diacylglycerols (DAG) and triacylglycerols (TAG) (Bansal-Mutalik *et al*., 2014).
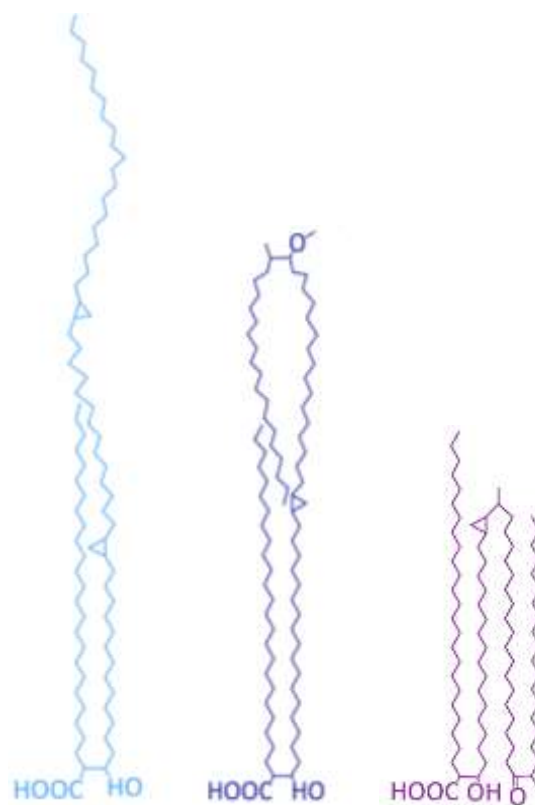
Figure 7. Structures of α-, keto- and methoxy-mycolic acids. Each structure has both a long beta-hydroxy chain and a shorter alpha-alkyl side chain. Adapted from Batt *et al.*, 2020.

1.4.6. Synthesis of Mycolic Acids

The synthesis of mycolic acids can be described in five stages, starting with fatty acid synthase I (FAS-I) (Figure 8). *fas* (Rv2524c) synthesises short-chain fatty acids as part of FAS-I, the only *de novo* system of fatty acid synthesis in mycobacteria. The fatty acids produced by FAS-I either form the α-alkyl short chain (C_{24}) moiety or are elongated by FAS-II to form the longer mero-chain fatty acids (C_{56}) (K. Bloch *et al.*, 1977; Peterson *et al.*, 1977). FabD (Rv2243) transfers a malonyl extender unit to AcpM (Rv2244) from malonyl-CoA (Kremer *et al.*, 2001). Subsequently FabH (Rv0533c) catalyses a condensation reaction in which AcpM and palmitoyl-CoA are utilised, forming a β-

ketoacyl-AcpM intermediate (Choi *et al.*, 2000). MabA (Rv1483), a keto-reductase, reduces the β-ketoacyl-AcpM intermediate, forming β-hydroxylacyl-AcpM (Marrakchi *et al.*, 2002), which is subsequently dehydrated to form an enoyl-AcpM intermediate by the heterodimers HadAB (Rv0635-Rv0636) and HadBC (Rv0636-Rv0637) (Brown *et al.*, 2007; Sacco *et al.*, 2007). InhA (Rv1484) then reduces enoyl-AcpM to acyl-AcpM (Banerjee *et al.*, 1994). The KasA (Rv2245) and KasB (Rv2246) β-ketoacyl synthases initiate subsequent cycles of acylation, from the involvement of MabA to the reduction by InhA (Kremer *et al.,* 2002; Schaeffer *et al.*, 2001). The meromycolate chain is either elongated to C_{42-62} or altered through the addition of keto- or methoxy-groups, methylations or *cis-/trans*-cyclopropanations (Barkan *et al.*, 2010; Barry *et al.*, 1998; Glickman, 2003; Glickman *et al.*, 2000). The meromycolyl-AcpM is activated by the fatty acyl-AMP ligase, FadD32 (Rv3801c), forming meromycolyl-AMP, which is attached to Pks13 (Rv3800c) at the N-terminal ACP (Léger *et al.*, 2009; Portevin *et al.*, 2004; Trivedi *et al.*, 2004). The ACCase complex carboxylates the α-alkyl branch and attaches it to Pks13 at the C-terminal ACP domain, which allows for a Claisen-type condensation reaction by Pks13 (Gande *et al.*, 2007; Gavalda *et al.*, 2014). Pks13 transfers the product of this reaction onto a trehalose to form an α-alkyl-β-keto-trehalose monomycolate (TMM*k*) (Gavalda *et al.*, 2014). The reduction of the keto group by CmrA (Rv2509) produces TMM (Bhatt *et al.*, 2008; Lea-Smith *et al.*, 2007), which is then translocated across the inner membrane into the periplasm by MmpL3 (Rv0206c) (Grzegorzewicz *et al.*, 2012; Tahlan *et al.*, 2012). Finally, mycolic acids are transferred from TMM to AG as part of the mAGP complex, or are bound to TMM forming TDM by a shuttle mechanism

in the Ag85 complex of proteins, Ag85A (Rv3804c), Ag85B (Rv1886c) and Ag85C (Rv0129c) (Belisle *et al.*, 1997; Jackson *et al.*, 1999).

Figure 8. The synthesis of mycolic acids. Mycolic acid synthesis features the FAS-I and FAS-II fatty acid synthase systems for the formation of α-alkyl short chains (C_{24}) and longer mero-chain fatty acids (C_{56}). Adapted from Batt *et al.*, 2020

1.4.7. Structure of PIMs, LM and LAM

The mycobacterial cell wall contains a number of biosynthetically-related glycolipids and lipoglycans, including phosphatidyl-*myo*-inositol mannosides (PIMs), lipomannan (LM) and lipoarabinomannan (LAM) (Figure 9). PIMs are important glycophospholipids which

are non-covalently bound to both the inner and outer membrane of the mycobacterial cell wall (Ortalo-Magné *et al.*, 1996; Pitarque *et al.*, 2008). The lipoglycans, LM and LAM, are formed through the glycosylation of PIMs. These three groups of glycolipids rely on an acylated *sn*-glycerol-3-phospho-(1-D-*myo*-inositol) (PI) unit as part of their structure, accompanied by up to six α-D-mannopyranosyl (Man*p*) residues and up to four acyl chains. In eukaryotes, a PI unit exists in the form of a glycophosphatidylinositol (GPI) anchor, which often binds proteins in the lipid bilayer (Ballou *et al.*, 1964; Chatterjee *et al.*, 1992; Severn *et al.*, 1998). In mycobacteria, the inositol-ring of the PI unit is instead glycosylated at the O-2 and O-6 positions with Man*p* residues, forming a mannosyl phosphate inositol (MPI) anchor. The properties of the acyl chains in the MPI unit, such as position and number, create a large amount of structural diversity in MPI anchors (Pitarque *et al.*, 2005). The most common forms of PIMs in *M. bovis* BCG, *M. tuberculosis* H37Rv and *M. smegmatis* are the tri-acylated and tetra-acylated phospho-*myo*-inositol di-mannosides and phospho-*myo*-inositol hexa-mannosides (Ac_1PIM_2, Ac_2PIM_2, Ac_1PIM_6 and Ac_2PIM_6 respectively) (Khoo *et al.*, 1995)*.* While the mannosylation of PIMs reaches a maximum of 6 mannose residues, LM and LAM are further mannosylated in chains of up to 34 mannose residues interspersed with monomannose branches (Chatterjee *et al.*, 1992).

Immunomodulation of the host's defence is a key function of the cell wall lipoglycans which is achieved through the presence of different LAM 'caps'. Depending on the type of cap, the immune response can be inhibited or stimulated. The presence of mannose caps (ManLAM) is believed to both subdue the response of the host's immune system and function as a ligand for phagocytosis (Schlesinger *et al.,* 1994)*,* while

phosphoinositol caps (PILAM) induce a heightened immune response to *Mtb* through

toll-like receptor 2 (TLR2) signalling (Shukla *et al.*, 2018).
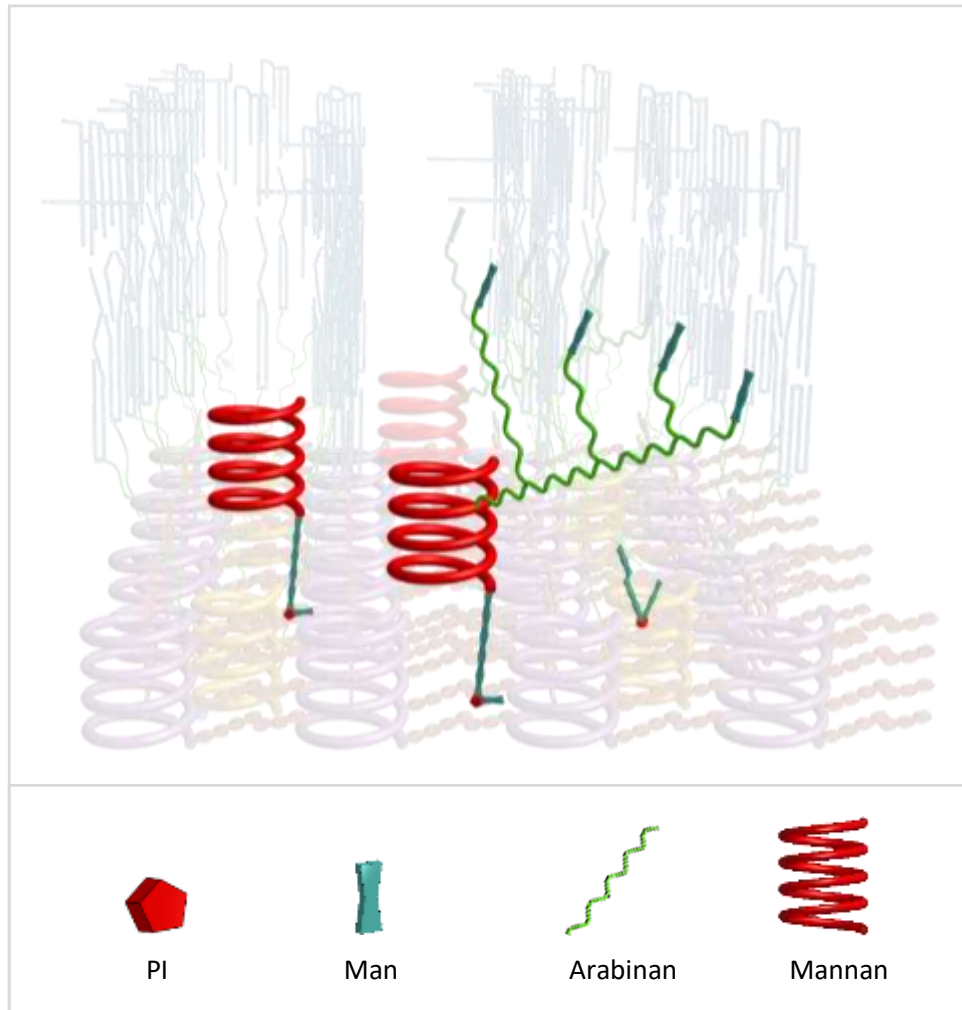
Figure 9. Structure of LM, LAM and AC$_1$PIM$_6$. The cell wall features have been made transparent, leaving LM (left), LAM (centre) and AC$_1$PIM$_6$ (right) in bold colour. Each of these macromolecules is bound to the cell membrane by a mannosyl phosphate inositol anchor and they are thought to protrude through the pores within the PG lattice. Figure produced using Onshape® software.

1.4.8. Synthesis of PIMS, LM and LAM

Formation of cell wall glycolipids begins with the synthesis of the phosphatidylinositol

(PI) anchor, *sn*-glycerol-3-phospho-(1-D-*myo*-inositol), which is essential for tethering

PIMs, LM and LAM to the cell membrane (Figure 10). The first enzyme involved in the synthesis of the PI anchor is PgsA1, a CDP-alcohol phosphotransferase, which catalyses the conjugation of D-*myo*-inositol-3-phosphate (ino-P) with cytidine diphosphate diacylglycerol (CDP-DAG), yielding phosphatidylinositol phosphate (PIP). PIP is immediately separated into phosphatidylinositol and phosphate by an unknown phosphatase (Jackson *et al.*, 2000; Grāve *et al.*, 2019).

The early steps in PIM biosynthesis rely on four α-mannopyranosyltransferases (Man*p*Ts): PimA (Rv2610c), PimB (Rv2188c), PimC and PimD. The formation of Ac_1PIM_1 and Ac_1PIM_2 is achieved by the addition of Man*p* residues from a GDP-Man*p* donor to the PI *myo*-inositol ring by PimA and PimB, and subsequent acylation by Rv2611c (Boldrin et al., 2014; Guerin et al., 2007, 2009; Korduláková et al., 2002). There is ambiguity surrounding the order of mannosylation and acylation, but the preferential formation of Ac_1PIM_1 over Ac_1PIM_2 has been demonstrated, suggesting that mannosylation by PimB likely occurs before acylation (Guerin *et al.*, 2009; Korduláková *et al.*, 2003; Škovierová *et al.*, 2009). Synthesis of the mannosylated PI anchor (MPI) is concluded by an unknown acyltransferase. The enzymes responsible for the addition of subsequent Man*p* residues to MPI remain un-determined, and it is possible that multiple pathways exist. Two likely Man*p*T candidates have been designated PimC and PimD (Kremer *et al.*, 2002).

It is at this stage, following the completion of Ac_1PIM_4/Ac_2PIM_4, that PIM_4 is exported from the cytoplasmic side of the membrane to the periplasmic space through the action of an unknown translocase, possibly Rv1747 (Glass *et al.*, 2017). The synthesis of higher

PIMs, LM and LAM is no longer dependent on the nucleotide derived sugar donor GDP-Man, but instead utilises polyprenyl-phosphate-based mannose donors (PPMs), the synthesis of which is catalysed by Ppm1 (Berg *et al.*, 2007; Gurcha *et al.*, 2002). Following the formation of Ac_1PIM_4/Ac_2PIM_4, higher PIM, LM and LAM synthesis is separated into two pathways by a lipoprotein, LpqW (Rv1166), which directs the tetramannosyl PIM towards higher PIM synthesis by PimE (Rv1159), or towards LM and LAM synthesis (Crellin *et al.*, 2008). PimE mediates the $\alpha(1{\rightarrow}2)$-linked fifth and sixth mannose transfers, resulting in Ac_1PIM_5/Ac_2PIM_5 and Ac_1PIM_6/Ac_2PIM_6 (Morita *et al.*, 2006).

If the tetramannosyl PIM is channelled towards LM and LAM synthesis, mannosylation continues to form an $\alpha(1{\rightarrow}6)$-linked core, distinct from the $\alpha(1{\rightarrow}2)$ linkages in Ac_1PIM_5/Ac_2PIM_5 and Ac_1PIM_6/Ac_2PIM_6, which implicates PIM_4 as the branch-point of divergence in PIM/LM biosynthesis. The $\alpha(1{\rightarrow}6)$-linked core of linear LM is synthesized by MptA (Rv2174) and MptB (Rv1459c) (Mishra *et al.*, 2007, 2008). MptC (Rv2181) is responsible for the transfer of additional mannose residues which form monomannose side chains (Kaur *et al.*, 2008; Mishra *et al.*, 2011).

The LM core is elaborated further to form LAM which is first primed with a small number of Ara*f* residues by an unknown arabinosyltransferase (Ara*f*T). Between 12 and 16 Ara*f* residues are added to the primed core with $\alpha(1{\rightarrow}5)$ linkages by EmbC, using β-D-arabinofuranosyl-1-monophosphoryldecaprenol (DPA) as the arabinose donor (Alderwick *et al.*, 2011; Libin Shi *et al.*, 2006), after which AftC, introduces branching with the addition of $\alpha(1{\rightarrow}3)$-linked Ara*f* residues (Birch *et al.*, 2008). Additional $\alpha(1{\rightarrow}3)$ branches are thought to be introduced by AftD (Škovierová *et al.*, 2009). Once LAM has

reached a total of 55-70 Ara$f$ residues, and its structure has a become highly branched, the nonreducing ends of the arabinan domain are terminated by AftB with β(1→2)-linkages (Jankute *et al.*, 2017). The arabinan termini are primed by a Man$p$T, termed CapA (Rv1635c) (Dinadayala *et al.*, 2006) in preparation for mannosylation by MptC, which adds one to three α(1→2) Man$p$ residues (Kaur *et al.*, 2008). A variation occurs in approximately one fifth of the mannose caps of *Mtb*, whereby mannose is replaced with an α-(1→4)-linked methylthio-D-xylose (MTX) residue (Angala *et al.*, 2017; Ludwiczak *et al.*, 2002; Turnbull *et al.*, 2004).
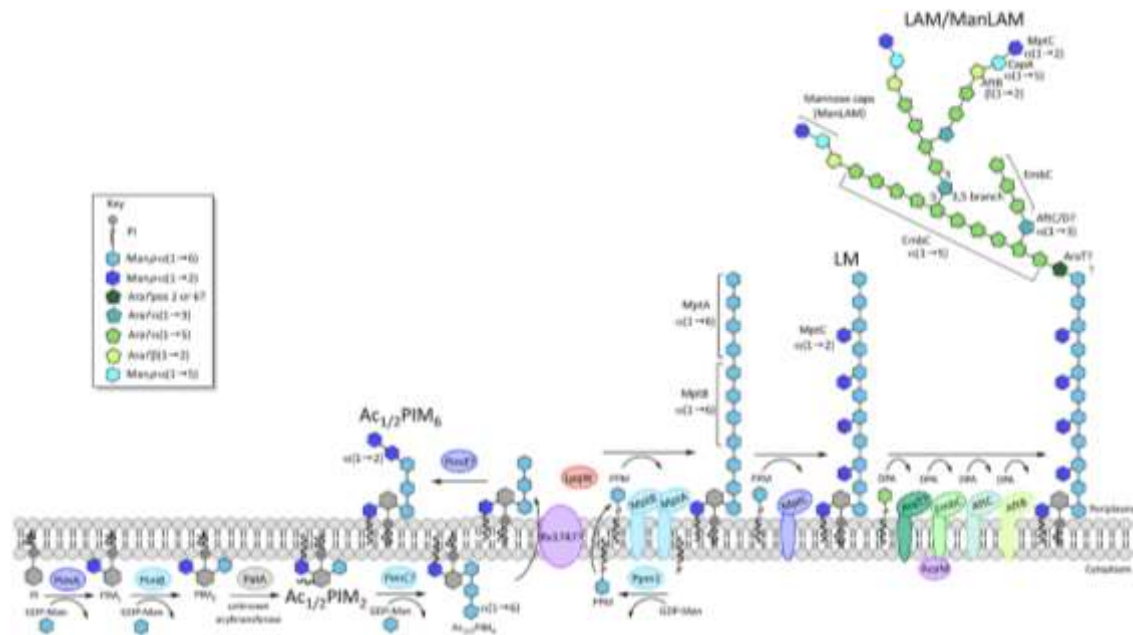
Figure 10. The synthesis of PIMs, LM and LAM. Synthesis begins on the cytoplasmic side of the membrane. AC$_{1/2}$PIM$_4$ is transported across the membrane to the periplasm where synthesis of higher PIMs as well as LM and LAM/ManLAM occurs. Adapted from Batt *et al.*, 2020.

1.4.9. Triacylglycerol (TAG) Synthesis

In *Mtb* TAGs are important energy storage molecules which can be found in intracellular lipid inclusion (ILI) bodies in the cytoplasm as well as in large quantities in the cell wall

(Christensen *et al.*, 1999; Garton *et al.*, 2002). ILI formation can be induced through nitrogen deprivation, in conditions replicating the environment of granulomas (Santucci *et al.*, 2019). TAGs are therefore considered to be involved in fuelling dormant *Mtb* within the host (Maurya *et al.*, 2019). Non-hydroxylated fatty acids matching the meromycolate components found in mycolic acids have also been identified in both DAG and TAG, which implies an involvement in the MOM outer leaflet (Kremer *et al.*, 2005; Rafidinarivo *et al.*, 2009). The first committed step of de novo TAG biosynthesis begins with the formation of DAG. Glycerol-3-phosphate is sequentially esterified by the PlsB/PlsC acylytansferase system to form the precursor to CDP-diacylglycerol, phosphatidic acid (PA) (Lightner *et al.*, 1980; Coleman *et al.*, 1992; Sohlenkamp *et al.*, 2015; Crotta Asis *et al.*, 2021). CDP-DAG is utilised in the synthesis of membrane phospholipids, whereas DAG and subsequent TAG formation require the dephosphorylation of PA by a phosphatidic acid phosphatase (PAP) (Parsons *et al.*, 2013; Crotta Asis *et al.*, 2021). A group of triacylglycerol synthase enzymes (Tgs enzymes) use Acyl-CoA to acylate DAG, forming TAG (Daniel *et al.*, 2004).

1.4.10. Other Lipids of the Mycobacterial Cell Wall

The cell envelope of *Mtb* houses a plethora of lipids with a range of structural and immunomodulatory functions, in addition to the major cell wall components, such as the mAGP complex, lipoglycans and mycolic acids. The phthiocerol and phenolphthiocerol dimycocerosate (PDIM) families, include glycolipids with important roles in virulence. PDIMs are present in all pathogenic members of the *Mtb* complex and have been identified in all clinical isolates of *Mtb* (Goren *et al.*, 1974; Onwueme *et al.*,

2005). At >90 carbons in size, PDIMs are large molecules, which are found as free lipids in the outer membrane. Attenuation of virulence can be achieved by serial *in vitro* passage, and often results in a reduction in or complete loss of PDIMs (Domenech *et al.*, 2009; Goren *et al.*, 1974), implicating PDIMs in *Mtb* virulence. Phenolic glycolipids (PGLs) are a related group of lipids similar in structure to PDIMs but with the modification of a group of antigenic oligosaccharides attached to the phenolic residue (Minnikin *et al.*, 2015). Like PDIMs, PGLs are important virulence factors, and disruption of PGLs in hypervirulent strains results in dramatic attenuation (Reed *et al.*, 2004).

1.5.   Treatment and Drug Resistance

The first anti-TB drugs were developed in the 1950s; since then, more antibiotics have been discovered to treat TB and increasingly complex treatment regimens have evolved to treat multi drug-resistant TB (MDR-TB) and extensively drug-resistant TB (XDR-TB). The slow-growing nature of *Mtb* makes rapid culturing of clinical isolates very challenging and as such, National Institute for Health and Care Excellence guidelines (NICE, 2016) recommend that treatment of TB should be started immediately if clinical signs and symptoms indicate TB, even if the infection has not been confirmed through laboratory tests. Treatment for drug susceptible TB begins with a cocktail of front-line drugs: Isoniazid (INH or H), Rifampicin (Rif or R), Pyrazinamide (PZA or Z) and Ethambutol (EMB or E). Depending on the susceptibility of the strain to these drugs, the duration of the initial phase of treatment can vary, but is advised to last at least 2 months (WHO, 2017) followed by a four month continuation of INH and Rif to form the 2HRZE/4HR treatment regimen (WHO, 2020). This regimen is often also accompanied by a

prescription of pyridoxine hydrochloride as a prophylaxis against isoniazid-induced neuropathy (Porter, 1992). In drug susceptible infections, it is estimated that 85% of patients are successful after the first 6 months of treatment (WHO, 2017). If infection persists or if the infection is resistant to any of the first-line drugs, a number of alternative second-line drugs can be used. These include, but are not limited to, levofloxacin, bedaquiline, pyrazinamide, meropenem, amikacin and ethionamide (WHO, 2020). Studies have shown that daily dosing in TB treatments results in a better outcome than intermittent dosing, such as thrice-weekly treatments (Gopalan *et al*., 2018; Johnston *et al*., 2017). In order to improve compliance and provide support to patients undergoing TB treatment, directly observed treatment (DOT) can be offered, where patients are seen either at home or in a community healthcare setting taking their medication. Daily dosing naturally has an operational disadvantage compared to intermittent dosing if a DOT regimen is to be carried out by healthcare providers. Recently, video observed treatment (VOT) has been offered as an alternative (WHO, 2020).

The treatment of any infection with such an extensive cocktail of drugs naturally leads to complications. For example, access to all the necessary chemotherapeutics may be limited in areas with less developed healthcare systems, which can lead to patients receiving an incomplete course of treatment. Even in countries with the most advanced healthcare systems, patient compliance is a serious issue due to the long duration and unpleasant side effects of treatment. In addition to these four drugs, patients are treated with a low dose of pyridoxine hydrochloride as a prophylactic against isoniazid induced neuropathy. Recently, WHO updated their guidelines to advise against the use

of alternative 4 month treatments which used fluoroquinolone, as they were not shown to be any more effective than 2HRZE/4HR (WHO, 2017).

The above average rates of non-compliance not only lead to poor patient outcomes, but are also a contributing factor to the rising incidence of multidrug-resistant TB (MDR-TB) rifampicin-resistant TB (RR-TB) and extensively drug-resistant TB (XDR-TB) cases worldwide (Morris, 2009). An estimated 132,222 new cases of MDR-TB/RR-TB, meaning they were resistant to INH and RIF, occurred in 2020, accounting for over 5% of bacteriologically confirmed cases (WHO, 2015). A further 25,681 patients in the same year had pre-XDR-TB or XDR-TB; the strains of TB they carried were also resistant to rifampicin and any fluoroquinolone drug (pre-XDR-TB), and either bedaquiline or linezolid (XDR-TB) (WHO, 2015). The distribution of MDR/RR-TB in previously treated cases of TB shows a heavy burden of drug resistance in countries in the region of the Russian Federation (Figure 11).With treatment success for drug-resistant TB only a little over 50%, there is an urgent need for new chemotherapeutics to be developed (Sugawara *et al*., 2014).
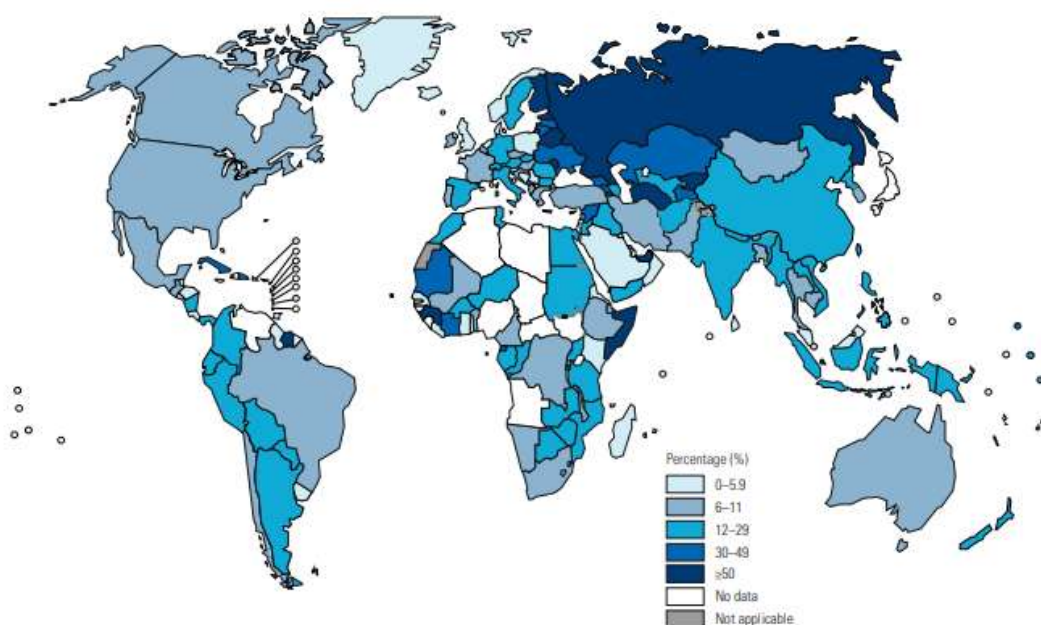
Figure 11. Global distribution of previously treated TB cases with MDR/RR-TB from WHO TB report (2020). Rates of drug resistant, previously treated infections are presented by region and a higher percentage of cases is indicated by a darker colour.

1.6.   First-Line Antibiotics

1.6.1. Isoniazid (INH)
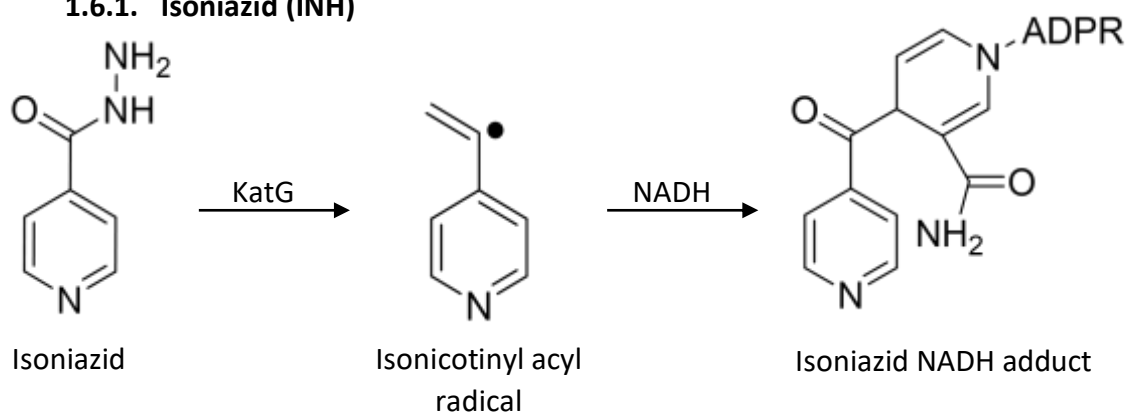
Figure 12 Isoniazid activation. Structures of the first line TB drug isoniazid, the isonicotinyl acyl radical formed by KatG and an isoniazid-NADH adduct, bound to adenosine diphosphate ribose (ADPR).

INH is a first-line drug which inhibits mycolic acid synthesis through competitive inhibition of InhA, a FAS-II enoyl-CoA reductase (Banerjee *et al.*, 1994). InhA is essential for the synthesis of mycolic acids in *M. tuberculosis* (Quémard *et al.*, 1995). It is a pro-

drug which passively diffuses into the cell in its inactive, non-toxic form (Bardou *et al.*, 1998). Activation of INH is carried out by the catalase-peroxidase KatG (Zhang *et al.*, 1992) which catalyses the formation of an isonicotinyl acyl radical, a reactive intermediate, which spontaneously couples with (reduced nicotinamide adenine dinucleotide) NADH to form a covalently bound INH-NAD adduct (Rawat *et al.*, 2003) (Figure 12). The nitrogen-containing pyridine ring of the INH-NADH adduct binds tightly and competitively to InhA, leaving the binding pocket occupied and blocking the binding of NADH alone (Rozwarski *et al.*, 1998). As with other pro-drugs, changes to the protein that activates the drug, in this case KatG, can result in a reduction or complete loss of activity (Zhang *et al.*, 2009). In isolates selected with resistance related to impairment of KatG, a second mutation is often found in AhpC, an alkyl-hydroperoxide reductase, which is thought to be a compensatory upregulation mutation (Sherman *et al.*, 1996). Resistance to InhA can also occur through mutations to a serine residue in the InhA binding pocket (Rozwarski *et al.*, 1998; Torres *et al.*, 2015), as well as other modifications which reduce the affinity of the INH-NADH adduct (Banerjee *et al.*, 1994; Dessen *et al.*, 1995; Rozwarski *et al.*, 1998). An unfortunate consequence of mutations directly affecting InhA, is the cross-resistance to ethionamide which, when activated to form an adduct with NAD, also binds InhA (Baulard *et al.*, 2000; DeBarber *et al.*, 2000; Vannelli *et al.*, 2002). The first clinical trials of INH in the early 1950s were a huge success, with the severity of all participants' symptoms being relieved, and 25% of patients' sputum tested negative for infection after 4-15 weeks (Herbert Fox, 1952; Robitzek *et al.*, 1952; Selikoff *et al.*, 1952). In recent years, however, resistance to INH has become a major

challenge to global health, with mutations to *katG* reported in up to 82% of MDR-TB cases (Torres *et al.*, 2015).

1.6.2. Rifampicin (RIF)
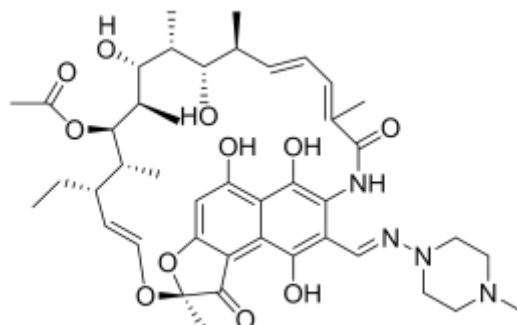
Rifampicin
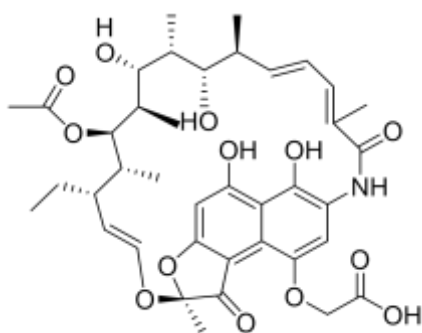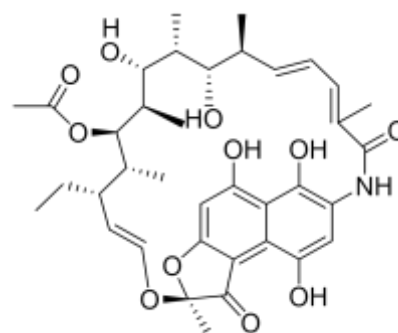
Rifamycin B   Rifamycin SV

Figure 13. Structures of rifampicin, rifamycin B and rifamycin SV

RIF was first discovered in 1965 as a potent antibiotic and an important front-line treatment for TB (Maggi *et al.*, 1965). RIF is an RNA polymerase inhibitor (Hartmann *et al.*, 1967; Umezawa *et al.*, 1968), derived from rifamycin B, an essentially inactive compound without anti-TB effects that degrades into the potent antimicrobial, rifamycin SV, through oxidation and hydrolysis (Figure 13). It is a polyketide with a heterocyclic structure and a naphthoquinone core. The naphthoquinone is responsible

for the characteristic red-orange colour of the drug, that often discolours the urine, sweat and tears of patients.

The mechanism of action of RIF is interesting in that it does not inhibit the activity of the RNA polymerase by binding the active site, but binds to a pocket in the β subunit, and physically prevents elongation in the DNA/RNA channel (Campbell *et al*., 2001). The RNA transcript is blocked from the 5' end after the addition of two or three nucleotides, and further bonds cannot be formed (Campbell *et al*., 2001; Feklistov *et al*., 2008). In virtually all cases, resistance to RIF is associated with mutations to *rpoB,* the gene encoding the β subunit (Ezekiel *et al*., 1968; Heep *et al*., 2000; Ramaswamy *et al*., 1998). This is true of almost every species in which RIF resistance has been studied, including *Mtb*. In fact, in *Mtb*, mutations are so commonly found in a single area dubbed the 'rifampcin resistance determining region' or RRDR, they can be used for rapid detection of drug-resistant infections (Telenti *et al*., 1993). Approximately 86% of RIF resistance in clinical isolates of *Mtb* can be attributed to three amino acid substitutions (Telenti *et al*., 1993): the substitution of Serine-531 for Leucine (Ser531Leu) accounts for 41% of mutations and causes a conformational change to the binding pocket which prevents RIF from tightly binding; when Histidine-526 is replaced by Tyrosine (His526Tyr) in 36% of cases, RIF binding is sterically blocked; and the substitution of Asparagine-516 with Valine (Asp516Val) affects the charge of the binding pocket, thus repelling RIF and preventing binding, which accounts for 9% of resistance mutations (Artsimovitch *et al*., 2005; Campbell *et al*., 2001; Gill *et al*., 2011; Molodtsov *et al*., 2017).

1.6.3. Pyrazinamide (PZA)
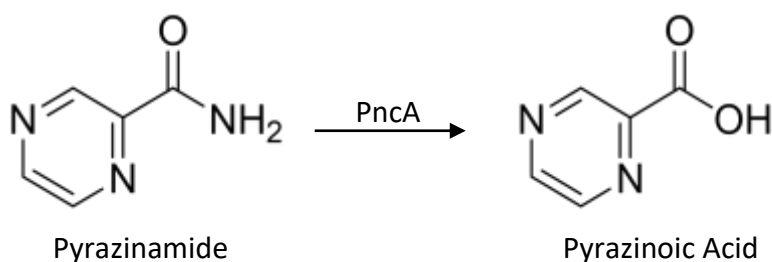
Figure 14 Structure of pyrazinamide and pyrazinoic acid, which is converted by PncA.

PZA, a structural analogue of nicotinamide (also known as vitamin B3), was first isolated in 1939 (Dalmer, 1936). Nicotinamide was identified as a compound with activity against *Mtb* in the 1940s (Chorine, 1945) and investigations into the effect of PZA on *Mtb* soon followed. In 1949, PZA clinical trials began, and by 1952 the promising results demonstrating the effect of PZA on pulmonary tuberculosis had been published (Yeager *et al.*, 1952).

Unlike the majority of antibiotics used in the treatment of TB, PZA is almost completely inactive against growing cells, yet has valuable antimicrobial properties against non-replicating 'persisters' (Hu *et al.*, 2006). Prior to the 1970s, PZA was routinely only used as a second-line drug, due to the high dose required, and associated hepatotoxicity (Zhang *et al.*, 2014). When administered in combination with other drugs such as INH, however, PZA is far more effective at clearing infection and can be used at lower concentrations. As such, it is now prescribed as part of a combination therapy regimen (McCune *et al.*, 1956).

PZA is a pro-drug which diffuses easily into the *Mtb* granuloma, where it is activated by the mycobacterial pyrazinimidase, PncA, which converts it to pyrazinoic acid (Scorpio *et*

al., 1996) (Figure 14). While some of the pyrazinoic acid accumulates within the cell, much of it diffuses out into the acidic environment of the granuloma. Under acidic conditions, pH5.5, protonation of pyrazinoic acid occurs, and the resulting conjugate acid diffuses back into the cell where it accumulates (Zhang *et al.*, 1999, 2003). This is thought to lead to a higher concentration of the more acidic pyrazinoic acid within the cell and causes cell damage and eventual cell death (Zhang *et al.*, 2014).

The exact mechanism of action of PZA has long been debated, but recent studies have identified Coenzyme A (CoA) as an indirect target of pyrazioic acid, and the aspartate decarboxylase, PanD, as a direct target (Gopal *et al.*, 2016; Gopal, *et al.*, 2017; Gopal *et al.*, 2017; Shi *et al.*, 2014). PanD is involved in the synthesis of pantothenate, commonly known as vitamin B5, which is required for CoA synthesis. PZA binds to PanD and only weakly inhibits it but is thought to act as a target degrader. The caseinolytic protease ClpC1-ClpP is responsible for the degradation of PanD, triggered by the binding of PZA to PanD (Gopal *et al.*, 2017; Shi *et al.*, 2014; Zhang *et al.*, 2017).

1.6.4. Ethambutol (EMB)
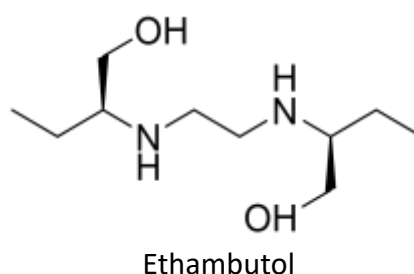
Ethambutol

Figure 15 Structure of ethambutol

EMB (Figure 15) is a bacteriostatic antibiotic, discovered in 1961. It efficiently inhibits cell wall synthesis by targeting arabinotransferases in the EmbCAB operon (Belanger *et*

al., 1996). Treatment of *M. smegmatis* with EMB affects arabinogalactan (AG) synthesis, resulting in incomplete, truncated AG, which has been attributed to inhibition of EmbA/EmbB (Deng *et al*., 1995; Safi *et al*., 2008, 2010; Starks *et al*., 2009; Takayama *et al*., 1989). It has recently been demonstrated through structural studies, that ethambutol binds to EmbA, EmbB and EmbC (Zhang *et al*., 2020). Inhibition of EmbC prevents the α(1→5) Ara*f* elongation, interfering with LAM synthesis (Alderwick *et al*., 2011; Shi *et al*., 2006). It has also been observed that *M. smegmatis* treated with ethambutol is unable to form the termini of AG which links the mycolic acid layer and the cell wall (Takayama *et al*., 1989). Resistance to EMB is almost exclusively associated with mutations to EmbB, which occur in as many as 93% of EMB resistant strains, and in 72% of all MDR strains. The most common EmbB mutation, accounting for at least half of cases, is the substitution of Methionine-306 with Valine, Leucine or Isoleucine (Zhao *et al*., 2015).

1.7. Second-Line Antibiotics

In the event of the first phase of treatment not completely clearing the infection, patients will be prescribed a combination of second-line drugs. The WHO separates these drugs into three groups based on effective combinations of therapeutics and the priority of their use. Group A, consisting of four drugs, levofloxacin or moxifloxacin, bedaquiline and linezolid, three of which should be prescribed together (with one of levofloxacin or moxifloxacin included). Group B consists of just two drugs, and either one or both should be added to the regimen where appropriate. Group C, consists of 10

drugs, of which two are added to the regimen to replace any drugs from A and B which

cannot be used (WHO, 2021) (Table 1).

Table 1 Second-line antibiotics used to treat drug-resistant tuberculosis. Drugs are divided into groups based on priority of use. Adapted from WHO consolidated guidelines on tuberculosis, 2021.

WHO grouping	Drug	Mechanism of Action
Group A	Levofloxacin or moxifloxacin	Inhibition of DNA gyrase and topoisomerase IV
	Bedaquiline	Inhibition of adenosine triphosphate (ATP) synthase
	Linezolid	Inhibition of protein synthesis
Group B	Clofazimine	Inhibition of ATP synthesis via F-ATP synthase interference
	Cycloserine or terizidone	Inhibition of cell wall biosynthesis (both)
Group C	Ethambutol	Inhibition of cell wall biosynthesis
	Delamanid	Inhibition of cell wall biosynthesis
	Pyrazinamide	Interferes with CoA synthesis via PanD degradation
	Imipenem-cilastatin or meropenem	Inhibition of cell wall biosynthesis (Imipenem and meropenem) and prevention of renal metabolism of imipenem (cilastatin)
	Amikacin or streptomycin	Inhibition of protein synthesis (both)
	Ethionamide or prothionamide	Inhibition of cell wall biosynthesis (ethionamide) and inhibition of peptide synthesis (prothionamide)
	P-aminosalicylic acid	Inhibition of folate synthesis

1.8.   Drug Discovery

The search for novel antimycobacterial drugs is driven by the need to combat existing

drug resistance and minimise the chance of resistance to new drugs occurring. While

drug targets vary between different pathogens, common techniques are used for the

identification of new drugs and targets for infectious diseases in the drug discovery pipeline (Abrahams, 2020). The success of a drug candidate is dependent on a number of criteria which determines its suitability as a treatment and its viability as a commercial drug. Perhaps the most important attributes of a new drug are its compatibility with existing therapeutics so that it is suitable for use in: (i) combination therapies, (ii) a short treatment duration (which is particularly important in TB drug discovery), (iii) a low mutation frequency and, preferably, (iv) low production costs.

New TB drugs are required to act rapidly in a bactericidal manner, preferably with a treatment duration under 6 months, and a novel mode of action is beneficial to ensure the susceptibility of MDR-TB strains which are resistant to existing drugs. Additionally, it is essential that novel therapeutics are suitable for co-administration with existing TB drugs (Mdluli *et al.*, 2015). The (L)ADME(T) (liberation, absorption, distribution, metabolism, excretion, and toxicity) properties of prospective drugs must be carefully assessed (Kenakin, 2017). Absorption usually refers to absorption of a compound into the bloodstream through a mucous membrane, before distribution to the effector site. The metabolism of a drug is important, as the breakdown of a parent compound into metabolites may result in inactivity of the drug, or in the case of a pro-drug might be essential for its activation. Excretion simply refers to the method through which a compound and its metabolites are eliminated from the body. Finally, liberation and toxicity need to be considered. The liberation of a compound describes the separation of an active compound or a pro-drug from the vehicle used for administration. The toxicity is perhaps the most important property to consider, as damage to human cells

caused by an antibiotic can render the drug useless, no-matter how desirable its other properties (Kenakin, 2017).

The physiology of *Mtb* and its epidemiological characteristics raise additional challenges in drug discovery, including the need to tackle physiologically distinct populations of replicating and non-replicating bacteria (Bhat *et al.*, 2015; Du *et al.*, 2016; Colangeli *et al.*, 2020). The waxy cell membrane, rich in mycolic acids, makes the cell wall of *Mtb* particularly hard to penetrate (Batt, *et al*., 2020). The issue of cell permeability is further exacerbated by the fact that *Mtb* are often protected within the microenvironment of the TB granuloma which is equally challenging to penetrate (Dartois, 2014).

Drug discovery can be approached by two distinct methods; (i) target-to-drug discovery, or (ii) drug-to-target discovery. In target-to-drug methodologies, drugs are screened with the intention of directly inhibiting a pre-determined target, such as a defined cellular process or enzyme. This allows the researcher to select for certain desirable target properties. Ideally drugs selected to combat the growing threat of antibiotic resistance should target enzymes or cellular processes with no previously known resistance to other drugs. This has led to a concerted effort to identify 'novel' drug targets which are not involved in the mechanism of action of any commercial drugs. Another aspect to be taken into consideration is the existence of human orthologues to the target gene. A drug that inhibits an enzyme or cellular process in the target organism may also have activity against mammalian cells, potentially rendering the drug unusable. Identifying targets with no human orthologues early in the drug discovery process may increase the chances of drugs reaching clinical trials. Finally, the cellular location of a

target is crucial for success. If a target is inaccessible to the drug, be it due to poor permeability of the cell or efflux of the drug before it can reach the target, it is not a viable target. The extracellular surface of the cell is a particularly desirable location for drug targets, which circumvents any issues with entry into the cell. Only three drugs have been approved by the US Food and Drug Administration (FDA) in the past 50 years, bedaquiline, delamanid and pretomanid, all of which were identified through whole cell screening (Mahajan, 2013; Ryan *et al.*, 2014; FDA, 2019).

A major drawback of target-to-drug based research is that the direct inhibition of a target in biochemical assays does not necessarily translate to killing or inhibition in whole cell assays. This obstacle is avoided in drug-to-target based discovery, in which compound libraries are commonly screened against whole cells to identify phenotypic hits, selected based on their activity. Additionally, growth conditions can be altered to reflect the conditions within the host and macrophage infection models can easily be employed. While drug-to-target screening provides an early indication of a drugs ability to inhibit a pathogen, however it provides little insight into the mechanism of action and requires the retrospective identification of targets. Target deconvolution can be achieved through a number of strategies including the generation and sequencing of resistant mutants, RNA sequencing, chemoproteomic profiling, morphological profiling and metabolomics (Abrahams, 2020).

Whole genome sequencing (WGS) of resistant mutants is a popular technique for target identification which is relatively straightforward to carry out. Resistant mutants are generated through incubation with high concentrations of a drug and following DNA

extraction their genomes are sequenced to determine mutations, such as single nucleotide polymorphisms (SNPs) or insertions or deletions (InDels) which may confer resistance. The rationale for this method is that mutations which confer resistance are likely to occur in the target gene, however it is not infallible. In some instances, mutations occur in genes encoding resistance mechanisms, such as efflux pumps which result in resistance without target mutations (Milano *et al*., 2009). In addition, genes responsible for pro-drug activation can mutate, preventing activation and cause strains to appear resistant, despite remaining susceptible to the active form of the drug (Abrahams *et al*., 2020). If a drug has more than one target, WGS of resistant mutants can be misleading and result in alternative targets being overlooked (Chiarelli *et al*., 2018). In the event of WGS yielding no definitive results, or if the generation of resistant mutants is simply not possible, a combination of technologies can be exploited to elucidate the target. RNA sequencing is another relatively low-cost solution to target delineation that relies on changes occurring in the transcriptome following exposure to a drug. It can provide insights into the mechanism of action, and is particularly useful if a transcriptional regulator is implicated as the target (Abrahams 2020; Yang *et al*., 2020).

In chemoproteomic profiling, a drug is immobilised on a Sepharose bead matrix forming an affinity probe and is incubated with a cell lysate. Following elution, mass spectrometry is used to analyse proteins that bind to the drug. Moreover, competition assays can be carried out using 'free' compound to distinguish between non-specifically bound proteins and those which bind competitively. Naturally, this process will only identify protein targets and is unsuitable for determining structural targets.

Morphological profiling simply involves incubating cells with a drug and analysing changes to their morphological features compared to the parental strain. Incubation of cells with control drugs with known targets, which cause known morphological changes can aid target identification (Ii *et al*., 2020). This method may not provide sufficient information to determine the involvement of a specific protein but helps to narrow down which cellular processes are being targeted.

Metabolomic analysis requires cells to be cultured in the presence and absence of a drug before extracting the cell metabolites. Similarly to chemoproteomic profiling, these can be analysed by mass spectrometry and the treated and untreated profiles compared to identify significant changes and determine which metabolic pathways are targeted (Zampieri *et al*., 2018).

It is now widely accepted that the most efficient route to producing new commercially viable drugs is the simultaneous application of target-based and drug-based approaches (Abrahams *et al.*, 2020). In order to exploit the whole cell nature of drug-to-target screening with a more refined focus on a specific target, protein overexpression and knockdown techniques can be employed. Overexpression of a target gene can be used as an indicator of target engagement in high-throughput screening (HTS). When a protein is expressed in higher amounts, the concentration of drug required to inhibit it must increase, resulting in a measurable increase in minimal inhibitory concentration (MIC) compared to a wild type (WT) strain. Following the same principle, if a gene is knocked-down by the innovative genetic tool clustered regularly interspaced short palindromic repeat interference (CRISPRi), less drug is required to inhibit the remaining

activity, and as such, the MIC will be reduced. This technique can also be deployed to test the effect of considerably reducing the expression of different proteins in order to select an appropriate target.

Typically, drug discovery encompasses: the identification of hits; the refinement of hits through pharmacokinetic (PK) and pharmacodynamic (PD) assessments and structure-activity relationship (SAR) studies to determine lead compounds (hit-to-lead); the optimisation of lead compounds to improve structure and deliver the maximum potency and (L)ADME(T) properties (Kenakin, 2017; Gianti *et al.*, 2021) (Figure 16). Preclinical development sees the introduction of *in vivo* testing and continued *in vitro* testing. The primary objective of preclinical development is to establish safe starting doses for human trials and further understand the toxicity of leads. The no-observed-adverse-effect level (NOAEL), the concentration of drug at which an organism experiences no statistically significant adverse effects, is established in pre-clinical trials. Following successful pre-clinical trials, compounds go through three phases of human trials as part of the drug development process (Figure 16). Phase I clinical trials use healthy participants to ascertain whether the safe doses established in pre-clinical trials are suitable, and changes to dosing are made where appropriate. The data collected in Phase I trials is used to inform phase II trials, in which participants are usually a small number of patients who have the disease targeted by the drug candidates. The final phase of clinical trials prior to a request for approval by a regulatory authority (e.g., the FDA in the USA or the Medicines and Healthcare products Regulatory Agency in the UK), involves large scale testing of patients with the targeted disease. If the drug meets the required standard of safety and efficacy as dictated by the regulatory authority, it will

be licensed for use. The development of new drugs and the collection of data about their safety and efficacy continues past the point of approval. A fourth round of clinical trials (phase IV) can be requested as a condition of approval, and follow-up drug discovery studies may continue (Salazar *et al.*, 2017).
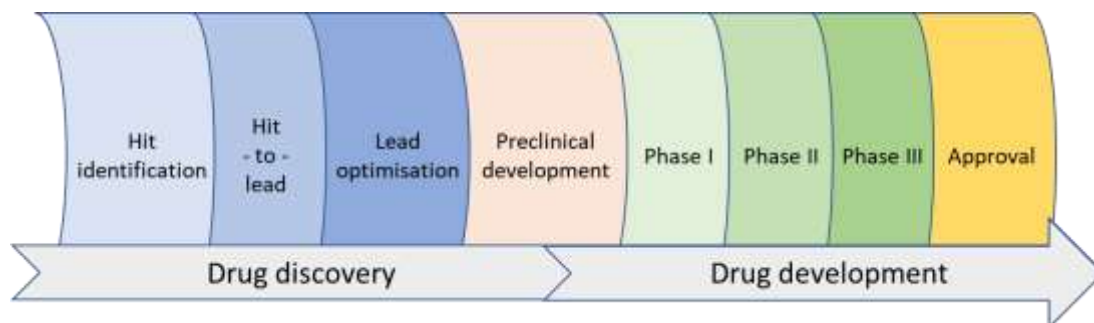
Figure 16 The steps involved in drug discovery and development. Drug candidates undergo three stages of drug discovery prior to their use in preclinical animal testing. Three stages of human clinical trials are routinely used, with more extensive testing required in each phase.

1.9.   Revisiting Existing Drugs for *Mtb* Target Identification

Revisiting existing drugs in the hope of identifying new anti-TB activities or previously undescribed targets is an important strategy in drug discovery and drug development. For the numerous families of drugs that exist to treat TB and other diseases, scientific research has barely scratched the surface and there is often scope to understand and exploit these compounds further. Two groups of drugs with promising activity against Mycobacteria which have formed much of the focus of this thesis are the BM212 series MmpL3 inhibitors and triacylglycerol synthase inhibitors.

1.9.1. BM212 Series MmpL3 Inhibitors

Countless proteins encoded by *Mtb* have been investigated as possible drug targets in recent decades as part of the concerted effort to tackle MDR-TB (Abrahams *et al*., 2018; Batt *et al*., 2020). An essential protein that has attracted considerable attention is MmpL3, one of the 13 MmpLs (mycobacterial membrane protein large) of *Mtb*, which is conserved across mycobacterial species (Cole *et al*., 1998). MmpL3 is thought to act as a flippase in the transport of trehalose monomycolate (TMM) and has been shown to bind phosphatidylethanolamine (PE) (Grzegorzewicz *et al*., 2012; Tahlan *et al*., 2012). Precursors to TMM accumulate when MmpL3 activity is reduced, leading to incomplete cell wall biosynthesis and eventual cell death (Deidda *et al*., 1998; Domenech *et al*., 2005; Graham *et al*., 2018; La Rosa *et al*., 2012; Li, K *et al*., 2014; Li, W *et al*., 2014; Onajole *et al*., 2013; Protopopova *et al*., 2005; Rao *et al*., 2013; Remuiñán *et al*., 2013; Stanley *et al*., 2012). Collectively, the MmpL proteins play an important role in the translocation of a wide variety of lipids across the plasma membrane, although MmpL3 is the only essential member of the MmpL family (Degiacomi *et al*., 2017; Domenech *et al*., 2005). The recent elucidation of the MmpL3 crystal structure reveals that MmpL3 consists of 12 transmembrane α-helices and two periplasmic domains which are situated between α-helices 1 and 2, and 7 and 8 (Zhang *et al*., 2019). A cavity, which is important for TMM transportation, is formed between the two periplasmic domains (Su *et al*., 2019; Zhang *et al*., 2019). Two essential pairs of aspartic acid and tyrosine residues (Asp256-Tyr646 and Tyr257-Asp645) are situated centrally within the transmembrane helices, where they bind α-helices 4 and 10, and are facilitators of proton translocation

(Bernut *et al.*, 2016; Shao *et al.*, 2020; Zhang *et al.*, 2019). The transmembrane region has been identified as a key location for drug interactions through co-crystallisation with four MmpL3 drugs (SQ109, AU1235, ICA38 and Rimonabant) which bind within the domain (Zhang *et al.*, 2019). A conformational change occurs upon binding, disrupting the hydrogen bonds between α-helices 4 and 10, thus inhibiting the transporter (Zhang *et al.*, 2019). A further six compounds (BM212, NITD-349, GSK2200150A, C215, PIPD1 and HC2091) are predicted to bind in the same location (Bolla, 2020; Zhang *et al.*, 2019).

The numerous inhibitors of MmpL3 reported to date have an unusual variety of structural characteristics (Abrahams *et al.*, 2018). Known inhibitors include pyrrole and pyrazole derivatives, such as BM212 and Rimonabant; benzimidazoles, like C215; indole-2-carboxamides and even more structurally diverse compounds, such as the ethylenediamine, SQ109 (Figure 17) (Graham *et al.*, 2018; La Rosa *et al.*, 2012; Onajole *et al.*, 2013; Protopopova *et al.*, 2005; Remuiñán *et al.*, 2013).

A common characteristic of MmpL3 inhibitors is their promiscuity; secondary targets have been identified for a number of drugs, some of which also inhibit non-MmpL3-containing pathogens (Li, K. *et al.*, 2014). SQ109, which is currently undergoing clinical trials as a TB drug, inhibits a wide variety of organisms, such as *Helicobacter pylori* (Makobongo *et al.*, 2013)*, Saccaromyces cerevisiae* and *Candida albicans* (Li, K. *et al.*, 2014), and has anti-parasitic properties against *Trypanosoma cruzi* (Veiga-Santos *et al.,*2015), *Plasmodium falciparum* (Kai Li *et al.*, 2014) and *Leismania* spp (García-García *et al.*, 2016; Gil *et al.*, 2020).

Prior to the structural characterisation of MmpL3, the mechanisms of action of its inhibitors were widely contested (Abrahams *et al.*, 2018; Batt *et al.*, 2020). Due to the structural diversity of inhibitors, it was proposed that MmpL3 could have an efflux function, which would explain its frequent detection through the generation of resistant mutants (Viljoen *et al.*, 2017). Cross-resistance to other drugs is a common consequence of mutations to efflux pumps (Li *et al.*, 2009). At least two other proteins from the same family, MmpL5 and MmpL7, have also been identified as likely efflux pumps (Pasca *et al.*, 2005), mutations to which result in bedaquiline (Hartkoorn *et al.*, 2014) and azole (Milano *et al.*, 2009) resistance.

The co-crystallisation of MmpL3 with a selection of inhibitors gives sufficient cause to believe that it is a direct target of these drugs (Bolla, 2020; Zhang *et al.*, 2019). There is, however, evidence of secondary targets for an increasing number of MmpL3 inhibitors. SQ109, for example, inhibits two enzymes implicated in menaquinone biosynthesis, MenA and MenB, in addition to MmpL3 (Berube *et al.*, 2019; Li, K. *et al.*, 2014). The tetrahydropyrazol[1,5-a]pyrimidine-3-carboxamide (THPP) has also been probed for secondary targets, having been identified as an MmpL3 inhibitor through spontaneous resistant mutant generation (Remuiñán *et al.*, 2013). Competitive inhibition assays using THPP bound to immobilised beads identified EchA6 as an additional target (Cox *et al.*, 2016), demonstrating the importance of thorough investigation into drugs even after initial target discovery (Abrahams *et al.*, 2018).
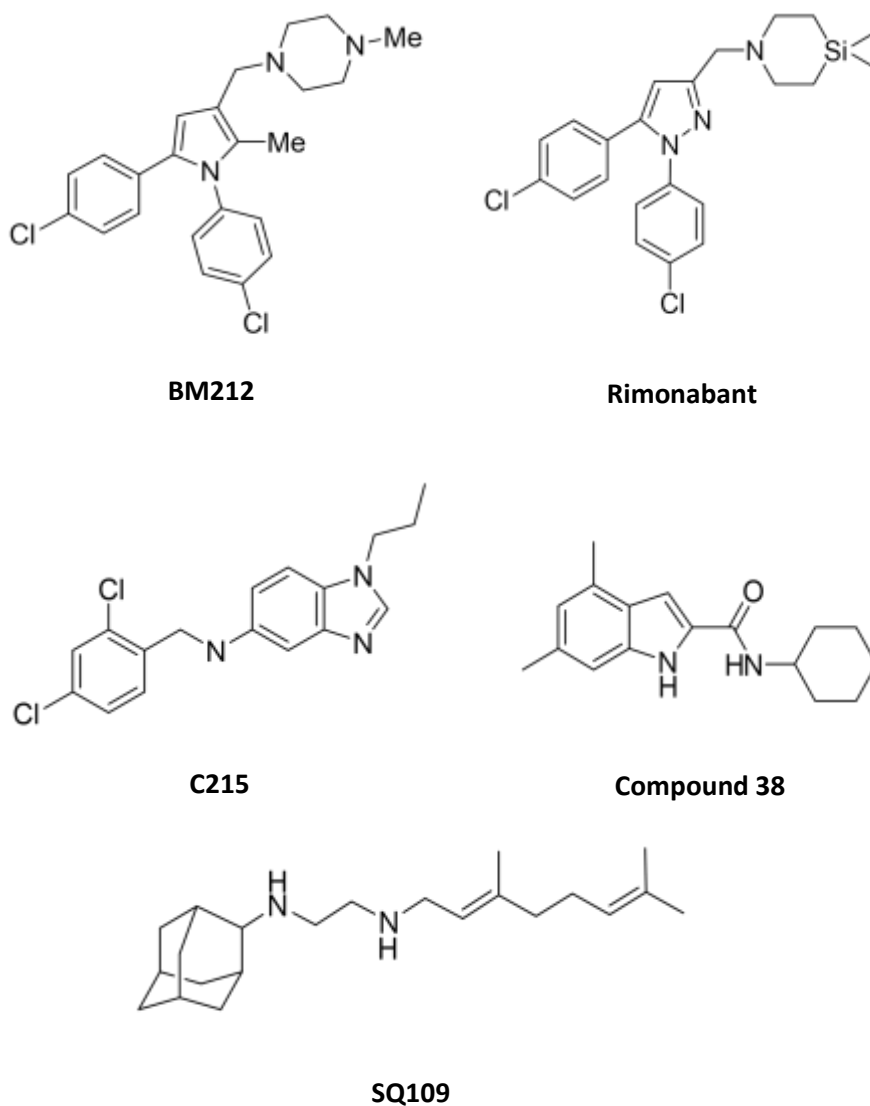
Figure 17 MmpL3 inhibitors are structurally diverse. A – BM212 **B –** BM212 pyrrole derivative, Rimonabant, **C –** Benzimidazole derivative, C215 **D** - indole-2-carboxamide, compound 38 **E –** SQ109, an ethylenediamine currently undergoing clinical trials.

1.9.2. Triacylglycerol Synthase Inhibitors

In TB infections, granuloma formation begins with the phagocytosis of TB bacilli by alveolar macrophages upon inhalation of the pathogen. Once phagocytosed, the TB bacillus prevents the phagolysosome compartment from undergoing acidification

(Sturgill-Koszycki *et al.*, 1994), and triggers accelerated growth and division of the pathogen (Russell *et al.*, 2009). An acquired immune response follows, leading to the formation of an early granuloma comprised of infected macrophages surrounded by foamy macrophages, phagocytes and lymphocytes (Peyron *et al.*, 2008; Russell *et al.*, 2009). The presence of *Mtb,* specifically the oxygenated mycolic acids on the surface of the cell, in the granuloma triggers increased differentiation of monocyte-derived macrophages into foamy macrophages, leading to a build-up of lipid-loaded macrophages (Peyron *et al.*, 2008). A mature granuloma also features a fibrous capsule which surrounds the immune cells and the number of blood vessels supplying the granuloma decreases, creating a hypoxic environment (Kim *et al.*, 2010).

Safely ensconced within the granuloma, the TB bacilli undergo further phenotypic changes triggered by the growth-limiting conditions of the granuloma. The most clinically important change is the phenotypic tolerance to many antibiotics, including rifampicin, isoniazid, ethambutol and pyrazinamide. These antibiotics are particularly efficient at targeting bacteria which are actively growing and replicating, but their activity is significantly reduced in latent TB infections (Roupie *et al.*, 2007).

The significance of fatty acids in TB persistence was first realised over 50 years ago when fatty acids of varying chain lengths were shown to stimulate oxygen uptake in *Mtb* (H. Bloch *et al.*, 1956)*.* Fatty acids can be utilised by *Mtb* for both the release of energy and the synthesis of carbohydrates. The tricarboxylic acid cycle (TCA) is a pathway by which lipids can be converted to adenosine triphosphate (ATP) and carbon dioxide through the oxidation of acetyl-CoA. The glyoxylate cycle, or shunt, is a variation of the TCA where

acetyl-CoA is converted to succinate, a dicarboxylic acid involved in carbohydrate synthesis (Lorenz *et al*., 2002). Under the hypoxic conditions of latent TB, a number of biochemical changes occur, resulting in reduced metabolic activity (Wayne *et al*., 1996). When both the TCA and the glyoxylate cycle run in parallel, fatty acids can be used as the main carbon source of *Mtb* in a hypoxic environment.

In both eukaryotic and prokaryotic organisms, fatty acids are stored as triacylglycerols (TAGs) (Turkish *et al.*, 2007; Serafim *et al.*, 2018). In most mammals, storage of TAG occurs in the adipose tissue, whereas in bacteria, TAG is accumulated as lipid inclusion bodies, aggregates of lipids within the cell (Turkish *et al.*, 2007; Serafim *et al.*, 2018). Dormant *Mtb* exhibits a particularly high number of inclusion bodies, consisting primarily of TAG (Garton *et al.*, 2002). In *Mtb,* there are fifteen genes which have been identified as having triacylglyerol synthase (TGS) activity (Drancourt, 2009) (Table 2). Tgs1 is of particular interest as it is powerfully inducible in the dormancy gene regulon, a collection of 48 genes mediated by DevR which is involved in the response to hypoxic stress (Voskuil *et al.*, 2003; Chauhan *et al.*, 2009). Tgs1 is thought to be a mycobacterial diacylglycerol acetyltransferase or triacylglycerol synthase. Diacylglycerol transferases are enzymes responsible for catalysing the terminal reaction between fatty acyl-CoAs and 1,2-diacylglycerols (Cases *et al*., 1998). Deletion of *tgs1* results in a significant reduction but not total elimination of TAG accumulation. Latent *Mtb* inside lipid-labelled macrophages have been shown to accumulate host TAG; when host TAG was labelled with triolein [glycerol-1,2,3–^{3}H, carboxyl-1-^{14}C], the label was shown to be incorporated into the TAG inside the *Mtb* cells (Daniel *et al*., 2011).

Diacylglycerol-transferases in humans are encoded by two genes; *DGAT1* and *DGAT2* (Cases *et al.*, 1998, 2001; Oelkers *et al.*, 1998). Inhibition of DGAT1 results in a reduction of TAG pools in macrophages, preventing foamy macrophage formation (Cao *et al.*, 2011; Knight *et al.*, 2018). There has been speculation that by reducing the availability of host TAG, the growth of *Mtb* could be inhibited (Shim *et al.*, 2020). Human DGAT1 is already implicated in a number of health conditions from metabolic disorders to the hepatitis C virus, and clinical trials have already begun on a number of DGAT1 inhibiting drugs (DeVita *et al.*, 2013).

Table 2. Confirmed and putative *tgs* genes in *Mtb* H37Rv. Subcellular location is recorded where known. All 15 *tgs* genes are considered non-essential for in vitro growth in rich media (Dejesus *et al.*, 2017; Griffin *et al.*, 2011; Minato *et al.*, 2019), however essentiality has been observed in specific conditions for certain genes. [1] Mawuenyega *et al.*, 2005; [2] Xiong *et al.*, 2005; [3] Gu *et al.*, 2003; [4] de Souza *et al.*, 2011; [5] Rengarajan *et al.*, 2005; [6] Tsolaki *et al.*, 2004; [7] Sassetti *et al.*, 2003.

Gene name	Location within the cell	Notes on essentiality
Rv3130c (*tgs1*)	Cell wall	
	Cell membrane[1,2]	
Rv3734c (*tgs2*)	Cell membrane[1,2,3]	
Rv3234c (*tgs3*)	Unknown	
Rv3088 (*tgs4*)	Unknown	
Rv0221	Cell membrane[3]	
Rv0895	Cell wall[1]	Essential in primary murine macrophages[5]
Rv1425	Cell membrane[1]	
Rv1760	Unknown	Non-essential, deletion observed in clinical isolates[6]
Rv2285	Cell membrane[4]	
Rv2484c	Cell membrane[1]	
Rv3087	Unknown	Essential in C57BL / 6J mouse spleen[7]
Rv3233c	Unknown	
Rv3371	Cell membrane[1]	
Rv3480c	Unknown	Essential in primary murine macrophages[5]
Rv3740	Unknown	

It is therefore logical to explore the possibility of applying DGAT1 inhibitors to the treatment of mycobacterial infections. Interestingly, while DGAT2 is also responsible for the production of host TAG, it is non-competitively inhibited by niacin, a lipid-regulating agent produced by *Mtb* (Ganji *et al.*, 2004). The production of niacin by mycobacterial species has been known since the 1960s, when it was observed that the human pathogen *Mtb* produced a far higher amount of niacin than bovine strains, which led to the development of the niacin test as a method of differentiating mycobacterial species (Greenberg *et al.*, 1960).

1.10.   Project Aims

There is an undeniable need to address the growing issue of antibiotic resistance and to tackle the rising incidence of MDR-TB and XDR-TB. The development of new TB drugs is an essential part of the global effort to reduce TB. High-throughput screening programmes and the development of analogues based on existing drugs has produced numerous phenotypic hits which require target elucidation. Additionally, the multi-target nature of some TB drugs has become increasingly apparent, and as such there is an argument for re-examining drugs with previously identified cellular targets. This thesis describes the research into three groups of drug candidates, with an overarching aim of target identification.

1.   Investigate alternative targets of BM212, an inhibitor of the mycobacterial trehalose monomycolate (TMM) transporter MmpL3.

a. Identify targets by chemoproteomic profiling using bead immobilisation assays (carried out by Glaxo Smith Kline)

b. Assess the effect of BM212 in whole cell assays, using target overexpression strains.

c. Investigate whether drug boosting interactions occur between BM212 and ethionamide (ETA), an *Mtb* pro-drug whose activation is regulated by one of the alternative BM212 targets identified in objective 1a.

d. Investigate the binding of BM212 and selected analogues to the alternative targets identified in objective 1a.

2. Identify the target(s) of selected inhibitors of human diacylglycerol transferase 1 (DGAT1), which have shown promising activity against *M. tuberculosis.*

a. Carry out minimum inhibitory concentration (MIC) testing of DGAT1 inhibitors against *M. bovis* BCG overexpressing mycobacterial triacylglycerol synthases.

b. Examine the effect of DGAT1 inhibitors on the lipid profile of *M. bovis* BCG overexpressing mycobacterial triacylglycerol synthases to identify any phenotypic changes.

c. Explore the effect of DGAT1 inhibitors on *M. bovis* BCG following nitrogen deprivation induced triacylglycerol accumulation.

d. Develop biochemical assays to explore binding and inhibition of purified Tgs proteins.

e. Generate resistant mutants to DGAT1 inhibitors in *Mtb* for target identification

3. Investigate a set of compounds selected for their activity against *Mtb.*

   a. Carry out thorough MIC testing of compounds in multiple mycobacterial strains.

   b. Generate resistant mutants to selected compounds in *Mtb*.

   c. Generate strains over expressing hits identified by WGS of resistant mutants and test for MIC shifts.

Chapter 2

Target Promiscuity in an MmpL3 Inhibitor:
BM212 Family Compounds Bind EthR2

2. Target Promiscuity in an MmpL3 Inhibitor: BM212 Family Compounds Bind EthR2

2.1. Introduction

The dual target nature of a number of MmpL3 inhibitors has recently been observed (section 1.9.1.). Given the notable diversity in the structure of MmpL3 inhibitors, there is reason to believe that other compounds in this varied range of inhibitors have previously unidentified targets in addition to MmpL3. In this chapter, carried out in collaboration with GlaxoSmithKline, we investigated alternative potential targets for the pyrrole derived MmpL3 inhibitor BM212 and its analogues using bead immobilised assays for competitive binding. In addition to chemoproteomic profiling, whole-cell and biochemical assays were utilised to determine binding and examined possible synergy with ethionamide (ETA).

2.2.   Results

2.2.1. Chemical Proteomic Studies

In order to elucidate the mode of action of the (thio)morpholine analogue, GSK074A, chemoproteomic profiling was carried out. Bead immobilisation assays required the addition of funtionalised linkers in order to bind GSK704A to the NHS-Sepharose beads. These 3-aminopropyl linkers were attached to the phenyl substituent either at N1 or at C5, producing GSK569A and GSK574A, respectively (Figure 18). The immobilised GSK074A analogues were used in competition-based assays, in which *M. bovis* BCG extracts, containing increasing concentrations of free GSK074A or GSK303A, was incubated with the immobilized bead matrix, competing for binding of any targeted proteins.
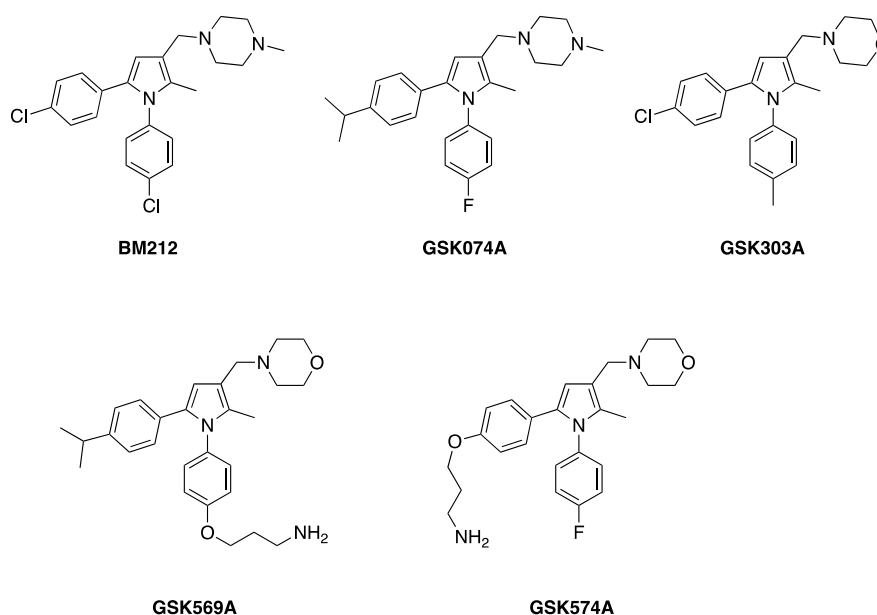
Figure 18. Structures of BM212 and analogues used in this work. BM212 and its derivatives were all synthesized by Glaxo Smith Kline.

Once the matrix-bound target proteins had been eluted, they were trypsinised and analysed by LC-MS/MS. Proteins which were present in substantially lower amounts (at least a 2-fold reduction) when incubated in the presence of GSK074A compared to the control were identified as target proteins. A total of four proteins were identified from 10 experiments, BCG_3853 (Rv3519), BCG_0174 (Rv0138), BCG_0109 (Rv0078) and BCG_0108c (Rv0077c) (Figure 19). Two of these proteins, BCG_0174 (Rv0138) and BCG_0109 (Rv0078), were consistently, competitively bound in 6 experiments, while BCG_3853 (Rv3519) and BCG_0108c (Rv0077c) were only identified in 3 of the 10 experiments. Due to the inconsistent binding of BCG_0108c (Rv0077c) and BCG_3853 (Rv3519), it was not possible to generate K_D values. For BCG_0174 (Rv0138) and BCG_0109 (Rv0078), however, the apparent K_D values were calculated as 7.3 µM and 2.9 µM, respectively (Figure 20). Only one protein, BCG0109 (Rv0078), was competed by both GSK074A and GSK303A. The difference in K_D and IC_{50} values can be attributed to the fact that IC_{50} calculations are expected to vary depending on assay conditions, while K_D values are measured as constants.
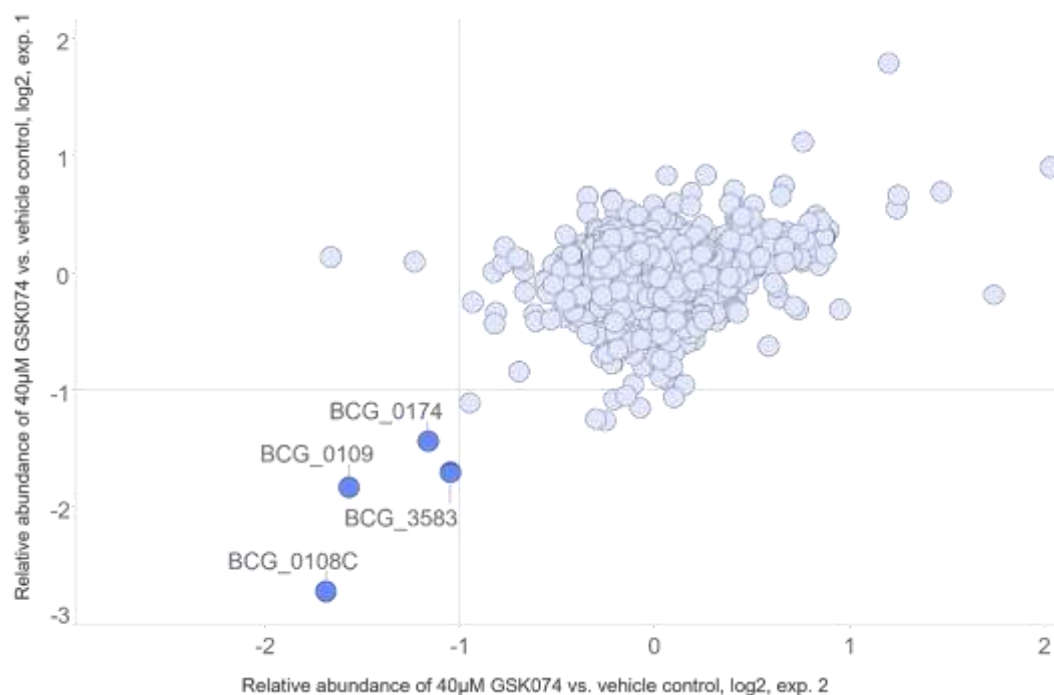
Figure 19 Chemoproteomic profiling of GSK074A. Four proteins, BCG_3853 (Rv3519), BCG_0174 (Rv0138), BCG_0109 (Rv0078) and BCG_0108c (Rv0077c), were identified as potential alternative targets of BM212 based on a >2-fold reduction in reduction in protein in bead immobilisation assays.
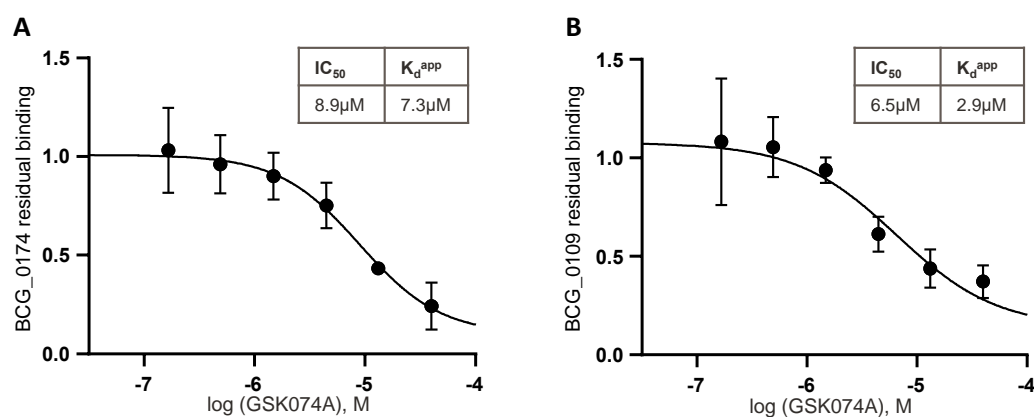
Figure 20 Residual binding curves of BCG_0174 (Rv0138) and BCG_0109 (Rv0078). Amine-functionalized analogues were immobilized to NHS Sepharose beads and incubated with aliquots of *Mycobacterium bovis* BCG protein extract containing GSK074A at different concentrations. The reduction of binding to the bead matrices was quantified by quantitative mass spectrometry. The IC_{50} values for BCG_0174 and BCG_0109 competition were calculated from the average of 6 independent experiments and standard deviations were calculated (**A** Rv0138 BCG_0174 IC_{50} 8.9 μM +/- 1.1 μM; **B** Rv0078 BCG_0109 IC_{50} 6.5 μM +/- 1.5 μM).

2.2.2. Microbiology Studies

2.2.2.1. Generation of Expression Strains

In total, six strains of BCG were cloned, overexpressing Rv0077c (EthA2), Rv0078 (EthR2), Rv3854c (EthA), Rv3855 (EthR), Rv0138 and Rv3519. PCR was used to generate the gene fragments for insertion into pMV216 (Figure 21) using the primers in Table 13. Colony PCR was used to check the size of each gene fragment that had been ligated into pMV261 and Top10 *E.coli* were transformed with the plasmids, prior to samples being selected for sequencing by Source Bioscience.
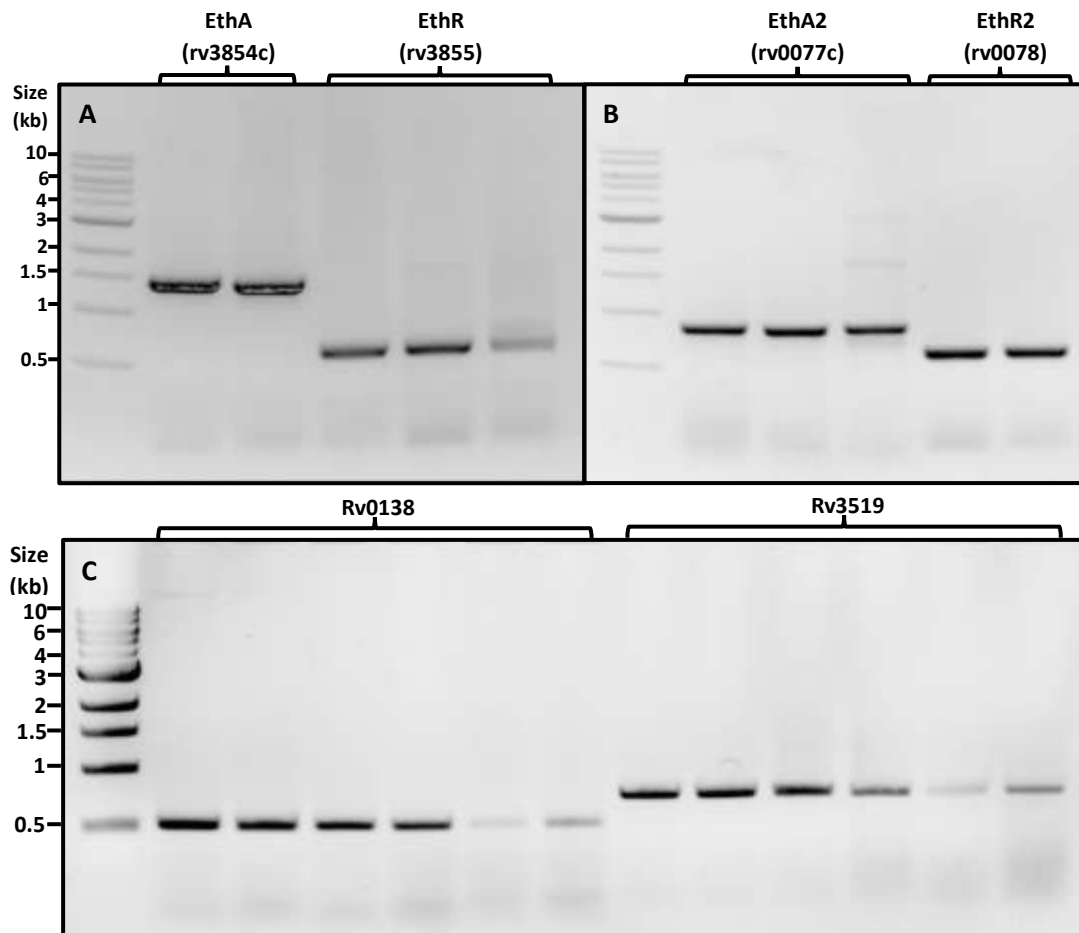
Figure 21 PCR of gene inserts. *Mtb* genes were amplified using PCR for insertion into plasmid vectors. PCR products were run on 1% agarose gels to confirm the size of the inserts. **A -** Lane 1 - 10kb ladder; lanes 2 and 3 - Rv3854c (1470bp); lanes 4 − 6 - Rv3855 (651bp). **B -** Lane 1 - 10kb ladder; lanes 2 − 4 − Rv0077c (831bp); lanes 5 and 6 − Rv0078 (606bp). **C –** Lane 1 - 10kb ladder; lanes 2 − 6 − Rv0138 (504bp); lanes 7 − 12 - Rv3519 (711bp). The first band for each gene insert (A − lanes 2 and 4; B − lanes 2 and 5; C − lanes 2 and 8) were selected to be sequenced by Source Bioscience.

2.2.2.2. Determination of Minimal Inhibitory Concentrations (MICs)

Microbiological studies were carried out using *M. bovis* BCG with two distinct aims: firstly, to ascertain whether the binding observed in bead immobilisation assays produced any detectable changes to the MIC of BM212 when the genes encoding the target proteins were overexpressed; and secondly to investigate whether any synergy occurred between BM212 and ETA.

The MIC_{90} of BM212 was established for wild type (WT) *M. bovis* BCG, and *M. bovis* BCG overexpressing Rv0077c (EthA2), Rv0078 (EthR2), Rv3854c (EthA), Rv3855 (EthR), Rv0138 and Rv3519. BM212 consistently inhibited WT *M. bovis* BCG, *M. bovis* BCG pMV261 *ethA2* and *M. bovis* BCG pMV261 *ethR2* at 4 µg/mL, whereas overexpression of Rv0138 and Rv3519 yielded an MIC_{90} of 3.2 µg/mL and >4 µg/mL, respectively.

Overexpression of the transcriptional regulators EthR and EthR2 conferred a higher tolerance to ETA than the control *M. bovis* BCG containing empty vector pMV261 (EV) on solid media, with MIC90 ranges of 3.7 – 11 µg/mL for pMV261 EV, 11 – 33 µg/mL for pMV261-*ethR* and >33 µg/mL for pMV261-*ethR2*. Overexpression of ETA activators EthA and EthA2 resulted in stunted growth on solid media, and an ETA MIC90 of 11 – 33 µg/mL on solid media. The MIC90 for pMV261-*ethA2* in liquid media was 2 µg/mL, half that of pMV261-EV indicating increased susceptibility. These results appear to support the logical assumption that overexpression of the repressors EthR and EthR2 (and resulting downregulation of ETA activators) leads to an increase in MIC, while overexpression of the activators EthA and EthA2 results in a lower MIC due to the increased amount of active drug availability in the cell as reported previously (Baulard

et al., 2000). The solid MICs should, however, be used as a guide. There is considerable variation between strains in the density of colonies on no drug plates, making it difficult to correctly determine the relative change in growth at increasing concentrations, and it was not possible to define a precise MIC.

2.2.2.3. Determination of Drug Interactions Between BM212 and Ethionamide (ETA)

In light of the apparent binding of BM212 compounds to EthA2 and EthR2, the possible outcomes of drug interactions between BM212 and ethionamide (ETA) were considered. Both EthA2 and EthR2, two of the proteins identified in competitive binding assays, are involved in the activation of the pro-drug ETA (Figure 22 A). Inhibition of EthA2 or EthR2 individually would theoretically result in either a reduction or increase in ETA activation. Inhibition of EthR2 might be expected to prevent the repression of EthA2, thus allowing the unrestricted conversion of ETA to its active form (Figure 22 B). Inhibition of EthA2, however would prevent or significantly reduce its function and therefore confer resistance to ETA through the failure to activate it (Figure 22 C). The result of inhibiting both proteins would depend on the affinity of the drug to either protein, as inhibition of EthA2 would potentially reverse the ETA boosting effects of EthR2 inhibition.

In order to quantitively determine whether there was a synergistic, additive/indifferent or antagonistic interaction between BM212 and ETA, chequerboard assays were performed in triplicate, and the results were analysed using Equation 5 (Figure 23).

The FIC values were calculated using the sub-lethal concentration of both drugs needed to inhibit 75% of growth. The MIC_{75} values for BM212 and ETA were 3μg/mL and 2μg/mL, respectively. The $\sum FIC_{75}$ for WT BCG of 0.83 indicates that the interaction is additive/indifferent.
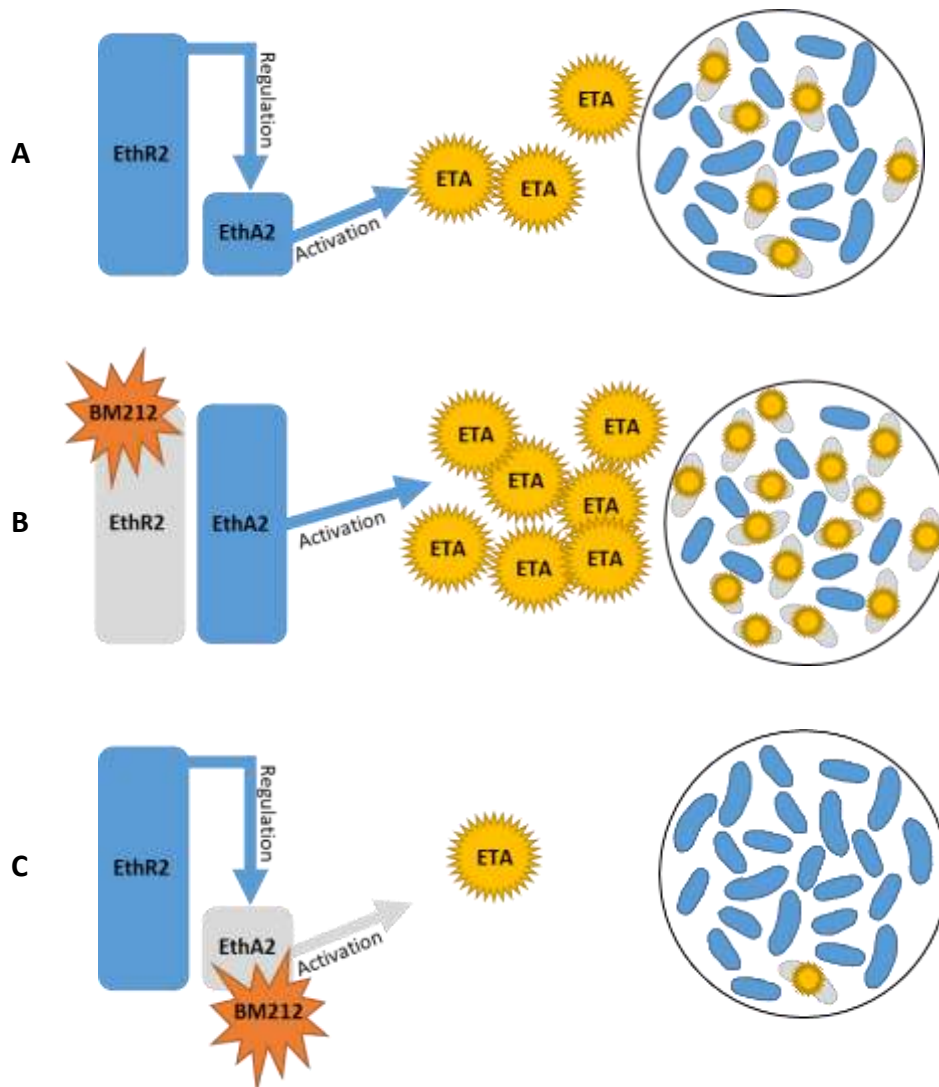
Figure 22 Schematic showing three predicted scenarios of the effect of BM212 on ETA activation. A – ETA treatment in the absence of BM212: EthR2 regulates EthA2, which activates ETA. Active ETA has an antibacterial effect. **B –** inhibition of EthR2 by BM212 is expected to increase EthA2 activity through a loss of regulation, EthA2 is able to activate an increased amount of ETA, and thus increase the antibacterial affect. **C –** inhibition of EthA2 by BM212 reduces the activation of ETA and in turn reduces the antibacterial effect.
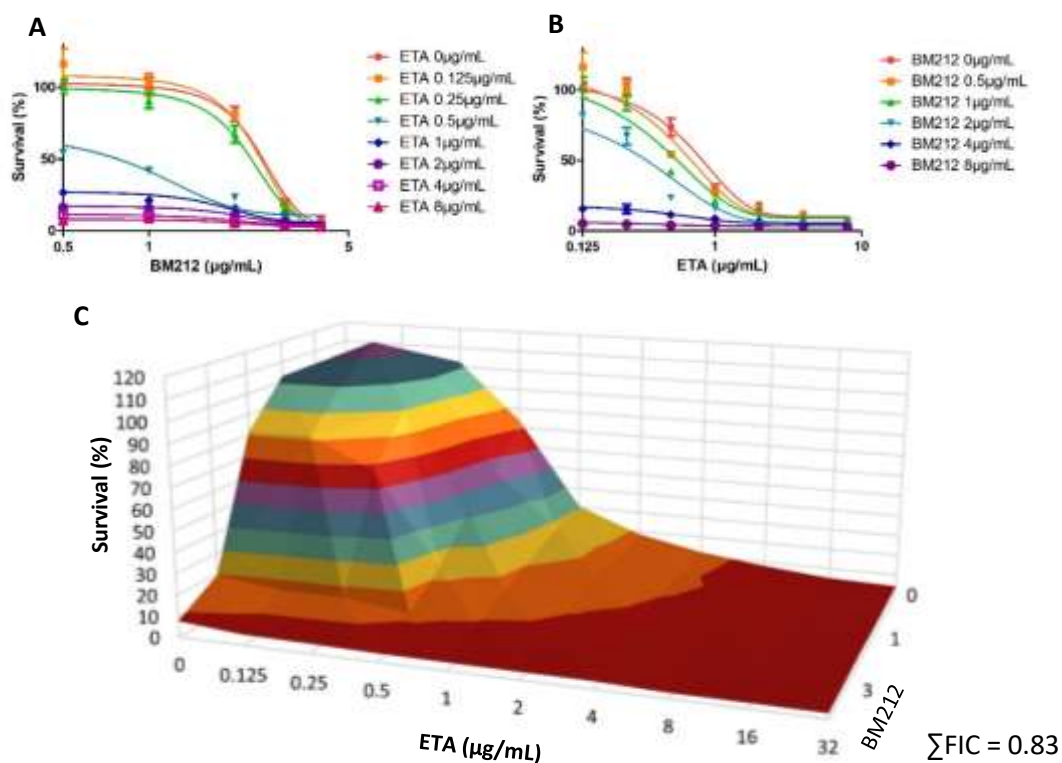
Figure 23. **Dual drug treatment of *M. bovis* BCG with BM212 and ETA. A and B –** Survival analysis of *M. bovis* BCG treated with ETA and BM212 at varying concentrations. Survival was measured after 7 days and normalised as a percentage. Data shown as an average of 3 technical repeats. **C –** Chequerboard analysis of *M. bovis* BCG treated with BM212 and ETA. Dark red area indicates survival below 10%. FIC analysis indicates no synergy between BM212 and ETA. Survival was measured after 7 days and normalised as a percentage. Data shown as an average of 3 technical repeats. The FIC was calculated at 0.83 indicating an additive/indifferent effect.

2.2.3. Biochemical Studies

2.2.3.1. Generation of Overexpression Constructs and Purification of Target Proteins

Purification was attempted for the four proteins identified as binding BM212 in bead immobilisation assays, Rv0077c (EthA2), Rv0078 (EthR2), Rv0138 and Rv3519 in order to obtain further binding data to support the results reported previously. Briefly, gene fragments were amplified by PCR (Figure 24), ligated into pET28a and pET41c and the

sequences confirmed by sequencing with Source Bioscience. *E.coli* BL21 DE3 were transformed with the appropriate plasmids. Both EthR2 and Rv0138, the two proteins which showed the most consistent binding in competitive binding assays, were easily purified with a high yield by nickel affinity chrotrmatography using a HisTrap column. EthA2 and Rv3519 proved more challenging to express and purify and, due to time constraints, EthR2 and Rv0138 were prioritised based on the promising binding data (Figures 24 and 25).

The purified recombinant, poly-histidine tagged proteins were confirmed by Western blot. The substantial band present in lanes 7 and 8 of Figure 24 which were pooled and dialysed, was clearly identifiable by Western blot at the expected size of Rv0138 (Figure 26). The 50 mM imidazole fraction of EthR2 showed only one distinct band at the expected size of 22 kDa. The Western blot was not run immediately upon purification of EthR2 and, interestingly, by the time a second gel was run for Western blotting, two bands were visible (Figure 27). EthR2 has been shown to form dimers, with two EthR2 dimers binding a single operon sequence (Samanovic *et al*., 2018; Wohlkönig *et al*., 2017). It is possible that dimerisation had occurred, and the two bands represented EthR2 in monomer and dimer forms.
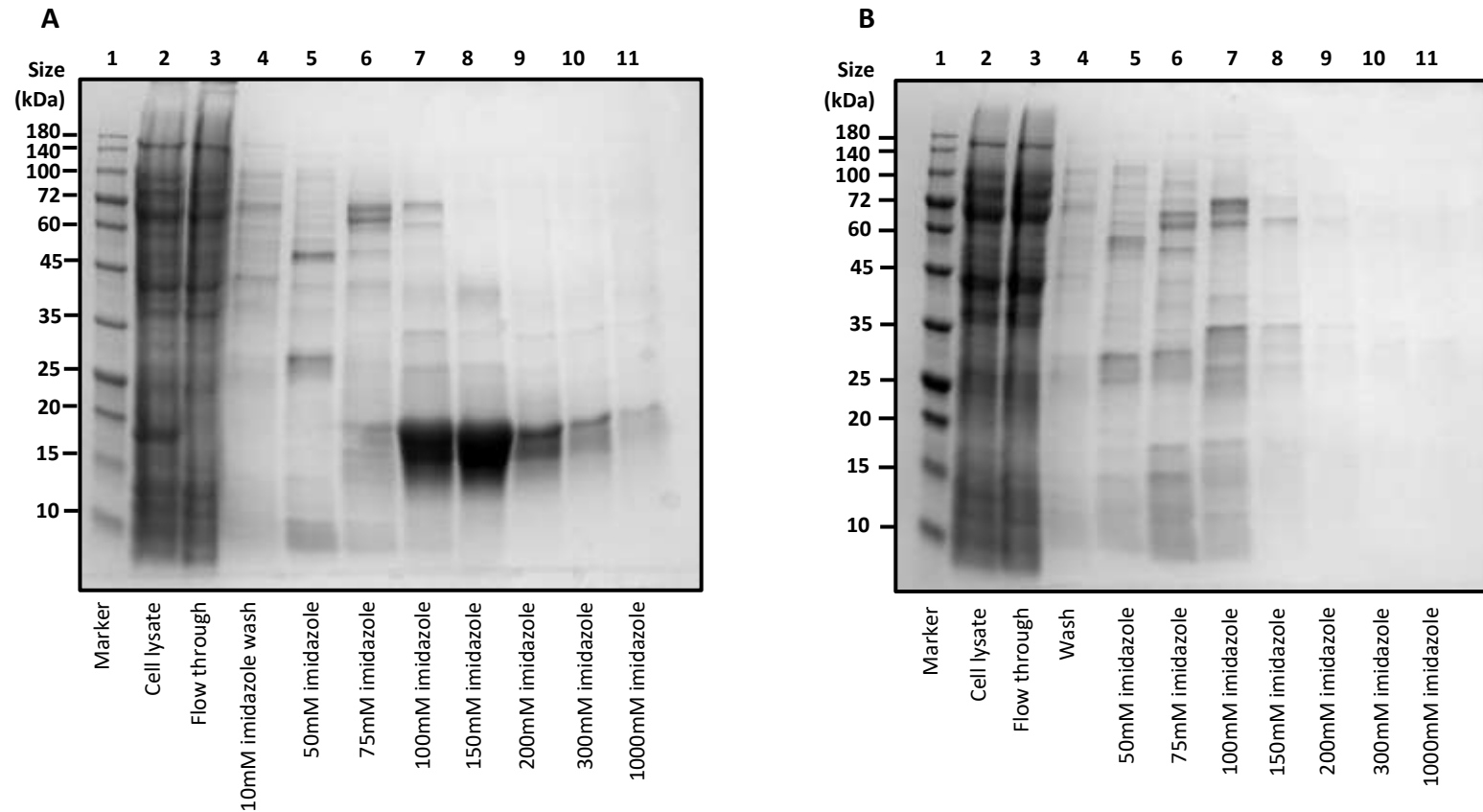
Figure 24 SDS PAGE of fractions from the purification of Rv0138 and Rv3519 by nickel affinity. Recombinant Rv0138 and Rv3519 were expressed in *E. coli* BL21 DE3 induced with 1 mM IPTG. Harvested cells were lysed and purified using a HisTrap column and eluted with increasing concentrations of imidazole. Purification was achieved using a HisTrap column. Samples from lysis and elution steps of the purification were boiled in SDS and separated by SDS PAGE **A –** a band corresponding to Rv0138, 18.94kDa, is visible at high concentration in lanes 7 and 8, and at a lower concentration in lanes 9 – 11. **B –** Rv3519, a protein of 25kDa, may be visible in lanes 5, 6, and 7 at low concentration, but requires Western blotting and an expression trial.
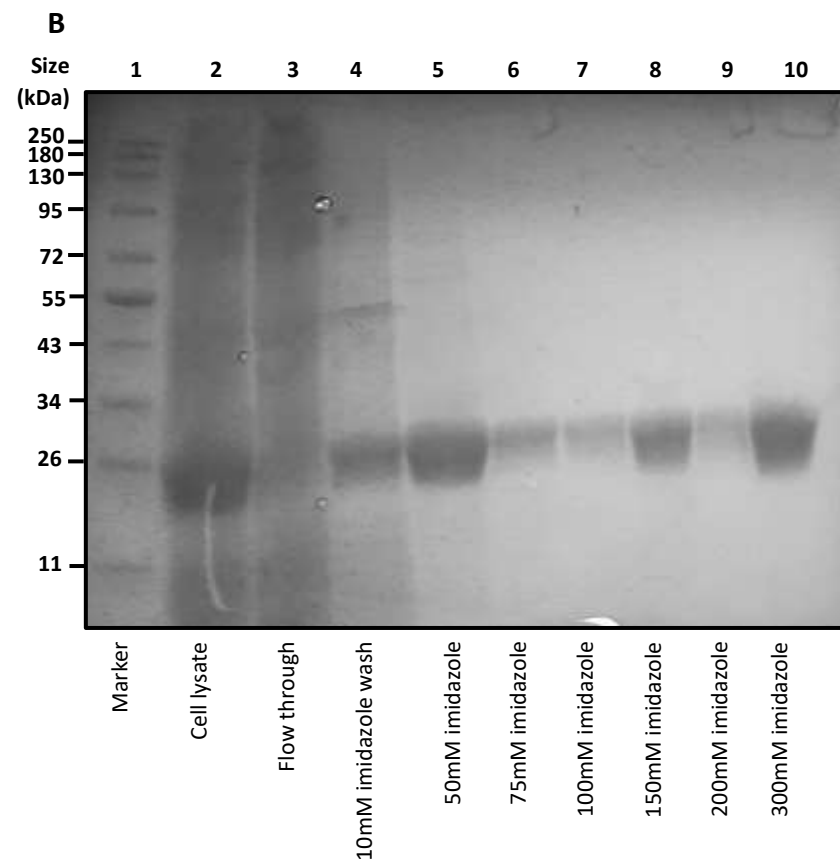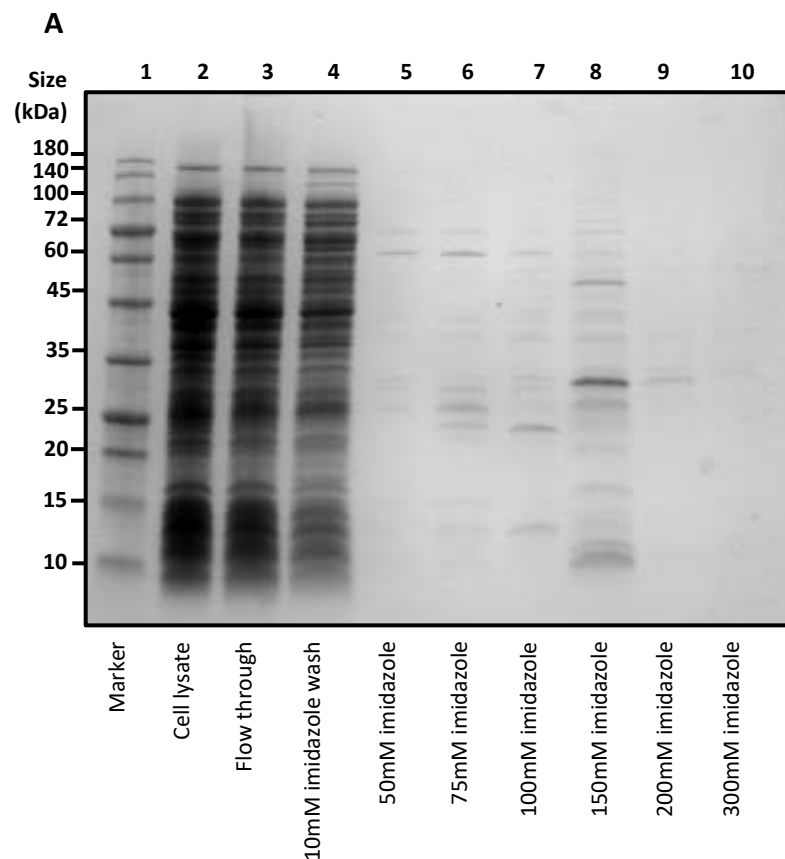
Figure 25 SDS PAGE of fractions from the purification of Rv0077c (EthA2) and Rv0078 (EthR2) by nickel affinity. Recombinant Rv0077c and Rv0078 were expressed in *E. coli* BL21 DE3 induced with 1 mM IPTG. Harvested cells were lysed and purified using a HisTrap column and eluted with increasing concentrations of imidazole. Purification was achieved using a HisTrap column. Samples from lysis and elution steps of the purification were boiled in SDS and separated by SDS PAGE **A** – Rv0077c, a protein of 19.69kDa, does not appear to be over expressed in any of the elution lanes, nor is it present in any large quantity in the lysate, flow through or wash. A thorough expression trial of soluble, insoluble and membrane proteins is required. **B** – a band corresponding to Rv0078, 21.9kDa, is visible at high concentration in elution lanes 5 – 10.
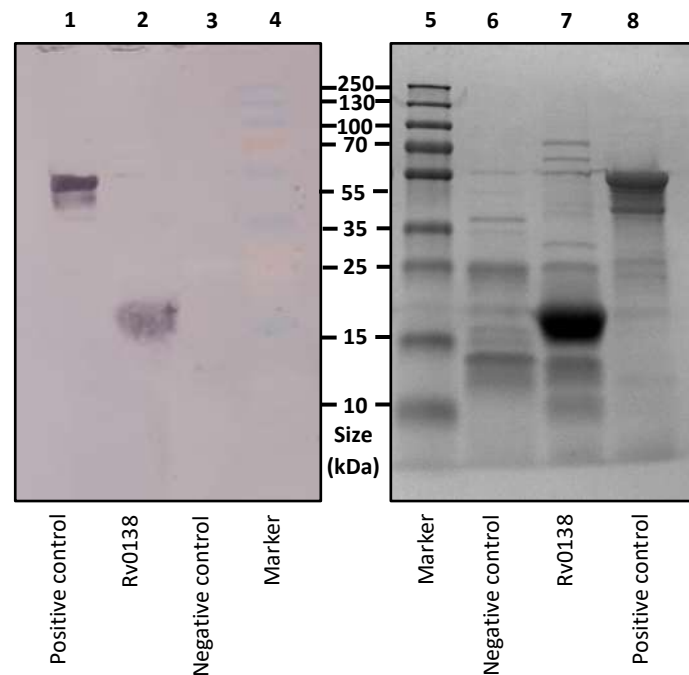
Figure 26 Western blot of fractions from the purification of Rv0138 by nickel affinity chromatography. Western blot carried out with Penta-His Mouse IgG primary antibody (Qiagen). Anti-Mouse IgG-Alkaline Phosphatase secondary antibody (Sigma). Recombinant Rv0138 appears as a band close 20kDa in both the Western blot (lane 2), and the corresponding SDS PAGE gel (lane 7).
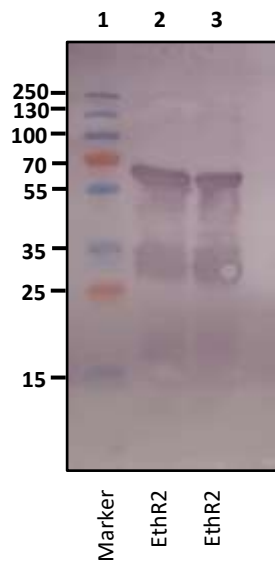
Figure 27 Western blot of fractions from the purification of Rv0078 (EthR2) by nickel affinity chromatography. Western blot carried out with Penta-His Mouse IgG primary antibody (Qiagen). Anti-Mouse IgG-Alkaline Phosphatase secondary antibody (Sigma). Two bands are clearly visible between 25-35kDa and 55-70kDa are thought to be Rv0078 in monomer and dimer formation.

74

2.2.3.2. Intrinsic Tryptophan Fluorescence Binding Assays

In addition to bead immobilised binding assays, intrinsic tryptophan (Trp) fluorescence quenching was used to ascertain whether binding occurred between target proteins and BM212 and its analogues (Figure 28). Ordinarily, binding results in the quenching of fluorescence of Trp residues in the binding site. Trp is one of three amino acids found in proteins which are intrinsically fluorescent, and it is the most abundant. Selective excitation at 295nm, where there is very little absorption by other residues, allows the study of Trp fluorescence. Changes to the microenvironment of these fluorescent residues can affect the fluorescence spectrum, as well as the intensity of fluorescence. In addition to local changes, Trp fluorescence can be affected by conformational changes or denaturing, where internal residues become exposed, or exposed residues become hidden. EthR2 was titrated against BM212, and the two analogues GSK303A and GSK074A, and saturation ligand-binding curves produced. In contrast to the earlier competitive binding assays, no change to the intrinsic fluorescence of EthR2 was observed in the presence of GSK074A, and as such no k_D was generated. BM212 bound with a k_D of 0.66 µM, but the drug with highest affinity was GSK303A, with a k_D of 0.19 µM.

Saturation binding experiments were repeated with Rv0138, which showed consistent binding to BM212 and GSK303A with k_D values of 3.94 µM and 6.82 µM, respectively, despite the fact that GSK303A did not competitively bind to GSK303A in previous experiments. Interestingly, all assays of Rv0138 Trp fluorescence, performed in triplicate, consistently resulted in an increase in fluorescence with binding. Furthermore, at high ligand concentrations (4 times k_D) the fluorescence reduced.

The increase in fluorescence could have been caused by a conformational change to the protein. BCG_0174, the *M. bovis* BCG target identified in competition assays, is a SnoaL-like domain, which contains an orthologue to Rv0138. The predicted structure of Rv0138 bears similarities with SnoaL which comprises an α β barrel, the hydrophobic cavity of which is the active site (Figure 29). Multiple control assays were carried out to rule out DMSO toxicity or drug precipitation as the cause of the reduction in fluorescence at high concentrations. One possibility is that high concentrations of drugs affected the environment of the protein causing aggregation or denaturing.
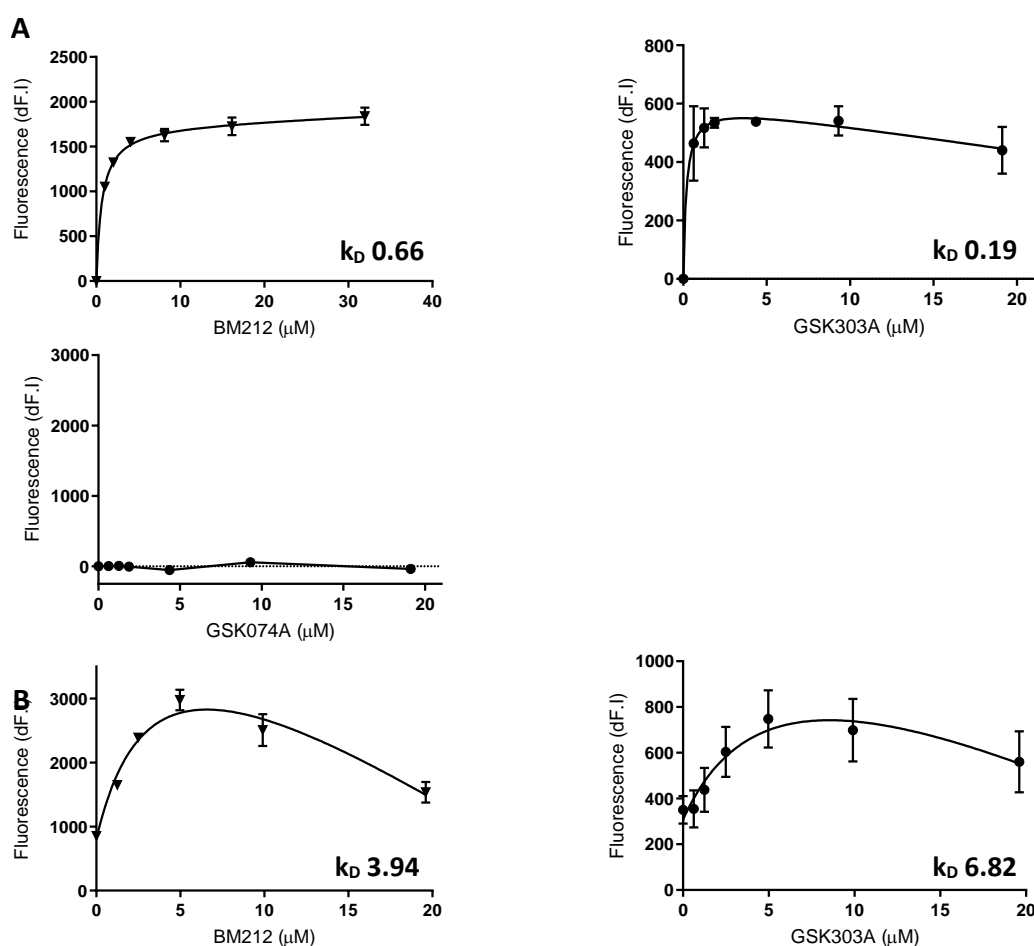
Figure 28 Intrinsic tryptophan fluorescence assays indicate that BM212 and analogues bind to Rv0078 (EthR2) and rv0138. BM212 and analogues were titrated against EthR2 and rv0138. Saturation ligand-binding curves were generated with GraphPad prism software using the change in fluorescence. **A** – EthR2 bound to BM212 and GSK303A with a k_D of 0.66 μM and 0.19 μM respectively. Trp fluorescence of EthR2 was not altered by the addition of GSK074A and no K_D was able to be calculated. **B** – Rv0138 bound to BM212 with a k_D of 3.94 μM, and also to GSK303A with a k_D of 6.82 μM.
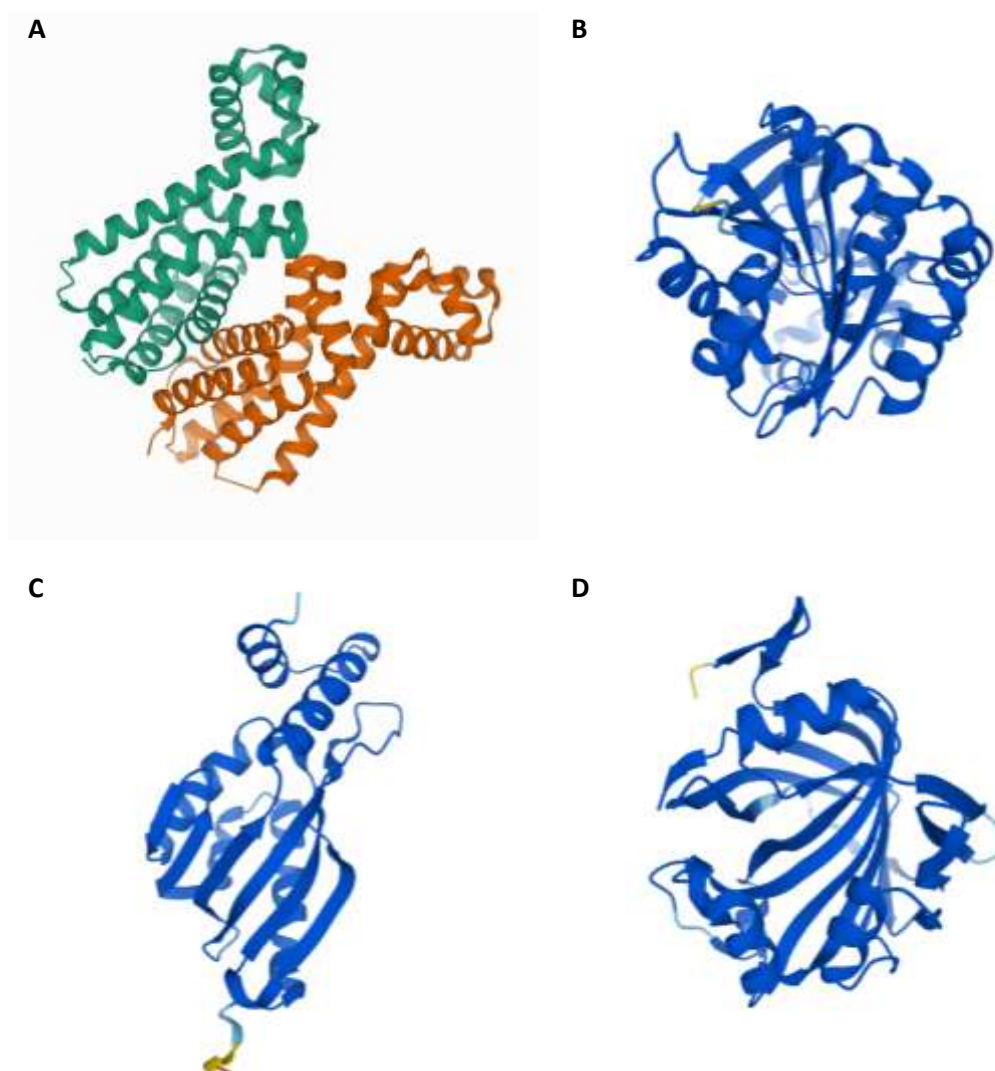
Figure 29 Four distinct proteins were identified as potential alternative BM212 targets by competitive binding assays. A – ribbon representation of the Rv0078 (EthR2) dimer with helix-turn-helix motifs PDB ref: 5N1I (Blondiaux *et al*., 2017) **B** – predicted structure of EthA2 **C** – predicted structure of SnoaL-like Rv0138 **D** – predicted structure of Rv3519. Structures of B, C and D were predicted by AlphaFold (Jumper *et al*., 2021).

2.2.3.3. Crystal Screening

Using the MIDAS screen from Molecular Dimensions, crystal screens were set up for EthR2 with 6x concentration of ligand (BM212). Crystals appeared in multiple conditions, with different physical characteristics. The three most frequently occurring forms were flat crystals, star shaped crystals that formed a larger lattice, and thin pointed shards. Wells of each protein shape were selected for treatment with JBS True Blue stain to give an indication of whether they were macromolecular protein crystals, or simply buffer components that had crystalised (Figure 30). Absorption of the blue dye indicates probable protein crystals, while salt for example should remain uncoloured. Positive conditions for crystallisation were recorded for optimisation, but unfortunately due to time constraints, it was not possible to set up secondary screens (Table 3). Crystals were seen for EthR2 with and without ligand, which was promising; if crystals from co-crystallisation of protein and ligand are not suitable for the elucidation of their crystal structure, it may be possible to soak EthR2 crystals in ligand and solve the ligand-bound crystal structure through this method.
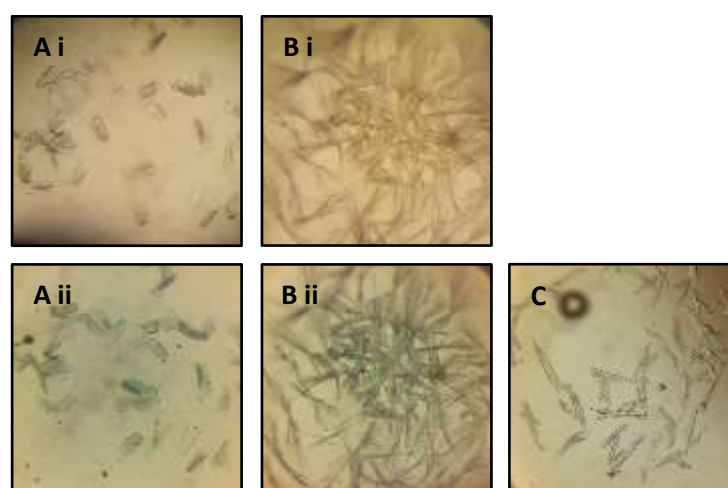
Figure 30. Crystals of EthR2. Crystal trays were set up using the MIDAS screen from Molecular Dimensions for the co-crystallisation of EthR2 and BM212 at a concentration of 1 : 6. A variety of different crystal forms were visible in different crystallization conditions. JBS True Blue dye was applied to wells to differentiate macromolecular crystals from other crystalline forms such as salt crystals. **A i** and **A ii** – flat crystals were the most abundant form of crystal and appeared to absorb the blue colour. **B i** and **B ii** – a star shaped lattice of crystals appeared in a small number of wells and absorbed the blue stain. **C** – An example of thin crystals which were not positively stained as macromolecular protein crystals.

Table 2 Conditions of Molecular Dimensions' MIDAS screen which yielded crystals. Rows highlighted in blue indicate wells in which EthR2 was crystalised; rows highlighted in green indicate wells with EthR2 and ligand.

Well		% conc	Precipitant	% conc	Salt/Additive	pH	% conc	Buffer
B	1	20% v/v	Jeffamine D2000	0.2 M	sodium chloride	5.5	0.1 M	MES- NaOH
B	2	15 % v/v	pentaerythritol propoxylate (5/4 PO/OH	0.2 M	sodium thiocyanate	7	0.1 M	HEPES-NaOH
B	3	5 % w/v	polyvinyl alcohol type II	0.2 M	potassium acetate	7	0.1 M	HEPES-NaOH
B	5	8 % w/v	polyvinyl alcohol type II	10 % v/v	1- propanol	7	0.1 M	HEPES-NaOH
B	7	40 % v/v	polypropylene glycol 400	0.2 M	imidazole	7		
B	9	35 % v/v	Jeffamine SD2001	0.1 M	sodium chloride	8	0.1 M	Tris-HCl
C	1	15 % w/v	Jeffamine ED2003	10 % v/v	ethanol			
C	2	30 % w/v	Jeffamine ED2003	0.2 M	sodium chloride	6	0.1 M	MES- NaOH
C	3	25 % v/v	Jeffamine SD2001	0.1 M	sodium malonate	5.5	0.1 M	MES- NaOH
C	4	15 % v/v	pentaerythritol propoxylate(5/4 PO/OH)	0.2 M	sodium chloride	6	0.1 M	MES- NaOH
C	6	40 % v/v	pentaerythritol propoxylate (5/4 PO/OH)	15 % v/v	ethanol			
C	7	50 % v/v	pentaerythritol propoxylate (5/4 PO/OH)			8	0.1 M	Tris-HCl
C	8	12.5 % w/v	polyvinyl pyrrolidone K15	0.2 M	sodium chloride	8	0.1 M	Tris-HCl
C	9	25 % v/v	pentaerythritol propoxylate (5/4 PO/OH)	0.1 M	sodium chloride			
D	1	60 % v/v	polypropylene glycol 400			8	0.1 M	Tris-HCl
D	2	30 % v/v	pentaerythritol ethoxylate (15/4 EO/OH)			7.5	0.1 M	HEPES-NaOH
D	3	45 % v/v	polypropylene glycol 400	10 % v/v	ethanol			
D	4	10 % v/v	pentaerythritol ethoxylate (3/4 EO/OH)	10 % v/v	1-butanol			
D	6	6 % w/v	polyvinyl pyrrolidone K15			6.5	0.1 M	HEPES-NaOH
D	7	20 % w/v	Jeffamine ED2003			6.5	0.1 M	HEPES-NaOH
D	8	20 % v/v	glycerol ethoxylate	10% v/v	tetrahydrofuran	8	0.1 M	Tris-HCL
E	2	35 % v/v	pentaerythritol propoxylate (5/4 PO/OH)	0.2 M	potassium acetate			
E	3	20 % v/v	pentaerythritol ethoxylate (15/4 EO/OH)	0.2 M	potassium chloride	9.5	0.1 M	Glycine
E	4	40 % v/v	pentaerythritol propoxylate (5/4 PO/OH)	0.2 M	sodium thiocyanate	7	0.1 M	HEPES-NaOH

						pH		
E	5	15 % v/v	Jeffamine T403	0.2 M	potassium chloride	6.5	0.1 M	HEPES-NaOH
E	6	15 % v/v	pentaerythritol ethoxylate (15/4 EO/OH),	0.2 M	potassium acetate	6	0.1 M	MES- NaOH
E	9	25 % w/v	Jeffamine ED2003	0.1 M	lithium sulfate	8	0.1 M	Tris-HCl
E	10	10 % v/v	Jeffamine T403			8	0.1 M	Tris-HCl
F	1	40 % v/v	Jeffamine D2000			6.5	0.1 M	HEPES-NaOH
F	4	20 % w/v	polyacrylate 2100, sodium salt	0.2 M	sodium chloride	9	0.1 M	Bicine
F	7	20 % v/v	Jeffamine M2070	20 % v/v	dimethyl sulfoxide			
F	12	20 % w/v	Sokalan® HP 56	0.2 M	sodium sulfate	8	0.1 M	Tris-HCl
G	1	25 % v/v	Sokalan® CP 7	0.1 M	potassium chloride	7	0.1 M	HEPES-NaOH
G	9	25 % v/v	Sokalan® CP 42	10 % v/v	tetrahydrofuran	7	0.1 M	Tris-HCl
G	10	20 % v/v	Sokalan® CP 42	0.1 M	lithium acetate	6	0.1 M	Bis-Tris-NaOH
H	3	20 % v/v	glycerol ethoxylate			8.5	0.1 M	Tris-HCl
H	9	25 % w/v	Sokalan® HP 56	0.2 M	ammonium acetate	7	0.1 M	HEPES-NaOH
H	10	25 % v/v	Sokalan® CP 5			8.5	0.1 M	Tris-HCl
H	12	15 % w/v	Poly(vinyl pyrrolidone) K 15			8	0.1 M	Tris-HCl

2.2.3.4. Molecular Docking

Molecular docking was carried out further investigate the binding by EthR2 of BM212 using Chimera (Pettersen *et al.,* 2004; Butt *et al.,* 2020) and AutoDock Vina (Trott *et al.,* 2010; Eberhardt *et al.,* 2021) software. The chimera models, with docking scores ranging from -5.8 to -5.4, showed BM212 bound in a cavity at the dimer interface in multiple different poses (Figure 31). Conversely, exististing crystal structures of ligand-bound EthR2 show that small molecule inhibitors more commonly bind to a cavity within each monomer partner of EthR2 where they cause a conformational change to the helix-turn-helix region and restrict DNA binding (Wohlkönig *et al.,* 2017). Tryptophan residues have been highlighted in yellow in panel B, showing that Trp113 is the residue affected in the intrinsic Trp fluorescence quenching assays. Considering the lack of synergy between

BM212 and ethionamide, and the binding determined by molecular docking, it is likely that the interaction between BM212 and the inter-dimer cavity does not cause sufficient disruption to EthR2 to restrict DNA binding. It is worth considering that modifications to BM212 could produce a more favourable interaction with EthR2. Using the same apprcoah, molecular docking was carried out to predict the binding by Rv0138 of BM212. All AutoDock Vina predictions showed BM212 bound within the SnoAL-like barrel of Rv0138 (Figure 32). It is likely that BM212 causes a change in the environment surrounding Trp31 and Trp61 leading to a change in detectable fluorescence.
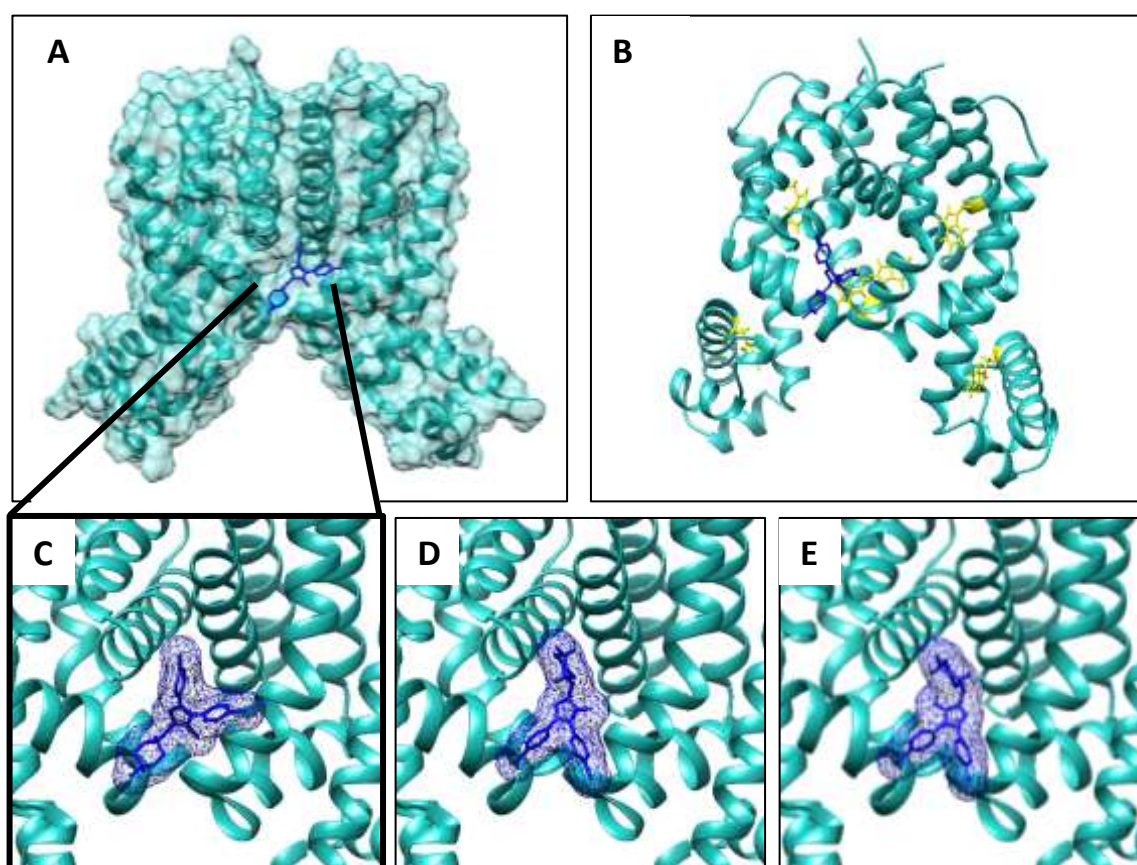
Figure 31. Chimera and AutoDock Vina were used to create binding models of EthR2 (PDB: 5N1I unliganded form) and BM212 (CID: 456926). **A -** placement of highest scoring BM212 pose in the EthR2 dimer; **B –** View of EthR2 with Tryptophan residues highlighted in yellow; **C -** close up of highest scoring BM212 pose (docking score -5.8) binding in the dimer interface of EthR2; **D -** close up of second highest scoring BM212 pose (docking score -5.7) binding in the dimer interface of EthR2; **E -** close up of third highest scoring BM212 pose (docking score -5.6) binding in the dimer interface of EthR2.
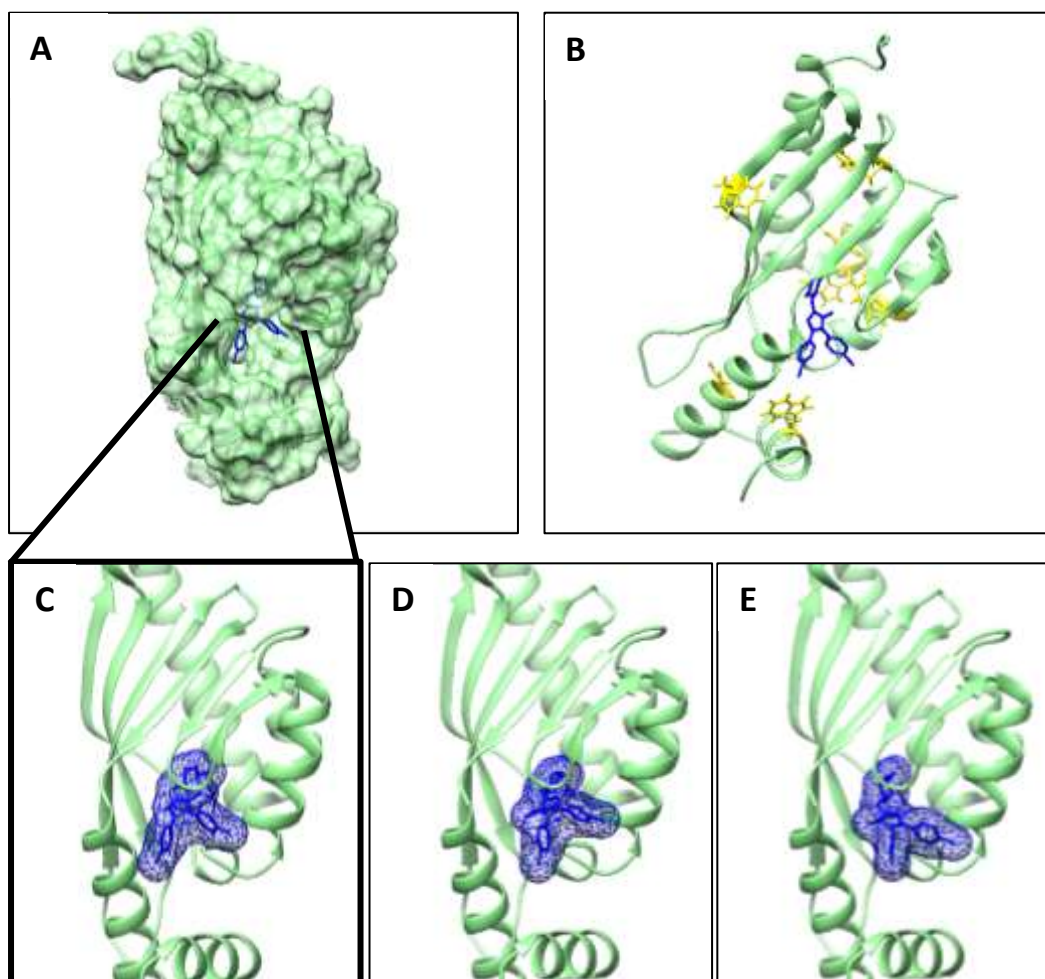
Figure 32. Chimera and AutoDock Vina were used to create binding models of Rv0138 (PDB file obtained from AlphaFold) and BM212 (CID: 456926). **A -** placement of highest scoring BM212 pose in the Rv0138 dimer; **B -** View of Rv0138 with Tryptophan residues highlighted in yellow; **C -** close up of highest scoring BM212 pose (docking score -9.1) binding in the SnoAL-like barrel of Rv0138; **D -** close up of second highest scoring BM212 pose (docking score -8.4) binding in the SnoAL-like barrel of Rv0138; **E -** close up of third highest scoring BM212 pose (docking score -8.2) binding in the SnoAL-like barrel of Rv0138.

2.3.   Discussion

The requirement of chemotherapeutics to tackle MDR-TB is indisputable. While high-throughput screening programmes seeking novel compounds with anti-TB activity are yielding promising results, there is still a significant benefit to the continued research into existing TB drugs. A collection of analogues was synthesised based on the structure of BM212, two of which were modified for and bound to Sepharose beads for competitive inhibition studies. The objective of this line of inquiry was twofold: to seek alternative targets of the BM212 family of MmpL3 inhibitors, and to explore the binding affinity of different analogues.

Chemoproteomic profiling uncovered 4 proteins with previously unreported binding to BM212 family compounds: Rv0077c (designated EthA2), Rv0087 (designated EthR2), Rv0138 and Rv3519. Both Rv0138 and Rv3519 are uncharacterised proteins. Himar1 mutagenesis experiments indicate that *rv0138* is a non-essential gene for the *in vitro* growth of *M. tuberculosis* strain H37Rv (Griffin *et al*., 2011; Minato *et al*., 2019; Sassetti, Boyd, *et al*., 2003). In fact, disruption of *rv0138 in vitro* appears to be advantageous for H37Rv growth (Dejesus *et al*., 2017). Rv3519 is also non-essential, and has been found in membrane fractions of H37Rv (Gu *et al*., 2003; Sinha *et al*., 2005; Xiong *et al*., 2005). Orthologues of both Rv0138 and Rv3519 in *M. smegmatis* (MSMEG_6475 and MSMEG_5919) are preceded by a conserved motif in the intergenic region, which is commonly found in the promotor region of genes controlled by the TetR-type regulator Rv3594 (Kendall *et al*., 2007).

EthA2 and EthR2 are known functional analogues of EthA and EthR. EthA and EthA2 are responsible for the activation of the pro-drug ethionamide which, like isoniazid, targets InhA, an NADH-specific enoyl-acyl carrier protein reductase involved in mycolic acid biosynthesis (Banerjee *et al*., 1994; Quemard *et al*., 1992). InhA is essential for elongation of short-chain fatty acids as part of the type II fatty acid synthase system (FAS-II) (Batt *et al*., 2020; Marrakchi *et al*., 2000). Interestingly, EthA exhibits wide subject-specificity, acting as an activator for multiple inhibitors of mycolic acid biosynthesis, including thiacetazone and isoxyl (Bhowruth *et al*., 2006; Dover *et al*., 2007). EthA-EthR deficient strains exhibit a phenotypic change to mycolic acid composition, and increased adherence to mammalian cells, suggesting that the biological role of EthA relates to mycolic acid synthesis (Ang *et al*., 2014).

EthR and EthR2 are TetR-type transcriptional regulators of EthA and EthA2 (Blondiaux *et al*., 2017; Dover *et al*., 2004). EthA and EthR share a promotor region, as do EthA2 and EthR2, which are regulated by EthR and EthR2, respectively. Research has demonstrated that the inactivation of EthR2 by the small molecules aborting resistance (SMARt) family of spiroisoxazolines results in the reversal of resistance to ethionamide through the induction of the alternative activation pathway involving EthA2. SMARt-420 is the most potent of the SMARt EthR2 inhibitors tested; elucidation of the crystal structure of EthR2 bound to SMARt-420 reveals that it induces a conformational change in EthR2 by binding to both molecules in the homodimer. The helix-turn-helix (HTH) motifs are disrupted, with a ~6Å increase in distance between HTHs, preventing EthR2 from efficiently binding to DNA (Blondiaux *et al*., 2017).

SMARt-420 is not the first compound to be utilised for its potentiating capabilities. Pharmacokinetic enhancers or 'drug boosters' have been discovered for treating a variety of infectious diseases; they are compounds which, when applied in combination with an existing drug, boost its pharmacokinetic effect. Boosters are particularly useful for drugs with low efficacy, or low bioavailability, which would otherwise need to be prescribed in high doses, with negative side effects. β-lactam enhancers have been applied to a range of Gram-positive bacteria to restore susceptibility in MDR strains, including *Mtb* in which carbapenem resistance can be restored with clavulanic acid treatment (Kurz *et al*., 2012; Ramón-Garciá *et al*., 2016). Recent studies also have demonstrated the effectiveness of the combination of zidebactam (enhancer) and cefepime (β-lactam antibiotic) against Gram-negative bacteria (Bhagwat *et al*., 2019, 2021; Moya *et al*., 2021). In antiretroviral treatments, bioavailability can be hampered by the metabolism of therapeutics by cytochrome P450, meaning a higher oral dose is required to be effective. Inhibition of the metabolism of HIV drugs can be achieved using enhancers such as Cobicistat or Ritonavir (Danner *et al*., 1995; Hsu *et al*., 1998; Larson *et al*., 2014).

Following chemoproteomic profiling, assays were carried out using changes to the intrinsic tryptophan fluorescence of EthR2 and Rv0138 as an indicator for binding. Initially, both proteins were tested with BM212 in its original form and consistently bound, EthR2 with a K_D of 0.66 μM and Rv0138 with a K_D of 3.94 μM. Further structural analogues from the BM212 family were tested in the same manner, and GSK303A consistently bound to both EthR2 and Rv0138. Of the compounds tested, GSK303A bound with the lowest K_D of 0.19 μM to EthR2, considerably lower than the apparent K_D

of 9.3 µM obtained from bead immobilised assays. GSK303A also bound to Rv0138 in tryptophan fluorescence assays, with a K_D of 6.82 µM; it was not, however, competitively bound in bead immobilised assays. Interestingly, GSK074A, around which the competitive binding assays were based and which had an apparent K_D of 2.9 µM, did not induce any change to Trp fluorescence when titrated against EthR2 and as such no K_D was determined.

In order to clearly demonstrate binding of BM212 series compounds to EthR2, preliminary screens were carried out for protein-ligand co-crystallisation. Due to time constraints, it was not possible to solve a crystal structure of EthR2 with ligand, although crystals were generated in 10 conditions of the MIDAS screen from Molecular Dimensions. These results could be developed by optimisation screens of the crystallisation conditions. A high number of conditions resulted in the formation of EthR2 crystals without ligand; the most promising crystals could be selected for ligand soaking in order to generate a protein-ligand structure. Computational molecular docking experiments revealed that BM212 likely binds to EthR2 at a shallow cavity in the dimer interface unlike conventional EthR2 inhibitors which affect the TetR-like helix-turn-helix region.

Neither EthA or EthR is essential to *Mtb* and their deletion does not appear to incur a fitness cost. The same is assumed of EthA2 and EthR2, but no studies have yet reported the result of EthA2 or EthR2 deletion. It is improbable that the antimicrobial activity of BM212 is a direct result of inhibition of one or both of EthA2 or EthR2. It seems more likely that the binding of EthA2 and EthR2 in competition binding experiments is the

result of off-target effects also observed across the BM212 compound series and other MmpL3 inhibitors.

Strains of *M. bovis* BCG overexpressing EthA, EthR, EthA2 and EthR2 were generated for a series of survival assays to assess the efficacy of ETA. The MIC90 ranges determined for the transcriptional regulators EthR and EthR2 on solid media were increased compared to the empty vector control, demonstrating that an increase in the activity of the repressor leads to a reduction in activator activity, limiting the generation of the ETA-NAD adduct and thus increasing the MIC90. The generation of solid MIC90 values for strains overexpressing the activators EthA and EthA2 was hindered by the fact that these overexpression strains had a negative impact on cell growth, even in the absence of drug. MIC90 values appeared to be within the same range or slightly lower than the empty vector control. When EthA2 was grown in liquid, however, an MIC90 of 2 μg/mL was obtained, half that of the empty vector control, indicating an increase in ETA efficacy.

Guided by the assumption that EthA2 and EthR2 are not directly responsible as targets for the potent activity of BM212, and that there may be an additional, off-target interaction between one or both proteins and BM212, the dynamics of dual drug treatment with BM212 an ETA was investigated. The antibacterial activity of BM212 was established first on its own, and later in combination with ETA. FIC values, calculated from chequerboard plates, indicated that the simultaneous application of both drugs to *M. bovis* BCG had an additive/indifferent effect. The outcome of such combinatory treatments depends on the affinity of BM212 for EthA2 and EthR2. Taken together with

the competitive binding experiments, these data suggest that BM212 binds to both EthA2 and EthR2. While EthR2 bound most consistently in competitive binding assays and was identified as a likely secondary target of the BM212 family of compounds, EthA2 also appeared to bind to analogues, albeit in a small number of experiments. It is possible that any ETA boosting properties of BM212 resulting from EthR2 binding are counteracted by the binding of BM212 to EthA2.

Chapter 3

DGAT1 inhibitors prevent triacylglycerol synthesis in *Mtb*

3. DGAT1 Inhibitors Prevent Triacylglycerol Synthesis in *Mtb*

3.1.   Introduction

Triacylglycerol (TAG) is an important energy storage molecule in *Mtb* and proteins involved in the synthesis of TAG have the potential to be exploited as drug targets (section 1.9.2.). To successfully inhibit the production and accumulation of TAG in *Mtb*, three TAG sources must be addressed: *DGAT1* and *DGAT2* in humans, and the *tgs* genes in *Mtb*. In collaboration with GlaxoSmithKline, four DGAT1 inhibitors have been selected to be investigated for their anti-TB effects. These compounds have shown good drug metabolism and pharmacokinetic properties in mice. In unpublished preliminary studies, a DGAT1 inhibitor was used in a chronic TB mouse model, resulting in a reduction of colony forming units in the lungs of infected mice and acting as a proof-of-concept for the use of DGAT1 inhibitors against TB.

In this study, the antimycobacterial properties of DGAT1 inhibitors were explored, with a specific focus on their effect on mycobacterial triacylglycerol synthases. Overexpression studies focussing on four different TGS genes, *tgs1, tgs2, tgs3* and *tgs4,* were used to ascertain whether these known TAG synthases were involved in the mechanism of action of the most potent of the DGAT1 inhibitors tested. Through lipid profiling and MIC testing, Tgs3 was identified as a probable target, and a variety of biochemical techniques were employed to further elucidate the interaction between GSK2 and Tgs3.

3.2. Results

3.2.1. Preliminary Screening of DGAT1 Inhibitors Against TB, Carried out by GSK

Screening programmes performed by GSK identified inhibitors of human DGAT1 with activity against TB. Four DGAT1 inhibitors currently under clinical development were selected based on their superior DMPK (drug metabolism and pharmacokinetics) properties. As a proof-of-concept, two of the selected DGAT1 inhibitors were tested against TB infected THP-I cells, all demonstrating reasonable anti-TB activity (Table 4).

Table 4. Response of TB infected THP-I macrophages to treatment by four DGAT1 inhibitors.
Preliminary data provided by GSK shows the anti-TB effects of GSK1 and GSK2 when used to treat THP-I macrophages infected with TB.

Compound	Intracell IC50 (µM)	Intracell IC90 (µM)
GSK1	2.25	22.82
GSK2	3.42	10.9

3.2.2. Inhibition of *M. bovis* BCG by DGAT1 Inhibitors

Evaluation of DGAT inhibitor MICs against *M. bovis* BCG was carried out using a resazurin assay. GSK2, was determined to be the most potent inhibitor of the four, with an MIC of 30 µM. An MIC of 80 µM was recorded for GSK4, considerably higher than GSK2 but nevertheless active against *M. bovis* BCG. Neither GSK1 nor GSK3 exhibited a strong inhibitory effect against *M. bovis* BCG below 150 µM and as such both drugs were not progressed for further investigation (Figure 33, Table 5).
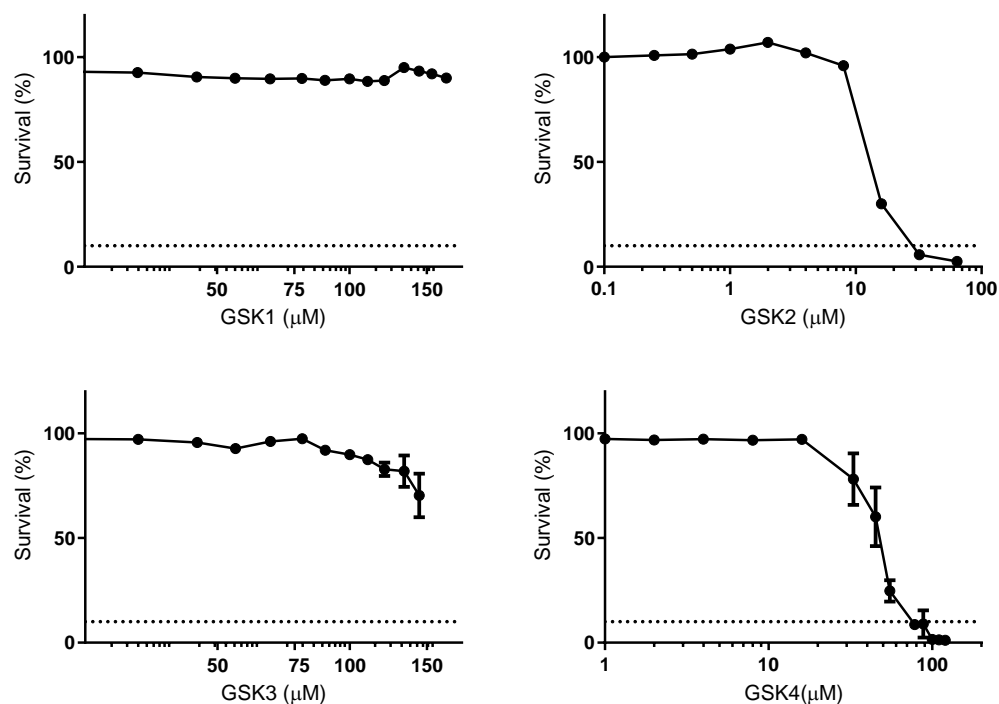
Figure 33. MICs of four DGAT1 inhibitors. *M. bovis* BCG was incubated in the presence of DGAT1 inhibitors for 7 days after which a resazurin assay was used to determine cell survival. Results were normalised by percentage normalisation. Graphs were produced using GraphPad prism showing the mean of 3 technical repeats with standard deviation.

Table 5. MIC values of four DGAT1 inhibitors tested against M. bovis BCG. *M. bovis* BCG was incubated in the presence of DGAT1 inhibitors for 7 days after which an end point resazurin assay was used to determine cell survival. MICs were calculated as the concentration needed for 90% inhibition of cell survival, and data represents the mean of three technical repeats.

Compound	*M. bovis* BCG MIC (μM)
GSK1	>150
GSK2	30
GSK3	>150
GSK4	80

3.2.3. Minimum Inhibitory Concentrations (MICs) of GSK2 Against *M. bovis* BCG Overexpressing *Mtb* Triacylglycerol Synthases

Four strains of *M. bovis* BCG overexpressing *Mtb* triacylglycerol synthases *tgs1*, *tgs2*, *tgs3* and *tgs4* were constructed using a pMV261 expression vector. These genes were selected on the basis that Tgs1, Tgs2, Tgs3 and Tgs4 exhibit higher triacylglycerol synthase activity than the 11 putative mycobacterial Tgs proteins (Jaiyanth Daniel *et al*., 2004). The MICs of GSK2, the DGAT1 inhibitor with the lowest MIC against WT *M. bovis* BCG, were established for each overexpression strain. The concentration range tested was based on a WT MIC of 30 µM and aimed to identify whether overexpression of any of these *tgs* genes conferred a level of resistance to GSK2 and increased the MIC. *M. bovis* BCG pMV261-empty, referred to as EV, was used as a control, and had an MIC equal to that of WT. Expression of pMV261-*tgs1* and pMV261-*tgs2* did not produce a change in MIC; expression of pMV261-*tgs3* and pMV261-*tgs4*, however, resulted in an increase of MIC from 30 µM to 50 µM and 40 µM, respectively (Figure 34, Table 6).
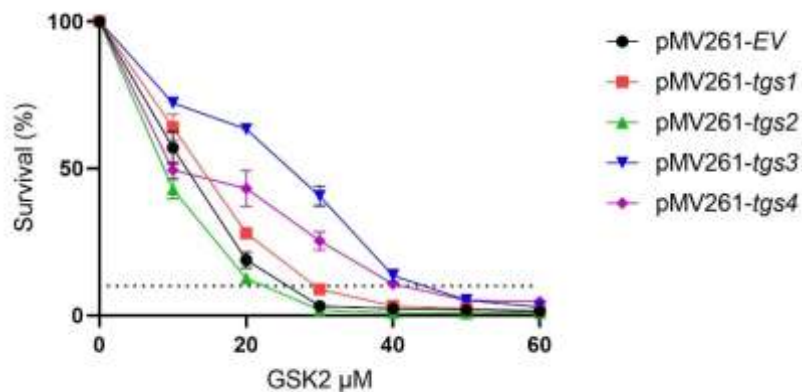
Figure 34. MICs of GSK2 against *M. bovis* BCG expressing *Mtb* triacylglycerol synthases. Five overexpression strains of *M. bovis* BCG were incubated in the presence of GSK2 for 7 days after which a resazurin assay was used to determine cell survival. Results were normalised by percentage normalisation. GraphPad prism was used to generate a graph showing the mean of 3 technical repeats with standard deviation.

Table 63. MIC values of GSK2 against M. bovis BCG expressing Mtb triacylglycerol synthases *M. bovis* BCG strains were incubated in the presence of GSK2 for 7 days after which an end point resazurin assay was used to determine cell survival. MICs were calculated as the concentration needed for 90% inhibition of cell survival, and data represents the mean of three technical repeats.

Strain	*M. bovis* BCG MIC (µM)
M. bovis BCG pMV261-empty	30
M. bovis BCG pMV261-*tgs1*	30
M. bovis BCG pMV261-*tgs2*	30
M. bovis BCG pMV261-*tgs3*	50
M. bovis BCG pMV261-*tgs4*	40

3.2.4. Minimal Inhibitory Concentrations (MICs) of GSK2 in Minimal Media

The endurance of mycobacteria within granulomas and in harsh extracellular environments has been linked to the formation of ILIs (Santucci *et al*., 2019). Particularly in low carbon environments, ILIs act as a valuable source of carbon due to the accumulation of lipids, such as TAG. Additionally, ILIs are associated with tolerance to antibiotics (Deb *et al*., 2009; Hammond *et al*., 2015). Studies have shown that nitrogen deprivation can induce the formation of ILIs *in vitro*, and the accumulation of TAG within those lipid bodies. With this in mind, the MICs of GSK2 against *M. bovis* BCG expressing pMV261-*tgs1*, pMV261-*tgs2*, pMV261-*tgs3* and pMV261-EV were obtained in nitrogen limiting minimal media. A significant reduction in MIC was observed in the empty vector control and strains expressing *tgs1* and *tgs2*, all of which had MICs below 10 µM (Figure 35, Table 7). The strain overexpressing *tgs3*, however, had an MIC of 30 µM, still a reduction from the MIC in nutrient media, but considerably higher than the empty vector control.
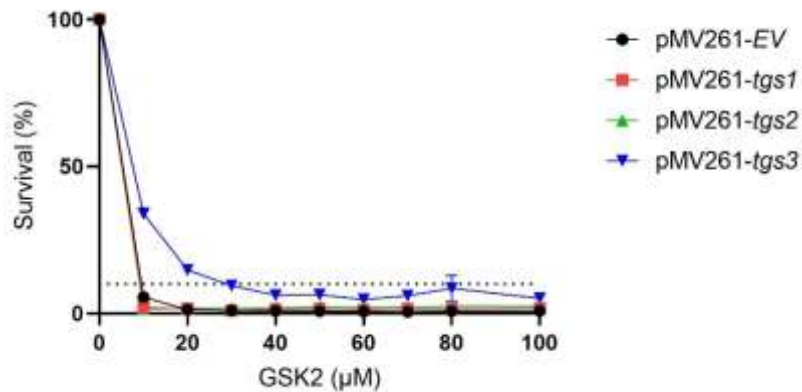
Figure 35. MICs of GSK2 against *M. bovis* BCG expressing triacylglycerol synthases in nitrogen limiting media. . Four overexpression strains of *M. bovis* BCG were incubated in nitrogen limiting media in the presence of GSK2 for 7 days after which a resazurin assay was used to determine cell survival. Results were normalised by percentage normalisation. The strain expressing Tgs3 was the only strain to survive above 10μM GSK2. GraphPad prism was used to generate a graph showing the mean of 3 technical repeats with standard deviation.

Table 7. MICs of GSK2 against M bovis BCG expressing triacylglycerol synthases in nitrogen limiting media. *M. bovis* BCG strains were incubated in the presence of GSK2 for 7 days after which an end point resazurin assay was used to determine cell survival. MICs were calculated as the concentration needed for 90% inhibition of cell survival, and data represents the mean of three technical repeats.

Strain	*M. bovis* BCG MIC (μM) low N
M. bovis BCG pMV261-EV	<10
M. bovis BCG pMV261-*tgs1*	<10
M. bovis BCG pMV261-*tgs2*	<10
M. bovis BCG pMV261-*tgs3*	30

3.2.5. Minimum Inhibitory Concentrations (MICs) of GSK2 on Solid Media

The generation and whole genome sequencing of resistant mutants is a straightforward method of determining the target and mode of action of antibiotics (Abrahams *et al*., 2018). When used in combination with other techniques, it can be a valuable indicator of genes of interest. Before spontaneous resistant mutants could be raised, a solid GSK MIC was established for *Mtb* H37Rv (Figure 36, Table 8) and for *Mtb* H37Rv *ΔleuDΔpanCD* (mc^{2}7000). The attenuated strain of *Mtb* H37Rv *ΔleuDΔpanCD* (mc^{2}7000), was used for mutant generation at 5x the solid MIC of 20 µM. Colonies that formed on high drug concentrations were transferred to liquid media before being re-streaked onto 5x MIC plates for re-testing.
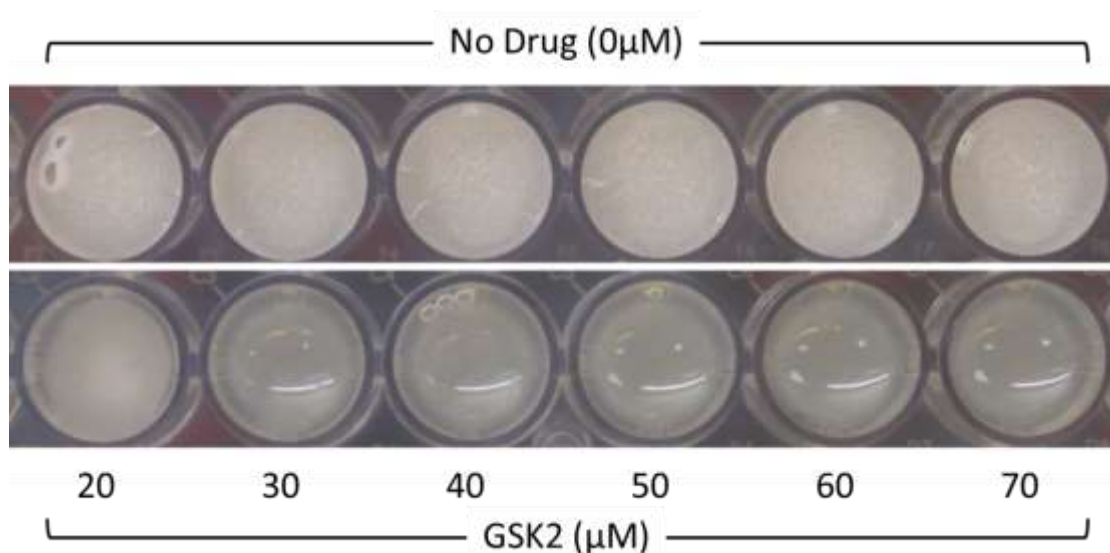
Figure 36*. Solid MIC of GSK2 against *Mtb* H37Rv. Multi-well plates containing concentrations of GSK2 in 7H11 solid media were prepared and *Mtb* H37Rv was added to each well. Plates were incubated until a lawn of bacterial was visible on the no drug control wells. The solid MIC was defined as 30 µM, the lowest concentration on which no visible growth was present.

Table 8. Solid MICs of GSK2 against *Mtb* H37Rv and *Mtb* H37Rv *ΔleuDΔpanCD* (mc²7000).

Strain	Solid MIC (µM)
M. tuberculosis H37Rv	20
M. tuberculosis H37Rv *ΔleuDΔpanCD* (mc²7000)	30

1.1.1. Lipid Profiles of GSK2 Treated *M. bovis* BCG Overexpressing Triacylglycerols

Apolar lipids extracted from WT *M. bovis* BCG treated with GSK2 were spotted onto silica TLC plates at a concentration of 10,000 cpm per TLC, and run in solvent systems A-D (Figure 67). Autoradiographs reveal a slight increase in phthiocerol dimycocerosates (PDIMs), relative to TAG in system A at high concentrations of GSK2. Since equal counts were loaded onto each TLC, an apparent increase in PDIMs could be due to a decrease in other labelled lipids separated in the same solvent systems. A decrease in TAG in system A, for example could cause PDIMs to appear to be more prominent on the TLC plates in their respective solvent systems.

A decrease in TAG is a likely outcome given the activity of compound GSK2 as an inhibitor of human diacylglycerol O-Acyltransferase 1. If TAG synthesis is indeed disrupted, an accumulation of TAG precursors is likely to occur. Synthesis of DAG is the first committed step in TAG biosynthesis, which involves the acylation of DAG. In system C, there is a distinct difference in the intensity of FFAs, lipids which are incorporated in the final step of TAG synthesis.

Polar lipid fractions, separated in solvent systems D_2 and E, revealed no changes upon treatment with GSK2 (Figure 67). FAMEs and MAMEs fractions extracted from TBAH treated delipidated cells, were run in a 1D TLC system, which did not show any significant change to FAMEs or to α or keto MAMEs with GSK2 treatment (Figure 37). Lipid profiling was limited to single replicates for apolar, polar and FAMEs and MAMEs due to availability of GSK2 drug.
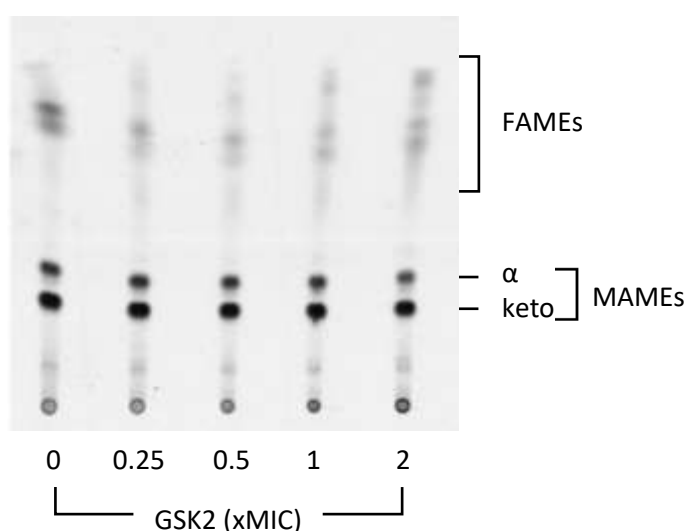
Figure 37. FAMEs and MAMEs of WT *M. bovis* BCG treated with GSK2. *M. bovis* BCG was cultured in the presence of GSK2 for 24 hours and labelled with [14C] acetic acid. Cells were harvested by centrifugation and FAMEs and MAMEs were extracted. Aluminium backed silica TLC plates loaded with 10,000 cpm FAMEs and MAMEs were run in Petroleum ether / acetone (95 : 5). Autoradiograph films were exposed to the TLC plates for 6 days. Treatment with GSK2 did not have a significant effect on the FAMEs and MAMEs.

strains overexpressing *tgs1*, *tgs2*, *tgs3* and *tgs4* to ascertain whether treatment with GSK2 resulted in a phenotypic change. The lipid profile of *M. bovis* BCG pMV261-empty was also assessed and showed no changes compared to WT (Figure 67). Upon overexpression of three of these key TAG synthases there was a change to the apolar lipids in the absence of drug. *M. bovis* BCG containing the constructs pMV261-*tgs1*, pMV261-*tgs2* and pMV261-*tgs3* exhibited a change in PGLs (Figures 68, 69 and 70).

Expression of *tgs1* resulted in a marked reduction in PGLs, while *tgs2* and *tgs3* overexpressors showed a complete lack of PGLs. As with WT BCG, treatment with GSK2 induced FFA accumulation in *M. bovis* BCG pMV261-*tgs1*, pMV261-*tgs2* and pMV261-*tgs4* (Figures 67, 68, 69 and 71). Notwithstanding the absence of PGLs, the apolar lipid profile of *M. bovis* BCG pMV261-*tgs3* treated with GSK2 revealed a reversion to untreated WT phenotype.

1.1.2. Accumulation of Triacylglycerol (TAG) in Minimal Media

Three types of media were used to probe the effect of nutrient limitation on GSK2 activity. Middlebrook 7H9 media supplemented with OADC, Tween80 and glycerol was used as a standard nutrient media. An intermediate minimal medium was used, in addition to a reduced nitrogen minimal media. Nitrogen deprivation in this media has been shown to result in the accumulation of TAG (Santucci *et al.*, 2019). GSK2 MICs were established for *M. bovis* BCG overexpressing *tgs1, tgs2* and *tgs3* for 7H9 media and minimal media with reduced nitrogen (Table 7) and it was evident that *M. bovis* BCG overexpressing *tgs3* retained an MIC similar to WT BCG in nutrient media, while all other strains showed significant reductions to their MICs. *M. bovis* BCG pMV261-EV and pMV261-*tgs3* were grown in 7H9, minimal media and minimal media with low nitrogen, treated with GSK2 at 0x, 0.5x 1x and 2x the MIC of WT BCG in nutrient media, and labelled with [^{14}C]-acetic acid. The apolar lipids were extracted and separated by 1D TLC (Figure 38). The position of TAG was confirmed by running TAG standards alongside labelled samples. The density of TAG was calculated and normalised so that 0x GSK2

samples represent 100 % TAG and subsequent drug concentrations show a percentage of TAG relative to the untreated controls (Figure 39).

The amount of TAG extracted from *M. bovis* BCG pMV261-empty reduces significantly (P<0.05) when cultures have been treated with GSK2 relative to other lipid products present in the apolar lipid extracts. The most considerable reduction is seen in strains grown in minimal media with normal nitrogen (Figure 40). *M. bovis* BCG pMV261-*tgs3*, exhibits a slight reduction in TAG when treated with GSK2 in 7H9 media (P=ns) and a significant reduction in TAG in minimal media. Low nitrogen minimal media however, which in *M. bovis* BCG pMV261-empty results in exaggerated depletion of TAG, causes a restoration of TAG in *M. bovis* BCG pMV261-*tgs3.*

These changes in MIC, and phenotypic response to GSK2 upon overexpression of *tgs3* suggests the involvement of Tgs3 as a target and indicates that GSK2 is more potent in nitrogen deprivation conditions. Granuloma formation, hypoxia and nitrogen deprivation conditions have all been implicated in tolerance to antibiotics. These results are particularly promising, because they show an increase in potency rather than a reduction in harsh conditions.
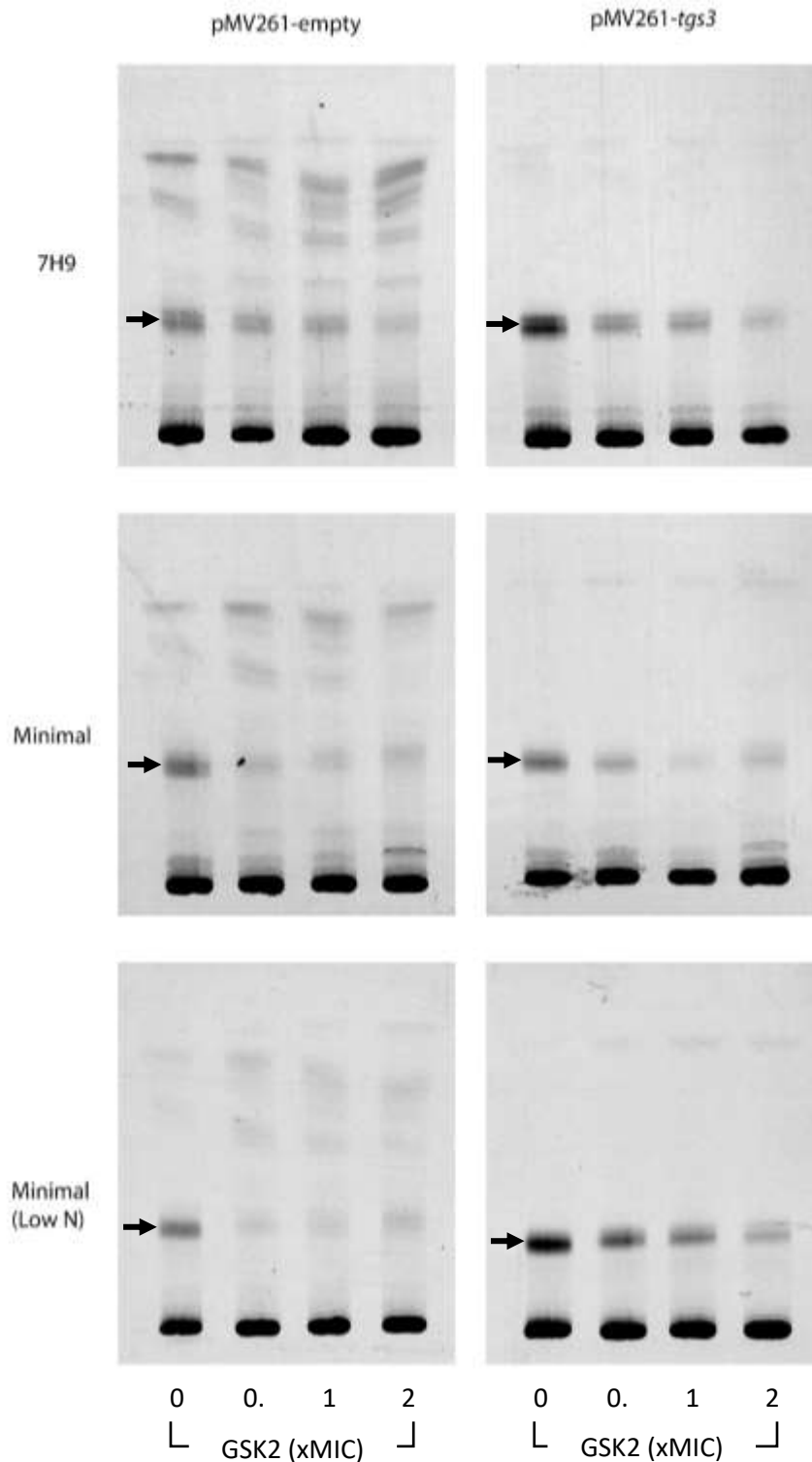
Figure 38. Autoradiographs of 1D TLC plates showing TAG in *M. bovis* BCG following GSK2 treatment. Cultures of *M. bovis* BCG expressing pMV261-empty and pMV261-*tgs3* were grown in 7H9, minimal media or minimal media - low nitrogen and treated with GSK2. Cultures were labelled with [^{14}C] acetic acid and apolar lipids were extracted. 10,000 cpm of apolar lipids were loaded onto aluminium-backed silica TLC plates which were run in Petroleum ether / diethyl ether (90 : 10). Blue autoradiograph films were exposed to the TLC plates, scanned then transformed to grayscale and cropped using Adobe Photoshop. The contrast of the whole image was adjusted for image clarity. This image represents one replicate of TLCs run in triplicate. Black arrows indicate TAG.

7H9 Media

Minimal Media

Minimal Media (Low N)
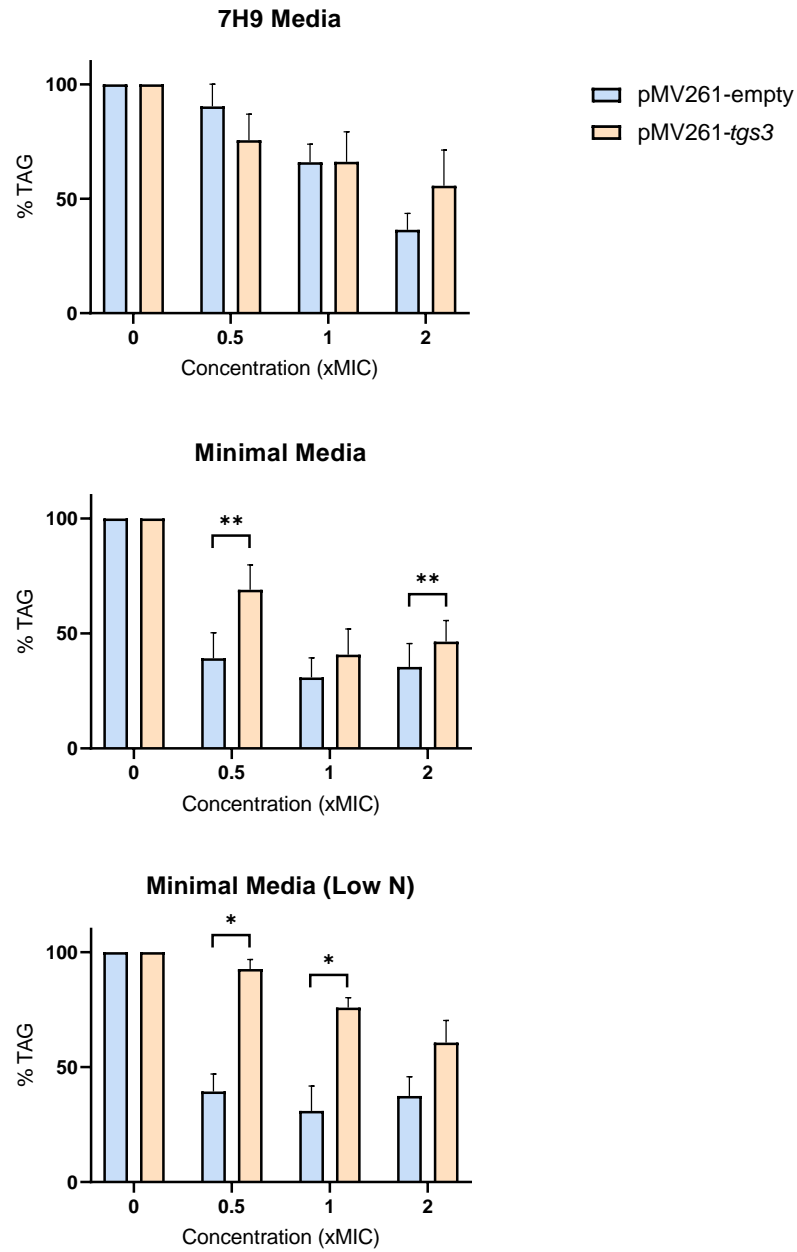
Figure 39. Relative change in TAG of *M. bovis* BCG expressing pMV261-empty and pMV261-*tgs3* treated with GSK2 in three types of media. The density of bands was calculated using Image Lab software. Data are normalised to show untreated cultures as having 100% TAG. The TAG of cultures treated with GSK2 is shown as a percentage of the untreated control. Data represent the mean of TLCs run in triplicate ± SD. Paired t-tests were carried out to compare the two strains; * corresponds to P<0.05 and ** corresponds to P<0.01
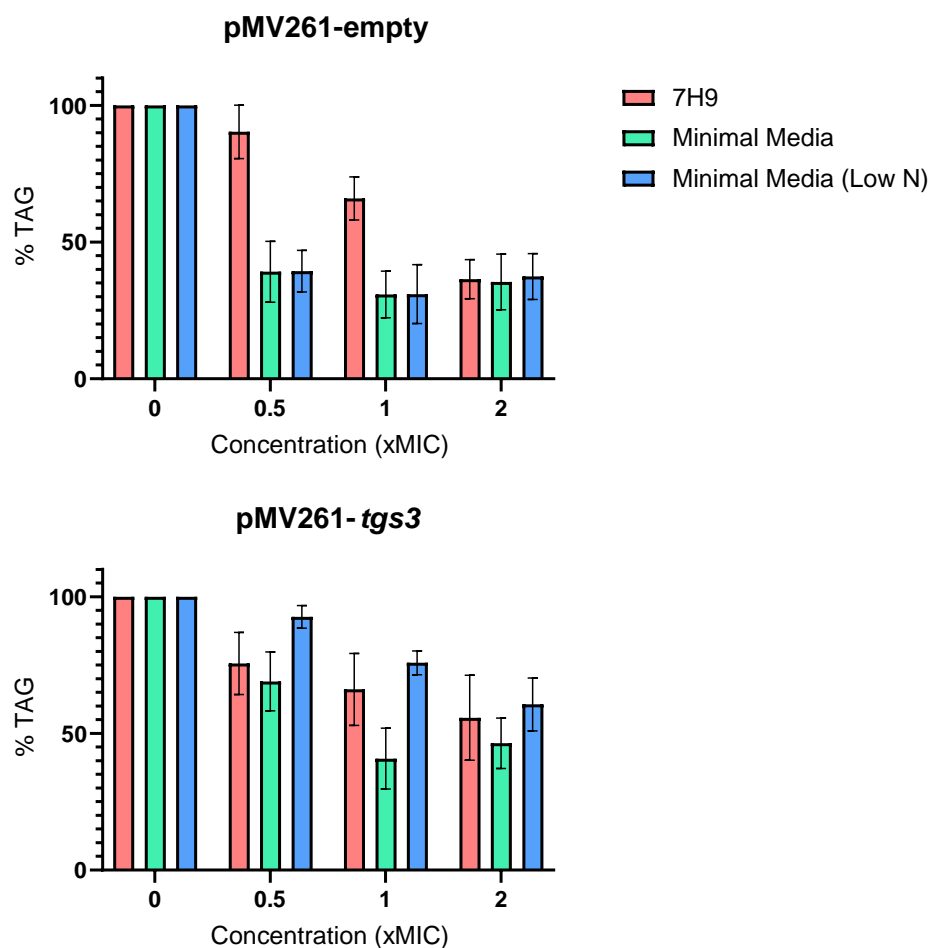
Figure 40. The effect of media type on the potency of GSK2 against *M. bovis* BCG. Over expression of *tgs3* results in a less pronounced reduction in TAG with GSK2 treatment, particularly when cultures are grown in nitrogen deprivation conditions. The density of bands was calculated using Image Lab software. Data are normalised to show untreated cultures as having 100% TAG. The TAG of cultures treated with GSK2 is shown as a percentage of the untreated control. Data represent the mean of TLCs run in triplicate ± SD.

1.1.3. Lipid Profiling of *M. bovis* BCG Treated with GSK4

The DGAT1 inhibitor with the second lowest MIC of those tested was GSK4. Lipid profiling was carried out for WT *M. bovis* BCG treated with GSK4 (Figure 72). In a similar outcome to that seen in GSK2 treatment, high concentrations of GSK4 cause an apparent increase in PDIMs in apolar system A, which in fact represents a relative decrease in TAG (Figures 41 and 42). In systems B and C, we see the familiar increase in FFA, which is characteristic of TAG inhibition. The amount of extractable lipids at high concentrations of GSK4 was low and there were insufficient counts of [^{14}C]-labelled polar lipids from the 2x MIC treatment to run TLC plates in systems D and E.

Restricting nutrients in the growth media had surprisingly little effect on TAG accumulation when WT *M. bovis* BCG was treated with GSK4, compared to the dramatic impact of nitrogen deprivation on the response to GSK2 treatment (Figures 40 and 42). Due to the high MIC of GSK4, growing cultures in 2x MIC used a considerable amount of compound, and as such there was insufficient drug available to run TLCs in triplicate.
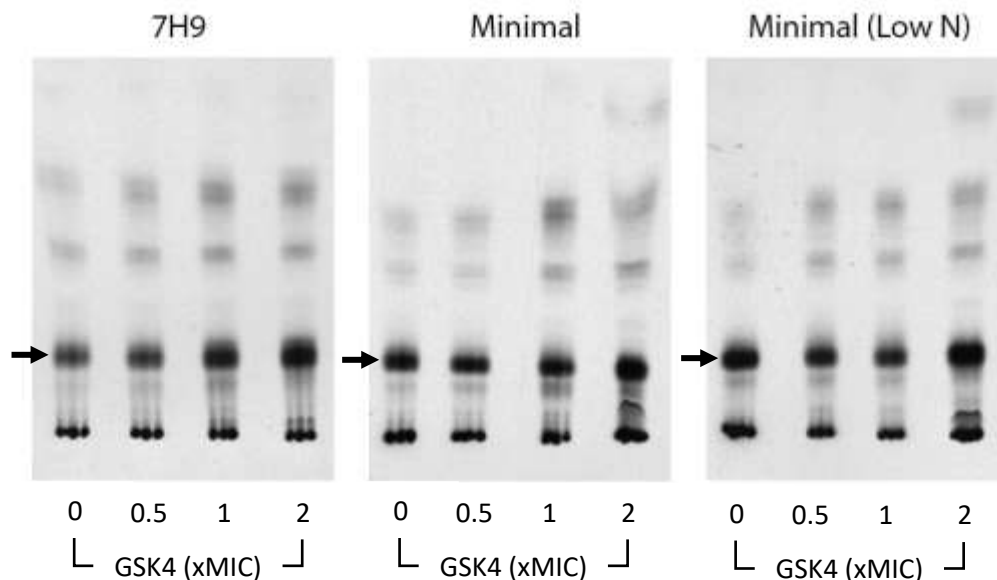
Figure 41. Autoradiographs of 1D TLC plates showing TAG depletion in *M. bovis* BCG following GSK4 treatment. Cultures of WT *M. bovis* BCG were grown in 7H9, minimal media or minimal media - low nitrogen and treated with GSK4. Cultures were labelled with [^{14}C] acetic acid and apolar lipids were extracted. 10,000 cpm of apolar lipids were loaded onto aluminium-backed silica TLC plates which were run in Petroleum ether / diethyl ether (90 : 10). Blue autoradiograph films were exposed to the TLC plates, scanned then transformed to grayscale and cropped using Adobe Photoshop. The contrast of the whole image was adjusted for image clarity. Black arrows indicate TAG.
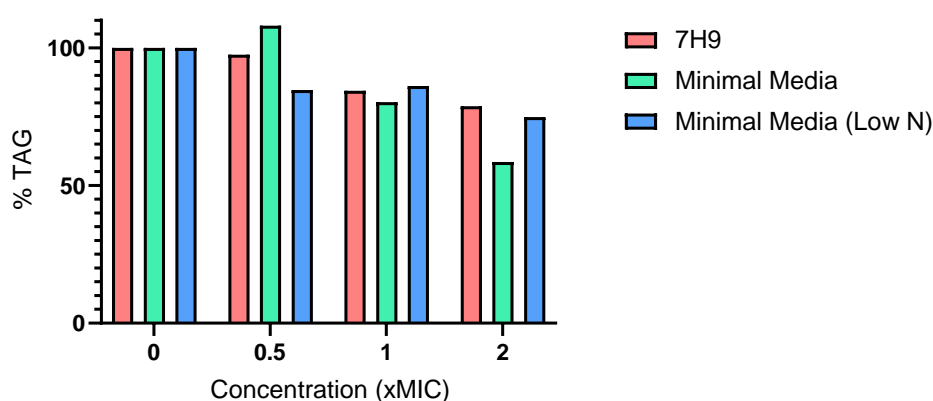
Figure 42. The effect of media type on the potency of GSK4 against WT *M. bovis* BCG. TAG reduces considerably with GSK4 treatment. The density of bands was calculated using Image Lab software. Data are normalised to show untreated cultures as having 100% TAG.

1.1.4. Construction of Recombinant *E. coli* Protein Expression Strains

Four strains of *E. coli* expressing Rv3130c (Tgs1), Rv3734c (Tgs2), Rv3234c (Tgs3) and Rv3088 (Tgs4) were constructed. Gene fragments for insertion into pET28a were generated by PCR. Restriction digest was used to check the size of each gene fragment that had been ligated into pET28a (Figure 43) before the Top10 *E. coli* were transformed with the plasmids for amplification and storage. The sequences of ligated plasmids were confirmed by Source Bioscience. *E. coli* BL21 DE3 were transformed with plasmids with correct sequences.
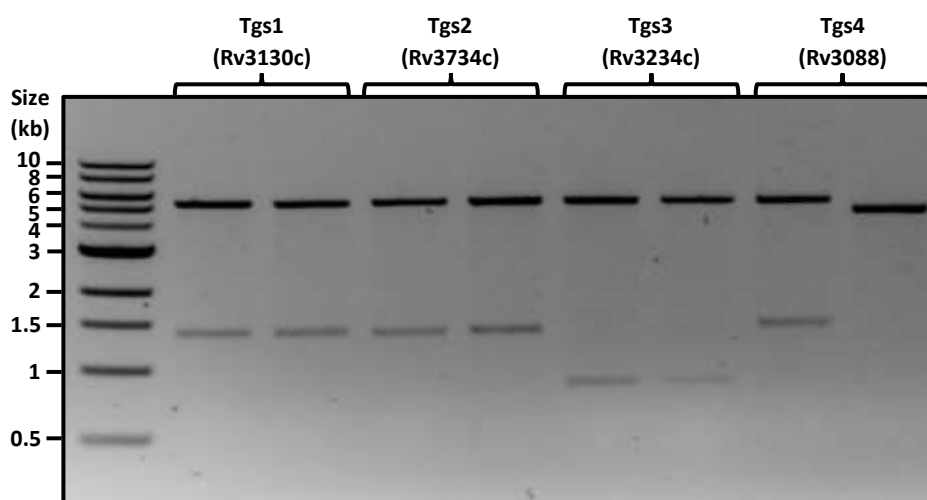
Figure 43. Restriction digest of pET28a gene inserts. *Mtb* genes were amplified using PCR for insertion into plasmid vectors. Restriction digests were carried out to confirm the presence of gene inserts, digested products were run on 1% agarose gels to confirm the size of the inserts. Lane 1 – 10kb ladder; lanes 2 and 3 – Rv3130c (1392bp); lanes 4 and 5 – Rv3734c (1365bp); lanes 6 and 7 – Rv3234c (816bp); lanes 8 and 9 – Rv3088 (1425bp). Lanes 2, 5, 6 and 8 were selected to be sequenced by Source Bioscience.

1.1.5. Purification of *Mtb* Triacylglycerol Synthases

Purification was attempted for each of the four Tgs1, Tgs2, Tgs3 and Tgs4. An initial expression trial with each protein expressed in *E. coli* grown in terrific broth and induced with IPTG at an OD_{600} of 0.8. Tgs1, Tgs2 and Tgs4 were identified by Western blot in the cell lysate (Figure 44). Purification of Tgs1 was successfully achieved by nickel affinity chromatography. A band corresponding to the approximate size of Tgs1 (50kDa) is visible in all elution fractions (Figure 45). Samples from lanes 8, 9 and 10 were pooled and concentrated, and the band at ~50kDa confirmed by Western blot (Figure 44).
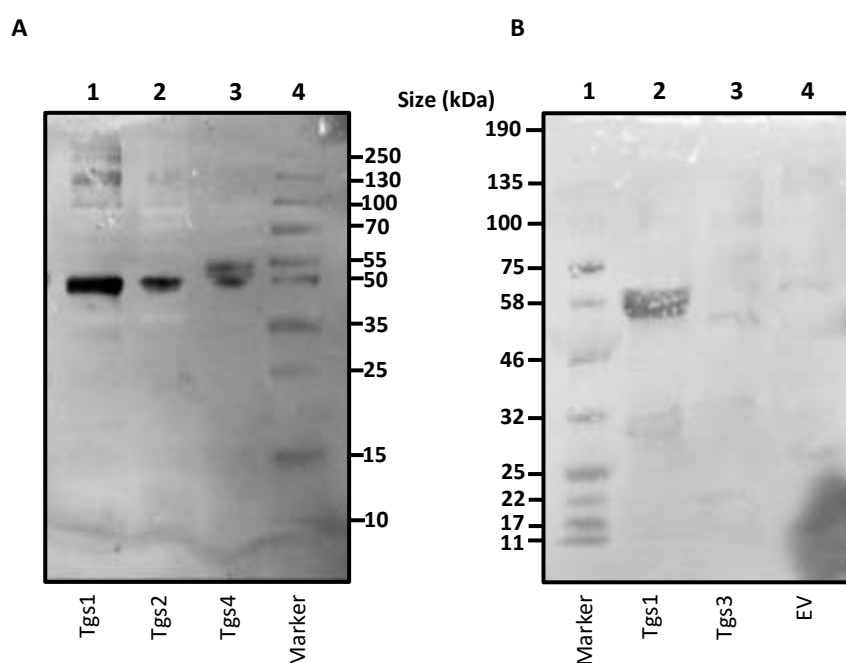
Figure 44. Western blots of Tgs proteins overexpressed in *E. coli.* A – Positive identification of Tgs1, Tgs2 and Tgs4 with bands corresponding to their sizes of 50kDa, 49kDa and 50kDa respectively. B – Tgs1 was used as a positive control, visible between 46kDa and 58kDa. No band was detected for Tgs3 (30kDa) or *E. coli* containing an empty vector plasmid (EV).
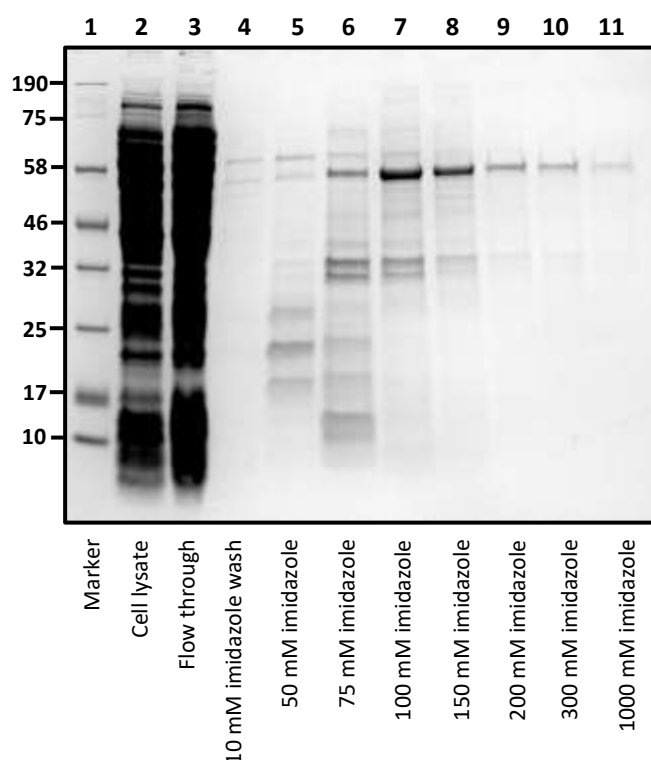
Figure 45. SDS PAGE of fractions from the purification of Tgs1 (Rv3130c) by nickel affinity. Recombinant Rv3130c was expressed in *E. coli* BL21 DE3 induced with 1mM IPTG. Purification was achieved using a HisTrap column. Samples from lysis and elution steps of the purification were boiled in SDS and separated by SDS PAGE. A band corresponding to the size of Tgs1 is visible in all lanes containing imidazole elutions. Lanes 8, 9 and 10 were pooled and concentrated.

1.1.6. Triacylglycerol Synthase Activity Assays

Treatment with GSK2 causes phenotypic changes to *M. bovis* BCG overexpressing Tgs3 and Tgs4 in the form of an increased MIC and, in the case of Tgs3, changes to the lipid profile. In order to further probe the possible interactions between GSK2 and the three selected Tgs proteins (excluding Tgs3 which could not be identified by Western blot in expression assays), enzymatic assays were carried out. Due to the difficulties in purifying Tgs proteins, the synthesis of TAG was assayed using cell lysate from *E. coli* BL21 DE3 overexpressing each of the four Tgs proteins. *E. coli* BL21 DE3 containing an empty vector (EV) was used as a control. Briefly, in the reaction described by McFie *et. al* (2011), NBD-tagged palmitoyl-CoA is incubated with DAG and a triacylglycerol synthase (in this

case, present in the cell lysate). In the presence of an active triacylglycerol synthase, the NBD-tagged fatty acyl chain is separated from CoA and transferred to DAG, forming NBD-TAG. Separation of the reaction product is achieved by solvent extraction and the product run on a preparative TLC. The TAG product, identified under UV light, is scraped from the TLC and the fluorescence measured (Figure 46).
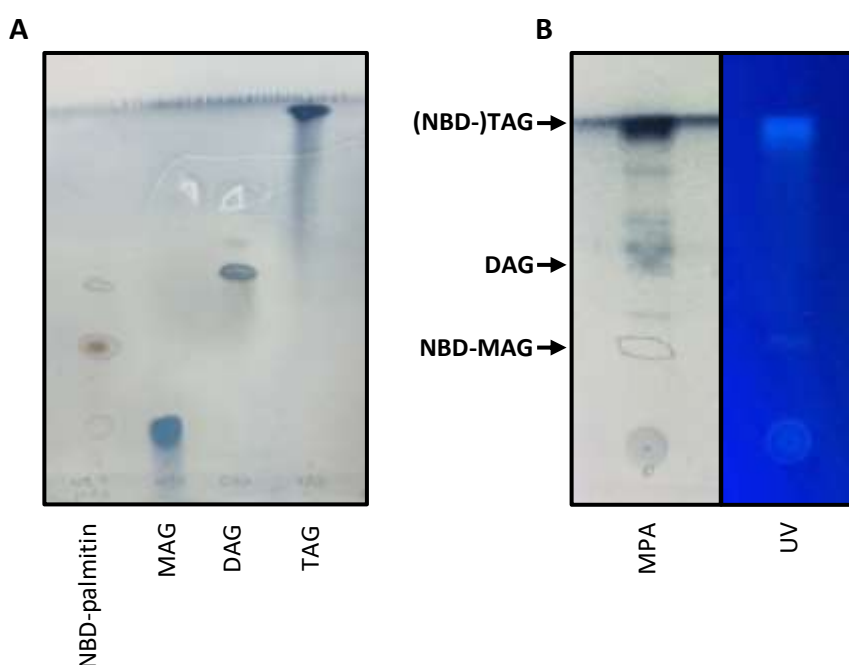
Figure 46 TLC separation of NBD-TAG from *tgs* activity assay substrates. The activity of *Mtb* triacylglycerol synthases was assayed as described by McFie *et al.* (2011). The products were extracted and separated by TLC in Petroleum ether / diethyl ether (90 : 10) and viewed under UV light. A – standards run to determine relative positions of mono- (MAG), di- (DAG) and tri-acylglycerols (TAG). NBD-palmitin was marked first by pencil under UV light before staining with MPA. B – Two panels show the product of tgs synthesis in *E. coli* overexpessing *Mtb* Tgs1. The same TLC has been imaged after staining with MPA (left) and under UV light (right). The highest band running close to the solvent front shows TAG, which was extracted from prep-TLCs for fluorescent quantitation.

The assay was carried out with and without GSK2, and in all samples of cell lysate there was a reduction in fluorescence (indicating a reduction in TAG) in the presence of drug (Figure 47). The most significant reduction occurred in the EV control, suggesting that native *E. coli* proteins were acting as triacylglycerol synthases and were too inhibited by GSK2. While the production of high yields of TAG is characteristic of Actinomycetes such

as *Mtb*, other prokaryotes have systems for the synthesis of a smaller proportion of TAG (Rucker *et al*., 2013). With this in mind, it is clear that there is too much background activity in *E. coli* cell lysate for this assay to be used, however it does help to further validate GSK2 as a DGAT inhibitor. The activity of Tgs1, Tgs2 and Tgs4 did not exceed the activity of EV, suggesting that they may have been enzymatically inactive.
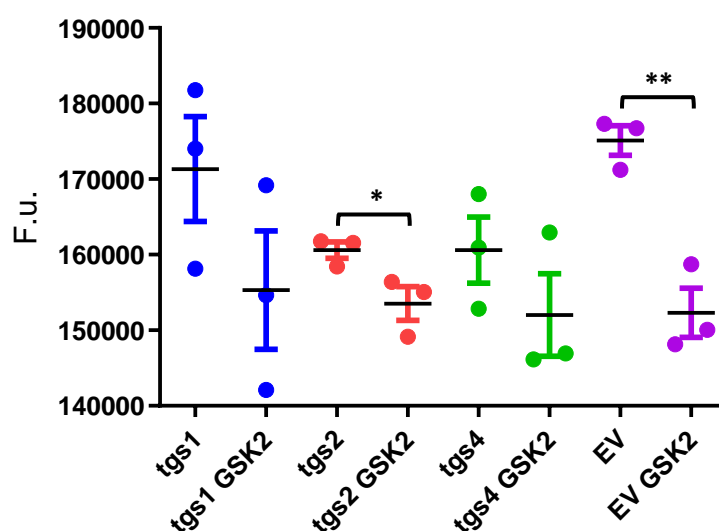
Figure 47 Triacylglycerol synthase activity of cell lysate of *E. coli* expressing *Mtb* Tgs proteins. The activity of *Mtb* triacylglycerol synthases was assayed as described by McFie *et al.* (2011). The products were extracted and separated by TLC in Petroleum ether / diethyl ether (90 : 10) and the bands of TAG were scraped from the TLC plate. Scraped silica was suspended in petroleum ether in a 96 well plate and the fluorescence was measured with a BMG plate reader. Treatment with GSK2 resulted in a reduction in fluorescence of cell lysate expressing Tgs1, Tgs2 and Tgs4. EV *E. coli* shows clear DGAT activity and the most significant reduction in fluorescence in the presence of drug. TLCs were carried out in triplicate and significance is indicated by asterisks, calculated by T-test. * P=0.0458 ** P=0.0039

1.1.7. Tryptophan Fluorescence Quenching Assay

Intrinsic tryptophan (Trp) quenching was used to ascertain whether GSK2 bound to Tgs1 which was successfully purified in this work. Tgs1 was titrated against GSK2, and saturation ligand-binding curves were produced. Tgs1 bound to GSK2 with a K_D of 36.04

µM and R^2 value of 0.934 indicating a good fit of the curve (Figure 48). Based on the lack of phenotypic changes seen in strains overexpressing Tgs1 when treated with GSK2, binding was unexpected. Four of the six Tryptophan residues of Tgs1 are predicted to be localised on a beta-sheet, with the other two residues close by (Figure 48). This gives some indication of the location of binding and could be further investigated through co-crystallisation of Tgs1 and GSK2. Unfortunately, when the TAG synthesis assays were carried out using purified Tgs1, no activity was detected, suggesting that the protein was inactive. As such, it was not possible to enzymatically assess the effect of GSK2.
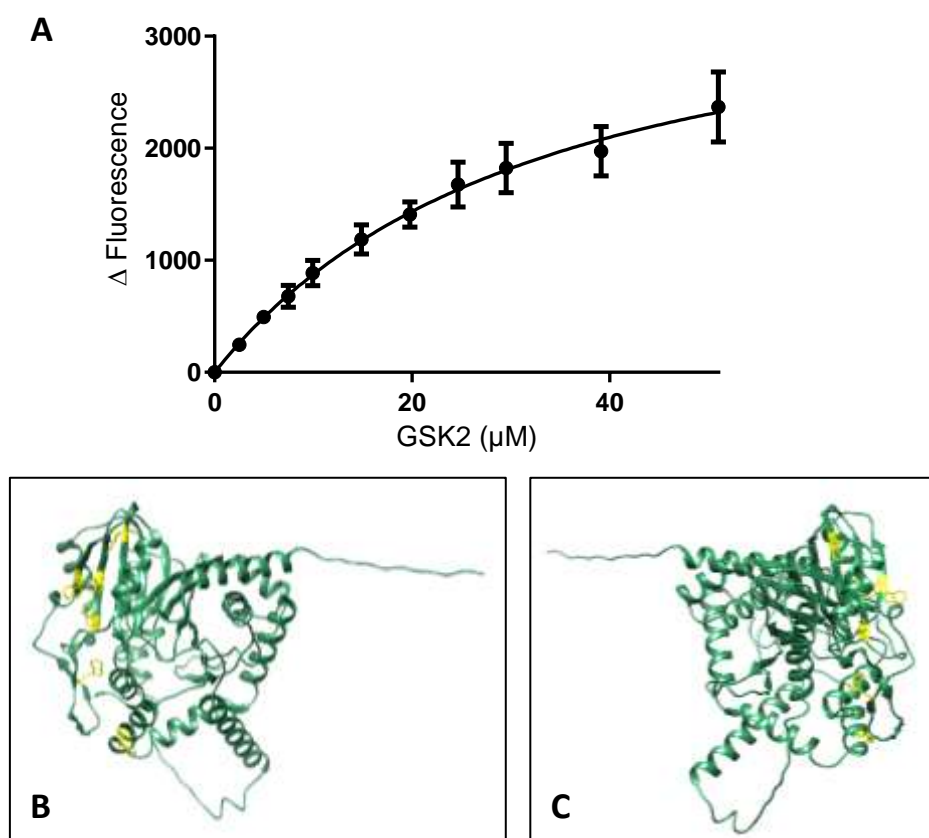
Figure 48. Saturation binding curve of Tgs1 and GSK2. A - GSK2 was titrated against Tgs1 and Intrinsic tryptophan fluorescence quenching was used to determine the binding of GSK2 to Tgs1. Saturation ligand-binding curves were generated with GraphPad prism the K_D was calculated to be 36.04 µM. **B** and **C –** Two views of Tgs1 showing six Tryptophan residues localised in one area of the protein, with four of the Trp residues present on a beta-sheet (structure obtained from AlphaFold and visualised using Chimera).

The amino acid sequences of Tgs1, Tgs2, Tgs3 and Tgs4 were compared by pairwise alignment to establish the amount of similarity between the proteins. The highest similarity was 45.3 % between Tgs4 and Tgs2, while the lowest was 25.0 % between Tgs3 and Tgs4 (Figure 49). The 15 putative *tgs* genes from *Mtb* share similar active site motifs, 11 of which have a characteristic HHxxxDG sequence (Figure 50). This site is thought to participate in acyl-CoA acyltransferase reactions which are key for TGS synthesis (Jaiyanth Daniel *et al*., 2004). Tgs3 is one of 2 Tgs proteins with modifications to the double histidine at the start of the motif; the second histidine of Tgs3 is replaced with a glutamine residue. The penultimate residue is also different for Tgs3, where aspartic acid is substituted for asparagine. These active-site similarities could be responsible for the apparent binding of Tgs1. While it doesn't appear to be implicated as a target of GSK2 in other assays, there appears is an affinity between GSK2 and Tgs1.
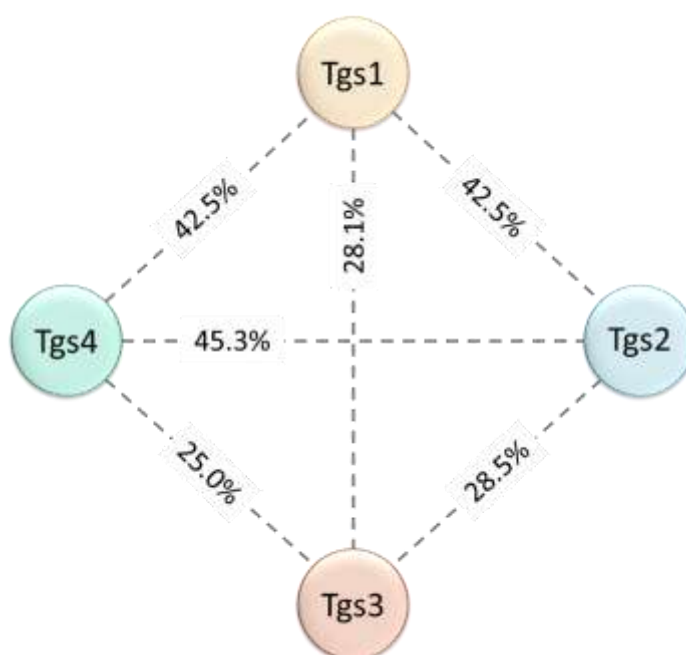
Figure 49. Amino acid sequence similarities between four Tgs proteins. Percentage similarities between all possible pairings of Tgs1, Tgs2, Tgs3 and Tgs4 were calculated based on their amino acid sequences.

```
tgs1    WEVWVIEGLADSKWAILTKLHHCMADGIAATHLLAGLSDESMS-DSFASNIHTTMQSQS-      173
tgs2    WELHVVEGLNDGRFAMYTKMHHALIDGVSAMKLAQRTLSADPD-DAEVRAIWNLPPRPRT      176
tgs3    WEMYLVEGLEKNRIALYTKSHQALINGVTALAIGHVIADRTRRPPAFPEDIWVPERDPGT      176
tgs4    WECYIIDGIERGRIAILLKVHHALIDGEGGLRAMRNFLSDSPD-DTTLAGPWMSAQGADR      172
```

Figure 50. The characteristic active-site motif of Tgs1, Tgs2, Tgs3 and Tgs4. For 11 of the 15 putative Tgs proteins, the motif (highlighted in yellow) follows a HHxxxDG pattern.

1.1.8. Generation and Sequencing of Spontaneous Resistant Mutants

Spontaneous resistant mutants were generated by culturing *Mtb* H37Rv *ΔleuDΔpanCD* (mc^{2}7000) on high concentrations of GSK2. A single colony was isolated from a 5x MIC plate (150 µM GSK2) and was transferred to liquid media containing no GSK2. Following incubation, the culture was re-tested on a 5x MIC plate alongside WT cells to check whether the cells were resistant to GSK2 (Figure 51). Colonies were only generated by the resistant mutant strain, and not by wild type. Genomic DNA extraction was carried out and the DNA was sent for whole genome sequencing by Microbes NG, who also carried out variant calling (Figure 51). Indels and SNPs were reviewed and filtered first by 90 % frequency and 10x read depth and second, more broadly, by 10 % frequency and 3x read depth, where frequency refers to the percentage of reads have the variant, and read depth refers to the number of times a base occurs at a particular position within all the sequencing reads. No variants of any significance were detected in the sequencing data, specifically no SNPs or indels occurred with high frequency which caused changes to amino acids compared to the reference genome, nor were any mutations detected in essential genes. Without evidence of genetic resistance there are a number of other potential reasons that this single colony was generated on a high concentration drug plate. Firstly, in the event of poor mixing of the compound into the

113

agar, colonies are able to grow on areas of the plate where the concentration of drug is lower. Similarly, degradation of the compound could lead to areas of the plate having lower concentrations than expected. The practice of retesting mutants on high concentration plates should usually prevent these false positives from being identified as mutants. Phenotypic drug tolerance is another possible phenomenon, distinct form drug resistance as it is not inherited in the form of resistance genes and cannot be shared as a mobile genetic element (Liu *et al.*, 2020). Metabolically-dormant bacteria can survive in the presence of antibiotics despite genetic susceptibility to them through tolerance by slow growth, or tolerance by lag (Brauner *et al.*, 2016; Fridman *et al.*, 2014).
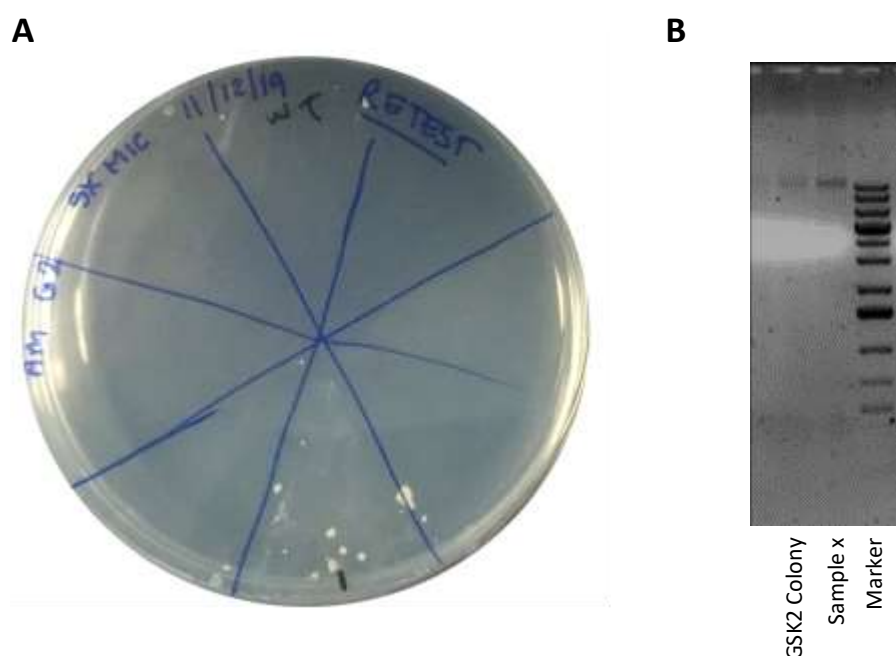
Figure 51. Spontaneous resistant mutant generation. *Mtb* was grown on solid media containing GSK2 at 5x MIC. A single colony was picked and retested on solid media before genomic DNA was extracted and sequenced by Microbes NG. A – Retest plate showing growth of colonies in the lower octant of the apparent resistant mutant, and no colonies in the upper WT octant. B – Agarose gel showing genomic DNA extracted from a colony grown on solid media containing GSK2 at 5x MIC. A faint band of DNA is visible at the top of the marker. Sample x is not relevant to this experiment.

1.2. Discussion

The urgent requirement for therapeutic regimens to combat MDR-TB has led to a concerted effort to identify novel compounds with anti-TB activities and to examine existing drugs which may be repurposed for use against TB. The focus of this work has been to validate the activity of a group of human DGAT1 inhibitors against mycobacteria and to identify their targets in *Mtb*. Preliminary data provided by GSK demonstrated the promising effects of four DGAT1 inhibitors against TB infected THP-1. Of the four DGAT1 inhibitors selected from the screening programmes by GSK, two exhibited activity against *M. bovis* BCG with MICs of 30 μM and 80 μM. The most potent of these compounds, termed GSK2, exhibited an IC90 of 10.9 μM in the initial macrophage studies (Table 4).

As inhibitors of human DGAT1, these compounds are known to reduce the accumulation of TAG in host macrophages. While a reduction of host TAG may contribute to the inhibition of TB in macrophages treated with DGAT1 inhibitors, it is not their sole mechanism of action against TB, as they effectively inhibit mycobacteria grown in the absence of macrophages. The storage of fatty acids as TAG for use as carbon and energy sources in both prokaryotes and eukaryotes has been well documented. Guided by the primary function of these drugs as DGAT1 inhibitors in humans, investigations into the mechanism of action of GSK2 against mycobacteria began with a focus on TAG synthesis in *Mtb.* Overexpression studies were employed to probe the effect of DGAT1 inhibitors on four Tgs proteins selected from the 15 putative Tgs proteins identified in *Mtb* (Table 2)*.* MIC testing revealed an increased tolerance of GSK2 in strains of *M. bovis* BCG

overexpressing the *Mtb* genes encoding *tgs3* and *tgs4* (Table 6, Figure 34)*.* An MIC increase in an overexpression strain can indicate that a function that was inhibited in WT has been restored, implicating the overexpressed gene as a potential target.

To further probe the mechanism of action of GSK2, lipid profiling was carried out for WT *M. bovis* BCG and for *M. bovis* BCG expressing *tgs1, tgs2, tgs3* and *tgs4* (Figures 37, 67, 68, 69 and 70). Two noteworthy changes occurred in the lipid profile of WT *M. bovis* BCG upon treatment with GSK2. The amount of TAG present in extractable apolar lipids was considerably depleted in treated cultures, and the FFAs from the same extractable fractions were more abundant. FFAs are of importance in the final step of TAG synthesis. The changes to both of these lipid groups are key indicators that GSK2 acts on TAG synthesis. Overexpressing TAG synthases in *M. bovis* BCG results in changes to PGLs in the absence of drugs, with *tgs3* and *tgs4* apparently lacking any PGLs, but the lipid profiles of all untreated strains otherwise matched that of WT *M. bovis* BCG. Overexpression of *tgs1, tgs2* and *tgs4* resulted in a similar accumulation of FFAs to WT *M. bovis* BCG with GSK2 treatment, and there were no significant changes to the lipid profiles. The amount of FFA present in treated samples of *M. bovis* BCG overexpressing *tgs3* was much reduced compared to treated WT, and its lipid profile was distinct in the absence of changes induced by GSK2 treatment.

Taken together, the increased MIC and lipid profile of *M. bovis* BCG pMV261-*tgs3* show that increased expression of Tgs3 reduces the effect of GSK2. The apolar lipids of WT *M. bovis* BCG and the Tgs3 overexpressor were more deeply examined through the utilisation of a variety of growth media. Growth in nitrogen deprivation conditions can

alter production of TAG and induce the formation of TAG containing ILIs (Santucci *et al.*, 2019). When grown in low nitrogen minimal media, *M. bovis* BCG pMV261-*tgs3* was the only strain to withstand treatment with GSK2, with an MIC of 30 μM (Table 7). Apolar lipids extracted from WT *M. bovis* BCG and *M. bovis* BCG pMV261-*tgs3* grown in 7H9, minimal media and low nitrogen minimal media showed significant differences between the two strains (Figures 38, 39 and 40). There was a particularly stark contrast between the survival of both strains in low nitrogen conditions, in which the strain expressing Tgs3 accumulated higher levels of TAG than in nutrient media, and WT *M. bovis* BCG exhibited extremely reduced TAG in low nitrogen conditions.

The lipid profile of WT *M. bovis* BCG treated with a second DGAT1 inhibitor, GSK4, was also assessed. With an MIC of 60 μM, GSK4 is an effective antimycobacterial, albeit considerably less potent than GSK2 which had an MIC of 30 μM. The lipid profile of WT *M. bovis* BCG showed the characteristic reduction in TAG and increase in FFA when treated with GSK2 typical of a TAG synthesis inhibitor. The high MIC for this drug unfortunately meant that testing sufficiently high concentrations of drug on multiple overexpressor strains was not feasible. As such, GSK2 was prioritised for target identification studies.

In an attempt to demonstrate the activity of GSK2 enzymatically, a number of techniques were employed. Firstly, Tgs1, Tgs2, Tgs3 and Tgs4 were expressed in *E. coli* BL21 DE3 for the purposes of purification and whole cell assays. Purification of Tgs2, Tgs3 and Tgs4 proved challenging, and the only protein expressed and purified to a suitable quality was Tgs1. Although the exact cellular locations of all 15 *Mtb* TAG

synthases have not been determined, many have been identified in cell membrane fractions (de Souza *et al*., 2011; Gu *et al*., 2003; Mawuenyega *et al*., 2005; Xiong *et al*., 2005). Membrane proteins are notoriously difficult to purify due to the need for detergents for solubilization and can be challenging to express in sufficient quantities, which may explain the need for further expression and purification trials for the majority of the proteins used in this work.

In the absence of purified protein, cell lysates from *E. coli* overexpressing TAG synthases was obtained for use in a fluorescent assay to quantitatively evaluate the *in vitro* activity of TAG synthesis. The assay measures the formation of the fluorescently labelled reaction product NBD-TAG which is synthesised when Tgs-containing cell lysate is incubated with NBD-palmitoyl-CoA and DAG (Coleman *et al.*, 1976; Coleman, 1992; McFie *et al.*, 2011). Unfortunately, TAG synthase activity was seen in the negative control, likely due to native *E. coli* Tgs proteins, and therefore the activity of individual Tgs proteins could not be determined. It was however interesting to note that inhibition of the native Tgs activity of *E. coli* cell lysate could be achieved with the addition of GSK2, further validating its activity an inhibitor of TAG synthesis (Figure 47).

Tgs1, the most well documented *Mtb* tgs protein, was purified with a sufficient yield to use in saturation binding assays which utilised the proteins intrinsic Trp fluorescence. Unexpectedly, a significant change in fluorescence was observed indicating the binding of GSK2 to Tgs1 with a K_D of 36.04 µM. Overexpression of Tgs1 in *M. bovis* BCG did not result in any significant changes to the lipid profile or MIC compared to WT *M. bovis* BCG and there were no other indications that the protein is targeted by GSK2. The binding

could be attributed to the fact that the TAG synthases of *Mtb* share an active site motif, and the similarities in binding site could be sufficient for off target binding to occur. Unfortunately, the protein showed no triacylglycerol synthase activity, suggesting a need for optimisation of the purification conditions, which meant that the activity of GSK2 against Tgs1 could not be established.

Of the triacylglycerol synthases used in this study, Tgs3 appears to be the primary target of GSK2. As a non-essential gene however, it is possible that Tgs3 is one of multiple GSK2 targets which together are responsible for the antimycobacterial effect. The generation of resistant mutants is a reliable way to validate potential drug targets when used in combination with other techniques. The incubation of *Mtb* H37Rv *ΔleuDΔpanCD* (mc^{2}7000) on high concentrations of GSK2 resulted in the generation of one single spontaneous resistant mutant colony. Analysis of whole genome sequencing did not reveal any high frequency mutations to genes of interest, and no mutations within essential genes. For the sequencing of spontaneous resistant mutants to provide reliable results, multiple colonies should ideally be sequenced revealing mutations to the same gene(s). Resistant mutant generation experiments can be repeated until a desired number of mutants have been obtained, but this can be time consuming and may simply not be possible if the target is an essential gene. Furthermore, it can be argued that the easy generation of resistant mutants, whilst a useful tool for target identification, is not desirable in the development of a new drug to combat MDR-TB.

In summary, the evidence presented in this chapter demonstrates the effectiveness of DGAT1 inhibitors in their use against TB. The results of experiments carried out to

elucidate the mechanism of action of GSK2 strongly suggest that Tgs3 is the target of this compound. The application of DGAT1 inhibitors in the treatment of TB could be an efficient way of denying the pathogen access to the valuable carbon source of host derived TAG, while also inhibiting the synthesis of mycobacterial TAG (Jaiyanth Daniel *et al.*, 2011). Specifically, the antimycobacterial characteristics of GSK2 have the potential to boost a host focused pharmacology approach (Shim, 2020), where DGAT1 is inhibited pharmacologically and DGAT2 is inhibited by the high levels of secreted Niacin which occurs in TB infections (Greenberg *et al.*, 1960; Ganji *et al.*, 2004). The risk of developing drug resistance with such an approach is low because, in the event of *Mtb* developing resistance to the direct antimicrobial effects of a DGAT1 inhibitor, inhibition of host TAG synthesis will continue to inhibit the growth of the pathogen. Administration of DGAT1 inhibitors with existing TB drugs could present an attractive treatment combination profile.

Further research is required to fully explain the mechanism of action of GSK2. The purification of Tgs3 and other triacylglycerol synthases should be prioritised so that binding assays, activity assays and crystallisation experiments can be carried out and hopefully demonstrate with more certainty the interaction between GSK2 and Tgs3. Additionally, the activity against *Mtb* of a wider range of DGAT1 inhibitors should be explored, delving deeper into their mechanisms of action. The precise functions of many of the putative *tgs* genes are yet to be confirmed. In *M. bovis* BCG, a group of proteins (Tgs1 (BCG_3153c), Tgs2 (BCG_3794c), BCG_1169c, BCG_1489c and BCG_1721) have been associated with lipid droplet formation, some of which thought to have bi-functional roles both in promoting the build-up of TAG and in the hydrolysis of TAG (Low

et al., 2010). A better understanding of the role of Tgs3 and other triacylglycerol synthases in *Mtb* is needed in order to exploit the synthesis, accumulation and hydrolysis of TAG as targets of antimycobacterial compounds.

Chapter 4

Target Elucidation of Human Kinase Inhibitors that Target *Mycobacterium tuberculosis*

2. Target Elucidation of Human Kinase Inhibitors that Target *Mycobacterium tuberculosis*
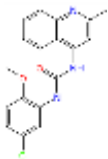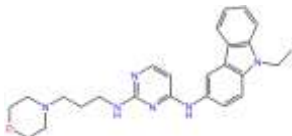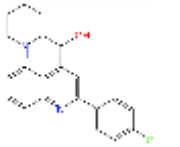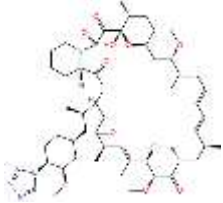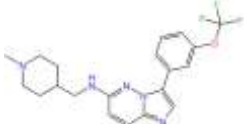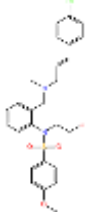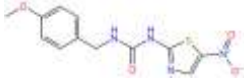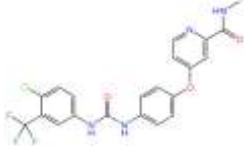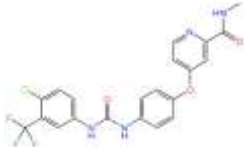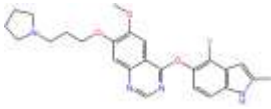
2.1. Introduction
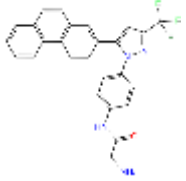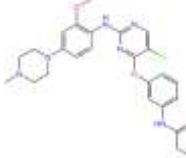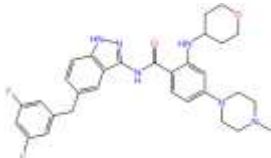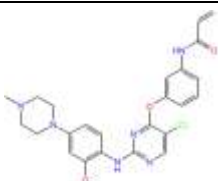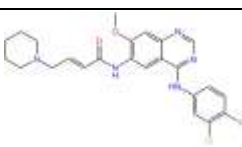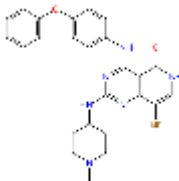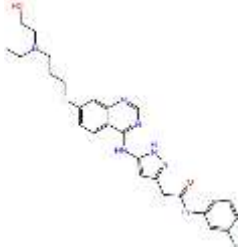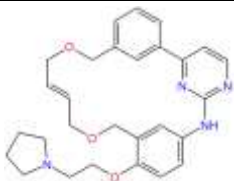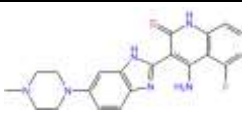
In this chapter, methods of target identification were explored for a group of 30 phenotypic hits, selected from a HTS programme on the basis of their activity against *Mtb* at 20 µM. The first strategy used was the generation of resistance mutants against the 30 compounds, all of which were commercially available compounds with activity against human kinases. Mutants raised to the kinase inhibitors were subjected to genomic analysis to determine genes of interest. Subsequently, protein overexpression techniques were used to probe potential targets. Finally, tools for the biochemical characterisation of potential hits were evaluated and consideration was given to the suitability of the methods used in this study.
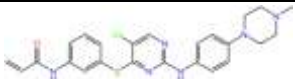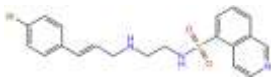
2.2. Results

2.2.1. Minimum Inhibitory Concentrations (MICs) on Solid

A large group of human kinase inhibitors were screened in liquid against *Mtb* in a preliminary study carried out by collaborators (Dr Reynolds, University of Alabama). A group of 30 hits exhibiting the greatest activity against *Mtb* were selected based on the percentage inhibition at 20 µM and their MIC90s. These compounds were carried forward for further whole cell testing in different mycobacterial species and for target elucidation studies. The 30 most potent compounds which showed inhibition of over 90% of growth at 20 µM are displayed in Table 9. The MIC90s for four compounds (BR18, BR21, BR15, BR5) were below 5 µM and a further 9 compounds had MIC90s below 10 µM. The hits from the preliminary screening were re-tested against *M.bovis* BCG, *Mtb* H37Rv and *Mtb* H37Rv mc^{2}7000 on solid media in order to obtain MIC values for the generation of resistant mutants. The solubility of 5 compounds were considered to be poor and did not allow for sufficient concentrations to be reached in solid media without the compound precipitating. These inhibitors were excluded from further screening efforts. Solid MICs were determined as the lowest concentration of inhibitor tested on which there was no visible growth. A further 5 compounds did not inhibit growth at any of the concentrations tested, these too were excluded from further experiments as the MICs were deemed to be too high for resistant mutant generation at 5x and 10x MIC. The lowest MIC obtained against *M. bovis* BCG was for BR5 at 6 µM, and a total of 9 compounds had MICs of 10 µM or lower (Figures 52 and 53, and Table 10).

Table 94. 30 BR compounds selected based on their activity against *Mtb* H37Rv. Compounds have been ranked by their MIC90.

	Compound name	MIC90 (µM)	Structure
BR18	PFK15	3.28	
BR21	URMC-099	3.71	
BR15	LDK378	4.79	
BR5	Foretinib (GSK1363089)	4.96	
BR24	Akti-1/2	6.38	
BR17	GZD824	9.33	
BR10	Ponatinib (AP24534)	9.43	
BR14	Cabozantinib malate (XL184)	9.59	
BR9	AEE788 (NVP-AEE788)	9.65	

	Compound name	MIC90 (µM)	Structure
BR29	PQ 401	9.66	
BR20	EHop-016	9.69	
BR22	Vacquinol-1	9.95	
BR16	Zotarolimus(ABT-578)	9.97	
BR12	SGI-1776 free base	10.45	
BR25	KN-93 Phosphate	12.68	
BR27	AR-A014418	13.81	
BR26	Sorafenib	14.38	
BR3	Sorafenib Tosylate	15.19	
BR1	Cediranib (AZD2171)	16.51	

	Compound name	MIC90 (µM)	Structure
BR4	OSU-03012 (AR-12)	18.55	
BR19	WZ4003	18.71	
BR23	Entrectinib (RXDX-101)	18.92	
BR7	WZ4002	19.00	
BR13	Dacomitinib (PF299804, PF299)	19.34	
BR28	G-749	19.39	
BR6	Barasertib (AZD1152-HQPA)	19.42	
BR30	Pacritinib (SB1518)	19.54	
BR2	Dovitinib (TKI-258, CHIR-258)	19.77	

	Compound name	MIC90 (µM)	Structure
BR8	WZ8040	19.82	
BR11	H 89 2HCl	19.98	

Screening of 17 inhibitors, selected for their superior solubility, against *Mtb* H37Rv revealed that 7 of the compounds had solid media MICs of 10 µM of less (Figure 54 and Table 10). A further 8 compounds inhibited growth with MICs up to 50 µM. MICs were not obtained for BR11 and BR27, as they inhibited all growth at the lowest concentrations tested (10 µM and 20 µM, respectively). Meanwhile BR12 and BR25 were considered to have MICs close to 15 µM, the highest concentration tested, but did not entirely inhibit visible growth at this concentration. The MICs of most compounds against *Mtb* strains were found to be similar or lower than the *M. bovis* BCG MICs.

Multi-well MIC plates were prepared and sent to Dr Alistair Brown at Newcastle University, who inoculated them with *Mtb* H37Rv *ΔleuDΔpanCD* (mc²7000). MICs were obtained for BR1, BR8, BR10, BR19, BR20, BR22, BR23, BR28 and BR29 and large 20cm solid plates were prepared for each compound at 0 x, 5 x and 10 x the MIC for mutant generation (Table 10).

Table 10 Solid MICs for *M. bovis* BCG, *Mtb* H37Rv, *Mtb* H37Rv mc^{2}7000 plates for BR compounds. Strains were grown on the appropriate solid media supplemented with a range of concentrations of BR compounds. MICs were determined as the lowest concentration at which growth was inhibited upon visual inspection of the plates.

Compound	MIC BCG (μM)	MIC *Mtb* H37Rv (μM)	MIC *Mtb* H37Rv mc^{2}7000 (μM)
BR1	20	-	10
BR4	10	15	-
BR5	6	7.5	-
BR6	>30	35	-
BR8	>30	50	50
BR9	20	15	-
BR10	15	15	10
BR11	25	<10	-
BR12	10	>15	-
BR13	20	-	-
BR14	15	10	-
BR16	>20	-	-
BR17	15	15	-
BR19	20	-	20
BR20	10	10	10
BR21	>20	-	-
BR22	10	7.5	7.5
BR23	25	20	20
BR24	10	7.5	-
BR25	10	>15	-
BR26	>30	35	-
BR27	>30	<15	-
BR28	10	-	10
BR29	10	-	12.5
BR30	>30	-	-
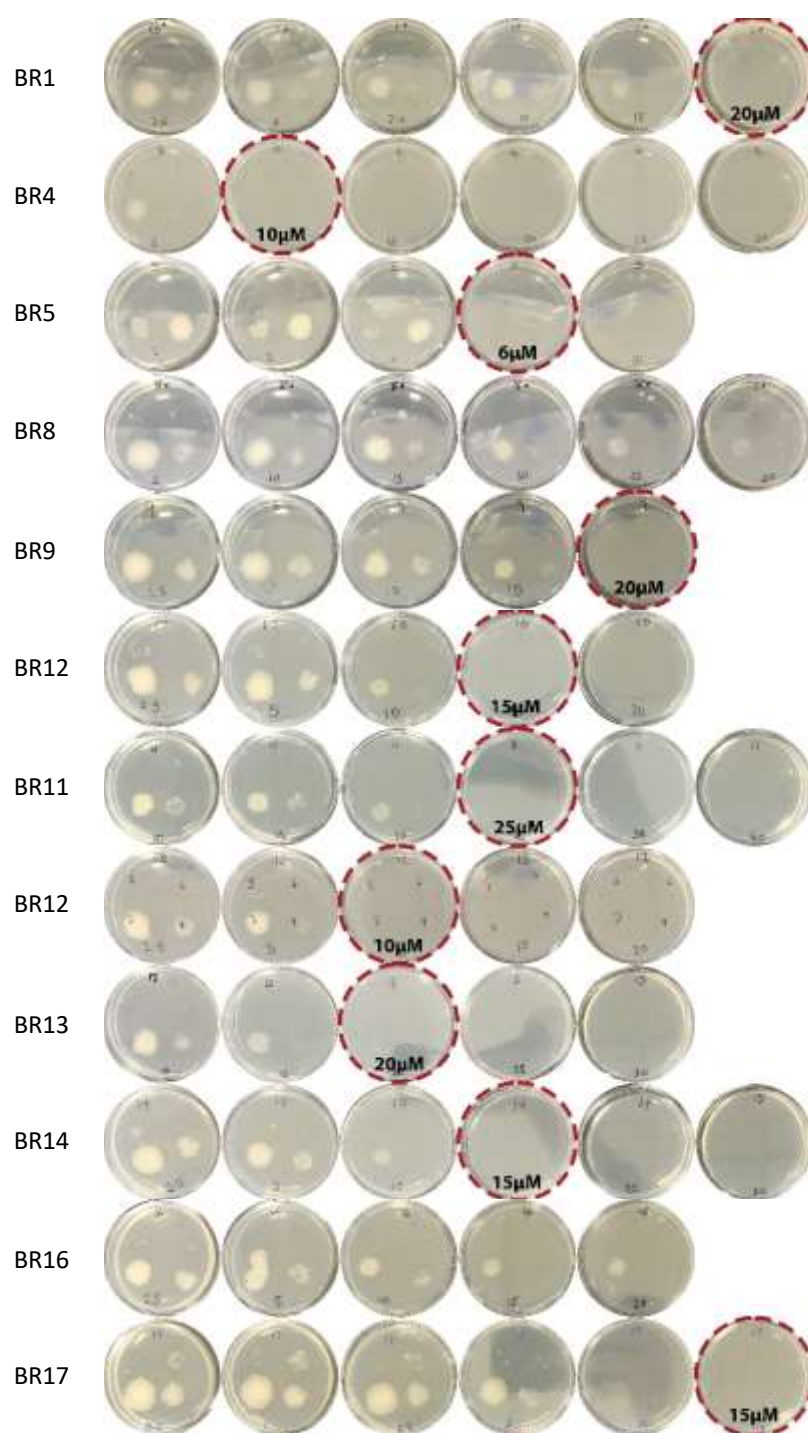
Figure 52. Solid *M. bovis* BCG MIC plates for BR compounds. *M. bovis* BCG was grown on 7H11 solid media supplemented with a range of concentrations of BR compounds. MIC values were determined by the lowest concentration at which no growth was visible (circled in red).
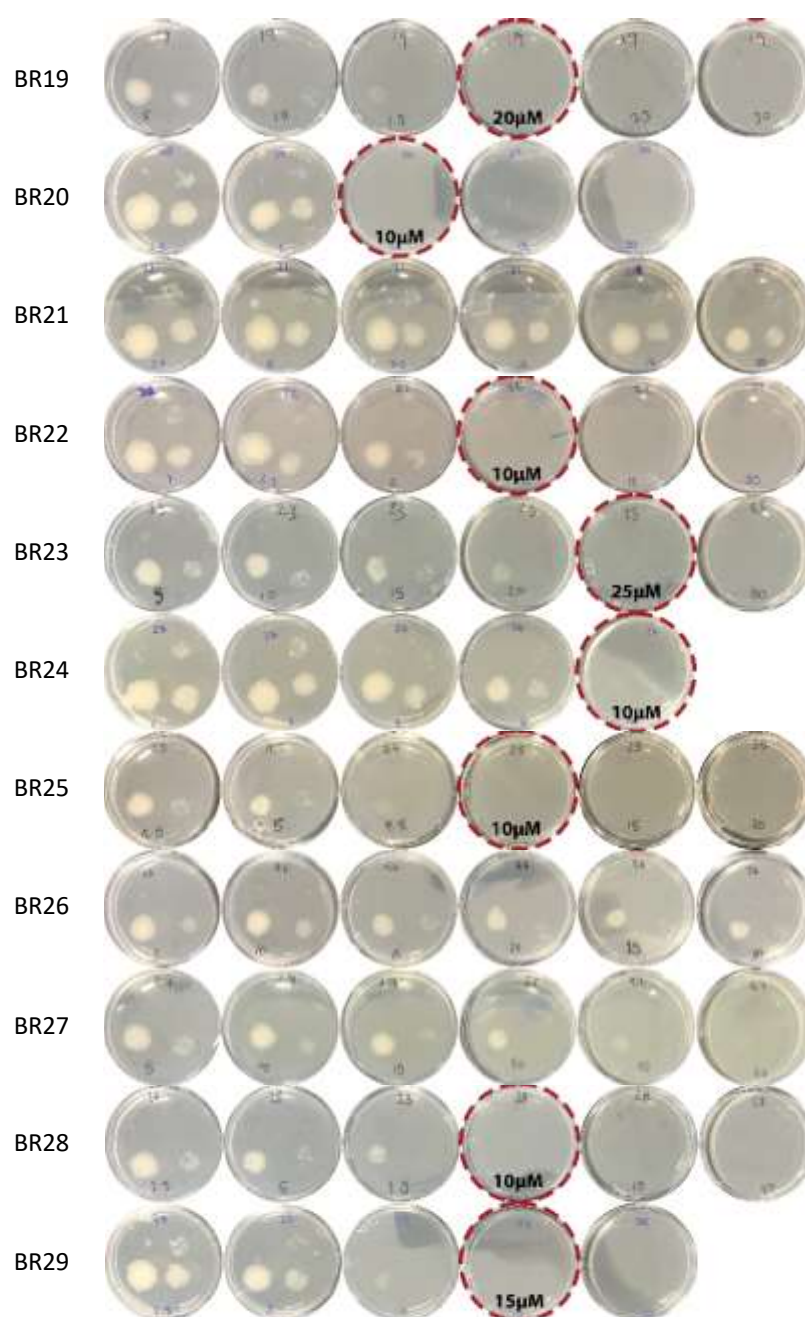
Figure 53. Solid *M. bovis* BCG MIC plates for BR compounds. *M. bovis* BCG was grown on 7H11 solid media supplemented with a range of concentrations of BR compounds. MIC values were determined by the lowest concentration at which no growth was visible (circled in red).
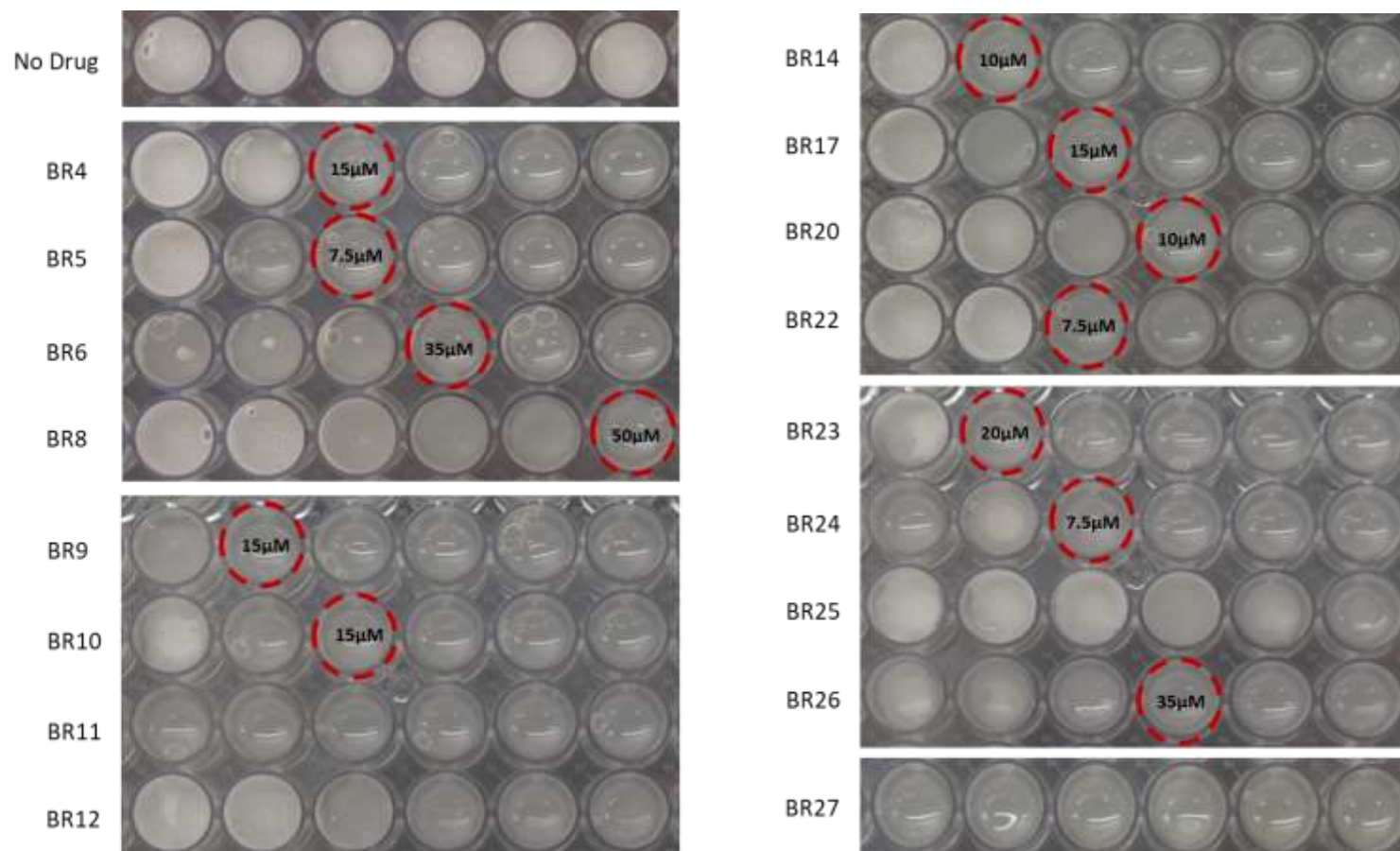
Figure 54. Solid *Mtb* H37Rv MIC plates for BR compounds. *Mtb* H37Rv was grown on the appropriate solid media supplemented with a range of concentrations of BR compounds. MIC values were determined by the lowest concentration at which no growth was visible (circled in red).

2.2.2.   Generation of Resistant Mutants

Colonies picked from high drug concentration plates were re-tested on 0 x, 5 x and 10 x

MIC plates alongside *Mtb* H37Rv *ΔleuDΔpanCD* (mc^{2}7000) which had not been exposed

to drug to confirm resistance (Figure 55). Colonies which grew on the high concentration

re-test plates were considered potential mutants if the parental strain did not grow and

were subsequently picked for genomic DNA extraction. Agarose gels were run to confirm

the presence of genomic DNA in the extracted samples and to check for degradation.

Samples were then sent for whole genome sequencing by Microbes NG (Figure 56).
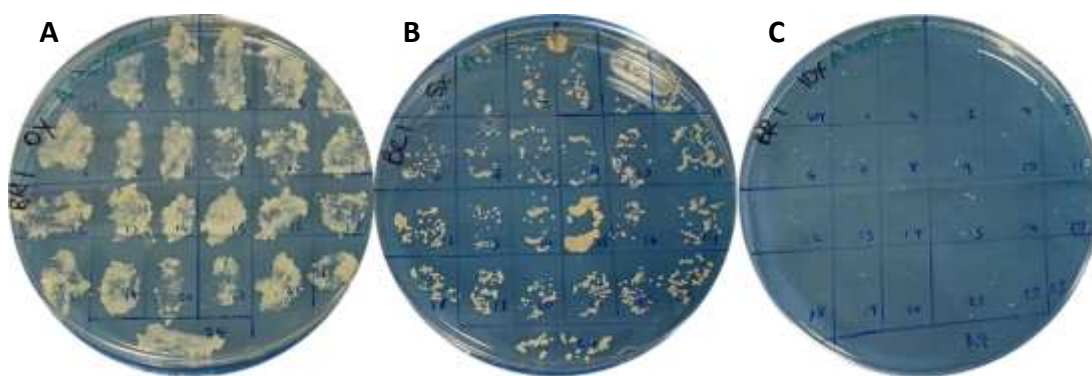
Figure 55. *Mtb* **H37Rv *ΔleuDΔpanCD* (mc^{2}7000) resistant mutant retest plates for BR1.** *Mtb* H37Rv *ΔleuDΔpanCD* (mc^{2}7000) mutants were raised on media containing BR compounds at concentrations in excess of their MICs. Colonies selected from high concentration mutant generation plates were retested at 0 x (A), 5 x (B) and 10 x (C) MIC plates alongside a control strain of *Mtb* H37Rv *ΔleuDΔpanCD* (mc^{2}7000) which had not previously been exposed to the drug.
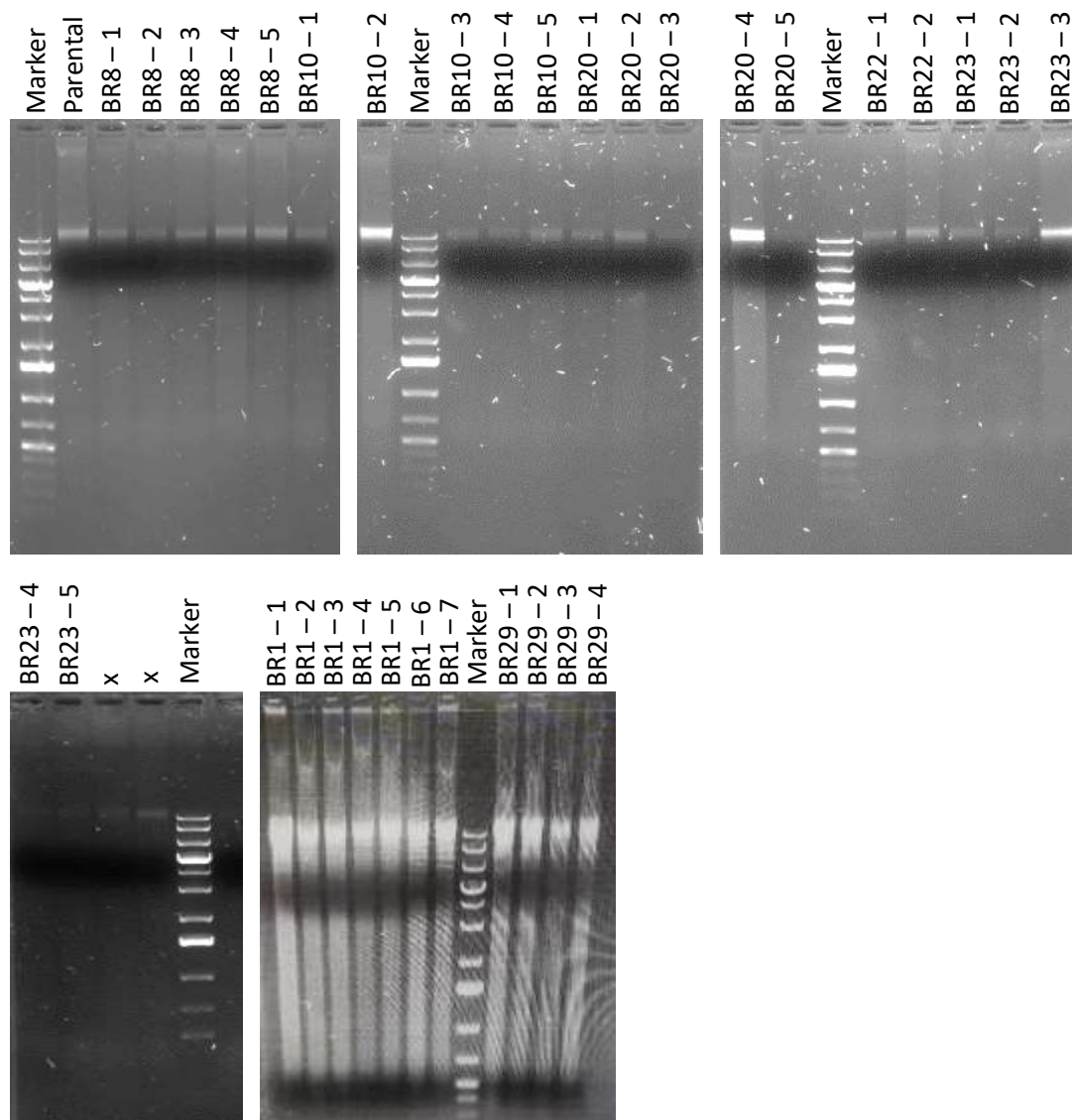
Figure 56. Agarose gels showing the presence of genomic DNA extracted from *Mtb* H37Rv mc²7000. Genomic extractions were carried out on colonies selected from high concentration BR plates. Extraction samples were separated by SDS PAGE and checked for the presence of a single band of genomic DNA towards the top of the gel before being sent for sequencing by Microbes NG. Lanes labelled x contain DNA samples not related to this set of resistant mutants.

The mutations were reviewed to identify any possible kinase involvement, off target mutations, such as efflux systems, and to determine which genes were essential (Tables 11 and 12). One mutation, a codon substitution in Rv3239c, which occurred in a mutant raised against BR1, may indicate efflux activity. Rv3239c is a probable transmembrane transport protein which is relatively conserved. It shares a 423 amino acid overlap (31.9% similarity) with Rv1250, another probable membrane transport protein which is implicated in drug export (Cole *et al*., 1998). Rv1250 is overexpressed in strains exposed to INH and RIF stress and is expressed at higher levels in MDR clinical isolates than drug susceptible strains (Guilian Li *et al*., 2015). It is likely that the mutation in Rv3239c is related to the export of BR1 rather than Rv3239c being a direct target of this drug.

Four affected genes were reported as essential in the literature: Rv2553c (Griffin *et al*., 2011; Minato *et al*., 2019; Sassetti and Rubin, 2003), *hemD* (Rv0511) (Dejesus *et al*., 2017; Griffin *et al*., 2011; Minato *et al*., 2019; Sassetti, Boyd, *et al*., 2003), *ponA1* (Rv0050) (Griffin *et al*., 2011; Minato *et al*., 2019) and *tyrA* (Rv3754) (Dejesus *et al*., 2017; Griffin *et al*., 2011; Minato *et al*., 2019). Rv2553c is a probable conserved protein about which little is known. Polymorphisms have been reported in Rv2553c in lab strains. Specifically a +3 bp indel at position 53 of 417 amino acids, a similar region to the +3 bp indel seen in mutant BR22 – 2 (Ioerger *et al*., 2010).

hemD, the probable uroporphyrin-III C-methyltransferase, catalyses methylation reactions as part of the cobalamin (vitamin B_{12}) biosynthetic pathway (Warren *et al.*, 1990a; Warren *et al.*, 1990b; Schubert *et al.*, 2002). The first reaction converts the macrocyclic tetrapyrrole uroporphyrinogen III into precorrin-1 before a second reaction

converts precorrin-1 to precorrin-2 (Warren *et al.*, 1990a; Warren *et al.*, 1990b; Schubert *et al.*, 2002).

A mutation was detected in BR29 – 2 in the essential gene *tyrA*, a shikimate pathway prephenate dehydrogenase which catalyses the dehydrogenation of prephenate to form tyrosine. In *Mtb,* TyrA forms part of the regulatory subunit of the aspartate kinase, MtbAKβ, which comprises two aspartate kinase, chorismate mutase, TyrA (ACT) domains (Yang *et al.*, 2011). BR29 (PQ401) inhibits type I insulin-like growth factor receptor (IGF-IR) signalling. Binding of IGF to receptors on the cell surface triggers signalling by a number of kinase mediated signalling pathways. IGF-IR is a receptor tyrosine kinase (Hua *et al.*, 2020).

PonA1 is an essential (probable) penicillin binding protein (PBP), with a role in cell elongation and division (Kieser *et al.*, 2015). During cell division, PonA1 is thought to be localised at the poles where it interacts with RipA, a peptidoglycan hydrolase (Hett *et al.*, 2010). The cytoplasmic tail of PonA1 acts as a substrate for PknB, a serine-threonine protein kinase in *Mtb* (Prisic *et al.*, 2010)*.* Specifically, PknB phosphorylates PonA1 at its T34 residue (Kieser *et al.*, 2015). The rate of cell elongation appears to be mediated by the phosphorylation of PonA1. Changes to the rate of PonA1 activity has a direct impact on cell survival. It could be hypothesised that a reduction in the rate phosphorylation of PonA1 due to kinase inhibition could impact PonA1 activity. In a single mutant raised to BR20 a PonA1 proline to serine codon substitution was observed at P631S.

Table 51. Whole genome sequencing results. Variants were reviewed based on their frequency and type (eg substitution or deletion). High frequency mutations are listed with the codon substitution and corresponding amino acid substitution. Where no substitute codon or amino acid is listed, the mutation is a frame shift. Sample number should be read with preceding drug number, eg BR1 – 1 to correspond with numbering used in Figure 56.

Drug	Sample number							Locus	Codon substitution	Amino acid substitution
	1	2	3	4	5	6	7			
BR1	●	●	●	●	●	○	●	Rv1543	Acc/Gcc	T233A
	○	○	○	●	○	○	○	Rv3239c	Cac/Tac	H260Y
	○	○	○	●	○	○	○	Rv2566	cgt/Gcgt	R13A?
	○	○	○	●	○	○	○	*amt*	tcT/tcC	S403
	○	○	○	●	○	○	○	Rv0074	ccg/AGCccg	P259SP
	○	○	○	●	○	○	○	*end*	ggc/	G202
	○	○	○	●	○	○	○	*hemD*	cgt/cCgt	R117P?
	○	○	○	●	○	○	○	*ilvE*	cct/	P183
	○	○	○	○	○	●	○	Rv3680	gtc/	V123
	○	○	○	●	●	●	○	*PE_PGRS54*	ggG/ggC	G1243
	○	○	○	●	●	○	●	*PE_PGRS54*	gCc/gAc	A1497D
	○	○	○	○	●	●	●	*PE_PGRS54*	gTc/gCc	V1444A
BR10	○	○	○	○	●	-	-	*PE_PGRS10*	Agg/Ggg	R225G
	○	○	○	○	●	-	-	*PE_PGRS10*	Cgc/Ggc	R227G
BR20	○	●	○	○	○	-	-	*PPE18*	Gtg/Acg	V55E
	○	●	○	○	○	-	-	*PPE18*	cGg/cAg	R287Q
	○	●	○	○	○	-	-	*PPE18*	gGt/gCt	G303A
	○	○	●	●	○	-	-	*PPE18*	Cag/Aag	Q30K
	○	○	○	●	○	-	-	*ponA1*	Ccg/Tcg	P631S
BR22	○	●	-	-	-	-	-	Rv2553c	gcc/gTGGcc	A58VA
BR23	○	●	●	○	○	-	-	*glnA2*	Tcg/Ccg	S332P
	○	○	●	○	○	-	-	Rv2553c	gcc/gTGGcc	A58VA
	○	○	○	○	●	-	-	*PPE18*	Cag/Aag	Q30K
	○	○	○	○	●	-	-	Rv1543	Acc/Gcc	T233A
BR29	●	○	●	○	-	-	-	Rv1635c	acc/	T456
	○	●	○	●	-	-	-	*Hsd4B*	Gca/Aca	A226T
	○	●	○	○	-	-	-	Rv3786c	gat/	D127
	○	●	○	○	-	-	-	*tyrA*	ggc/	G287
	●	●	●	●	-	-	-	*PE_PGRS54*	ggG/ggC	G1243
	●	○	●	●	-	-	-	*PE_PGRS54*	gCc/gAc	A1497D
	○	●	●	○	-	-	-	*PE_PGRS54*	gCc/gAc	A1702D
	●	○	○	●	-	-	-	*PE_PGRS54*	gAc/gGc	D754G
	●	●	●	●	-	-	-	*PE_PGRS54*	gTc/gCc	V1444A

Table 62. Mutations identified from whole genome sequencing of mutants raised to BR compounds. High frequency mutations were investigated to determine the essentiality and function of the genes in which the mutations were identified. [a] Mawuenyega *et al.*, 2005; [b] Griffin *et al.*, 2011; [c] Dejesus *et al.*, 2017; [d] Sassetti, Boyd and Rubin, 2003; [e] Minato *et al.*, 2019; [f] Sassetti and Rubin, 2003

Locus	Essentiality	Function
Rv0074	Non-essential [a,b,c]	Conserved protein with unknown function
Rv1543	Non-essential [b,d,e] (Griffin *et al.*, 2011; Minato *et al.*, 2019; Sassetti, Boyd, *et al.*, 2003)	Possible fatty acyl-CoA reductase
Rv1635c	Non-essential [c,d,e]	Probable mannosyltransferase/conserved transmembrane protein.
Rv2553c	Essential [b,e,f]	Probable conserved membrane protein
Rv2566	Non-essential [b,c,d]	Long conserved protein
Rv3239c	Non-essential [b,c,d,e]	Probable conserved transmembrane transport protein. Possible involvement in efflux system (probably sugar or drug transport).
Rv3680	Non-essential [c,e]	Probable anion transporter ATPase
Rv3786c	Non-essential [b,c,d,e]	Unknown protein
amt	Non-essential [b,c,d,e]	Probable ammonium-transport integral membrane protein.
end	Non-essential [b,d,e]	Probable endonuclease IV
glnA2	Non-essential [c,e]	Probable glutamine synthetase (GS-II)
hemD	Essential [b,c,d,e]	Probable uroporphyrin-III C-methyltransferase. Possible involvement in siroheme and cobalamin biosynthesis
hsd4B	Non-essential [c,d,e]	Probable dehydrogenase. Possible 2-enoyl acyl-CoA hydratase.
ilvE	Non-essential [b,c,d,e]	Branched-chain amino acid transaminase
PE_PGRS54	Non-essential [b,c]	Function unknown
PE_PGRS10	Non-essential [b,c]	Function unknown
ponA1	Essential [b,e] / Non-essential [c,d]	Probable bifunctional penicillin-binding protein
PPE18	Non-essential [c,d,e]	Function unknown
tyrA	Essential [b,d,e]	Prephenate dehydrogenase (PDH) (hydroxyphenylpyruvate synthase). Involved in tyrosine biosynthesis.

2.2.3. Construction of Strains Overexpressing Potential Targets

Overexpression strains were constructed for genes identified as potential targets by WGS of resistant mutants. Genomic DNA was sent for sequencing in batches as mutants were generated over a number of months. The first set of genes to be identified by WGS included Rv1543, Rv1196 (PPE18) and Rv2222c (*GlnA2*). Due to time constraints, it was not possible to produce overexpression constructs for other genes identified in later sequencing runs. Gene inserts were generated by PCR using the primers in Table 13 and the size of each insert was checked on agarose gels prior insertion into pMV261 (Figure 57). *M. bovis* BCG was transformed with ligated constructs sequenced by Source Bioscience.
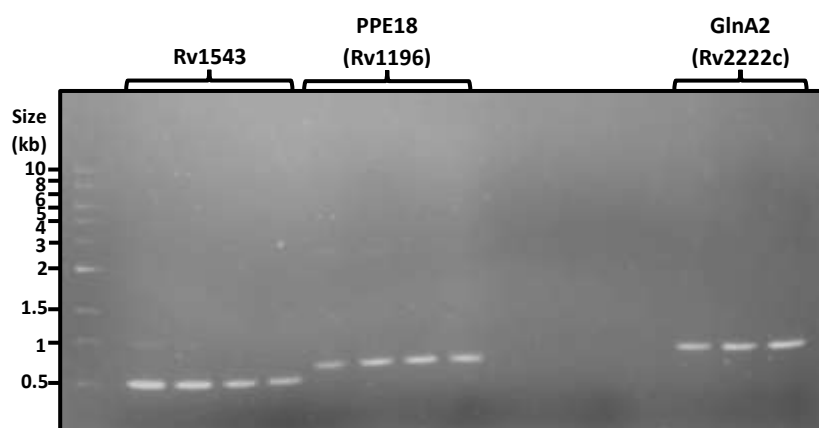
Figure 57. PCR of gene inserts. *Mtb* genes were amplified using PCR for insertion into plasmid vectors. PCR products were run on 1% agarose gels to confirm the size of the inserts. Lane 1 - 10kb ladder; lanes 2 - 5 - Rv1543; lanes 6 - 9 - PPE18 (Rv1196); lanes 10 - 13 - blank; lanes 14 - 16 - GlnA2 (Rv222c). The last band for each insert (lanes 5, 9 and 16) were selected to be sequenced by Source Bioscience.

2.2.4. Overexpression of Potential Target Genes

The genes that were overexpressed based on mutations found in WGS were tested against the corresponding BR compound that caused each mutation in order to determine MICs. The BR compounds were also tested against *M. bovis* BCG pMV261-

empty (EV) so as to compare MICs. No gene caused an increase in MIC in the overexpression strain compared to the empty vector (EV) control. BR1, BR23 and BR29 were tested against *M. bovis* BCG pMV261-Rv1543 with MICs of 20 µM, 50 µM and 20 µM respectively, compared to an EV MIC of >50 µM for all three compounds. BR20 and BR23 were tested against *M. bovis* BCG pMV261-*ppe18* with MICs of 10 µM and 50 µM respectively with an EV MIC of >50 µM for BR20 and 50 µM for BR23. Finally, BR23 was tested against *M. bovis* BCG pMV261-*glnA2* and EV with MICs of 20 µM and 50 µM, respectively (Figures 58 and 59).
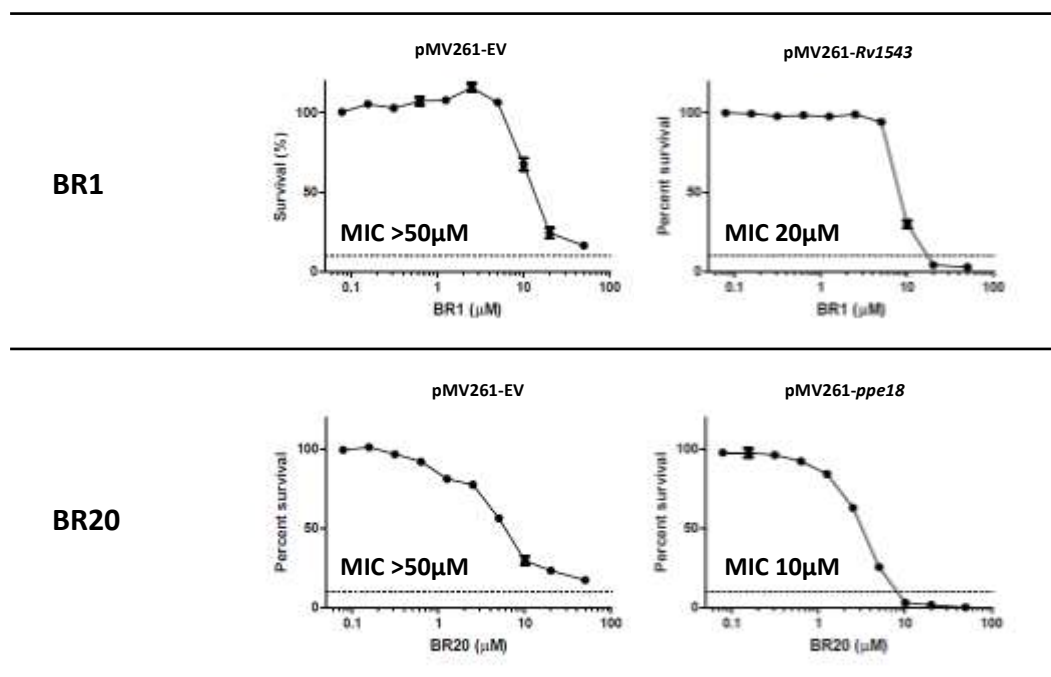
Figure 58. Minimal inhibitory concentrations of BR compounds against *M. bovis* BCG overexpressing genes identified as potential targets. Overexpression strains of *M. bovis* BCG were incubated in the presence of BR compounds for 7 days after which a resazurin assay was used to determine cell survival. Results were normalised by percentage normalisation. GraphPad prism was used to generate a graph showing the mean of 3 technical repeats with standard deviation.
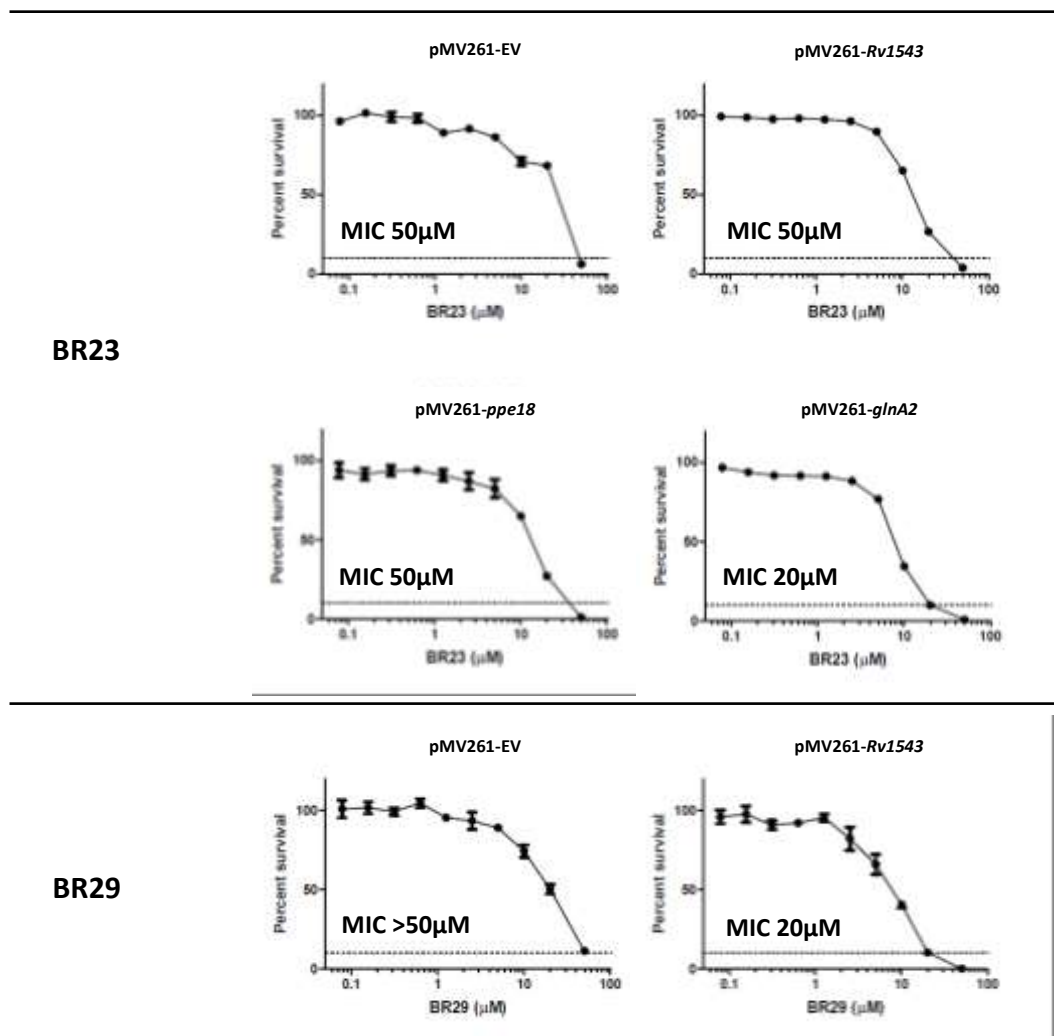
Figure 59. Minimal inhibitory concentrations of BR compounds against *M. bovis* BCG overexpressing genes identified as potential targets. Overexpression strains of *M. bovis* BCG were incubated in the presence of BR compounds for 7 days after which a resazurin assay was used to determine cell survival. Results were normalised by percentage normalisation. GraphPad prism was used to generate a graph showing the mean of 3 technical repeats with standard deviation.

2.3. Discussion

Kinases are a group of enzymes with phosphorylation activities, which act by transferring a phosphate from ATP to a substrate (Figure 60). They can be divided into four groups – protein kinases, carbohydrate kinases, lipid kinases and other kinases – based on their substrate preferences. This varied family of enzymes can be found in a wide range of organisms from humans to plants and bacteria. Up to 30% of the human proteome undergoes modification by the 518 human protein kinases, encoded for by approximately 2% of human genes (Manning *et al*., 2002).
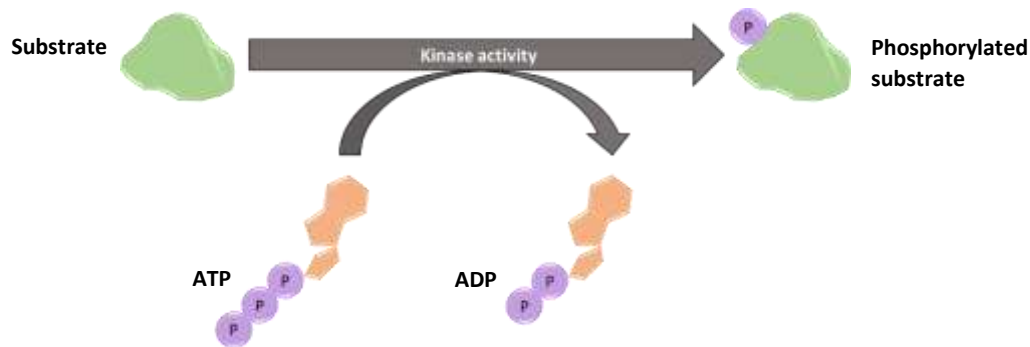
Figure 60. Kinase phosphorylation activity. Kinase proteins catalyse the phosphorylation of specific substrates, using a phosphate group from adenosine triphosphate (ATP).

Kinases are of importance to many cellular processes including metabolism, signalling, transport and the regulation of proteins. The deregulation of kinases is a hallmark of numerous diseases (Knapp, 2018). In many oncological conditions for example, protein kinases cease to function in a controlled manner, which leads to various aspects of cell growth and death becoming unregulated. Other disease groups affected by protein kinase deregulation include immunological, inflammatory, cardiovascular, degenerative and metabolic conditions (Fabbro, 2015; Ferguson *et al*., 2018; Müller *et al*., 2015; Xie *et al*., 2021). Due to the significance of kinase function in pathology, they have been

widely researched and a wealth of drugs exist to regulate or inhibit human kinases primarily for the treatment of cancers. There are currently 283 protein kinase inhibitors listed on PKIDB, an online database of protein kinase inhibitors, 69 of which have been approved by the FDA (Bournez *et al.*, 2020; Carles *et al.*, 2018) (accessed 02 October 2021). The successful development of human kinase inhibitors for cancer treatment has resulted in a large body of data demonstrating the LADMET and DMPK properties, and the performance of specific drugs in clinical trials as well as their specific mechanisms of action. This abundance of data has contributed to the development of a further 10 FDA approved protein kinase inhibitors for non-oncological conditions. Protein kinase inhibitors have two classifications: monoclonal antibodies (mAbs) and small molecule kinase inhibitors (SMKIs). SMKIs have gained popularity due to their relatively low production costs and stability compared to mAbs (Xie *et al.*, 2021; Zhan *et al.*, 2016).

The ubiquity of kinases across eukaryotic and prokaryotic species led to suggestions that human kinase inhibitors could be repurposed for the treatment of infectious diseases. The activity of kinase inhibitors in infectious diseases treatment can either work through the direct inhibition of the pathogen, or modulation of the host's response to the pathogen through host kinase inhibition. Recently there has been particular interest in using kinase inhibitors for the treatment of COVID-19. The Janus Kinase (JAK) family of human transmembrane protein kinases are involved in cytokine signalling (Xie *et al.*, 2021). Inhibiting JAKs has the potential to improve COVID-19 outcomes by managing the host's inflammatory response to the virus (Virtanen *et al.*, 2019; Spinelli *et al.*, 2020; Guimarães *et al.*, 2021; Hayek *et al.*, 2021; Petrone *et al.*, 2021; Walz *et al.*, 2021). Tofacitinib (Guimarães *et al.*, 2021) and baricitinib (Petrone *et al.*, 2021) are among the

many licenced kinase inhibitors which have been trialled in COVID-19 treatments to improve patient outcomes.

Screening of SMKIs against a variety of pathogens and parasites including *Staphylococcus aureus* (Le *et al*., 2020), *Plasmodium falciparum* (Hallyburton *et al*., 2017; Kesely *et al*., 2020) and *M. tuberculosis* (Shapira *et al*., 2020) has been carried out with numerous positive outcomes. While the activity of kinases against eukaryotes has been known for twenty years (Burk *et al.*, 2002), activity against *P. falciparum* kinases has only recently been reported in a number of human kinases, which are now being investigated as treatment options for malaria (Arendse *et al*., 2021; Hallyburton *et al*., 2017; Kesely *et al*., 2020). Major challenges arise when using human kinase inhibitors to inform the design of pathogen kinase inhibitors. The highly conserved ATP binding site of kinases means that drug specificity over human orthologues can be difficult to achieve (Arendse *et al*., 2021). Nevertheless, they offer a novel class of drugs for many infections.

The use of kinases inhibitors for host-directed treatment of *Mtb* has been proposed based on a number of *in vivo* and *ex vivo* studies (Shapira *et al*., 2020; Young *et al*., 2020). Imatinib, for example, reduced granuloma formation and bacterial load in mice (Napier *et al*., 2011), while the epidermal growth factor receptor (EGFR) tyrosine kinase, Gefitinib, reduced the growth of *Mtb* in infected macrophages through increased lysosomal biogenesis (Sogi *et al*., 2017).

In this study, 30 compounds with known activity against human kinases, were selected from a high-throughput screen in which there were discovered to inhibit the growth of *Mtb* by >90% at 20 µM. A combination of target-based and drug-based approaches were

used to test the activity of these compounds against multiple mycobacterial species and to probe their cellular targets. The generation of resistant mutants was considered a logical starting point for target identification studies as it has the potential to provide precise information on genes of interest without the need for proteins to be extracted (chemoproteomics) which is unsuitable if the target protein is unstable or for metabolites to be extracted (metabolomics), both of which are time consuming and expensive when dealing with multiple compounds.

MICs were established for 25 kinase inhibitors against *M. bovis* BCG, 17 against *Mtb* H37Rv and 9 against *Mtb* H37Rv mc^{2}7000. Guided by the MICs, mutant generation plates were set up at high drug concentrations for the 9 compounds tested against *Mtb* H37Rv mc^{2}7000, resulting in mutant colonies on 6 compound plates. WGS of the mutant genomes identified a total of 33 mutations of potential interest in 19 different genes. Literature searches did not uncover any kinases in the list of genes, however 4 of the 33 genes were found to be essential and 2 genes (*ponA1* and *tyrA*) were involved in the activity of other kinase enzymes. At least one gene, Rv3239c, is implicated in drug efflux and the mutation likely conferred resistance by encoding the export of BR1 out of the cell.

PonA1, a probable PBP, was mutated by way of a SNP in one strain grown on BR20. The role of PonA1 in cell elongation and division is highly regulated by phosphorylation by PknB, an *Mtb* serine-threonine protein kinase (Hett *et al*., 2010; Kieser *et al*., 2015; Prisic *et al*., 2010). BR20, also known as EHop-016, is an inhibitor of Rac, a Rho family GTPase in humans (Montalvo-Ortiz *et al*., 2012). It also inhibits the activity of p21-activated

kinase (PAK), a Rac downstream effector (Castillo-Pichardo *et al*., 2014). Rac GTPases are involved in the regulation of cytoskeletal dynamics including cell polarity regulation and, like PonA1, are regulated themselves by phosphorylation (Chardin, 2006; Heasman *et al*., 2008). PonA1 and Rac GTPases are similar in their role in the regulation of structural features of the cell. A frame shift mutation was detected in TyrA, a shikimate pathway prephenate dehydrogenase which is a key component of the aspartate kinase regulatory subunit MtbAKβ. The mutation arose in cells exposed to BR29, an IGF-IR inhibitor known as PQ401 which is interrupts kinase signalling.

Once WGS data was processed, genes of interest were cloned into the mycobacterial expression vector pMV261 for overexpression studies. Genomic DNA was sent for sequencing in batches as mutants were generated over a number of months. The first set of genes interested detected from sequencing results included Rv1543, PPE18 and GlnA2. These genes were considered worth investigating because of the strength and frequency with which the mutations occurred, although there was no evidence of gene essentiality or involvement in kinase activity. No increase in MIC was seen with overexpression of these genes, on the contrary, in some cases the MIC decreased. The WGS sequencing data revealing mutations in Rv2553c, *hemD* (Rv0511), *ponA1* (Rv0050) and *tyrA* (Rv3754) was not received until the end of this project and there was insufficient time to prepare overexpression strains for these genes. Ideally *ponA1* and *tyrA* would be prioritised for future studies.

The information obtained from resistant mutant generation suggests that in this instance mutant generation was not the most suitable method for the target

identification process. Alternative methods of target-based and drug-based identification need to be employed to delineate the *Mtb* targets of the BR set of compounds. Protein kinases are not notoriously challenging or unstable proteins to extract, as such there is a good chance of identifying *Mtb* kinase targets through chemoproteomic profiling. Initially a small number of the most potent BR inhibitors could be selected for incorporation into Sepharose bead matrices for bead immobilisation assays. The inhibition of kinases involved in complex cellular pathways is likely to result in changes to the profile of metabolites, therefore metabolomic analysis would be well suited to accompany chemoproteomic profiling.

Morphological profiling should be considered as a lower priority strategy as it gives less clarity than methods which utilise mass spectrometry or sequencing. Describing the morphological profile of *Mtb* treated with Imatinib and Gefitinib, two known kinase inhibitors of *Mtb*, might give a sufficient standard with which to compare other drugs to identify kinase inhibitor activity.

Finally, overexpression trials could be further exploited. Any orthologues to the human kinases targeted by the BR collection of compounds should be investigated, and overexpression strains generated for these and other *Mtb* kinases. Screening all 30 BR compounds against mycobacteria overexpressing kinases and identifying MIC shifts as indicators of target engagement should be prioritised alongside chemoproteomic profiling.

Chapter 5

General Materials and Methods

3. General Materials and Methods

3.1.　　Media and buffers

3.1.1. Luria-Bertani (LB) broth

25g of LB broth granules were dissolved in 1L of dH$_2$O. LB broth was sterilised by autoclaving at 121°C for 20 minutes.

3.1.2. Luria-Bertani agar (LBA)

37g of LB agar granules were dissolved in 1L of dH$_2$O. LBA was sterilised by autoclaving at 121°C for 20 minutes.

3.1.3. Middlebrook 7H9 Liquid Media

2.35 g of 7H9 powder (Middlebrook) was dissolved in 450 mL of dH$_2$O, supplemented with 2 mL of glycerol (50% v/v), 1.25 mL of 20% Tween 80 and 50 mL of Middlebrook ADC enrichment (albumin, dextrose, catalase). 7H9 media was sterilised by filtration using a 0.22 micron filter unit.

3.1.4. Middlebrook 7H9 Liquid Media Supplemented for Maintenance of Deletion Mutants

500 mL 7H9 agar was prepared as described above and supplemented with 5 mL of glycerol (100% v/v), 1 mL of calcium pantothenate (24 mg/mL stock), 2mL of casamino acid (10% w/v stock), 1 mL of cycloheximide (10 mg/ml stock) and 1 mL of carbenicillin disodium salt (10 mg/ml) after sterilisation by autoclaving at 121°C for 20 minutes.

3.1.5. Middlebrook 7H11 Agar

7 g of 7H11 agar powder (Middlebrook) was dissolved in 270 mL of dH$_2$O, supplemented with 3 mL of glycerol (50% v/v). 30 mL of Middlebrook BBL OADC enrichment (oleic acid, albumin, dextrose, catalase) was added after sterilisation by autoclaving at 121°C for 20 minutes.

3.1.6. Middlebrook 7H11 Agar Supplemented for Maintenance of Deletion Mutants

1 L 7H11 agar was prepared as described above and supplemented with 5 mL of glycerol (100% v/v), 1 mL of calcium pantothenate (24 mg/mL stock), 2mL of casamino acid (10% w/v stock), 1 mL of cycloheximide (10 mg/ml stock) and 1 mL of carbenicillin disodium salt (10 mg/ml) after sterilisation by autoclaving at 121°C for 20 minutes.

3.1.7. Minimal Media

2 g Na$_2$HPO$_4$, 1 g KH$_2$PO$_4$, 0.5 g NaCl, 0.2 g MgSO$_4$, 20 mg CaCl$_2$ and 1 g NH$_4$Cl were dissolved in 1 L of dH$_2$O and sterilised by filtration using a 0.22 micron filter unit (Santucci *et al.*, 2019).

3.1.8. Minimal Media – Low Nitrogen

2 g Na$_2$HPO$_4$, 1 g KH$_2$PO$_4$, 0.5 g NaCl, 0.2 g MgSO$_4$, 20 mg CaCl$_2$ and 0.05 g NH$_4$Cl were dissolved in 1 L of dH$_2$O and sterilised by filtration using a 0.22 micron filter unit (Santucci *et al.*, 2019).

3.1.9. Terrific Broth

14.3 g of terrific broth was dissolved in 1 L of dH_2O and supplemented with 8 mL of glycerol (50% v/v). Terrific broth was sterilised by autoclaving at 121°C for 20 minutes.

3.1.10. Lysis Buffer

Protein purification Tgs1: 20mM imidazole, 50mM Tris pH8, 200mM NaCl, 10% glycerol

Protein purification EthR2: 10mM imidazole, 50mM NaH_2PO_4 and 300mM NaCl

3.1.11. Dialysis Buffer

EthR2: 25mM Tris, 300mM NaCl and 10% glycerol

3.1.12. Phosphate Buffered Saline (PBS)

One PBS tablet was dissolved in dH^2O (100 mL) and autoclaved at 121°C for 20 minutes.

3.1.13. Tris - Glycine - SDS Buffer

25 mM Tris-HCl, 192 mM glycine, 0.1 % SDS

3.1.14. Western Transfer Buffer

25 mM Tris-HCl, 192 mM glycine, 10 % methanol

3.1.15. Tris Buffered Saline (TBS)

20 mM Tris-HCl pH 7.5, 150 mM sodium chloride

3.1.16. Tris Buffered Saline - Tween (TBS-T)

20 mM Tris-HCl pH 7.5, 150 mM sodium chloride, 0.05% v/v Tween 20

3.1.17. Tris base, Acetic acid, EDTA (TAE) Buffer

40 mM Tris-acetate pH8.3, 2 mM Na₂EDTA

3.2. General Methods

3.2.1. Growth Conditions for *E. coli*

E. coli strains used for the expression of recombinant proteins (BL21 DE3) and for plasmid DNA extraction (Top10) were grown in LB broth in culture tubes at 37°C with shaking (180 rpm) or grown on LBA at 37°C without shaking. For large scale protein production, flasks containing 1 L terrific broth were inoculated with overnight cultures of BL21 DE3 grown in LB broth (5 mL). Antibiotics for plasmid maintenance were included where appropriate (kanamycin 50 µg/mL).

3.2.2. Growth Conditions Mycobacterial Species

M. bovis BCG was cultured in Middlebrook 7H9 liquid media in culture flasks at 37°C with 5% CO_2 or grown on Middlebrook 7H11 solid media without shaking. Antibiotics for plasmid maintenance were included where appropriate (kanamycin 25 µg/mL). *M. tuberculosis* was cultured in Middlebrook 7H9 liquid media in culture flasks at 37°C with 5% CO_2 or grown on Middlebrook 7H11 solid media without shaking. *M. tuberculosis* H37Rv *ΔleuDΔpanCD* mc²7000 were cultured in Middlebrook 7H9 liquid media supplemented for maintenance of deletion mutants in culture flasks at 37°C with 5% CO_2 or grown on Middlebrook 7H11 solid media supplemented for maintenance of deletion mutants without shaking.

3.2.3. Chemically Competent *E. coli*

Flasks containing 100 mL LB broth were inoculated with 5 mL of overnight culture of *E. coli* and grown to an OD_{600} of 0.4 – 0.8 at 37°C with shaking (180 rpm). The cells were pelleted by centrifugation at 4,000 rpm at 4°C for 20 minutes in 50 mL falcon tubes, and the supernatant was discarded. Cell pellets were resuspended in 10 mL of filter sterilised 100 mM $CaCl_2$ and chilled on ice for 10 minutes before centrifugation was repeated. The supernatant was once again discarded and cells were resuspended 10 mL of filter sterilised 100 mM $CaCl_2$ and chilled on ice for 10 minutes, before a final centrifugation. The supernatant was discarded, and pellets were resuspended in 2.5 mL filter sterilised 100mM $CaCl_2$. Competent cells separated into 100 µL aliquots and submerged in liquid nitrogen for flash freezing. Aliquots were stored at -80°C and thawed on ice as required.

3.2.4. Electrocompetent *M. bovis* BCG

M. bovis BCG was grown in 50 mL of Middlebrook 7H9 liquid media in culture flasks at 37°C with 5% CO_2 until an OD_{600} of 0.4 – 0.8. The cells were pelleted by centrifugation at 4,000 rpm at 4°C for 20 minutes in 50 mL falcon tubes, and the supernatant was discarded. Cell pellets were resuspended in 10 mL of filter sterilised 10% glycerol in dH_2O and chilled on ice for 10 minutes before centrifugation was repeated. The supernatant was once again discarded and cells were resuspended 10 mL of filter sterilised 10% glycerol in dH_2O and chilled on ice for 10 minutes, before a final centrifugation. The supernatant was discarded, and pellets were resuspended in 2.5 mL filter sterilised 10% glycerol in dH_2O. Competent cells separated into 200 µL aliquots and submerged in liquid nitrogen for flash freezing. Aliquots were stored at -80°C and thawed on ice as required.

3.2.5. Transformation of *E. coli* Strains

Plasmid DNA and competent cells were thawed on ice. Plasmid DNA (1 μL) was added to 50 μL of competent cells and gently mixed, then left to chill on ice for 10 minutes. The mixture was transferred to a heating block set to 42°C for 30 seconds before being transferred to a 1.5 mL Eppendorf tube containing 250 μL of LB broth. Cells were allowed to recover for 1 hour at 37°C with shaking (180 rpm) and were then spread onto LBA solid media containing the relevant selection antibiotics. The plates were incubated overnight at 37°C.

3.2.6. Electroporation of *M. bovis* BCG

Plasmid DNA and competent cells were thawed on ice. Plasmid DNA (1 μL) was added to 200 μL of competent cells and gently mixed, then left to chill on ice for 10 minutes. The mixture was transferred to an electroporation cuvette (1 mm gap) which was pulsed at 1,800 V in an Eppendorf 2510 Electroporator. Electroporated cells were transferred to a culture tube containing 2 mL of Middlebrook 7H9 media and incubated at 37°C with shaking (180 rpm) for 24 hours. The cells were centrifuged at 4,000 rpm for 15 minutes and the supernatant discarded. The pellets were then resuspended in 100 μL of Middlebrook 7H9 media and spread onto 20 mL Middlebrook 7H11 agar plates containing antibiotic for plasmid maintenance (kanamycin 25 μg/mL). Plates were incubated at 37°C with 5% CO_2 wrapped in Parafilm to limit evaporation, for 3 weeks until colonies formed.

3.2.7. Preparation of Glycerol Stocks

For storage of bacterial strains, a culture was grown to mid-log (OD_{600} of 0.4-0.8) in the appropriate growth medium. Cell culture (750 μL) was mixed with 750 μL of 50% v/v glycerol (for a final concentration of 25% glycerol v/v) in a Cryo-vial (Nalgene) and flash frozen by submersion in liquid nitrogen. All bacterial stocks were stored at -80°C.

3.2.8. Construction of Recombinant Mycobacterial Strains

Overexpression strains of *M. bovis* BCG were constructed using pMV261, a mycobacterial overexpression vector with a kanamycin resistance cassette. Inserts of the desired *Mtb* Tgs genes were amplified by PCR using the primers shown in Table 13 supplied by Eurofins Genomics (method 3.2.18). Gene inserts and the pMV261 vector were digested using the restriction enzymes in Table 13 (NEB) before the ligation of the inserts into the vector (methods 3.2.22 and 3.2.24). Constructs were sequenced by Source Bioscience prior to electroporation into electrocompetent *M. bovis* BCG (method 3.2.6). Electroporated cells were centrifuged at 3,900 rpm for 10 minutes, resuspended in 100 μl of 7H9 and the entire volume then spread onto 20 mL 7H11 plates supplemented with 25 μg/mL of kanamycin. The plates were incubated at 37°C for approximately 4 weeks, until colonies formed. Colonies were selected and transferred to 7H9 media containing 25 μg/mL kanamycin for use in experiments, and glycerol stocks were prepared for storage (method 3.2.7). Additionally, an empty vector pMV261 strain, pMV261-empty or 'EV' was generated, with no gene inserted.

3.2.9. Generation of *E. coli* Overexpression Constructs

Over expression strains for the purification of target proteins were generated using pET28a, a bacterial expression vector with a kanamycin resistance cassette for transformant selection, in *E. coli*. Inserts were synthesised by PCR using the primers listed in Table 13, supplied by Eurofins Genomics (method 3.2.18). Inserts and vectors were digested with restriction enzymes from New England Biolabs (method 3.2.22), before the ligation of inserts into pET28a (method 3.2.24). *E. coli* BL21 (DE3) was transformed with plasmid constructs by heat shock at 42°C (method 3.2.5) and incubated in LB broth for 1 hr at 37°C. Following recovery in liquid media, 100 μL of each transformed culture was spread onto LBA (Kanamycin 50μg/mL) and plates were incubated at 37°C overnight. Colonies were selected and plasmid DNA extracted for sequencing by Source Bioscience (method 3.2.21). Prior to sequencing, colonies were check for the presence of an insert either by plasmid extraction and digest, or by colony PCR.

Table 13. Oligonucleotide primers and restriction enzymes used in the generation of overexpression constructs organised by thesis chapter. Primers were purchased from Eurofins genomics.

Chapter 2				
	Rv0077c	Forward	BamHI	CTAGCTAGGGATCCAATGTCGACGATCGACATTAG
		Reverse	HindIII	CTAGCTAGAAGCTTCTACGTGCGCACCGCGACCG
	Rv0078	Forward	BamHI	CTAGCTAGGGATCCAATGGAAATCAAGAGACGCAC
		Reverse	HindIII	CTAGCTAGAAGCTTCTAGCCGTTAAGCATCCCGTC
	Rv3854	Forward	BamHI	CTAGCTAGGGATCCAATGACCGAGCACCTCGACGTTG
pMV261		Reverse	HindIII	CTAGCTAGAAGCTTCTAAACCCCCACCGGGGCAG
	Rv3855	Forward	BamHI	CTAGCTAGGGATCCAGTGACCACCTCCGCGGCCAG
		Reverse	HindIII	CTAGCTAGAAGCTTTTAGCGGTTCTCGCCGTAAATG
	Rv0138	Forward	BamHI	CATGCATGGGATCCAGTGAGCGCTTCGGAGTTCTCC
		Reverse	HindIII	CATGCATGAAGCTTTTAAGGACCTCCATGCCGGCG
	Rv3519	Forward	BamHI	CATGCATGGGATCCAATGCCCGTCTCGCAACACACC
		Reverse	HindIII	CATGCATGAAGCTTTCAGATCGGGTGACCGTCGCC
	Rv0078	Forward	NdeI	CTAGCTAGCATATGGAAATCAAGAGACGCACCCAG
		Reverse	HindIII	CTAGCTAGAAGCTTCTAGCCGTTAAGCATCCCGTC
	Rv0077c	Forward	BamHI	CTAGCTAGGGATCCCTACGTGCGCACCGCGACCG
pET28a		Reverse	HindIII	CTAGCTAGAAGCTTATGTCGACGATCGACATTAG
	Rv0138	Forward	NdeI	CATGCATGCATATGGTGAGCGCTTCGGAGTTCTCC
		Reverse	XhoI	CATGCATCTCGAGAGGACCTCCATGCCGGCGCATC
	Rv3519	Forward	NdeI	CATGCATGCATATGCCCGTCTCGCAACACACCATC
		Reverse	XhoI	CATGCATCTCGAGGATCGGGTGACCGTCGCCGAAG
Chapter 3				
	Rv3130c	Forward	BamHI	GATCGATC GGATCC
	tgs1	Reverse	HindIII	GATCGATC AAGCTT TCACACAACCAGCGATAGCGC
	Rv3734c	Forward	BamHI	GATCGATC GGATCC
pMV261	*tgs2*	Reverse	HindIII	GATCGATC AAGCTT TTAGATCCCGACGGCCTGTTC
	Rv3234c	Forward	BamHI	GATCGATC GGATCC GTCACCCGGTTGTCTGCATC
	tgs3	Reverse	HindIII	GATCGATC AAGCTT TCAGCACCACGTCGTGGAG
	Rv3088	Forward	BamHI	GATCGATC GGATCC ACCCGCATCAATCCGATCGATC
	tgs4	Reverse	HindIII	GATCGATC AAGCTT
	Rv3130c	Forward	NdeI	GATCGATC CATATG
	tgs1	Reverse	HindIII	GATCGATC AAGCTT TCACACAACCAGCGATAGCGC
pET28a	Rv3734c	Forward	NdeI	GATCGATC CATATG
	tgs2	Reverse	HindIII	GATCGATC AAGCTT TTAGATCCCGACGGCCTGTTC
	Rv3234c	Forward	NdeI	GATCGATC CATATG GTCACCCGGTTGTCTGCATC
	tgs3	Reverse	HindIII	GATCGATC AAGCTT TCAGCACCACGTCGTGGAG
Chapter 4				
	Rv1543	Forward	PstI	CTAGCTAG CTGCAGAA
		Reverse	HindIII	CTAGCTAG AAGCTT TCACCAATGGATCCCTCGGG
pMV261	Rv1196	Forward	BamHI	CTAGCTAG GGATCCA
		Reverse	HindIII	CTAGCTAG AAGCTT
	Rv2222c	Forward	MscI	CTAGCTAG TGGCCAAG
		Reverse	HindIII	CTAGCTAG AAGCTT CTACAGCGACAGGTAGGTGC

3.2.10. Genomic DNA Extraction

Mycobacterial strains were grown in the appropriate liquid media at 37°C to an OD_{600} of 0.6 -

0.8 and centrifuged at 3,500 rpm for 35 minutes at room temperature to pellet the cells. The

cell pellet was resuspended in 450 μL of GTE-RNAse buffer (200 μl RNAse A, 20 mL GTE buffer –

25 mM tris pH8, 10 mM EDTA pH8, 50 mM glucose) and lysozyme (50 μL, 10 mg/mL stock) was

added. Following an overnight incubation at 37°C, RNAse A (10 μL, 10 mg/ml stock) was added

and the mixture incubated at 37°C for 30 mins, then SDS (100 μL, 10%) and Proteinase k (20 μL,

15 mg/ml stock) were added and the mixture was incubated again, this time at 55°C for 3 hours.

NaCl (200 μL, 5M) and chloroform : isoamylalcohol (1 mL, 24 : 1, v / v) were added to the cells

and the mixture was centrifuged at 13,000 rpm for 10 minutes. The aqueous layer was removed

and 700 μL ice cold isopropanol was added. The tube was centrifuged at 13,000 rpm for 30

minutes at 4°C, the supernatant discarded, the pellet washed with 700 μL ice cold ethanol and

the centrifugation repeated. The ethanol was removed and the pellet was allowed to dry before

being resuspended in 10 μL elution buffer (QIAGEN, 10 mM Tris-Cl, pH 8.5). Samples were run

on 1% agarose gels and the concentration of DNA was measured using a Nanodrop.

3.2.11. Minimum Inhibitory Concentrations (MICs) in Liquid Media

Liquid MICs were determined in triplicate using 96-well, black microtiter plates

(Greiner). V-bottom 96-well plates (Greiner) were used for the preparation of compound

stock plates at 100x the final desired concentration of drug. Compounds were diluted

from the stock plate, (1 μL) was transferred to each well of the MIC plate, followed by

99 μL of mid-log cultures of WT *M. bovis* BCG and *M. bovis* BCG expressing pMV261

constructs diluted in 7H9 media to a density of $1x10^5$ cells *per* well. Antibiotics, used for

selection, were omitted from the media used in the preparation of MIC plates. After 7

days of static incubation at 37°C with 5 % CO_2, survival was measured by a resazurin survival assay (method 3.2.15).

3.2.12. Minimal Inhibitory Concentrations (MICs) in Minimal Media

Minimal media compound stock plates were prepared as described in (method 3.2.11) and drug (1 µL) was transferred to each well of the 96-well, black microtiter MIC plates (Greiner). *M. bovis* BCG expressing pMV261 constructs were grown to mid-log in 7H9 before being centrifuged at 3,000 rpm for 10 minutes and resuspended in PBS to wash the cells. After repeating the wash step twice, cells were resuspended in either 7H9 or low nitrogen minimal media (methods 5.1.5, 3.1.7 and 3.1.8) at an OD_{600} of 0.1, and cultures were allowed to grow to mid-log. Culture (99 µL) was added to each well at a concentration of $1x10^5$ cells *per* well. Plates were then incubated statically for 7 days at 37°C with 5 % CO_2 before resazurin survival assays were carried out (method 3.2.15).

3.2.13. Minimum Inhibitory Concentrations (MICs) on Solid Media for *M. bovis* BCG

7H11 media was prepared as described in method 3.1.65. For *M. bovis* BCG, solid MICs were carried out using 10 mL plates. Dilutions of drug compounds were prepared in 50 mL falcon tubes and 7H11 was mixed with each drug dilution before being transferred into 10 mL plates by pouring. 4 distinct spots of $1x10^3$, $1x10^4$ $1x10^5$ and $1x10^6$ cells were added to each plate once the media had set and cooled. Plates were then incubated for 3 weeks at 37°C with 5 % CO_2 until the control wells containing no drug had grown sufficiently. The lowest concentration at which no growth was visible was determined as the solid MIC.

3.2.14. Minimal Inhibitory Concentrations (MICs) on Solid Media for *Mtb*

H37Rv and H37Rv *ΔleuDΔpanCD* (mc²7000)

Standard 7H11 media and 7H11 media supplemented for the growth of mc²7000 were prepared as described in method 3.1.6. Media (1 mL) was mixed with each concentration of drug in 1.5 mL microcentrifuge tubes before being transferred by pipetting into a 48-well plate (Corning Costar, 48-well cell culture cluster, 3548). *Mtb* was added to the plates at a concentration of 1x10⁵ cells *per* well from a mid-log culture. Plates were then incubated for 3 weeks at 37°C with 5 % CO_2 until the control wells containing no drug had grown sufficiently. The lowest concentration at which no growth was visible was determined as the solid MIC.

3.2.15. Resazurin Survival Assay

Following the incubation of 96-well MIC plates for 7 days, 42μL resazurin (0.02% v/v) was added to each well and the plates were incubated at 37°C for a further 24 hours, before being read using a BMG plate reader (excitation 544nm, emission 590nm). Data were processed by percentage normalisation using positive and negative controls (Equation 1).

3.2.16. Percentage Normalisation

Data from resazurin survival assays were normalised using Equation 1, which determines percentage survival based on positive and negative controls.

Equation 1. Percentage normalisation of MIC data. x is the experimental value, n$\bar{x}$ is the mean of the negative controls and p$\bar{x}$ is the mean of the negative controls.

$$normalised \% = \left(\frac{x - n\bar{x}}{p\bar{x} - n\bar{x}}\right) \times 100$$

3.2.17. Resistant Mutant Generation

Resistant mutants were generated using *Mtb* H37Rv *ΔleuDΔpanCD* (mc^{2}7000). Supplemented 7H11 plates were prepared as described in method 3.1.6, and drug compounds were added in a maximum of 1 % total volume DMSO at concentrations of 5x and 10x their MICs against *Mtb* H37Rv *ΔleuDΔpanCD* (mc^{2}7000). Inoculation of plates and culture of *Mtb* H37Rv *ΔleuDΔpanCD* (mc^{2}7000) was carried out by Dr Alistair Brown at Newcastle University. Briefly, *Mtb* H37Rv *ΔleuDΔpanCD* (mc^{2}7000) was grown to mid-log and adjusted to 1x10^9 cells *per* mL. 100 µL of cells was spread onto each agar plate, and plates were incubated at 37°C with 5 % CO$_2$ for approximately 1-2 months until colonies formed. Genomic DNA was extracted using method 3.2.10 and was sent to Mircobes NG for sequencing.

3.2.18. Polymerase Chain Reaction (PCR)

PCRs were carried out using primers supplied by Eurofins Genomics, all other reagents were supplied by New England Biolabs (NEB). A master mix was prepared on ice with the volumes listed in Table 14, before being aliquoted into multiple PCR tubes. The reactions were carried out using a thermocycler set to the conditions in Table 15. For colony PCRs, a small amount of bacterial colony (<1 µL) was used instead of template DNA.

Table 14. Components of a PCR master mix sufficient for 5 PCR reactions. Forward and reverse primers were ordered from Eurofins Genomics, all other components were from NEB.

Component	125 µL reaction volume
5x Q5 Reaction Buffer	25 µL
5x Q5 High GC Enhancer	25 µL
10 mM DNTPs	2.5 µL
100 µM Forward primer	1.25 µL
100 µM Reverse primer	1.25 µL
Template DNA (<1 µg)	2.5 µL or <1 µL bacterial colony
DNA polymerase	1.25 µL
dH$_2$O	66.25 µL

Table 15. Thermocycler conditions used for standard PCRs.

Step	Temperature	Time (mm:ss)	Cycles
Initial denaturation	98°C	03:00	1
Denaturation	98°C	00:30	
Annealing	50 – 75°C	00:30	30
Elongation	72°C	00:30 per kb	
Final extension	72°C	05:00	1

3.2.19. PCR Cleanup (QIAquick)

PCR cleanup was carried out on gene inserts amplified by PCR following the QIAquick PCR Cleanup Kit protocol from QIAGEN. All centrifugation steps were run at 13,000 rpm for 1 minute. Buffer PB (5 volumes) was added to 1 volume of the PCR reaction If the colour of the dissolved gel was orange or violet, 10 µL of 3 M sodium acetate (pH5.0) was added. The mixture was transferred to a QIAquick spin column in a 2 mL collection tube and then centrifuged. The flow-through was discarded and 750 µL of Buffer PE (10 mM Tris-HCl pH 7.5, 80 % Ethanol) was added to the QIAquick column, which was centrifuged, the flowthrough discarded and then centrifuged once more. The QIAquick column was transferred to a fresh 1.5 mL Eppendorf tube and 50 µL of Buffer EB (10 mM Tris-Cl, pH 8.5) was added. The column was allowed to stand for 1 minute before a final

centrifugation. The DNA concentration was measured using a Nanodrop spectrophotometer and DNA was stored at -20°C.

3.2.20. Agarose Gel

Agarose gels were prepared as 1% w/v as standard by adding Agarose (1 g) to TAE Buffer (100 mL) and heating the mixture for 1 minute in a microwave with occasional stirring. Midori Green Advance (2.5 μL) from Nippon Genetics was added to the liquid gel which was poured into a tray and a comb inserted before the gel set. The solid gel was submerged in a tank filled with TAE buffer and, following removal of the comb, samples of DNA mixed with 6X Gel Loading Dye Purple (NEB) were added to the wells in volumes up to 20 μL. A DNA ladder, Quick-Load Purple 1 kb DNA Ladder (NEB) was added to an empty well. Gels were run at 140 V, 400 mA for 45 minutes before being imaged using a Bio-Rad Gel Doc XR+ UV.

3.2.21. Plasmid Extraction (QIAprep)

Plasmid extraction was carried out using the QIAprep Spin Miniprep Kit protocol from QIAGEN. All centrifugation steps were carried out at 13,000 rpm. *E. coli* Top10 containing the plasmid to be amplified was grown overnight in 5 mL of LB broth with the relevant selection antibiotic at 37°C with shaking (180 rpm). Cells were pelleted by centrifugation for 10 minutes and the supernatant discarded. The pellet was resuspended in 250 μL of Buffer P1 and transferred to a 1.5 mL Eppendorf tube. Buffer P2 (250 μL) was added and the tube mixed thoroughly by inverting it 5 times. Once the solution turned blue, 350 μL of Buffer N3 was added and immediately mixed by inverting the tube 5 times which resulted in the solution turning colourless. Following a 10 minute centrifugation of the

tube, 800 µL of the supernatant was transferred to a QIAprep 2.0 spin column, which was centrifuged for 1 minute. The supernatant was discarded and 0.5 mL of Buffer PB was added, and the tube centrifuged again for 1 minute. The column was washed by adding 0.75 µL of Buffer PE and centrifuging for 1 minute, before again discarding the supernatant. A further 1 minute centrifugation removed the residual wash buffer from the column, which was then transferred to a fresh 1.5 mL Eppendorf tube. Buffer EB (50 µL) was added to the column which was allowed to stand for 1 minute before a final centrifugation step of 1 minute. The DNA concentration was measured using a Nanodrop spectrophotometer and plasmid DNA was stored at -20°C.

3.2.22. Restriction Digest

A mixture of plasmid DNA or vector DNA (1 µg), NEB CutSmart Buffer (2.5 µL), two restriction enzymes (1 µL of each) and dH_2O (adjusted for a total reaction volume of 25 µL) were incubated at 37°C for 1 hour as standard. All restriction enzymes were provided by NEB.

3.2.23. Gel Extraction (QIAquick)

Gel extractions were carried out as described in the QIAquick Gel Extraction Kit protocol from QIAGEN. All centrifugation steps were run at 13,000 rpm for 1 minute. Bands of DNA were cut from agarose gels under UV light using a clean scalpel and transferred to 15 mL Falcon tubes. After weighing the gel fragment, 3 volumes of Buffer QG (5.5 M guanidine thiocyanate, 20 mM Tris-HCl pH 6.6) were added to 1 volume of agarose gel and the tube was incubated at 50°C for 10 minutes with occasional vortexing. If the colour of the dissolved gel was orange or violet, 10 µL of 3 M sodium acetate (pH 5.0)

was added. Isopropanol (1 gel volume) was added to the tube and the mixture was

transferred to a QIAquick spin column in a 2 mL collection tube and then centrifuged. In

an optional step, the flow-through was discarded and 500 μL of Buffer QG was added to

the column which was then centrifuged. The flow-through was discarded and 750 μL of

Buffer PE (10 mM Tris-HCl pH 7.5, 80 % Ethanol) was added to the QIAquick column

which was allowed to stand for 2 minutes before being centrifuged. The flow-through

was discarded and the column centrifuged again to remove residual buffer. The column

was transferred to a fresh 1.5 mL Eppendorf collection tube and 50 μL of Buffer EB (10

mM Tris-Cl, pH 8.5) was added before centrifugation to elute the DNA. The final

centrifugation was repeated once more.

3.2.24. DNA Ligation

Restriction digested vector DNA (50 ng), restriction digested insert DNA (calculated using

Equation 2), NEB T4 DNA ligase (1 μL), NEB 10x T4 DNA Ligase Buffer (2 μL), and dH_2O

(asjusted for a total reaction volume of 20 μL) were mixed and incubated overnight at

room temperature.

Equation 2. Calculation of the amount of insert DNA required for ligation into vector.

$$\frac{Vector\ DNA\ (ng) \times Insert\ size\ (kb)}{Vector\ size\ (kb)} \times 3 = Insert\ DNA\ (ng)$$

3.2.25.   Protein Biochemistry

3.2.25.1. Purification

E. coli was used for the expression of recombinant proteins for purification. Cultures

were grown as described in method 3.2.1 until an OD_{600} of 0.4 − 0.8, when they were

induced with 1 mM IPTG and incubated for a further 12 hours at 16°C. Cells were harvested by centrifugation at 3,900 rpm for 45 minutes and the supernatant was discarded. Pellets were resuspended in lysis buffer method 3.1.10 and lysed using a MSE Soniprep 150 set to 30 seconds on, 30 seconds off for 12 sonication cycles. Tubes were kept in an ice bath during sonication. The cell lysate was centrifuged at 18,000 rpm for 45 minutes to pellet cell debris, and supernatant was passed through a 0.45 micron filter, resulting in clarified cell lysate (CCL). The CCL was loaded onto a nickel charged 1 mL HisTrap HP column (GE Healthcare) pre-equilibrated with lysis buffer at a rate of 1 mL/minute using a peristaltic pump and the flowthrough was collected. A 50 mL wash buffer (lysis buffer containing 10 or 20 mM imidazole) was passed through the column and collected. An increasing gradient of imidazole ranging from 25 mM to 1000 mM was passed through the column in 10 mL volumes and the elution fractions collected.

3.2.25.2. Sodium Dodecyl Sulphate – Polyacrylamide Gel Electrophoresis (SDS – PAGE)

Protein samples were mixed with 3x Blue Protein Loading Dye (62.5 mM Tris-HCl (pH 6.8), 2% (w/v) SDS, 10% glycerol, 0.01% (w/v) bromophenol blue) (NEB) and boiled for 10 minutes. Samples were then loaded onto a Mini-PROTEAN TGX Pre-Cast Gel (Bio-Rad) placed in a protein gel tank (Bio-Rad) containing Tris – Glycine - SDS running buffer (method 3.1.13). A protein ladder, Blue Prestained Protein Standard Broad Range (NEB), was added to an empty well and the gel was run at 200 V, 50 mA for 30 minutes. Instant Blue stain (Expedeon) was used to stain the gel for at least 20 minutes, and then the gel was destained in dH$_2$O.

3.2.25.3. Western Blot

Protein samples were run on Bio-Rad Mini-PROTEAN gels as described in method 3.2.25.2. For Western blotting, gels were run in duplicate and one gel was stained with Instant Blue stain (Expedeon) for a direct comparison with Western blots. Nitrocellulose paper was cut to the same size as the second gel and placed on top of it. The gel and nitrocellulose were sandwiched between squares of blotting paper and Western blot sponges, all of which were loaded into a Western transfer cassette containing Western transfer buffer (method 3.1.14). The transfer was run at 20 V and 300 mA for 1 hour after which the nitrocellulose was carefully placed in a blocking buffer consisting of TBS - T (method 3.1.16) containing and 5% w/v skimmed milk powder for a minimum of 30 minutes. The blocking buffer was then discarded and replaced with 50 mL of TBS - T containing 0.1% w/v skimmed milk powder and 5 µL of Penta-His Mouse IgG primary antibody (Qiagen). After 30 minutes of incubation at room temperature with primary antibody, the nitrocellulose was washed in TBS – T for 15 minutes; this step was repeated a further 2 times. After the third wash, the nitrocellulose was submerged in 50 mL of TBS - T containing 2 µL Anti-Mouse IgG-Alkaline Phosphatase secondary antibody (Sigma) for 30 minutes. The nitrocellulose was then washed twice in TBS – T for 15 minutes, before a final wash of TBS without Tween 20. The nitrocellulose was finally incubated at room temperature in BCIP solution (1 SigmaFAST BCIP/NBT tablet (Sigma) dissolved in 10 mL dH_2O) until bands appeared, at which point the BCIP solution was discarded and the nitrocellulose rinsed in dH_2O and allowed to dry.

3.2.25.4. Intrinsic Tryptophan Quenching Assay

Fluorescence spectroscopy was used to test the change in fluorescence emission of target proteins in the presence of inhibitors. Protein (6 µM of EthR2, 12 µM of Rv0138 or 6 µM Tgs1) was added to a crystal cuvette containing 400 µL buffer which was adjusted depending on the protein (50 mM Tris pH8 or pH7.4, 200 mM or 300 mM NaCl and 10% glycerol). The cuvette was equilibrated to 25°C for 10 minutes with constant stirring. Inhibitor (1 mM stock in DMSO) was titrated in at volumes of 0.5 µL, 1 µL or 2 µL until a total volume of 16 µL. With each addition of drug, the mixture was allowed to equilibrate for 1 minute with stirring, and 3 readings (excitation 295nm, emission 300-400nm) were taken to ensure that the fluorescence was stable. A DMSO control was subtracted from binding data for normalisation, and the data was plotted using the saturation binding model from GraphPad Prism (Equation 3).

Equation 3 Change in fluorescence emission. ΔFemission is calculated using the maximum fluorescence (Fmax), the ligand concentration (L) and the K_D.

$$\Delta Femission = Fmax \times \frac{L}{(k_D + L)}$$

3.3. Chapter 2 Methods

3.3.1. General synthetic procedures

3.3.1.1. General Procedure A - Stetter reaction.

Triethylamine (2.0 eq) and 3-buten-2-one (1.2 eq) were added sequentially to a solution of the corresponding benzaldehyde (1.0 eq) and 3-ethyl-5-(2-hydroxyethyl)-4-methylthiazolium bromide (0.2 eq) in anhydrous acetonitrile (0.325 M) in a Schlenk flask

under nitrogen. The flask was maintained under a nitrogen atmosphere and heated at 80 °C. After 24 h, the mixture was quenched with 2 M hydrochloric acid, extracted with EtOAc ($\times$ 3), and washed sequentially with saturated NaHCO$_3$ solution and brine. The organic layers were combined, dried with Na$_2$SO$_4$ and concentrated under reduced pressure. The residue was purified by column chromatography (cyclohexane/EtOAc 8:1 to 3:1, gradient) to afford the desired product.

3.3.1.2.   General Procedure B - Paal-Knorr reaction.

Camphorsulfonic acid (0.25 eq) was added to a solution of the 1,4-diketone (1.0 eq) and the aniline (1.2 eq) in anhydrous methanol (0.15 M) in a microwave vial under nitrogen. The mixture was heated at 150 °C for 20 min in a microwave reactor. The solvent was then evaporated under reduced pressure and the crude product was directly purified by column chromatography (cyclohexane/EtOAc 8:1 to 3:1, gradient) to afford the desired product.

3.3.1.3.   General Procedure C - Mannich Reaction.

A solution of the secondary amine (1.0 eq) and formaldehyde (37%, 1.0 eq) in acetic acid (1 M) was added at room temperature and in one portion to a solution of 1,2,5-trisubstituted pyrrole (1.0 eq) in anhydrous acetonitrile (0.125 M) under a nitrogen atmosphere. After 15 h, the reaction was quenched with sodium hydroxide solution (10%), extracted with EtOAc ($\times$ 3), and washed sequentially with water ($\times$ 3) and brine. The organic layers were combined, dried with Na$_2$SO$_4$, and concentrated under reduced pressure. The crude product was purified by column chromatography (cyclohexane/EtOAc 4:1 to 2:1, gradient) to afford the desired product.

3.3.1.4. General Procedure D - Mitsunobu reaction.

A solution of (cyanomethylene)tributylphosphorane (1 M in toluene, 1.5 eq) was added under nitrogen to a solution of phenol derivative (1.0 eq) and benzyl (3-hydroxypropyl)carbamate (1.1 eq) in anhydrous toluene (0.4 M) in a microwave vial. The reaction vial was placed in a microwave reactor and heated at 140 °C for 30 min. The reaction solvent was then evaporated under reduced pressure and the crude product purified by column chromatography (cyclohexane/EtOAc 4:1 to 1:4, gradient) to afford the desired product.

3.3.1.5. General Procedure E - Hydrogenolysis.

Nitrogen gas was bubbled through a solution of Cbz-protected compound (1.0 eq) in MeOH (0.15 M). Palladium on carbon (5 eq) was subsequently added. The atmosphere was displaced and maintained with hydrogen under atmospheric pressure. After 15 min, the palladium residues were filtered off, the solvent was removed from the filtrate under reduced pressure and the crude product was purified by preparative HPLC to afford the desired product.

3.3.2. Chemical Synthesis (Carried Out by Glaxo Smith Kline)

3.3.2.1. Analytical Methods

All chemical synthesis was carried out by Glaxo Smith Kline. Reactions were carried out under nitrogen using dry solvents. All reagents were used as received from commercial suppliers. NMR data were recorded on a Bruker AVIII300, Bruker DPX400 or AVIII400 spectrometer. Chemical shifts (δ) are quoted in ppm and coupling constants (J) are

reported in Hz to one decimal place. Spectra were recorded in deuterated chloroform (unless otherwise indicated) and calibrated using residual solvent resonances (^{1}H = 7.26 ppm; ^{13}C = 77.16 ppm). The multiplicities of ^{1}H NMR resonances are abbreviated as follows: s (singlet), d (doublet), t (triplet), q (quartet), m (multiplet). Data for ^{1}H NMR spectra are reported as follows: chemical shift (multiplicity, coupling constant, number of protons); and for proton-decoupled ^{13}C NMR spectra: chemical shift. 2-Dimensional homonuclear (^{1}H-^{1}H) and heteronuclear (^{1}H-^{13}C) NMR experiments were used to make unequivocal assignments. The progress of reactions was monitored by thin layer chromatography using Merck silica gel 60 F$_{254}$ plates, which were visualised with UV light and subsequent staining using *p*-anisaldehyde, acidic potassium permanganate or ninhydrin.

LCMS analysis was conducted on an Agilent HPLC. Method: neutral with ammonium carbonate pH 7. (4.5 min chromatogram). Initial conditions: 70:30 ammonium carbonate:MeCN. The UV detection was an averaged signal from wavelength of 210 nm to 350 nm. Mass spectra were recorded on a Waters ZMD mass spectrometer using alternate-scan positive- and negative-mode electrospray ionisation (ES +ve and ES –ve), mass range 100 – 1200. In those compounds where significantly populated isotopes are present (Cl, Br), only the lower isotopomer is reported.

Microwave reactions were conducted using a Biotage Initiator microwave. The initial absorption was set as 'high' and 15 s of pre-stirring was applied before heating commenced. Flash column chromatography was carried out using Davisil 60 Å silica gel and the indicated solvent systems. Preparative HPLC separation was conducted on an Agilent 1200 or on an Agilent 1100, using either an X-Bridge C18 column (19 mm × 150

mm, i.d. 5 µm packing diameter) or an X-Bridge C18 column (30 mm × 150 mm, i.d. 5 µm

packing diameter) at 35 °C. The solvents employed were: A = 0.1 M formic acid in water;

B = 0.1 M formic acid in acetonitrile. The purification was run as a gradient (A:B) over

either 20 min, with a flow rate of 17 mL/min (19 mm × 150 mm, i.d. 5 µm packing

diameter) or 35 mL/min (30 mm × 150 mm, i.d. 5 µm packing diameter). The UV

detection wavelengths were 210 nm and 350 nm. All final products were lyophilised

prior to their use in any biological assay. The purity of final compounds was greater than

95% by LCMS (HPLC: Acquity UPLC BEH C18 1.7u 3 × 50 mm, 35 °C. Method: ammonium

acetate 25 mM + 10% acetonitrile at pH 6.6/acetonitrile. 0 – 0.2 min 100:0; 0.2 – 1.0 min

10:90; 1.0 – 1.8 min 10:90; 1.8 – 2.0 min 100:0. Flow: 0.8 mL/min. The UV detection

wavelength was 254 nm and 210 nm.)

3.3.2.2.　Chemical Synthesis of BM212

As outlined in Supplementary Scheme 1 (Figure 62), 1-(4-chlorophenyl)pentane-1,4-

dione was prepared following (method 3.3.1.1) using 4-chlorobenzaldehyde (2.81 g,

20.0 mmol). The 1,4-dione product was isolated as a white solid (3.65 g, 87%). ^{1}H NMR

(300 MHz, CDCl$_3$) δ_H 7.97 – 7.84 (m, 2H), 7.46 – 7.35 (m, 2H), 3.26 – 3.19 (m, 2H), 2.92 –

2.77 (m, 2H), 2.25 (s, 3H);^{13}C NMR (101 MHz, CDCl$_3$) δ_C 207.2, 197.3, 139.6, 135.0, 129.5,

128.9, 37.0, 32.3, 30.1; m/z (EI) C$_{11}$H$_{11}$ClO$_2$, found [M]$^+$ 210.1. Spectroscopic data were

in agreement with those reported in the literature (Chochois *et al*., 2006).

1,2-Bis(4-chlorophenyl)-5-methyl-1*H*-pyrrole was prepared following (method 3.3.1.2)

using 1-(4-chlorophenyl)pentane-1,4-dione (666 mg, 3.16 mmol) and 4-chloroaniline

(484 mg, 3.79 mmol). The resulting pyrrole product, (1,2-bis(4-chlorophenyl)-5-methyl-

1*H*-pyrrole), was isolated as a yellowish solid (955 mg, 95%). ^{1}H NMR (400 MHz, CDCl$_3$) δ_H 7.39 – 7.32 (m, 2H), 7.17 – 7.10 (m, 2H), 7.10 – 7.05 (m, 2H), 6.99 – 6.93 (m, 2H), 6.34 (d, J = 3.5 Hz, 1H), 6.09 (dq, J = 3.5, 0.6 Hz, 1H), 2.13 (d, J = 0.6 Hz, 3H); ^{13}C NMR (101 MHz, CDCl$_3$) δ_C 137.7, 133.5, 133.0, 132.1, 131.71, 131.68 129.6, 129.4, 128.9, 128.3, 109.4, 108.1, 13.3; m/z (EI) C$_{17}$H$_{13}$Cl$_2$N, found [M]$^+$ 302.1. ^{1}H NMR Spectroscopic data consistent with those reported in the literature (Kamal *et al*., 2016).

1-((1,5-Bis(4-chlorophenyl)-2-methyl-1*H*-pyrrol-3-yl)methyl)-4-methylpiperazine was prepared following (method 3.3.1.3) using 1,2-bis(4-chlorophenyl)-5-methyl-1*H*-pyrrole (50 mg, 0.16 mmol) and *N*-methylpiperazine (18 µL, 0.16 mmol). 1,2,4,5-Tetrasubstituted pyrrole product [BM212, 1-((1,5-bis(4-chlorophenyl)-2-methyl-1*H*-pyrrol-3-yl)methyl)-4-methylpiperazine] was isolated as a white solid (45 mg, 66%).^{1}H NMR (400 MHz, CDCl$_3$) δ_H 7.37 – 7.30 (m, 2H), 7.13 – 7.08 (m, 2H), 7.07 – 7.01 (m, 2H), 6.96 – 6.90 (m, 2H), 6.35 (s, 1H), 3.47 (s, 2H), 3.04 – 2.38 (br m, 8H), 2.30 (s, 3H), 2.06 (s, 3H). ^{13}C NMR (101 MHz, CDCl$_3$) δ_C 137.7, 133.4, 131.9, 131.6, 131.5, 130.2, 129.7, 129.4, 128.8, 128.3, 116.7, 111.7, 55.0, 54.3, 52.6, 46.0, 11.2; m/z (EI) C$_{23}$H$_{25}$Cl$_2$N$_3$, found [M]$^+$ 414.2. Spectroscopic data were in agreement with those reported in the literature (More *et al*., 2016).

3.3.2.3.   Chemical Synthesis of GSK074A

As outlined in Supplementary Scheme 2 (Figure 63), 1-(4-isopropylphenyl)pentane-1,4-dione was prepared following (method 3.3.1.1) using 4-isopropylbenzaldehyde (1.48 g, 10.0 mmol). The 1,4-dione product was isolated as a yellow oil (1.1 g, 50%). ^{1}H NMR (400 MHz, CDCl$_3$) δ_H 7.95 – 7.89 (m, 2H), 7.33 – 7.28 (m, 2H), 3.28 – 3.22 (m, 2H), 3.07 – 2.90

(m, 1H), 2.90 – 2.83 (m, 2H), 2.25 (s, 3H), 1.26 (d, J = 6.9 Hz, 6H); ^{13}C NMR (101 MHz, CDCl$_3$) δ_C 207.5, 198.2, 154.7, 134.5, 128.3, 126.7, 37.1, 34.3, 32.3, 30.1, 23.7; m/z (EI) C$_{14}$H$_{18}$O$_2$, found [M]$^+$ 218.3. ^{1}H-NMR Spectroscopic data were in agreement with those reported in the literature (Biava *et al.*, 2008).

1-(4-Fluorophenyl)-2-(4-isopropylphenyl)-5-methyl-1*H*-pyrrole was prepared following (method 3.3.1.2) using 1-(4-isopropylphenyl)pentane-1,4-dione (1.10 g, 5.0 mmol) and 4-fluoroaniline (574 µL, 6.0 mmol). The 1,2,5-trisubstituted pyrrole product was isolated as a yellow oil that solidified upon standing (1.25 g, 85%). ^{1}H NMR (400 MHz, CDCl$_3$) δ_H 7.19 – 7.11 (m, 2H), 7.10 – 6.95 (m, 6H), 6.33 (d, J = 3.4 Hz, 1H), 6.09 (dd, J = 3.4, 0.6 Hz, 1H), 2.83 (heptet, J = 6.9 Hz, 1H), 2.13 (d, J = 0.6 Hz, 3H), 1.21 (d, J = 6.9 Hz, 6H).^{13}C NMR (101 MHz, CDCl$_3$) δ_C 161.6 (d, J = 247.1 Hz), 146.4, 135.6, 134.4, 131.4, 130.8, 130.1 (d, J = 8.4 Hz), 127.7, 126.1, 115.9 (d, J = 22.7 Hz), 108.3, 107.5, 33.6, 23.9, 13.3; m/z (ES+) C$_{20}$H$_{20}$FN, found [M + H]$^+$ 294.2. ^{1}H-NMR Spectroscopic data were in agreement with those reported in the literature (Biava *et al.*, 2008).

1-((1-(4-Fluorophenyl)-5-(4-isopropylphenyl)-2-methyl-1*H*-pyrrol-3-yl)methyl)-4-methylpiperazine (GSK074A) was prepared following (method 3.3.1.3) using 1-(4-fluorophenyl)-2-(4-isopropylphenyl)-5-methyl-1*H*-pyrrole (160 mg, 0.5 mmol) and *N*-methylpiperazine (60 µL, 0.5 mmol). The 1,2,4,5-tetrasubstituted pyrrole product (GSK074A) was isolated as an off-white solid (99 mg, 45%). ^{1}H NMR (400 MHz, CDCl$_3$) δ_H 7.29 – 6.90 (m, 8H), 6.32 (s, 1H), 3.47 (s, 2H), 2.80 (heptet, J = 6.9 Hz, 1H), 2.73 – 2.34 (m, 8H), 2.29 (s, 3H), 2.05 (s, 3H), 1.18 (d, J = 6.9 Hz, 6H). ^{13}C NMR (101 MHz, CDCl$_3$) δ_C 161.6 (d, J = 247.1 Hz), 146.3, 135.7, 135.7, 133.3, 130.6, 130.2 (d, J = 8.5 Hz), 129.5,

127.5, 126.1, 116.2, 115.8 (d, J = 22.6 Hz), 110.76, 110.75, 55.2, 54.4, 52.7, 46.0, 33.6, 23.9, 11.2; m/z (ES+) $C_{26}H_{32}FN_3$, found $[M + H]^+$ 406.4.

3.3.2.4. Chemical Synthesis of GSK303A

As outlined in Supplementary Scheme 3 (Figure 64), 2-(4-chlorophenyl)-5-methyl-1-(4-methylphenyl)-1H-pyrrole was prepared following (method 3.3.1.2) using 1-(4-chlorophenyl)pentane-1,4-dione (200 mg, 0.9 mmol) and p-toluidine (115 µL, 1.1 mmol). The pyrrole product was isolated as a yellow solid (194 mg, 73%). ^{1}H NMR (400 MHz, CDCl$_3$) δ_H 7.22 – 7.15 (m, 2H), 7.14 – 7.08 (m, 2H), 7.06 – 7.02 (m, 2H), 7.01 – 6.97 (m, 2H), 6.36 (d, J = 3.5 Hz, 1H), 6.10 (dd, J = 3.5, 0.7 Hz, 1H), 2.40 (s, 3H), 2.14 (d, J = 0.7 Hz, 3H). ^{1}H-NMR Spectroscopic data were in agreement with those reported in the literature (Biava et al., 2008).

4-((5-(4-Chlorophenyl)-2-methyl-1-(4-methylphenyl)-1H-pyrrol-3-yl)methyl)morpholine) (GSK303A) was prepared following (method 3.3.1.3) using 2-(4-chlorophenyl)-5-methyl-1-(4-methylphenyl)-1H-pyrrole (194 mg, 0.7 mmol) and morpholine (60 µL, 0.7 mmol). The 1,2,4,5-tetrasubstituted pyrrole product (GSK303A) was isolated as an off-white solid (150 mg, 57%). ^{1}H NMR (400 MHz, CDCl$_3$) δ_H 7.19 – 7.15 (m, 2H), 7.11 – 7.05 (m, 2H), 7.03 – 6.99 (m, 2H), 6.98 – 6.94 (m, 2H), 6.35 (s, 1H), 3.79 – 3.69 (m, 4H), 3.43 (s, 2H), 2.52 (br s, 4H), 2.38 (s, 3H), 2.06 (s, 3H); ^{13}C NMR (101 MHz, CDCl$_3$) δ_C 137.5, 136.6, 131.90, 131.88, 131.3, 130.4, 129.8, 128.6, 128.3, 128.1, 116.2, 111.0, 67.1, 55.1, 53.5, 21.2, 11.2; m/z (ES+) $C_{23}H_{25}ClN_2O$, found $[M + H]^+$ 381.3. Data were in agreement with those reported in the literature (Poce et al., 2013).

3.3.2.5. Chemical Synthesis of GSK569A

As outlined in Supplementary Scheme 4 (Figure 65), 4-(2-(4-isopropylphenyl)-5-methyl-1*H*-pyrrol-1-yl)phenol was prepared following (method 3.3.1.2) using 1-(4-isopropylphenyl)pentane-1,4-dione (437 mg, 2.0 mmol) and 4-aminophenol (261 mg, 2.4 mmol). The 1,2,5-trisubstituted pyrrole product was isolated as a purple oil (563 mg, 97%). ^{1}H NMR (400 MHz, CDCl$_3$) δ_H 7.09 – 7.01 (m, 2H), 7.00 (s, 4H), 6.84 – 6.78 (m, 2H), 6.30 (d, *J* = 3.4 Hz, 1H), 6.06 (dd, *J* = 3.4, 0.7 Hz, 1H), 4.76 (s, 1H), 2.81 (heptet, *J* = 6.9 Hz, 1H), 2.11 (d, *J* = 0.7 Hz, 3H), 1.19 (d, *J* = 6.9 Hz, 6H); ^{13}C NMR (101 MHz, CDCl$_3$) δ_C 154.6, 146.2, 134.3, 132.6, 131.5, 131.0, 129.7, 127.6, 126.0, 115.7, 107.9, 107.0, 33.6, 23.9, 13.3; m/z (ES+) C$_{20}$H$_{21}$NO, found [M + H]$^+$ 291.9.

Benzyl (3-(4-(2-(4-isopropylphenyl)-5-methyl-1*H*-pyrrol-1-yl)phenoxy)propyl)carbamate was prepared following (method 3.3.1.4) using 4-(2-(4-isopropylphenyl)-5-methyl-1*H*-pyrrol-1-yl)phenol (250 mg, 0.86 mmol) and benzyl (3-hydroxypropyl)carbamate (Miller *et al.*, 2004) (198 mg, 0.94 mmol). The carbamate product was isolated as a yellow oil (402 mg, 97%). ^{1}H NMR (400 MHz, CDCl$_3$) δ_H 7.40 – 7.26 (m, 5H), 7.11 – 7.00 (m, 2H), 6.99 (s, 4H), 6.88 – 6.79 (m, 2H), 6.30 (d, *J* = 3.4 Hz, 1H), 6.05 (dd, *J* = 3.4, 0.8 Hz, 1H), 5.11 (s, 2H), 4.99 (s, 1H), 4.03 (t, *J* = 5.8 Hz, 2H), 3.44 (app q, *J* = 6.4 Hz, 2H), 2.87 – 2.74 (m, 1H), 2.10 (d, *J* = 0.8 Hz, 3H), 2.07 – 1.97 (m, 2H), 1.18 (d, *J* = 6.9 Hz, 6H); ^{13}C NMR (101 MHz, CDCl$_3$) δ_C 157.7, 156.4, 146.1, 134.3, 132.6, 131.6, 131.0, 129.7, 129.5, 128.6, 128.2, 127.6, 126.0, 114.6, 107.9, 107.0, 66.7, 66.0, 38.6, 33.6, 29.5, 23.9, 13.3, 1 × aromatic C not observed, possible resonance overlap; m/z (ES+) C$_{31}$H$_{34}$N$_2$O$_3$, found [M + H]$^+$ 483.2.

Benzyl (3-(4-(5-(4-isopropylphenyl)-2-methyl-3-(morpholinomethyl)-1*H*-pyrrol-1-yl)phenoxy)propyl)-carbamate was prepared following (method 3.3.1.3) using benzyl (3-(4-(2-(4-isopropylphenyl)-5-methyl-1*H*-pyrrol-1-yl)phenoxy)propyl) carbamate (400 mg, 0.82 mmol) and morpholine (75 μL, 0.82 mmol). The morpholine product was isolated as an orange oil (250 mg, 50%). ^{1}H NMR (400 MHz, CDCl$_3$) δ_H 7.39 – 7.28 (m, 5H), 7.12 – 7.03 (m, 2H), 6.99 (s, 4H), 6.87 – 6.83 (m, 2H), 6.33 (s, 1H), 5.11 (s, 3H), 4.03 (t, *J* = 5.8 Hz, 2H), 3.77 – 3.71 (m, 4H), 3.49 – 3.37 (m, 4H), 2.80 (heptet, *J* = 6.9 Hz, 1H), 2.53 (s, 4H), 2.08 – 1.95 (m, 5H), 1.18 (d, *J* = 6.9 Hz, 6H); ^{13}C NMR (101 MHz, CDCl$_3$) δ_C 157.7, 156.5, 146.1, 136.6, 133.2, 132.7, 130.8, 129.8, 129.6, 128.6, 128.2, 127.4, 126.1, 115.7, 114.6, 110.3, 67.1, 66.7, 65.9, 55.1, 53.5, 38.6, 33.6, 29.5, 23.9, 11.2, 1 × aromatic C not observed, possible resonance overlap or not well resolved; m/z (ES-) C$_{36}$H$_{43}$N$_3$O$_4$, found [M − H]$^+$ 580.4.

3-(4-(5-(4-Isopropylphenyl)-2-methyl-3-(morpholinomethyl)-1*H*-pyrrol-1-yl)phenoxy)propan-1-amine (GSK569A) was prepared following general procedure E using benzyl (3-(4-(5-(4-isopropylphenyl)-2-methyl-3-(morpholinomethyl)-1*H*-pyrrol-1-yl)phenoxy)propyl)carbamate (250 mg, 0.43 mmol). The primary amine product (GSK569A) was isolated as an off-white solid (156 mg, 84%). %). ^{1}H NMR (400 MHz, CDCl$_3$) δ_H 7.08 – 7.02 (m, 2H), 6.98 (s, 4H), 6.92 – 6.84 (m, 2H), 6.31 (s, 1H), 4.05 (t, *J* = 6.1 Hz, 2H), 3.78 – 3.69 (m, 4H), 3.44 (s, 2H), 2.93 (t, *J* = 6.8 Hz, 2H), 2.85 – 2.74 (m, 1H), 2.52 (s, 4H), 2.04 (s, 3H), 1.95 (app pentet, *J* = 6.4 Hz, 2H), 1.18 (d, *J* = 6.9 Hz, 6H), NH$_2$ not observed. ^{13}C NMR (101 MHz, CDCl$_3$) δ_C 158.0, 146.0, 133.2, 132.5, 130.8, 129.8, 129.6, 127.4, 126.0, 115.6, 114.6, 110.2, 67.1, 66.1, 55.1, 53.4, 39.2, 33.6, 33.0, 23.9, 11.1; m/z (ES+) C$_{28}$H$_{37}$N$_3$O$_2$, found [MH − morpholine]$^+$ 361.3.

3.3.2.6. Chemical Synthesis of GSK574A

As outlined in Supplementary Scheme 5 (Figure 66), 1-(4-hydroxyphenyl)pentane-1,4-dione was prepared following (method 3.3.1.1), heating at 80 °C but for 72 h using 4-hydroxybenzaldehyde (2.44 g, 20.0 mmol). The 1,4-dione product was isolated as a yellowish oil that solidified upon standing (702 mg, 18%). ^{1}H NMR (400 MHz, CDCl$_3$) δ_H 7.86 − 7.79 (m, 2H), 6.87 − 6.81 (m, 2H), 3.18 (t, J = 6.2 Hz, 2H), 2.83 (t, J = 6.2 Hz, 2H), 2.22 (s, 3H), OH not observed; ^{13}C NMR (101 MHz, CDCl$_3$) δ_C 208.9, 197.7, 161.8, 130.6, 128.7, 115.5, 37.2, 32.0, 30.1. Data were in agreement with those reported in the literature (Esumi *et al.*, 2016).

4-(1-(4-Fluorophenyl)-5-methyl-1*H*-pyrrol-2-yl)phenol was prepared following (method 3.3.1.2) using 1-(4-hydroxyphenyl)pentane-1,4-dione (702 mg, 3.7 mmol) and 4-fluoroaniline (420 µL, 4.4 mmol). The pyrrole product was isolated as a yellowish oil that solidified upon standing (436 mg, 45%). ^{1}H NMR (400 MHz, CDCl$_3$) δ_H 7.15 − 7.08 (m, 2H), 7.08 − 6.99 (m, 2H), 6.96 − 6.88 (m, 2H), 6.65 − 6.60 (m, 2H), 6.25 (d, J = 3.4 Hz, 1H), 6.07 (dd, J = 3.4, 0.7 Hz, 1H), 4.69 (br s, 1H), 2.12 (d, J = 0.7 Hz, 3H); ^{13}C NMR (101 MHz, CDCl$_3$) δ_C 161.6 (d, J = 247.3 Hz), 153.8, 135.4 (d, J 4.0 Hz), 134.1, 131.0, 130.1 (d, J = 8.5 Hz), 129.5, 126.3, 115.9 (d, J = 22.6 Hz), 115.0, 107.8, 107.3, 13.3; m/z (ES+) C$_{17}$H$_{14}$FNO, found [M + H]$^+$ 268.4.

Benzyl (3-(4-(1-(4-fluorophenyl)-5-methyl-1*H*-pyrrol-2-yl)phenoxy)propyl)carbamate was prepared following (method 3.3.1.4) using 4-(1-(4-fluorophenyl)-5-methyl-1*H*-pyrrol-2-yl)phenol (420 mg, 1.57 mmol) and benzyl (3-hydroxypropyl)carbamate (Miller *et al.*, 2004) (345 mg, 1.65 mmol). The carbamate product was isolated as a yellowish oil

(500 mg, 69%). ^{1}H NMR (400 MHz, CDCl$_3$) δ_H 7.39 – 7.29 (m, 5H), 7.14 – 7.08 (m, 2H), 7.08 – 7.01 (m, 2H), 6.99 – 6.93 (m, 2H), 6.68 (d, J = 8.7 Hz, 2H), 6.25 (d, J = 3.4 Hz, 1H), 6.06 (dd, J = 3.4, 0.6 Hz, 1H), 5.09 (s, 2H), 4.97 (br s, 1H), 3.95 (t, J = 5.8 Hz, 2H), 3.38 (app. q, J = 6.3 Hz, 2H), 2.12 (d, J = 0.6 Hz, 3H), 2.00 – 1.92 (m, 2H); ^{13}C NMR (101 MHz, CDCl$_3$) δ_C 161.6 (d, J = 247.2 Hz), 157.0, 156.4, 135.4, 134.1, 131.0, 130.0 (d, J = 8.5 Hz), 129.2, 128.5, 128.1, 126.3, 115.9 (d, J = 22.6 Hz), 114.1, 107.8, 107.4, 66.7, 65.7, 38.7, 29.4, 13.31, 1 × aromatic C and 1 × aromatic CH not observed, possible resonance overlap or not well resolved; m/z (ES+) C$_{28}$H$_{27}$FN$_2$O$_3$, found [M + H]$^+$ 459.2.

Benzyl (3-(4-(1-(4-fluorophenyl)-5-methyl-4-(morpholinomethyl)-1H-pyrrol-2-yl)phenoxy)propyl) carbamate was prepared following (method 3.3.1.3) using benzyl (3-(4-(1-(4-fluorophenyl)-5-methyl-1H-pyrrol-2-yl)phenoxy)propyl) carbamate (500 mg, 1.1 mmol) and morpholine (95 µL, 1.1 mmol). The morpholine product was isolated as an orange oil (193 mg, 32%). ^{1}H NMR (400 MHz, CDCl$_3$) δ_H 7.37 – 7.27 (m, 5H), 7.12 – 7.00 (m, 4H), 6.97 – 6.91 (m, 2H), 6.66 (d, J = 8.7 Hz, 2H), 6.26 (s, 1H), 5.09 (s, 2H), 4.99 (br s, 1H), 3.95 (t, J = 5.8 Hz, 2H), 3.76 – 3.72 (m, 4H), 3.44 (s, 2H), 3.41 – 3.33 (m, 2H), 2.53 (br s, 4H), 2.06 (s, 3H), 2.00 – 1.92 (m, 2H); ^{13}C NMR (101 MHz, CDCl$_3$) δ_C 161.6 (d, J 247.5 Hz), 157.0, 156.4, 135.5, 133.1, 130.2 (d, J 8.1 Hz), 129.2, 129.1, 128.5, 128.1, 126.1, 115.9 (d, J, 22.2 Hz), 114.1, 110.1, 67.1, 66.7, 65.7, 55.0, 53.5, 38.7, 29.4, 11.2, 2 × aromatic Cs not observed and 1 × aromatic CH not accounted for, probable resonance overlap; m/z (ES+) C$_{33}$H$_{36}$FN$_3$O$_4$, found [MH – morpholine]$^+$ 471.2.

3-(4-(1-(4-Fluorophenyl)-5-methyl-4-(morpholinomethyl)-1H-pyrrol-2-yl)phenoxy)propan-1-amine (GSK574A) was prepared following general procedure E

using benzyl (3-(4-(1-(4-fluorophenyl)-5-methyl-4-(morpholinomethyl)-1*H*-pyrrol-2-yl)phenoxy)propyl)carbamate (193 mg, 0.34 mmol). The amine product (GSK574A) was isolated as a colourless oil (65 mg, 44%). ^{1}H NMR (400 MHz, CDCl$_3$) δ_H 7.14 – 6.99 (m, 4H), 6.96 – 6.88 (m, 2H), 6.71 – 6.65 (m, 2H), 6.26 (s, 1H), 3.97 (t, *J* = 6.4 Hz, 2H), 3.75 – 3.71 (m, 4H), 3.43 (s, 2H), 2.87 (t, *J* = 6.4 Hz, 2H), 2.52 (br., 4H), 2.06 (s, 3H), 1.88 (app. pentet, *J* = 6.4 Hz, 2H), NH$_2$ not observed; ^{13}C NMR (101 MHz, CDCl$_3$) δ_C 161.5 (d, *J* 248.5 Hz), 157.2, 135.6, 133.1, 130.2 (d, *J* 9.1 Hz), 129.1, 125.8, 115.9 (d, *J*, 22.2 Hz), 114.1, 110.0, 67.1, 65.8, 55.1, 53.5, 39.3, 33.0, 11.1, 2 × aromatic Cs not observed; m/z (ES+) C$_{25}$H$_{30}$FN$_3$O$_2$, found [MH – morpholine]$^+$ 337.2.

A solution of benzyl chloroformate (2.84 mL, 20 mmol) in CH$_2$Cl$_2$ (10 mL) was added over 2 min to a solution of 3-aminopropan-1-ol (3.82 mL, 50 mmol) in CH$_2$Cl$_2$ (40 mL) at 0 °C. The mixture was allowed to warm to RT. After 3 h, the mixture was diluted with CH$_2$Cl$_2$ (25 mL) and washed sequentially with saturated NH$_4$Cl solution (3 × 40 mL) and brine (40 mL), dried over Na$_2$SO$_4$ and concentrated under reduced pressure. The residue was purified by flash column chromatography (gradient: EtOAc/cyclohexane 1:3 to 1:1) to afford benzyl (3-hydroxypropyl)carbamate as a white solid (3.27 g, 78%). ^{1}H NMR (400 MHz, CDCl$_3$) δ_H 7.40 – 7.28 (m, 5H), 5.11 (s, 2H), 5.02 (br s, 1H), 3.68 (app. q, *J* = 5.7 Hz, 2H), 3.36 (app. q, *J* = 6.3 Hz, 2H), 2.52 (br s, 1H), 1.75 – 1.66 (m, 2H). ^{1}H-NMR spectroscopic data in accordance with those reported in the literature (Miller *et al*., 2004).

3.3.3. Chemical Proteomic Studies

NHS-activated Sepharose beads were functionalised by the addition of compounds GSK569A at 0.3mM and 1mM, and GSK574A at 1mM. After equilibration in lysis buffer (50 mM Tris-HCl, pH 7.4, 0.02% – 0.4% Igepal-CA630, 1.5 mM $MgCl_2$, 5% glycerol, 150 mM NaCl, 25 mM NaF, 1 mM Na_3VO_4, 1 mM DTT, and one EDTA-free protease inhibitor tablet (Roche) per 25 mL) the beads were incubated with 0.1 mL *M. bovis* BCG extract (2.5mg/mL) and either a test compound (GSK074A or GSK303A, Figure 19) prepared as previously described (Abrahams *et al.*, 2016) or DMSO.

10 samples *per* experiments were multiplexed (Werner *et al.*, 2014) enabling the calculation of depletion values for 4 samples and calculation of the IC_{50} values for the remaining 6 samples. For samples 3 and 4, *M. bovis* BCG extracts were incubated with the bead matrix and protein binding was calculated following incubation. A second incubation was then carried out with the remaining unbound protein and fresh beads and the protein binding was measured again (Bantscheff *et al.*, 2011; Eberl *et al.*, 2019). The test compounds were titrated into samples 5 – 10 for the calculation of IC_{50} values. Samples 1 and 2 were vehicle controls. Following incubation, beads were transferred to filter plates (Durapore PVDF membrane, Merck Millipore) and washed thoroughly with lysis buffer. SDS sample buffer was used to elute proteins which were then digested with trypsin (Hughes *et al.*, 2014; Moggridge *et al.*, 2018). Peptides were labelled with TMT10 isobaric mass tags and lyophilised. LC-MS measurements were carried out using Q Exactive Orbitrap and Orbitrap Fusion spectrometers (Thermo Fisher Scientific) following protocols described by Penzo *et al.* (2019) and Sridharan *et al.* (2019).

3.3.3.1. Checkerboard Plates

Combination drug plates were set up at 100 x the desired final concentration using V-bottom 96-well plates (Greiner), with BM212 diluted along the ordinate from 400 µg/mL to 0 µg/mL, and ETA diluted along the abscissa from 3200 µg/mL to 0 µg/mL. Checkerboard plates were prepared in 96-well, clear-bottom microtiter plates (Greiner) with 1 µL of drug from the compound stock plates *per* well for a 1% (v/v). Cells were added, as described for MIC plates, at a starting OD_{600} of 0.1 and the plates were incubated at 37°C with 5% CO_2. The OD_{600} was read using a BMG plate reader after 6 days, and results were normalised using Equation 4.

Equation 4 Fractional response of MIC data. x is the experimental value, $n\bar{x}$ is the mean of the negative controls and $p\bar{x}$ is the mean of the negative controls.

$$Fractional\ response = \left(\frac{x - n\bar{x}}{p\bar{x} - n\bar{x}}\right)$$

3.3.3.2. Analysis of Drug Interactions

Data from checkerboard plates was used to analyse drug interactions based on the fractional inhibitory concentration (FIC) index. The OD_{600} after 6 days was normalised to give a fractional response, and the ΣFIC calculated with Equation 5, which uses the MIC required for specified level of inhibition by both drugs separately and in combination to determine whether they are acting synergistically (ΣFIC<0.5), additively/indifferently (ΣFIC = 0.5 – 4) or antagonistically (ΣFIC>4). For the assessment of interactions between

BM212 and ETA, the concentration of drugs separately and in combination required to

inhibit growth by 75% was used.

Equation 5 Fractional inhibitory concentration (FIC). A and B represent the concentrations of drugs A and B applied in combination needed to achieve a specified level of inhibition, and MICA and MICB are the MICs of drug A and drug B needed to achieve the same level of inhibition when applied separately.

$$\sum \text{FIC} = FIC_A + FIC_B = \frac{A}{MIC_A} + \frac{B}{MIC_B}$$

3.3.4. Biochemical Studies

3.3.4.1. Crystal Trays

To further probe the binding of EthR2 and compounds from the BM212 family, crystal

trays were set up using the MIDAS crystal screen from Molecular Dimensions

(Supplementary material - Table 18). Briefly, EthR2 was dialysed into fresh buffer with a

lower salt concentration (20 mM Tris-HCl (pH 7.4), 10 mM NaCl, and 10% (vol/vol)

glycerol), and was concentrated to 10 mg/mL. 96-well sitting drop vapour diffusion

plates (Swissci) were used for growing crystals (Figure 20). 40 µL of buffer was added to

reservoir 4 by pipetting. 2 µL from reservoir 4 was transferred to both reservoirs 1 and

2. EthR2 (2 µL, 10 mg/mL) was added to reservoir 1. EthR2 was mixed with BM212 at a

concentration of 1 : 6 protein / ligand, and 2 µL of the mixture was transferred to

reservoir 2. Reservoir 3 was left empty. Crystal trays were sealed with Crystal Clear

Sealing Film (Hampton Research), stored at 4°C and checked every 3 days for crystals.
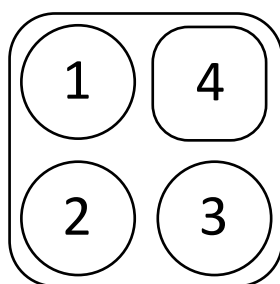
Figure 61. Layout of a single 96-well crystal tray sitting drop well. Reservoir 1 contains protein, reservoir 2 contains a mixture of protein and ligand, reservoir 3 was left empty, and reservoir 4 contains only buffer.

3.3.5. Molecular Docking

Molecular docking was carried out for EthR2 (PDB 5N1I) and BM212 (CID 456926) using Chimera and AutoDock Vina software, guided by an instructional publication from Butt *et al.* (2020).

3.4. Chapter 3 Methods

3.4.1. [^{14}C]-labelling of *M. bovis* BCG Cultures

Cultures of *M. bovis* BCG WT, and *M. bovis* BCG expressing pMV261-empty, pMV261-*tgs1*, pMV261-*tgs2*, pMV261-*tgs3* and pMV261-*tgs4* were grown overnight in 10 mL of 7H9 broth. Radiolabelled [1,2-^{14}C]-acetic acid (5 µl, was added and the cultures were incubated at 37°C for 24 hours. Cells were harvested by centrifugation at 3,500 rpm for 10 minutes and the supernatant discarded, and the pellet dried.

When testing the effect of diacylglycerol synthase inhibitors on WT BCG and BCG overexpressing *tgs1, tgs2, tgs3* and *tgs4*, drug was added to mid-log cultures 24 hours prior to radiolabelling. Drugs were tested at 0, 0.5, 1 and 2x MIC for all overexpression strains, an additional concentration of 0.25x MIC was tested for WT *M. bovis* BCG.

3.4.2. Extraction of Apolar and Polar Lipids from [^{14}C]-Labelled Cells

A mixture of methanol : 0.3 %NaCl (2 ml, 100 : 10 w / v) was added to cell pellets followed by 2 mL of petroleum-ether (60-80°) and mixed for 30 minutes on a rotator mixer. The tubes were then centrifuged for 5 minutes at 3000rpm and the upper layer transferred to a fresh tube (B). A further 2 mL of petroleum-ether (60-80°) was added to the lower layer, mixed for 30 minutes and centrifuged with the upper layer again transferred to tube B, which was then dried to afford the non-polar lipid fraction. A mixture of 2.3 mL chloroform : methanol : 0.3 % NaCl (2.3 mL, 90 : 100 : 30, v / v / v) was added to the lower layer and mixed for 1 hour before centrifugation. Supernatant was transferred to a fresh tube (C). A mixture of 750 µl chloroform : methanol : 0.3 % NaCl (0.75 mL, 50 : 100 : 40 v / v / v) was added to the pellet, mixed and centrifuged and the supernatant was added to tube C and this step was repeated. Chloroform (1.3 mL) and 0.3 % NaCl (1.3 mL) was added to tube C, mixed and centrifuged. The lower layer consisted of polar lipids, which were dried. The remaining pellet was saved for FAMEs and MAMEs extractions.

3.4.3. Extraction of Fatty Acid Methyl Esters (FAMEs) and Mycolic Acid Methyl Esters (MAMEs) from [^{14}C]-Labelled Cells

Dried pellets of delipidated cells were incubated with 5% tetrabutylammonium hydroxide (TBAH) (2 mL) overnight at 95°C. H_2O (2 mL), dichloromethane (2 mL) and iodomethane (30 µL) was added to the pellet following incubation with TBAH and mixed thoroughly for 1 hour and then centrifuged for 5 minutes at 3,500 rpm. The upper layer was discarded, and the lower layer was washed twice with H_2O (3 mL) and centrifuged.

The lower layer was transferred to a fresh tube, dried and resuspended in diethyl ether (4 mL). The tube was vortexed and centrifuged and the supernatant transferred to a fresh tube. Samples were dried, resuspended in dichloromethane (200 µL), dried again and finally resuspended in chloroform methanol (2 : 1, v / v).

3.4.4. Thin Layer Chromatography for [^{14}C]-Labelled Lipids

The counts per minute were calculated for each sample of polar and apolar lipids, and FAMEs and MAMEs. Samples were dried and resuspended in an appropriate volume of chloroform : methanol (2 : 1, v / v) for a concentration of 5,000 cpm per 1 µl where possible. Lipids were loaded onto the TLC plates by pipetting for a total amount of 10,000 cpm per plate. For the separation of lipids TLC was performed using Silica Gel 60 F_{254} TLC plates (Merck). The aluminium backed silica plates were cut to 6.7 cm by 6.7 cm for 2 directional solvent systems and 10 cm by 10 cm for 1 directional solvent systems. The lipid samples were added to the TLC plates approximately 1 cm from the bottom edge by pipetting and allowed to dry. Solvent systems were prepared and mixed in glass Duran bottles (Tables 16 and 17), then poured into a glass TLC tank to a depth of just under 1 cm. The lid was placed on the tank to allow equilibration, and after 3 minutes the TLC plates were stood vertically leaning against the wall of the tank, with the lipid sample origin sat just higher than the solvent level and the lid was replaced quickly. The TLC plates were removed once the solvent system had run to 1 cm from the top edge of the TLC plates and they were allowed to air dry. For TLC systems which required multiple runs in the same direction, TLCs were dried with a hair dryer set to cold until completely

dry before being run in fresh solvent. Once dry, TLC plates were exposed to autoradiography film for 6 days.

Table 16. Two dimensional solvent systems A-E used for the separation of apolar and polar lipids

System	Direction 1	Runs	Sample
A	Petroleum ether / ethyl acetate (98 : 2)	3	Apolar lipids
B	Petroleum ether / acetone (92 : 8)	3	Apolar lipids
C	Chloroform / methanol (96 : 4)	1	Apolar lipids
D	Chloroform / methanol / water (100 : 14 : 0.8)	1	Apolar / polar lipids
E	Chloroform / methanol / water (60 : 30 : 6)	1	Polar lipids
System	Direction 2	Runs	Sample
A	Petroleum ether / acetone (98 : 2)	1	Apolar lipids
B	Toluene / acetone (95 : 5)	1	Apolar lipids
C	Toluene / acetone (80 : 20)	1	Apolar lipids
D	Chloroform / acetone / methanol / water (50 : 60 : 2.5 : 3)	1	Apolar / polar lipids
E	Chloroform / acetic acid (glacial) / methanol / water (40 : 25 : 3 : 6)	1	Polar lipids

Table 17. Solvent systems used for the separation of FAMEs and MAMEs and apolar lipids

Direction 1	Runs	Sample
Petroleum ether / acetone (95 : 5)	1	FAMEs and MAMEs
Petroleum ether / diethyl ether (90 : 10)	1	Apolar

3.4.5. [^{14}C]-Labelling and Lipid Extraction of Cells Grown in Minimal Media

For minimal media experiments, *M. bovis* BCG expressing pMV261-empty and pMV261-*tgs3* were grown to mid-log in 7H9 before being centrifuged at 3,000 rpm for 10 minutes and

resuspended in PBS to wash the cells. After repeating the wash step twice, cells were resuspended in 7H9, minimal media or low nitrogen minimal media (methods 5.1.3, 3.1.7 and 3.1.8) at an OD_{600} of 0.1. When cultures reached mid-log, drug treatment and [^{14}C]-labelling was carried out as described above. Apolar lipids were extracted and loaded onto TLC plates (methods 3.4.1 and 3.4.2) and run in petroleum ether / diethyl ether (90 : 10, v / v) (Table 17).

3.4.6. Triacylglycerol Synthase Activity Assay

A fluorescence based assay was carried out as described by McFie and Stone (2011). Each reaction contained 1M Tris-HCl (20 µL, pH 7.6), 1M $MgCl_2$ (4 µL), 4 mM 1,2-dipalmitoyl-sn-glycerol (10 µL), BSA (10 µL, 12.5 mg/mL), 500 µM NBD-palmitoyl CoA (10 µL), and dH2O (96 µL). Each reaction was pre-incubated at 37°C for 2 minutes. Cell lysate (100 µg) was added, and the reaction incubated for 10 minutes at 37°C, shaking occasionally. The reaction was terminated with the addition of $CHCl_3$ / methanol (4 mL, 2 : 1 v / v) before H_2O (800 µL) was added. The mixture was left for 1 hour at room temperature before being vortexed and centrifuged at 3, 000 rpm to separate into a biphase. The lower phase was dried and lipids were resuspended in $CHCl_3$ / methanol (50 µL, 2 : 1 v / v). The extracted lipids were spotted onto TLC plates and run in triplicate in hexane / ethyl acetate / acetic acid (80 : 20 : 1). The bands of TAG were identified under UV light by comparison to standards run in parallel. The silica within the demarcated areas of the bands of TAG were scraped from the TLC plates and transferred to a 96 well plate where petroleum ether (50 µL) was added and mixed. After 20 minutes, the fluorescence of each well was read using a BMG plate reader.

Chapter 6

Conclusions and Future Work

4. Conclusions and Future Work

TB remains a leading cause of death worldwide and the global health significance of TB is indisputable (WHO, 2021). While improvements in the detection and management of TB have contributed significantly to a reduction in cases (WHO, 2015), and have improved outcomes, the increasing incidence of drug resistant TB threatens the progress of global strategies to stop TB. Multiple approaches have been employed in order to tackle the rise in drug resistance, including the introduction of directly- / video-observed treatment (D/VOT) as well as a concerted effort to introduce new anti-TB therapeutics (WHO, 2015). Since the 1970s, the production of new antibiotics to treat TB has virtually halted, while drug resistant cases increase. Screening programmes have made promising discoveries in recent years, with bedaquiline, delamanid and pretomanid achieving FDA approval having been identified through whole cell screening (Mahajan, 2013; Ryan *et al.*, 2014; FDA, 2019).

Methods of identifying anti-TB drugs vary from the discovery of novel small molecule inhibitors from the screening of vast compound libraries, to the repurposing of existing drugs used to treat different conditions (Abrahams, 2020). There are benefits to the discovery of novel targets, as they are less likely to be affected by resistance that has developed towards inhibitors of other targets, however, inhibitors of novel targets rarely make it through the early stages of drug discovery because there are often challenges surrounding delivery, which have already been solved for existing targets (Salazar *et al.*, 2017; Abrahams *et al.*, 2020).

In this work we set out to investigate potential anti-TB hits from a variety of screening programmes with a view to elucidating their targets. We studied existing anti-TB drugs for potential alternative targets, as well as exploring the anti-TB activity of drugs for other conditions, with a view to repurposing them in the future.

The BM212 series of compounds are known for their activity against MmpL3, a mycobacterial transmembrane protein responsible for the translocation of trehalose monomycolate (TMM) (Su *et al*., 2019). MmpL3 is described as a promiscuous target, which is vulnerable to inhibition by structurally diverse scaffolds. Despite being structurally diverse, MmpL3 inhibitors share the characteristic of being highly lipophilic, likely leading to their accumulation at high concentrations within the mycobacterial inner membrane where MmpL3 is situated (Li, W *et al*., 2018). Inhibitors that otherwise have poor activity due to weak binding may be present in high enough concentrations to sufficiently inhibit MmpL3, resulting in the frequent identification of such inhibitors from screening efforts. The promiscuous binding by MmpL3 of diverse compounds has been shown to mask alternative targets of MmpL3 inhibitors, such as THPP which also inhibits EchA6 (Cox *et al*., 2016). This has led to the re-evaluation of previously identified MmpL3 inhibitors, which may have unexplored alternative mechanisms of action. Through chemoproteomic profiling, we have demonstrated that analogues of the MmpL3 inhibitor BM212 bind to EthR2 (Rv0078), the regulator of EthA2 (Rv0077c) which is responsible for the activation of the pro-drug ethionamide (ETA). Guided by previous work which demonstrated the ETA boosting effects of EthR2 inhibitors (Blondiaux *et al*., 2017), we utilised microbiological and biochemical techniques to assess the pharmacokinetic enhancing properties of BM212. Despite the binding of BM212 to

EthR2 demonstrated in multiple assays, there was no evidence of synergy between BM212 and ETA. BM212 was observed to weakly and inconsistently bind to EthA2, the activator of ETA. If BM212 does indeed bind to EthA2 as well as EthR2, the ETA boosting effects of inhibiting the regulator, EthR2, are likely to be counteracted by the inhibition of the activator, EthA2. Alternatively, the binding of BM212 to EthR2 may be nonspecific and simply not inhibit the regulatory activity of EthR2. Nevertheless, we have demonstrated the importance of revisiting MmpL3 inhibitors for further target elucidation, as we predict there to be unexplored alternative targets of other inhibitors.

Drug repurposing is a desirable strategy for drug discovery because it invariably means that there is pre-existing (L)ADME(T) and PK/PD data that may facilitate faster progress through the drug discovery pipeline (Abrahams, 2020; Kenakin, 2017). A large portion of this research involved screening and target identification of two different groups of drugs: inhibitors of human diacylglycerol acyltransferase 1 (DGAT1) and inhibitors of a variety of human kinases. The methods employed for target identification were typical of the drug-to-target discovery pipeline, but an understanding of the targets of these drugs in humans was used to inform research decisions (Abrahams, 2020).

Limiting the energy source of a pathogen is an effective way of inhibiting growth and replication. *Mtb* has the advantage of being able to utilize host triacylglycerol (TAG) as an energy source as well as synthesising and accumulating native TAG (Daniel *et al.*, 2011; Maurya *et al.*, 2019). Inhibitors of human DGAT1 were shown in preliminary studies to significantly reduce infection in TB infected THP-1 macrophages with an IC90 10.9 μM. We explored the potential of DGAT1 inhibitors to directly inhibit *M. bovis* BCG

and investigated the target of one inhibitor with consistent activity against *M. bovis* BCG, GSK2. Through a series of overexpression studies, we have demonstrated the inhibition of TAG synthesis in *M. bovis* BCG by GSK2, and have identified Tgs3, a mycobacterial triacylglycerol synthase, as the target. Furthermore, we show that treatment with GSK2 prevents the accumulation of TAG induced by minimal media, specifically in nitrogen limiting conditions. When Tgs3 is overexpressed, the effect of GSK2 is diminished and the MIC of GSK2 increases. This promising research demonstrates the activity of a group of drugs currently in clinical trials for use in human metabolic disorders (Devita *et al.*, 2013; Denison *et al.*, 2014; Meyers *et al.*, 2016) against *Mtb* and identifies Tgs3 as a novel target of *Mtb* inhibition. Unfortunately, we were unable to establish the activity of GSK2 against Tgs3 in a biochemical assay, further attention could be given to producing soluble Tgs3 with the aid of detergents in order to test its activity in the assays we described in chapter 3. In addition, it would be useful to understand whether other DGAT1 inhibitors inhibit *Mtb* through the same target, and whether any of the additional 11 *tgs* genes in *Mtb* are targeted.

For the final portion of this research, we selected 30 compounds from a screen based on their activity against *Mtb* and we tested them against both *M. bovis* BCG and two strains of *Mtb.* By generating spontaneous mutants with resistance to the compounds, we sought to identify the targets using whole genome sequencing (WGS) and validate them using overexpression strains (Abrahams *et al.*, 2020). From the WGS data, 4 genes in which mutations were identified were found to be essential (Rv2553c, Rv0511, Rv0050 and Rv3754). Of these genes, two were considered to be genes of interest: *ponA1* (Rv0050) and *tyrA* (Rv3754). PonA1 is a probable penicillin binding protein (PBP)

involved in cell elongation and division (Kieser *et al.*, 2015). The cytoplasmic tail of PonA1 acts as a substrate for the serine-threonine protein kinase, PknB, which phosphorylates the T34 residue of PonA1 (Kieser *et al.*, 2015; Prisic *et al.*, 2010). The rate of cell elongation appears to be linked to the phosphorylation of PonA1. We hypothesise that the inhibition of PknB by a kinase inhibitor could impact the activity of PonA1, and the mutation in PonA1 has restored the activity resulting in resistance or a higher tolerance to the kinase inhibitor. The second essential mutation of interest was found in *tyrA*, which encodes a prephenate dehydrogenase, a protein which forms part of the regulatory subunit of the mycobacterial aspartate kinase (MtbAKβ) (Yang *et al.*, 2011).

Due to the slow, unpredictable process of resistant mutant generation and sequencing, and the limited time frame, further target characterization after the identification of these two mutations was not within the scope of this research. We propose a multistep plan for further target elucidation of the BR compounds which starts with chemoproteomic profiling of the most potent compounds, followed by morphological profiling using Imatinib and Gefitinib as standards. We recommend investigating genes of interest identified in the above steps using whole cell overexpression assays. Additionally, *Mtb* orthologues of human targets of the BR compounds could be overexpressed and used in whole cell assays.

To conclude, we must take a multifaceted approach to tackling antibiotic resistance in TB. It is important that in the many screening efforts to find anti-TB compounds, we do

not overlook existing drugs, and we take time to further our understanding of existing

drugs, as the discovery of alternative targets could reveal new avenues not yet explored.

Bibliography

Abdallah, A. M., Savage, N. D. L., van Zon, M., Wilson, L., Vandenbroucke-Grauls, C. M. J. E., van der Wel, N. N., Ottenhoff, T. H. M., & Bitter, W. 2008. The ESX-5 Secretion System of *Mycobacterium marinum* Modulates the Macrophage Response . *The Journal of Immunology*, *181*, 7166–7175. https://doi.org/10.4049/jimmunol.181.10.7166

Abdelgawad, H., Abuelsoud, W., Madany, M. M. Y., Selim, S., Zinta, G., Mousa, A. S. M., & Hozzein, W. N. 2020. Actinomycetes enrich soil rhizosphere and improve seed quality as well as productivity of legumes by boosting nitrogen availability and metabolism. *Biomolecules*, *10*, 1–19. https://doi.org/10.3390/biom10121675

Abrahams, K. A., & Besra, G. S. 2018. Mycobacterial cell wall biosynthesis: A multifaceted antibiotic target. In *Parasitology* (Vol. 145, Issue 2, pp. 116–133). https://doi.org/10.1017/S0031182016002377

Abrahams, K. A., & Besra, G. S. 2020. Mycobacterial drug discovery. In *RSC Medicinal Chemistry* (Vol. 11, Issue 12, pp. 1354–1365). https://doi.org/10.1039/d0md00261e

Abrahams, K. A., Chung, C. W., Ghidelli-Disse, S., Rullas, J., Rebollo-López, M. J., Gurcha, S. S., Cox, J. A. G., Mendoza, A., Jiménez-Navarro, E., Martínez-Martínez, M. S., Neu, M., Shillings, A., Homes, P., Argyrou, A., Casanueva, R., Loman, N. J., Moynihan, P. J., Lelièvre, J., Selenski, C., … Bates, R. H. 2016. Identification of KasA as the cellular target of an anti-tubercular scaffold. *Nature Communications*, *7*. https://doi.org/10.1038/ncomms12581

Abrahams, K. A., Cox, J. A. G., Spivey, V. L., Loman, N. J., Pallen, M. J., Constantinidou, C., Fernández, R., Alemparte, C., Remuiñán, M. J., Barros, D., Ballell, L., & Besra, G. S. 2012. Identification of Novel Imidazo[1,2-a]pyridine Inhibitors Targeting *M. tuberculosis* QcrB. *PLoS ONE*, *7*. https://doi.org/10.1371/journal.pone.0052951

Abrahams, K. A., Hu, W., Li, G., Lu, Y., Richardson, E. J., Loman, N. J., Huang, H., & Besra, G. S. 2020. Anti-tubercular derivatives of rhein require activation by the monoglyceride lipase Rv0183. *Cell Surface*, *6*. https://doi.org/10.1016/j.tcsw.2020.100040

Alderwick, L. J., Dover, L. G., Veerapen, N., Gurcha, S. S., Kremer, L., Roper, D. L., Pathak, A. K., Reynolds, R. C., & Besra, G. S. 2008. Expression, purification and characterisation of soluble GlfT and the identification of a novel galactofuranosyltransferase Rv3782 involved in priming GlfT-mediated galactan polymerisation in *Mycobacterium tuberculosis*. *Protein Expression and Purification*, *58*, 332–341. https://doi.org/10.1016/j.pep.2007.11.012

Alderwick, L. J., Lloyd, G. S., Ghadbane, H., May, J. W., Bhatt, A., Eggeling, L., Fütterer, K., & Besra, G. S. 2011. The C-terminal domain of the arabinosyltransferase *Mycobacterium tuberculosis* EmbC is a lectin-like carbohydrate binding module. *PLoS Pathogens*, *7*. https://doi.org/10.1371/journal.ppat.1001299

Alderwick, L. J., Lloyd, G. S., Lloyd, A. J., Lovering, A. L., Eggeling, L., & Besra, G. S. 2011. Biochemical characterization of the *Mycobacterium tuberculosis* phosphoribosyl-1-pyrophosphate synthetase. *Glycobiology*, *21*, 410–425. https://doi.org/10.1093/glycob/cwq173

Alderwick, L. J., Radmacher, E., Seidel, M., Gande, R., Hitchen, P. G., Morris, H. R., Dell, A., Sahm, H., Eggeling, L., & Besra, G. S. 2005. Deletion of *Cg-emb* in corynebacterianeae leads to a novel truncated cell wall arabinogalactan, whereas inactivation of *Cg-ubiA* results in an Arabinan-deficient mutant with a cell wall galactan core. *Journal of Biological Chemistry*, *280*, 32362–32371. https://doi.org/10.1074/jbc.M506339200

Alderwick, L. J., Seidel, M., Sahm, H., Besra, G. S., & Eggeling, L. 2006. Identification of a novel arabinofuranosyltransferase (AftA) involved in cell wall arabinan biosynthesis in *Mycobacterium tuberculosis*. *Journal of Biological Chemistry*, *281*, 15653–15661. https://doi.org/10.1074/jbc.M600045200

Andersen, C. S., Agger, E. M., Rosenkrands, I., Gomes, J. M., Bhowruth, V., Gibson, K. J. C., Petersen, R. V., Minnikin, D. E., Besra, G. S., & Andersen, P. 2009. A Simple Mycobacterial Monomycolated Glycerol Lipid Has Potent Immunostimulatory Activity. *The Journal of Immunology*, *182*, 424–432. https://doi.org/10.4049/jimmunol.182.1.424

Ang, M. L. T., Siti, Z. Z. R., Shui, G., Dianišková, P., Madacki, J., Lin, W., Koh, V. H. Q., Gomez, J. M. M., Sudarkodi, S., Bendt, A., Wenk, M., Mikušová, K., Korduláková, J., Pethe, K., & Alonso, S. 2014. An *ethA-ethR*-deficient *Mycobacterium bovis* BCG mutant displays increased adherence to mammalian cells and greater persistence *in vivo*, which correlate with altered mycolic acid composition. *Infection and Immunity*, *82*, 1850–1859. https://doi.org/10.1128/IAI.01332-13

Angala, S. K., McNeil, M. R., Shi, L., Joe, M., Pham, H., Zuberogoitia, S., Nigou, J., Boot, C. M., Lowary, T. L., Gilleron, M., & Jackson, M. 2017. Biosynthesis of the Methylthioxylose Capping Motif of Lipoarabinomannan in *Mycobacterium tuberculosis*. *ACS Chemical Biology*, *12*, 682–691. https://doi.org/10.1021/acschembio.6b01071

Arendse, L. B., Wyllie, S., Chibale, K., & Gilbert, I. H. 2021. Plasmodium Kinases as Potential Drug Targets for Malaria: Challenges and Opportunities. In *ACS Infectious Diseases* (Vol. 7, Issue 3, pp. 518–534). https://doi.org/10.1021/acsinfecdis.0c00724

Artsimovitch, I., Vassylyeva, M. N., Svetlov, D., Svetlov, V., Perederina, A., Igarashi, N., Matsugaki, N., Wakatsuki, S., Tahirov, T. H., & Vassylyev, D. G. 2005. Allosteric modulation of the RNA polymerase catalytic reaction is an essential component of transcription control by rifamycins. *Cell*, *122*, 351–363. https://doi.org/10.1016/j.cell.2005.07.014

Aufrecht. 1882. Die Aetiologie der Tuberculose. *Deutsche Medizinische Wochenschrift*, *8*, 283. https://doi.org/10.1055/s-0029-1196567

Bacon, J., Alderwick, L. J., Allnutt, J. A., Gabasova, E., Watson, R., Hatch, K. A., Clark, S. O., Jeeves, R. E., Marriott, A., Rayner, E., Tolley, H., Pearson, G., Hall, G., Besra, G. S., Wernisch, L., Williams, A., & Marsh, P. D. 2014. Non-replicating *Mycobacterium tuberculosis* elicits a reduced infectivity profile with corresponding modifications to the cell wall and extracellular matrix. *PLoS ONE*, *9*. https://doi.org/10.1371/journal.pone.0087329

Ballou, C. E., & Lee, Y. C. 1964. The Structure of a Myoinositol Mannoside from *Mycobacterium tuberculosis* Glycolipid. *Biochemistry*, *3*, 682–685. https://doi.org/10.1021/bi00893a014

Banerjee, A., Dubnau, E., Quemard, A., Balasubramanian, V., Um, K. S., Wilson, T., Collins, D., De Lisle, G., & Jacobs, W. R. 1994. *inhA*, a gene encoding a target for isoniazid and ethionamide in *Mycobacterium tuberculosis*. *Science*, *263*, 227–230. https://doi.org/10.1126/science.8284673

Bansal-Mutalik, R., & Nikaido, H. 2014. Mycobacterial outer membrane is a lipid bilayer and the inner membrane is unusually rich in diacyl phosphatidylinositol dimannosides. *Proceedings of the National Academy of Sciences of the United States of America*, *111*, 4958–4963. https://doi.org/10.1073/pnas.1403078111

Bantscheff, M., Hopf, C., Savitski, M. M., Dittmann, A., Grandi, P., Michon, A. M., Schlegl, J., Abraham, Y., Becher, I., Bergamini, G., Boesche, M., Delling, M., Dümpelfeld, B., Eberhard, D., Huthmacher, C., Mathieson, T., Poeckel, D., Reader, V., Strunk, K., … Drewes, G. 2011. Chemoproteomics profiling of HDAC inhibitors reveals selective targeting of HDAC complexes. *Nature Biotechnology*, *29*, 255–268. https://doi.org/10.1038/nbt.1759

Barberis, I., Bragazzi, N. L., Galluzzo, L., & Martini, M. 2017. The history of tuberculosis: From the first historical records to the isolation of Koch's bacillus. In *Journal of Preventive Medicine and Hygiene* (Vol. 58, Issue 1, pp. E9–E12). https://doi.org/10.15167/2421-4248/jpmh2017.58.1.728

Bardou, F., Raynaud, C., Ramos, C., Lanéelle, M. A., & Lanéelle, G. 1998. Mechanism of isoniazid uptake in Mycobacterium tuberculosis. *Microbiology*, *144*, 2539–2544. https://doi.org/10.1099/00221287-144-9-2539

Barkan, D., Rao, V., Sukenick, G. D., & Glickman, M. S. 2010. Redundant function of *cmaA2* and *mmaA2* in *Mycobacterium tuberculosis* cis cyclopropanation of oxygenated mycolates. *Journal of Bacteriology*, *192*, 3661–3668. https://doi.org/10.1128/JB.00312-10

Barreteau, H., Kovač, A., Boniface, A., Sova, M., Gobec, S., & Blanot, D. 2008. Cytoplasmic steps of peptidoglycan biosynthesis. In *FEMS Microbiology Reviews* (Vol. 32, Issue 2, pp. 168–207). https://doi.org/10.1111/j.1574-6976.2008.00104.x

Barry, C. E., Lee, R. E., Mdluli, K., Sampson, A. E., Schroeder, B. G., Slayden, R. A., & Yuan, Y. 1998. Mycolic acids: Structure, biosynthesis and physiological functions. In *Progress in Lipid Research* (Vol. 37, Issues 2–3, pp. 143–179). https://doi.org/10.1016/S0163-7827(98)00008-3

Basavannacharya, C., Moody, P. R., Munshi, T., Cronin, N., Keep, N. H., & Bhakta, S. 2010. Essential residues for the enzyme activity of ATP-dependent MurE ligase from *Mycobacterium tuberculosis*. *Protein and Cell*, *1*, 1011–1022. https://doi.org/10.1007/s13238-010-0132-9

Basavannacharya, C., Robertson, G., Munshi, T., Keep, N. H., & Bhakta, S. 2010. ATP-dependent MurE ligase in *Mycobacterium tuberculosis*: Biochemical and structural characterisation. *Tuberculosis*, *90*, 16–24. https://doi.org/10.1016/j.tube.2009.10.007

Batt, S. M., Burke, C. E., Moorey, A. R., & Besra, G. S. 2020. Antibiotics and resistance: the two-sided coin of the mycobacterial cell wall. In *Cell Surface* (Vol. 6). https://doi.org/10.1016/j.tcsw.2020.100044

Batt, S. M., Minnikin, D. E., & Besra, G. S. 2020. The thick waxy coat of mycobacteria, a protective layer against antibiotics and the host's immune system. In *Biochemical Journal* (Vol. 447, Issue 10, pp. 1983–2006). https://doi.org/10.1042/BCJ20200194

Baulard, A. R., Betts, J. C., Engohang-Ndong, J., Quan, S., McAdam, R. A., Brennan, P. J., Locht, C., & Besra, G. S. 2000. Activation of the pro-drug ethionamide is regulated in mycobacteria. *Journal of Biological Chemistry*, *275*, 28326–28331. https://doi.org/10.1074/jbc.M003744200

Belanger, A. E., Besra, G. S., Ford, M. E., Mikušová, K., Belisle, J. T., Brennan, P. J., & Inamine, J. M. 1996. The *embAB* genes of *Mycobacterium avium* encode an arabinosyl transferase involved in cell wall arabinan biosynthesis that is the target for the antimycobacterial drug ethambutol. *Proceedings of the National Academy of Sciences of the United States of*

America, *93*, 11919–11924. https://doi.org/10.1073/pnas.93.21.11919

Belánová, M., Dianišková, P., Brennan, P. J., Completo, G. C., Rose, N. L., Lowary, T. L., & Mikušova, K. 2008. Galactosyl transferases in mycobacterial cell wall synthesis. *Journal of Bacteriology*, *190*, 1141–1145. https://doi.org/10.1128/JB.01326-07

Belisle, J. T., Vissa, V. D., Sievert, T., Takayama, K., Brennan, P. J., & Besra, G. S. 1997. Role of the major antigen of *Mycobacterium tuberculosis* in cell wall biogenesis. *Science*, *276*, 1420–1422. https://doi.org/10.1126/science.276.5317.1420

Benson, T. E., Marquardt, J. L., Marquardt, A. C., Etzkorn, F. A., & Walsh, C. T. 1993. Overexpression, Purification, and Mechanistic Study of UDP-N-Acetylenolpyruvylglucosamine Reductase. *Biochemistry*, *32*, 2024–2030. https://doi.org/10.1021/bi00059a019

Berg, S., Kaur, D., Jackson, M., & Brennan, P. J. 2007. The glycosyltransferases of *Mycobacterium tuberculosis* - Roles in the synthesis of arabinogalactan, lipoarabinomannan, and other glycoconjugates. In *Glycobiology* (Vol. 17, Issue 6). https://doi.org/10.1093/glycob/cwm010

Bernut, A., Viljoen, A., Dupont, C., Sapriel, G., Blaise, M., Bouchier, C., Brosch, R., de Chastellier, C., Herrmann, J. L., & Kremer, L. 2016. Insights into the smooth-to-rough transitioning in *Mycobacterium bolletii* unravels a functional Tyr residue conserved in all mycobacterial MmpL family members. *Molecular Microbiology*, *99*, 866–883. https://doi.org/10.1111/mmi.13283

Berube, B. J., Russell, D., Castro, L., Choi, S. ryoung, Narayanasamy, P., & Parish, T. 2019. Novel MenA inhibitors are bactericidal against *Mycobacterium tuberculosis* and synergize with electron transport chain inhibitors. *Antimicrobial Agents and Chemotherapy*, *63*. https://doi.org/10.1128/AAC.02661-18

Besra, G. S., & Brennan, P. J. 1997. The mycobacterial cell wall: Biosynthesis of arabinogalactan and lipoarabinomannan. *Biochemical Society Transactions*, *25*, 845–850. https://doi.org/10.1042/bst0250845

Besra, G. S., McNeil, M. R., Brennan, P. J., Khoo, K. H., Dell, A., & Morris, H. R. 1995. A New Interpretation of the Structure of the Mycolyl—Arabinogalactan Complex of *Mycobacterium tuberculosis* as Revealed Through Characterization of Oligoglycosylalditol Fragments by Fast-Atom Bombardment Mass Spectrometry and 1H Nuclear Magnetic Resonance . *Biochemistry*, *34*, 4257–4266. https://doi.org/10.1021/bi00013a015

Bhagwat, S. S., Legakis, N. J., Skalidis, T., Loannidis, A., Goumenopoulos, C., Joshi, P. R., Shrivastava, R., Palwe, S. R., Periasamy, H., Patel, M. V., & Chatzipanagiotou, S. 2021. In vitro activity of cefepime/zidebactam (WCK 5222) against recent Gram-negative isolates collected from high resistance settings of Greek hospitals. *Diagnostic Microbiology and Infectious Disease*, *100*. https://doi.org/10.1016/j.diagmicrobio.2021.115327

Bhagwat, S. S., Periasamy, H., Takalkar, S. S., Palwe, S. R., Khande, H. N., & Patel, M. V. 2019. The Novel -Lactam Enhancer Zidebactam Augments the In Vivo Pharmacodynamic Activity of Cefepime in a Neutropenic Mouse Lung *Acinetobacter baumannii* Infection Model. *Antimicrobial Agents and Chemotherapy*, *63*. https://doi.org/10.1128/AAC.02146-18

Bhamidi, S., Scherman, M. S., Rithner, C. D., Prenni, J. E., Chatterjee, D., Khoo, K. H., & McNeil, M. R. 2008. The identification and location of succinyl residues and the characterization of

the interior arabinan region allow for a model of the complete primary structure of *Mycobacterium tuberculosis* mycolyl arabinogalactan. *Journal of Biological Chemistry*, *283*, 12992–13000. https://doi.org/10.1074/jbc.M800222200

Bhatt, A., Brown, A. K., Singh, A., Minnikin, D. E., & Besra, G. S. 2008. Loss of a Mycobacterial Gene Encoding a Reductase Leads to an Altered Cell Wall Containing β-oxo- Mycolic Acid Analogs and Accumulation of Ketones. *Chemistry and Biology*, *15*, 930–939. https://doi.org/10.1016/j.chembiol.2008.07.007

Bhatt, A., Kremer, L., Dai, A. Z., Sacchettini, J. C., & Jacobs, W. R. 2005. Conditional depletion of KasA, a key enzyme of mycolic acid biosynthesis, leads to mycobacterial cell lysis. *Journal of Bacteriology*, *187*, 7596–7606. https://doi.org/10.1128/JB.187.22.7596-7606.2005

Bhowruth, V., Brown, A. K., Reynolds, R. C., Coxon, G. D., Mackay, S. P., Minnikin, D. E., & Besra, G. S. 2006. Symmetrical and unsymmetrical analogues of isoxyl; active agents against *Mycobacterium tuberculosis*. *Bioorganic and Medicinal Chemistry Letters*, *16*, 4743–4747. https://doi.org/10.1016/j.bmcl.2006.06.095

Biava, M., Porretta, G. C., Poce, G., De Logu, A., Saddi, M., Meleddu, R., Manetti, F., De Rossi, E., & Botta, M. 2008. 1,5-Diphenylpyrrole derivatives as antimycobacterial agents. Probing the influence on antimycobacterial activity of lipophilic substituents at the phenyl rings. *Journal of Medicinal Chemistry*, *51*, 3644–3648. https://doi.org/10.1021/jm701560p

Birch, H. L., Alderwick, L. J., Bhatt, A., Rittmann, D., Krumbach, K., Singh, A., Bai, Y., Lowary, T. L., Eggeling, L., & Besra, G. S. 2008. Biosynthesis of mycobacterial arabinogalactan: Identification of a novel α(1→3) arabinofuranosyltransferase. *Molecular Microbiology*, *69*, 1191–1206. https://doi.org/10.1111/j.1365-2958.2008.06354.x

Bloch, H., & Segal, W. 1956. Biochemical differentiation of Mycobacterium tuberculosis grown *in vivo* and *in vitro*. *Journal of Bacteriology*, *72*, 132–141. https://doi.org/10.1128/JB.72.2.132-141.1956

Bloch, K., & Vance, D. 1977. Control mechanisms in the synthesis of saturated fatty acids. In *Annual review of biochemistry* (Vol. 46, pp. 263–298). https://doi.org/10.1146/annurev.bi.46.070177.001403

Blondiaux, N., Moune, M., Desroses, M., Frita, R., Flipo, M., Mathys, V., Soetaert, K., Kiass, M., Delorme, V., Djaout, K., Trebosc, V., Kemmer, C., Wintjens, R., Wohlkönig, A., Antoine, R., Huot, L., Hot, D., Coscolla, M., Feldmann, J., … Baulard, A. R. 2017. Reversion of antibiotic resistance in *Mycobacterium tuberculosis* by spiroisoxazoline SMARt-420. *Science*, *355*, 1206–1211. https://doi.org/10.1126/science.aag1006

Bohlin, J., Brynildsrud, O., Vesth, T., Skjerve, E., & Ussery, D. W. 2013. Amino Acid Usage Is Asymmetrically Biased in AT- and GC-Rich Microbial Genomes. *PLoS ONE*, *8*. https://doi.org/10.1371/journal.pone.0069878

Bolla, J. R. 2020. Targeting MmpL3 for anti-tuberculosis drug development. In *Biochemical Society Transactions* (Vol. 48, Issue 4, pp. 1463–1472). https://doi.org/10.1042/BST20190950

Bolla, J. R., Sauer, J. B., Wu, D., Mehmood, S., Allison, T. M., & Robinson, C. V. 2018. Direct observation of the influence of cardiolipin and antibiotics on lipid II binding to MurJ. *Nature Chemistry*, *10*, 363–371. https://doi.org/10.1038/nchem.2919

Boonkerd, N. 1998. Symbiotic association between Frankia and actinorhizal plants. In *Nitrogen Fixation with Non-Legumes* (pp. 327–331). https://doi.org/10.1007/978-94-011-5232-7_38

Bournez, C., Carles, F., Peyrat, G., Aci-Sèche, S., Bourg, S., Meyer, C., & Bonnet, P. 2020. Comparative assessment of protein kinase inhibitors in public databases and in PKIDB. *Molecules*, *25*. https://doi.org/10.3390/molecules25143226

Brauner, A., Fridman, O., Gefen, O., & Balaban, N. Q. 2016. Distinguishing between resistance, tolerance and persistence to antibiotic treatment. In *Nature Reviews Microbiology* (Vol. 14, Issue 5, pp. 320–330). https://doi.org/10.1038/nrmicro.2016.34

Brennan, P. J., & Nikaido, H. 1995. The envelope of mycobacteria. In *Annual Review of Biochemistry* (Vol. 64, pp. 29–63). https://doi.org/10.1146/annurev.bi.64.070195.000333

Brown, A. K., Bhatt, A., Singh, A., Saparia, E., Evans, A. F., & Besra, G. S. 2007. Identification of the dehydratase component of the mycobacterial mycolic acid-synthesizing fatty acid synthase-II complex. *Microbiology*, *153*, 4166–4173. https://doi.org/10.1099/mic.0.2007/012419-0

Bruning, J. B., Murillo, A. C., Chacon, O., Barletta, R. G., & Sacchettini, J. C. 2011. Structure of the *Mycobacterium tuberculosis* D-alanine:D-alanine ligase, a target of the antituberculosis drug D-cycloserine. *Antimicrobial Agents and Chemotherapy*, *55*, 291–301. https://doi.org/10.1128/AAC.00558-10

Burk, D. L., & Berghuis, A. M. 2002. Protein kinase inhibitors and antibiotic resistance. *Pharmacology and Therapeutics*, *93*, 283–292. https://doi.org/10.1016/S0163-7258(02)00197-3

Butt, SS., Badshah, Y., Shabbir, M., Rafiq, M., 2020., Molecular Docking Using Chimera and Autodock Vina Software for Nonbioinformaticians. *JMIR Bioinform Biotech* 1(1):e14232 doi: 10.2196/14232

Calmette, A. 1928. On preventive vaccination of the new-born against tuberculosis by B.C.G. *British Journal of Tuberculosis*, *22*, 161–165. https://doi.org/10.1016/S0366-0850(28)80052-4

Campbell, E. A., Korzheva, N., Mustaev, A., Murakami, K., Nair, S., Goldfarb, A., & Darst, S. A. 2001. Structural mechanism for rifampicin inhibition of bacterial RNA polymerase. *Cell*, *104*, 901–912. https://doi.org/10.1016/S0092-8674(01)00286-0

Cao, J., Zhou, Y., Peng, H., Huang, X., Stahler, S., Suri, V., Qadri, A., Gareski, T., Jones, J., Hahm, S., Perreault, M., McKew, J., Shi, M., Xu, X., Tobin, J. F., & Gimeno, R. E. 2011. Targeting acyl-CoA:Diacylglycerol Acyltransferase 1 (DGAT1) with small molecule inhibitors for the treatment of metabolic diseases. *Journal of Biological Chemistry*, *286*, 41838–41851. https://doi.org/10.1074/jbc.M111.245456

Carles, F., Bourg, S., Meyer, C., & Bonnet, P. 2018. PKIDB: A curated, annotated and updated database of protein kinase inhibitors in clinical trials. *Molecules*, *23*. https://doi.org/10.3390/molecules23040908

Cases, S., Smith, S. J., Zheng, Y. W., Myers, H. M., Lear, S. R., Sande, E., Novak, S., Collins, C., Welch, C. B., Lusis, A. J., Erickson, S. K., & Farese, R. V. 1998. Identification of a gene encoding an acyl CoA:diacylglycerol acyltransferase, a key enzyme in triacylglycerol

synthesis. *Proceedings of the National Academy of Sciences of the United States of America*, *95*, 13018–13023. https://doi.org/10.1073/pnas.95.22.13018

Cases, S., Stone, S. J., Zhou, P., Yen, E., Tow, B., Lardizabal, K. D., Voelker, T., & Farese, R. V. 2001. Cloning of DGAT2, a Second Mammalian Diacylglycerol Acyltransferase, and Related Family Members. *Journal of Biological Chemistry*, *276*, 38870–38876. https://doi.org/10.1074/jbc.M106219200

Castillo-Pichardo, L., Humphries-Bickley, T., De La Parra, C., Forestier-Roman, I., Martinez-Ferrer, M., Hernandez, E., Vlaar, C., Ferrer-Acosta, Y., Washington, A. V., Cubano, L. A., Rodriguez-Orengo, J., & Dharmawardhane, S. 2014. The Rac inhibitor EHop-016 inhibits mammary tumor growth and metastasis in a nude mouse model. *Translational Oncology*, *7*, 546–555. https://doi.org/10.1016/j.tranon.2014.07.004

Chardin, P. 2006. Function and regulation of Rnd proteins. In *Nature Reviews Molecular Cell Biology* (Vol. 7, Issue 1, pp. 54–62). https://doi.org/10.1038/nrm1788

Chatterjee, D., Hunter, S. W., McNeil, M., & Brennan, P. J. 1992. Lipoarabinomannan. Multiglycosylated form of the mycobacterial mannosylphosphatidylinositols. *Journal of Biological Chemistry*, *267*, 6228–6233. https://doi.org/10.1016/s0021-9258(18)42685-3

Chauhan, S., & Tyagi, J. S. 2009. Powerful induction of divergent *tgs1-Rv3131* genes in *Mycobacterium tuberculosis* is mediated by DevR interaction with a high-affinity site and an adjacent cryptic low-affinity site. *Journal of Bacteriology*, *191*, 6075–6081. https://doi.org/10.1128/JB.00310-09

Chen, K. T., Chen, P. T., Lin, C. K., Huang, L. Y., Hu, C. M., Chang, Y. F., Hsu, H. T., Cheng, T. J. R., Wu, Y. T., & Cheng, W. C. 2016. Structural Investigation of Park's Nucleotide on Bacterial Translocase MraY: Discovery of Unexpected MraY Inhibitors. *Scientific Reports*, *6*. https://doi.org/10.1038/srep31579

Chiarelli, L. R., Mori, G., Orena, B. S., Esposito, M., Lane, T., De Jesus Lopes Ribeiro, A. L., Degiacomi, G., Zemanová, J., Szádocka, S., Huszár, S., Palčeková, Z., Manfredi, M., Gosetti, F., Lelièvre, J., Ballell, L., Kazakova, E., Makarov, V., Marengo, E., Mikušová, K., … Pasca, M. R. 2018. A multitarget approach to drug discovery inhibiting *Mycobacterium tuberculosis* PyrG and PanK. *Scientific Reports*, *8*. https://doi.org/10.1038/s41598-018-21614-4

Chochois, H., Sauthier, M., Maerten, E., Castanet, Y., & Mortreux, A. 2006. 1,4-Carbonylative addition of arylboronic acids to methyl vinyl ketone: a new synthetic tool for rapid furan and pyrrole synthesis. *Tetrahedron*, *62*, 11740–11746. https://doi.org/10.1016/j.tet.2006.09.035

Choi, K. H., Kremer, L., Besra, G. S., & Rock, C. O. 2000. Identification and substrate specificity of β-Ketoacyl (Acyl carrier protein) synthase III (mtFabH) from mycobacterium tuberculosis. *Journal of Biological Chemistry*, *275*, 28201–28207. https://doi.org/10.1074/jbc.M003241200

Chorine, V. 1945. Action de l'amide nicotinique sur les bacilles du genre Mycobacterium. *Comp Rend Acad Sci (Paris)*, *220*, 150–151.

Christensen, H., Garton, N. J., Horobin, R. W., Minnikin, D. E., & Barer, M. R. 1999. Lipid domains of mycobacteria studied with fluorescent molecular probes. *Molecular Microbiology*, *31*, 1561–1572. https://doi.org/10.1046/j.1365-2958.1999.01304.x

Colangeli, R., Gupta, A., Vinhas, S. A., Chippada Venkata, U. D., Kim, S., Grady, C., Jones-López, E. C., Soteropoulos, P., Palaci, M., Marques-Rodrigues, P., Salgame, P., Ellner, J. J., Dietze, R., & Alland, D. 2020. *Mycobacterium tuberculosis* progresses through two phases of latent infection in humans. *Nature Communications*, *11*. https://doi.org/10.1038/s41467-020-18699-9

Cole, S. T., Brosch, R., Parkhill, J., Garnier, T., Churcher, C., Harris, D., Gordon, S. V., Eiglmeier, K., Gas, S., Barry, C. E., Tekaia, F., Badcock, K., Basham, D., Brown, D., Chillingworth, T., Connor, R., Davies, R., Devlin, K., Feltwell, T., … Barrell, B. G. 1998. Deciphering the biology of *Mycobacterium tuberculosis* from the complete genome sequence. In *Nature* (Vol. 393, Issue 6685, pp. 537–544). https://doi.org/10.1038/31159

Cole, S. T., Brosch, R., Parkhill, J., Garnier, T., Churcher, C., Harris, D., Gordon, S. V, Eiglmeier, K., Gas, S., Barry 3rd, C. E., Tekaia, F., Badcock, K., Basham, D., Brown, D., Chillingworth, T., Connor, R., Davies, R., Devlin, K., Feltwell, T., … et al. 1998. Deciphering the biology of *Mycobacterium tuberculosis* from the complete genome sequence [see comments] [published erratum appears in Nature 1998 Nov 12;396(6707):190]. *Nature*, *393*, 537–544.

Coleman, R. A. 1992. Diacylglycerol acyltransferase and monoacylglycerol acyltransferase from liver and intestine. *Methods in Enzymology*, *209*, 98–104. https://doi.org/10.1016/0076-6879(92)09013-S

Coleman, R., & Bell, R. M. 1976. Triacylglycerol synthesis in isolated fat cells. Studies on the microsomal diacylglycerol acyltransferase activity using ethanol-dispersed diacylglycerols. *Journal of Biological Chemistry*, *251*, 4537–4543. https://doi.org/10.1016/s0021-9258(17)33235-0

Cox, J. A. G., Abrahams, K. A., Alemparte, C., Ghidelli-Disse, S., Rullas, J., Angulo-Barturen, I., Singh, A., Gurcha, S. S., Nataraj, V., Bethell, S., Remuiñán, M. J., Encinas, L., Jervis, P. J., Cammack, N. C., Bhatt, A., Kruse, U., Bantscheff, M., Fütterer, K., Barros, D., … Besra, G. S. 2016. THPP target assignment reveals EchA6 as an essential fatty acid shuttle in mycobacteria. *Nature Microbiology*, *1*. https://doi.org/10.1038/nmicrobiol.2015.6

Crellin, P. K., Kovacevic, S., Martin, K. L., Brammananth, R., Morita, Y. S., Billman-Jacobe, H., McConville, M. J., & Coppel, R. L. 2008. Mutations in *pimE* restore lipoarabinomannan synthesis and growth in a *Mycobacterium smegmatis* lpqW mutant. *Journal of Bacteriology*, *190*, 3690–3699. https://doi.org/10.1128/JB.00200-08

Crotta Asis, A., Savoretti, F., Cabruja, M. *et al.* 2021. Characterization of key enzymes involved in triacylglycerol biosynthesis in mycobacteria. *Sci Rep* 11, 13257. https://doi.org/10.1038/s41598-021-92721-y

Daffe, M., Brennan, P. J., & McNeil, M. 1990. Predominant structural features of the cell wall arabinogalactan of *Mycobacterium tuberculosis* as revealed through characterization of oligoglycosyl alditol fragments by gas chromatography/mass spectrometry and by 1H and 13C NMR analyses. *Journal of Biological Chemistry*, *265*, 6734–6743. https://doi.org/10.1016/s0021-9258(19)39211-7

Dalmer O, Walter E, F. E. M. in D. 1936. *Verfahren zur Herstellung von Abkömmlingen der Pyrazinmonocarbonsäure*.

Daniel, J., Deb, C., Dubey, V. S., Sirakova, T. D., Abomoelak, B., Morbidoni, H. R., & Kolattukudy, P. E. 2004. Induction of a novel class of diacylglycerol acyltransferases and triacylglycerol accumulation in *Mycobacterium tuberculosis* as it goes into a dormancy-like state in

culture. *Journal of Bacteriology*, *186*, 5017–5030. https://doi.org/10.1128/JB.186.15.5017-5030.2004

Daniel, J., Maamar, H., Deb, C., Sirakova, T. D., & Kolattukudy, P. E. 2011. *Mycobacterium tuberculosis* uses host triacylglycerol to accumulate lipid droplets and acquires a dormancy-like phenotype in lipid-loaded macrophages. *PLoS Pathogens*, *7*. https://doi.org/10.1371/journal.ppat.1002093

Daniel, T. M. 2005. Leon Charles Albert Calmette and BCG vaccine. In *International Journal of Tuberculosis and Lung Disease* (Vol. 9, Issue 9, pp. 944–945).

Daniel, T. M. 2006. The history of tuberculosis. *Respiratory Medicine*, *100*, 1862–1870. https://doi.org/10.1016/j.rmed.2006.08.006

Danner, S. A., Carr, A., Leonard, J. M., Lehman, L. M., Gudiol, F., Gonzales, J., Raventos, A., Rubio, R., Bouza, E., Pintado, V., Aguado, A. G., Garcia de Lomas, J., Delgado, R., Borleffs, J. C. C., Hsu, A., Valdes, J. M., Boucher, C. A. B., & Cooper, D. A. 1995. A Short-Term Study of the Safety, Pharmacokinetics, and Efficacy of Ritonavir, an Inhibitor of HIV-1 Protease. *New England Journal of Medicine*, *333*, 1528–1534. https://doi.org/10.1056/nejm199512073332303

Dartois, V. 2014. The path of anti-tuberculosis drugs: From blood to lesions to mycobacterial cells. *Nature Reviews Microbiology*, *12*, 159–167. https://doi.org/10.1038/nrmicro3200

De La Rua-Domenech, R. 2006. Human *Mycobacterium bovis* infection in the United Kingdom: Incidence, risks, control measures and review of the zoonotic aspects of bovine tuberculosis. In *Tuberculosis* (Vol. 86, Issue 2, pp. 77–109). https://doi.org/10.1016/j.tube.2005.05.002

de Martino, M., Lodi, L., Galli, L., & Chiappini, E. 2019. Immune Response to *Mycobacterium tuberculosis*: A Narrative Review. *Frontiers in Pediatrics*. https://doi.org/10.3389/fped.2019.00350

De Smet, K. A. L., Kempsell, K. E., Gallagher, A., Duncan, K., & Young, D. B. 1999. Alteration of a single amino acid residue reverses fosfomycin resistance of recombinant MurA from Mycobacterium tuberculosis. *Microbiology*, *145*, 3177–3184. https://doi.org/10.1099/00221287-145-11-3177

de Souza, G. A., Leversen, N. A., Målen, H., & Wiker, H. G. 2011. Bacterial proteins with cleaved or uncleaved signal peptides of the general secretory pathway. *Journal of Proteomics*, *75*, 502–510. https://doi.org/10.1016/j.jprot.2011.08.016

Deb, C., Lee, C. M., Dubey, V. S., Daniel, J., Abomoelak, B., Sirakova, T. D., Pawar, S., Rogers, L., & Kolattukudy, P. E. 2009. A novel in vitro multiple-stress dormancy model for mycobacterium tuberculosis generates a lipid-loaded, drug-tolerant, dormant pathogen. *PLoS ONE*, *4*. https://doi.org/10.1371/journal.pone.0006077

DeBarber, A. E., Mdluli, K., Bosman, M., Bekker, L. G., & Barry, C. E. 2000. Ethionamide activation and sensitivity in multidrug-resistant *Mycobacterium tuberculosis*. *Proceedings of the National Academy of Sciences of the United States of America*, *97*, 9677–9682. https://doi.org/10.1073/pnas.97.17.9677

Degiacomi, G., Benjak, A., Madacki, J., Boldrin, F., Provvedi, R., Palù, G., Kordulakova, J., Cole, S. T., & Manganelli, R. 2017. Essentiality of mmpL3 and impact of its silencing on

Mycobacterium tuberculosis gene expression. *Scientific Reports*, *7*. https://doi.org/10.1038/srep43495

Deidda, D., Lampis, G., Fioravanti, R., Biava, M., Porretta, G. C., Zanetti, S., & Pompei, R. 1998. Bactericidal activities of the pyrrole derivative BM212 against multidrug-resistant and intramacrophagic *Mycobacterium tuberculosis* strains. *Antimicrobial Agents and Chemotherapy*, *42*, 3035–3037. https://doi.org/10.1128/aac.42.11.3035

Dejesus, M. A., Gerrick, E. R., Xu, W., Park, S. W., Long, J. E., Boutte, C. C., Rubin, E. J., Schnappinger, D., Ehrt, S., Fortune, S. M., Sassetti, C. M., & Ioerger, T. R. 2017. Comprehensive essentiality analysis of the *Mycobacterium tuberculosis* genome via saturating transposon mutagenesis. *MBio*, *8*. https://doi.org/10.1128/mBio.02133-16

Deng, L., Mikusova, K., Robuck, K. G., Scherman, M., Brennan, P. J., & McNeil, M. R. 1995. Recognition of multiple effects of ethambutol on metabolism of mycobacterial cell envelope. *Antimicrobial Agents and Chemotherapy*, *39*, 694–701. https://doi.org/10.1128/AAC.39.3.694

Denison, H., Nilsson, C., Löfgren, L., Himmelmann, A., Mårtensson, G., Knutsson, M., Al-Shurbaji, A., Tornqvist, H., & Eriksson, J. W. 2014. Diacylglycerol acyltransferase 1 inhibition with AZD7687 alters lipid handling and hormone secretion in the gut with intolerable side effects: A randomized clinical trial. *Diabetes, Obesity and Metabolism*, *16*, 334–343. https://doi.org/10.1111/dom.12221

Dessen, A., Quémard, A., Blanchard, J. S., Jacobs, W. R., & Sacchettini, J. C. 1995. Crystal structure and function of the isoniazid target of *Mycobacterium tuberculosis*. *Science*, *267*, 1638–1641. https://doi.org/10.1126/science.7886450

Devita, R. J., & Pinto, S. 2013. Current status of the research and development of diacylglycerol o -acyltransferase 1 (DGAT1) inhibitors. *Journal of Medicinal Chemistry*, *56*, 9820–9825. https://doi.org/10.1021/jm4007033

Dianišková, P., Korduláḱová, J., Sḱovierová, H., Kaur, D., Jackson, M., Brennan, P. J., & Mikusŏvá, K. 2011. Investigation of ABC transporter from mycobacterial arabinogalactan biosynthetic cluster. *General Physiology and Biophysics*, *30*, 239–250. https://doi.org/10.4149/gpb_2011_03_239

Dinadayala, P., Kaur, D., Berg, S., Amin, A. G., Vissa, V. D., Chatterjee, D., Brennan, P. J., & Crick, D. C. 2006. Genetic basis for the synthesis of the immunomodulatory mannose caps of lipoarabinomannan in *Mycobacterium tuberculosis*. *Journal of Biological Chemistry*, *281*, 20027–20035. https://doi.org/10.1074/jbc.M603395200

Dmitriev BA, Ehlers S, Rietschel ET. Layered murein revisited: a fundamentally new concept of bacterial cell wall structure, biogenesis and function. 1999 *Med Microbiol Immunol*. Mar;187(3):173-81. doi: 10.1007/s004300050090. PMID: 10206149.

Dmitriev, B. A., Ehlers, S., Rietschel, E. T., & Brennan, P. J. 2000. Molecular mechanics of the mycobacterial cell wall: From horizontal layers to vertical scaffolds. *International Journal of Medical Microbiology*, *290*, 251–258. https://doi.org/10.1016/S1438-4221(00)80122-8

Dmitriev, B. A., Toukach, F. V., Schaper, K. J., Holst, O., Rietschel, E. T., & Ehlers, S. 2003. Tertiary structure of bacterial murein: The scaffold model. *Journal of Bacteriology*. https://doi.org/10.1128/JB.185.11.3458-3468.2003

Dobson, M. J. 2015. *Murderous contagion : a human history of disease*. Quercus.

Doetsch, R. N. 1978. Benjamin Marten and his "New Theory of Consumptions." *Microbiological Reviews*, *42*, 521–528. https://doi.org/10.1128/mr.42.3.521-528.1978

Domenech, P., & Reed, M. B. 2009. Rapid and spontaneous loss of phthiocerol dimycocerosate (PDIM) from *Mycobacterium tuberculosis* grown in vitro: Implications for virulence studies. *Microbiology*, *155*, 3532–3543. https://doi.org/10.1099/mic.0.029199-0

Domenech, P., Reed, M. B., & Barry, C. E. 2005. Contribution of the *Mycobacterium tuberculosis* MmpL protein family to virulence and drug resistance. *Infection and Immunity*, *73*, 3492–3501. https://doi.org/10.1128/IAI.73.6.3492-3501.2005

Donoghue, H. D., Lee, O. Y. C., Minnikin, D. E., Besra, G. S., Taylor, J. H., & Spigelman, M. 2010. Tuberculosis in Dr Granville's mummy: A molecular re-examination of the earliest known Egyptian mummy to be scientifically examined and given a medical diagnosis. *Proceedings of the Royal Society B: Biological Sciences*, *277*, 51–56. https://doi.org/10.1098/rspb.2009.1484

Dover, L. G., Alahari, A., Gratraud, P., Gomes, J. M., Bhowruth, V., Reynolds, R. C., Besra, G. S., & Kremer, L. 2007. EthA, a common activator of thiocarbamide-containing drugs acting on different mycobacterial targets. *Antimicrobial Agents and Chemotherapy*, *51*, 1055–1063. https://doi.org/10.1128/AAC.01063-06

Dover, L. G., Corsino, P. E., Daniels, I. R., Cocklin, S. L., Tatituri, V., Besra, G. S., & Fütterer, K. 2004. Crystal structure of the TetR/CamR family repressor *Mycobacterium tuberculosis* EthR implicated in ethionamide resistance. *Journal of Molecular Biology*, *340*, 1095–1105. https://doi.org/10.1016/j.jmb.2004.06.003

Drancourt, M. 2009. Mycobacterium: genomics and molecular biology. In A. Brown (Ed.), *The Lancet Infectious Diseases* (Vol. 9, Issue 9). Caister Academic Press. https://doi.org/10.1016/s1473-3099(09)70221-x

Draper, P., Khoo, K. H., Chatterjee, D., Dell, A., & Morris, H. R. 1997. Galactosamine in walls of slow-growing mycobacteria. *Biochemical Journal*, *327*, 519–525. https://doi.org/10.1042/bj3270519

Du, P., Sohaskey, C. D., & Shi, L. 2016. Transcriptional and physiological changes during *Mycobacterium tuberculosis* reactivation from non-replicating persistence. *Frontiers in Microbiology*, *7*. https://doi.org/10.3389/fmicb.2016.01346

Eberhardt, J., Santos-Martins, D., Tillack, A.F., Forli, S. 2021. AutoDock Vina 1.2.0: New Docking Methods, Expanded Force Field, and Python Bindings. *Journal of Chemical Information and Modeling.*

Eberl, H. C., Werner, T., Reinhard, F. B., Lehmann, S., Thomson, D., Chen, P., Zhang, C., Rau, C., Muelbaier, M., Drewes, G., Drewry, D., & Bantscheff, M. 2019. Chemical proteomics reveals target selectivity of clinical Jak inhibitors in human primary cells. *Scientific Reports*, *9*. https://doi.org/10.1038/s41598-019-50335-5

Emami, K., Guyet, A., Kawai, Y., Devi, J., Wu, L. J., Allenby, N., Daniel, R. A., & Errington, J. 2017. RodA as the missing glycosyltransferase in Bacillus subtilis and antibiotic discovery for the peptidoglycan polymerase pathway. *Nature Microbiology*, *2*. https://doi.org/10.1038/nmicrobiol.2016.253

Eniyan, K., Dharavath, S., Vijayan, R., Bajpai, U., & Gourinath, S. 2018. Crystal structure of UDP-N-acetylglucosamine-enolpyruvate reductase (MurB) from *Mycobacterium tuberculosis*. *Biochimica et Biophysica Acta - Proteins and Proteomics*, *1866*, 397–406. https://doi.org/10.1016/j.bbapap.2017.11.013

Escuyer, V. E., Lety, M. A., Torrelles, J. B., Khoo, K. H., Tang, J. B., Rithner, C. D., Frehel, C., McNeil, M. R., Brennan, P. J., & Chatterjee, D. 2001. The Role of the *embA* and *embB* Gene Products in the Biosynthesis of the Terminal Hexaarabinofuranosyl Motif of Mycobacterium smegmatis Arabinogalactan. *Journal of Biological Chemistry*, *276*, 48854–48862. https://doi.org/10.1074/jbc.M102272200

Espitia, C., Laclette, J. P., Mondragón-Palomino, M., Amador, A., Campuzano, J., Martens, A., Singh, M., Cicero, R., Zhang, Y., & Moreno, C. 1999. The PE-PGRS glycine-rich proteins of *Mycobacterium tuberculosis*: A new family of fibronectin-binding proteins? *Microbiology*, *145*, 3487–3495. https://doi.org/10.1099/00221287-145-12-3487

Esumi, N., Suzuki, K., Nishimoto, Y., & Yasuda, M. 2016. Synthesis of 1,4-Dicarbonyl Compounds from Silyl Enol Ethers and Bromocarbonyls, Catalyzed by an Organic Dye under Visible-Light Irradiation with Perfect Selectivity for the Halide Moiety over the Carbonyl Group. *Organic Letters*, *18*, 5704–5707. https://doi.org/10.1021/acs.orglett.6b02869

Ezekiel, D. H., & Hutchins, J. E. 1968. Mutations affecting RNA polymerase associated with rifampicin resistance in *Escherichia coli.* 22. In *Nature* (Vol. 220, Issue 5164, pp. 276–277). https://doi.org/10.1038/220276a0

Fabbro, D. 2015. 25 Years of small molecular weight kinase inhibitors: Potentials and limitations. In *Molecular Pharmacology* (Vol. 87, Issue 5, pp. 766–775). https://doi.org/10.1124/mol.114.095489

Faria, S., Joao, I., & Jordao, L. 2015. General Overview on Nontuberculous Mycobacteria, Biofilms, and Human Infection. *Journal of Pathogens*, *2015*, 1–10. https://doi.org/10.1155/2015/809014

FDA. 2019. *FDA approves new drug for treatment-resistant forms of tuberculosis that affects the lungs*. Case Medical Research. https://doi.org/10.31525/cmr-1a2db41

Feklistov, A., Mekler, V., Jiang, Q., Westblade, L. F., Irschik, H., Jansen, R., Mustaev, A., Darst, S. A., & Ebright, R. H. 2008. Rifamycins do not function by allosteric modulation of binding of Mg 2+ to the RNA polymerase active center. *Proceedings of the National Academy of Sciences of the United States of America*, *105*, 14820–14825. https://doi.org/10.1073/pnas.0802822105

Ferguson, F. M., & Gray, N. S. 2018. Kinase inhibitors: The road ahead. In *Nature Reviews Drug Discovery* (Vol. 17, Issue 5, pp. 353–376). https://doi.org/10.1038/nrd.2018.21

Fisch, M. H., & Drabkin, I. E. 1952. Caelius Aurelianus: On Acute Diseases and on Chronic Diseases. In I. E. Drabkin (Ed.), *The Classical Weekly* (Vol. 45, Issue 10). https://doi.org/10.2307/4343144

Fridman, O., Goldberg, A., Ronin, I., Shoresh, N., & Balaban, N. Q. 2014. Optimization of lag time underlies antibiotic tolerance in evolved bacterial populations. *Nature*, *513*, 418–421. https://doi.org/10.1038/nature13469

Frith, J. 2014. History of tuberculosis. Part 2 - The sanatoria and the discoveries of the tubercle

bacillus. *Journal of Military and Veterans' Health*, *22*, 36–41.

Gande, R., Dover, L. G., Krumbach, K., Besra, G. S., Sahm, H., Oikawa, T., & Eggeling, L. 2007. The two carboxylases of corynebacterium glutamicum essential for fatty acid and mycolic acid synthesis. *Journal of Bacteriology*, *189*, 5257–5264. https://doi.org/10.1128/JB.00254-07

Ganji, S. H., Tavintharan, S., Zhu, D., Xing, Y., Kamanna, V. S., & Kashyap, M. L. 2004. Niacin noncompetitively inhibits DGAT2 but not DGAT1 activity in HepG2 cells. *Journal of Lipid Research*, *45*, 1835–1845. https://doi.org/10.1194/jlr.M300403-JLR200

García-García, V., Oldfield, E., & Benaim, G. 2016. Inhibition of Leishmania mexicana growth by the tuberculosis drug SQ109. *Antimicrobial Agents and Chemotherapy*, *60*, 6386–6389. https://doi.org/10.1128/AAC.00945-16

Garton, N. J., Christensen, H., Minnikin, D. E., Adegbola, R. A., & Barer, M. R. 2002. Intracellular lipophilic inclusions of mycobacteria in vitro and in sputum. *Microbiology*, *148*, 2951–2958. https://doi.org/10.1099/00221287-148-10-2951

Gavalda, S., Bardou, F., Laval, F., Bon, C., Malaga, W., Chalut, C., Guilhot, C., Mourey, L., Daffé, M., & Quémard, A. 2014. The polyketide synthase Pks13 catalyzes a novel mechanism of lipid transfer in mycobacteria. *Chemistry and Biology*, *21*, 1660–1669. https://doi.org/10.1016/j.chembiol.2014.10.011

Gianti, E., & Zauhar, R. J. 2021. Structure–activity relationships and drug design. In *Remington* (pp. 129–153). https://doi.org/10.1016/b978-0-12-820007-0.00007-6

Gil, Z., Martinez-Sotillo, N., Pinto-Martinez, A., Mejias, F., Martinez, J. C., Galindo, I., Oldfield, E., & Benaim, G. 2020. SQ109 inhibits proliferation of *Leishmania donovani* by disruption of intracellular Ca2+ homeostasis, collapsing the mitochondrial electrochemical potential (ΔΨm) and affecting acidocalcisomes. *Parasitology Research*, *119*, 649–657. https://doi.org/10.1007/s00436-019-06560-y

Gill, S. K., & Garcia, G. A. 2011. Rifamycin inhibition of WT and Rif-resistant *Mycobacterium tuberculosis* and *Escherichia coli* RNA polymerases *in vitro*. *Tuberculosis*, *91*, 361–369. https://doi.org/10.1016/j.tube.2011.05.002

Glass, L. N., Swapna, G., Chavadi, S. S., Tufariello, J. A. M., Mi, K., Drumm, J. E., Lam, T. K. T., Zhu, G., Zhan, C., Vilchéze, C., Arcos, J., Chen, Y., Bi, L., Mehta, S., Porcelli, S. A., Almo, S. C., Yeh, S. R., Jacobs, W. R., Torrelles, J. B., & Chan, J. 2017. *Mycobacterium tuberculosis* universal stress protein Rv2623 interacts with the putative ATP binding cassette (APC) transporter Rv1747 to regulate mycobacterial growth. *PLoS Pathogens*, *13*. https://doi.org/10.1371/journal.ppat.1006515

Glickman, M. S. 2003. The *mmaA2* gene of *Mycobacterium tuberculosis* encodes the distal cyclopropane synthase of the α-mycolic acid. *Journal of Biological Chemistry*, *278*, 7844–7849. https://doi.org/10.1074/jbc.M212458200

Glickman, M. S., Cox, J. S., & Jacobs, W. R. 2000. A novel mycolic acid cyclopropane synthetase is required for cording, persistence, and virulence of *Mycobacterium tuberculosis*. *Molecular Cell*, *5*, 717–727. https://doi.org/10.1016/S1097-2765(00)80250-6

Goffin, C., & Ghuysen, J.-M. 2002. Biochemistry and Comparative Genomics of SxxK Superfamily Acyltransferases Offer a Clue to the Mycobacterial Paradox: Presence of Penicillin-Susceptible Target Proteins versus Lack of Efficiency of Penicillin as Therapeutic Agent.

Microbiology and Molecular Biology Reviews, *66*, 702–738. https://doi.org/10.1128/mmbr.66.4.702-738.2002

Gopal, P., Nartey, W., Ragunathan, P., Sarathy, J., Kaya, F., Yee, M., Setzer, C., Manimekalai, M. S. S., Dartois, V., Grüber, G., & Dick, T. 2017. Pyrazinoic Acid Inhibits Mycobacterial Coenzyme A Biosynthesis by Binding to Aspartate Decarboxylase PanD. *ACS Infectious Diseases*, *3*, 807–819. https://doi.org/10.1021/acsinfecdis.7b00079

Gopal, P., Tasneen, R., Yee, M., Lanoix, J. P., Sarathy, J., Rasic, G., Li, L., Dartois, V., Nuermberger, E., & Dick, T. 2017. In Vivo-Selected Pyrazinoic Acid-Resistant *Mycobacterium tuberculosis* Strains Harbor Missense Mutations in the Aspartate Decarboxylase PanD and the Unfoldase ClpC1. *ACS Infectious Diseases*, *3*, 492–501. https://doi.org/10.1021/acsinfecdis.7b00017

Gopal, P., Yee, M., Sarathy, J., Liang Low, J., Sarathy, J. P., Kaya, F., Dartois, V., Gengenbacher, M., & Dick, T. 2016. Pyrazinamide resistance is caused by two distinct mechanisms: Prevention of coenzyme a depletion and loss of virulence factor synthesis. *ACS Infectious Diseases*, *2*, 616–626. https://doi.org/10.1021/acsinfecdis.6b00070

Gopalan, N., Santhanakrishnan, R. K., Palaniappan, A. N., Menon, P. A., Lakshman, S., Chandrasekaran, P., Sivaramakrishnan, G. N., Reddy, D., Kannabiran, B. P., Agiboth, H. K. K., Krishnamoorthy, V., Rathinam, S., Chockalingam, C., Manoharan, T., Ayyamperumal, M. M., Jayanthi, N., Satagopan, K., Narayanan, R., Krishnaraja, R., … Swaminathan, S. 2018. Daily vs intermittent antituberculosis therapy for pulmonary tuberculosis in patients with HIV a randomized clinical trial. *JAMA Internal Medicine*, *178*, 485–493. https://doi.org/10.1001/jamainternmed.2018.0141

Goren, M. B., Brokl, O., & Schaefer, W. B. 1974. Lipids of putative relevance to virulence in *Mycobacterium tuberculosis*: Phthiocerol dimycocerosate and the attenuation indicator lipid. *Infection and Immunity*, *9*, 150–158. https://doi.org/10.1128/iai.9.1.150-158.1974

Graham, J., Wong, C. E., Day, J., McFaddin, E., Ochsner, U., Hoang, T., Young, C. L., Ribble, W., DeGroote, M. A., Jarvis, T., & Sun, X. 2018. Discovery of benzothiazole amides as potent antimycobacterial agents. *Bioorganic and Medicinal Chemistry Letters*, *28*, 3177–3181. https://doi.org/10.1016/j.bmcl.2018.08.026

Grange, J. M. 1996. The biology of the genus Mycobacterium. *Journal of Applied Microbiology Symposium Supplement*, *81*. https://doi.org/10.1111/j.1365-2672.1996.tb04592.x

Grāve, K., Bennett, M. D., & Högbom, M. 2019. Structure of *Mycobacterium tuberculosis* phosphatidylinositol phosphate synthase reveals mechanism of substrate binding and metal catalysis. *Communications Biology*, *2*. https://doi.org/10.1038/s42003-019-0427-1

Greenberg, L., Eidus, L., & Diena, B. B. 1960. The Production of Niacin by Mycobacteria. *Canadian Journal of Comparative Medicine and Veterinary Science*, *24*, 187–191.

Griffin, J. E., Gawronski, J. D., DeJesus, M. A., Ioerger, T. R., Akerley, B. J., & Sassetti, C. M. 2011. High-resolution phenotypic profiling defines genes essential for mycobacterial growth and cholesterol catabolism. *PLoS Pathogens*, *7*. https://doi.org/10.1371/journal.ppat.1002251

Groenewald, W., Baird, M. S., Verschoor, J. A., Minnikin, D. E., & Croft, A. K. 2014. Differential spontaneous folding of mycolic acids from *Mycobacterium tuberculosis*. *Chemistry and Physics of Lipids*, *180*, 15–22. https://doi.org/10.1016/j.chemphyslip.2013.12.004

Grzegorzewicz, A. E., Pham, H., Gundi, V. A. K. B., Scherman, M. S., North, E. J., Hess, T., Jones, V., Gruppo, V., Born, S. E. M., Korduláková, J., Chavadi, S. S., Morisseau, C., Lenaerts, A. J., Lee, R. E., McNeil, M. R., & Jackson, M. 2012. Inhibition of mycolic acid transport across the *Mycobacterium tuberculosis* plasma membrane. *Nature Chemical Biology*, *8*, 334–341. https://doi.org/10.1038/nchembio.794

Grzelak, E. M., Choules, M. P., Gao, W., Cai, G., Wan, B., Wang, Y., McAlpine, J. B., Cheng, J., Jin, Y., Lee, H., Suh, J. W., Pauli, G. F., Franzblau, S. G., Jaki, B. U., & Cho, S. 2019. Strategies in anti-*Mycobacterium tuberculosis* drug discovery based on phenotypic screening. In *Journal of Antibiotics* (Vol. 72, Issue 10, pp. 719–728). https://doi.org/10.1038/s41429-019-0205-9

Gu, S., Chen, J., Dobos, K. M., Bradbury, E. M., Belisle, J. T., & Chen, X. 2003. Comprehensive proteomic profiling of the membrane constituents of a *Mycobacterium tuberculosis* strain. *Molecular & Cellular Proteomics : MCP*, *2*, 1284–1296. https://doi.org/10.1074/mcp.M300060-MCP200

Guerin, M. E., Kaur, D., Somashekar, B. S., Gibbs, S., Gest, P., Chatterjee, D., Brennan, P. J., & Jackson, M. 2009. New insights into the early steps of phosphatidylinositol mannoside biosynthesis in mycobacteria: PimB' is an essential enzyme of *Mycobacterium smegmatis*. *Journal of Biological Chemistry*, *284*, 25687–25696. https://doi.org/10.1074/jbc.M109.030593

Guimarães, P. O., Quirk, D., Furtado, R. H., Maia, L. N., Saraiva, J. F., Antunes, M. O., Kalil Filho, R., Junior, V. M., Soeiro, A. M., Tognon, A. P., Veiga, V. C., Martins, P. A., Moia, D. D. F., Sampaio, B. S., Assis, S. R. L., Soares, R. V. P., Piano, L. P. A., Castilho, K., Momesso, R. G. R. A. P., … Berwanger, O. 2021. Tofacitinib in Patients Hospitalized with Covid-19 Pneumonia. *New England Journal of Medicine*, *385*, 406–415. https://doi.org/10.1056/nejmoa2101643

Guirado, E., Schlesinger, L. S., & Kaplan, G. 2013. Macrophages in tuberculosis: Friend or foe. In *Seminars in Immunopathology* (Vol. 35, Issue 5, pp. 563–583). https://doi.org/10.1007/s00281-013-0388-2

Gupta RS, Lo B, Son J. Phylogenomics and Comparative Genomic Studies Robustly Support Division of the Genus Mycobacterium into an Emended Genus Mycobacterium and Four Novel Genera. 2018. *Front Microbiol*. 9:67. doi: 10.3389/fmicb.2018.00067.

Gurcha, S. S., Baulard, A. R., Kremer, L., Locht, C., Moody, D. B., Muhlecker, W., Costello, C. E., Crick, D. C., Brennan, P. J., & Besra, G. S. 2002. Ppm1, a novel polyprenol monophosphomannose synthase from *Mycobacterium tuberculosis*. *Biochemical Journal*, *365*, 441–450. https://doi.org/10.1042/BJ20020107

Gurcha, S. S., Usha, V., Cox, J. A. G., Fütterer, K., Abrahams, K. A., Bhatt, A., Alderwick, L. J., Reynolds, R. C., Loman, N. J., Nataraj, V., Alemparte, C., Barros, D., Lloyd, A. J., Ballell, L., Hobrath, J. V., & Besra, G. S. 2014. Biochemical and structural characterization of mycobacterial aspartyl-tRNA synthetase AspS, a promising TB drug target. *PLoS ONE*, *9*. https://doi.org/10.1371/journal.pone.0113568

Gutierrez, M., Brisse, S., Brosch, R., Fabre, M., Omaïs, B., Marmiesse, M., Supply, P., & Vincent, V. 2005. Ancient origin and gene mosaicism of the progenitor of Mycobacterium tuberculosis. *PLoS Pathogens*, *1*, 0055–0061. https://doi.org/10.1371/journal.ppat.0010005

Hallyburton, I., Grimaldi, R., Woodland, A., Baragaña, B., Luksch, T., Spinks, D., James, D., Leroy, D., Waterson, D., Fairlamb, A. H., Wyatt, P. G., Gilbert, I. H., & Frearson, J. A. 2017. Screening a protein kinase inhibitor library against *Plasmodium falciparum*. *Malaria Journal*, *16*. https://doi.org/10.1186/s12936-017-2085-4

Hammond, R. J. H., Baron, V. O., Oravcova, K., Lipworth, S., & Gillespie, S. H. 2015. Phenotypic resistance in mycobacteria: Is it because I am old or fat that I resist you? *Journal of Antimicrobial Chemotherapy*, *70*, 2823–2827. https://doi.org/10.1093/jac/dkv178

Harrison, J., Lloyd, G., Joe, M., Lowary, T. L., Reynolds, E., Walters-Morgan, H., Bhatt, A., Lovering, A., Besra, G. S., & Alderwick, L. J. 2016. Lcp1 is a phosphotransferase responsible for ligating arabinogalactan to peptidoglycan in *Mycobacterium tuberculosis*. *MBio*, *7*. https://doi.org/10.1128/mBio.00972-16

Hartkoorn, R. C., Uplekar, S., & Cole, S. T. 2014. Cross-resistance between clofazimine and bedaquiline through upregulation of *mmpl5* in *Mycobacterium tuberculosis*. *Antimicrobial Agents and Chemotherapy*, *58*, 2979–2981. https://doi.org/10.1128/AAC.00037-14

Hartmann, G., Honikel, K. O., Knüsel, F., & Nüesch, J. 1967. The specific inhibition of the DNA-directed RNA synthesis by rifamycin. *BBA Section Nucleic Acids And Protein Synthesis*, *145*, 843–844. https://doi.org/10.1016/0005-2787(67)90147-5

Hayek, M. E., Mansour, M., Ndetan, H., Burkes, Q., Corkern, R., Dulli, A., Hayek, R., Parvez, K., & Singh, S. 2021. Anti-Inflammatory Treatment of COVID-19 Pneumonia With Tofacitinib Alone or in Combination With Dexamethasone is Safe and Possibly Superior to Dexamethasone as a Single Agent in a Predominantly African American Cohort. *Mayo Clinic Proceedings: Innovations, Quality & Outcomes*, *5*, 605–613. https://doi.org/10.1016/j.mayocpiqo.2021.03.007

Haygood, T. M., & Briggs, J. E. 1992. World War II military led the way in screening chest radiography. In *Military Medicine* (Vol. 157, Issue 3, pp. 113–116). https://doi.org/10.1093/milmed/157.3.113

Hayman, J. 1984. Mycobacterium Ulcerans: an Infection From Jurassic Time? *The Lancet*, *324*, 1015–1016. https://doi.org/10.1016/S0140-6736(84)91110-3

Heasman, S. J., & Ridley, A. J. 2008. Mammalian Rho GTPases: New insights into their functions from in vivo studies. In *Nature Reviews Molecular Cell Biology* (Vol. 9, Issue 9, pp. 690–701). https://doi.org/10.1038/nrm2476

Heep, M., Rieger, U., Beck, D., & Lehn, N. 2000. Mutations in the beginning of the *rpoB* gene can induce resistance to rifamycins in both *Helicobacter priori* and *Mycobacterium tuberculosis*. *Antimicrobial Agents and Chemotherapy*, *44*, 1075–1077. https://doi.org/10.1128/AAC.44.4.1075-1077.2000

Herbert Fox, H. 1952. Synthetic tuberculostats. III. isonicotinaldehyde thiosemicarbazone and some related compounds. *Journal of Organic Chemistry*, *17*, 555–562. https://doi.org/10.1021/jo01138a007

Hershkovitz, I., Donoghue, H. D., Minnikin, D. E., Besra, G. S., Lee, O. Y. C., Gernaey, A. M., Galili, E., Eshed, V., Greenblatt, C. L., Lemma, E., Bar-Gal, G. K., & Spigelman, M. 2008. Detection and molecular characterization of 9000-year-old *Mycobacterium tuberculosis* from a neolithic settlement in the Eastern mediterranean. *PLoS ONE*, *3*. https://doi.org/10.1371/journal.pone.0003426

Hett, E. C., Chao, M. C., & Rubin, E. J. 2010. Interaction and modulation of two antagonistic cell wall enzymes of mycobacteria. *PLoS Pathogens*, *6*, 1–14. https://doi.org/10.1371/journal.ppat.1001020

Hingley-Wilson, S. M., Sambandamurthy, V. K., & Jacobs, W. R. 2003. Survival perspectives from the world's most successful pathogen, *Mycobacterium tuberculosis*. In *Nature Immunology* (Vol. 4, Issue 10, pp. 949–955). https://doi.org/10.1038/ni981

Hippocrates. 1849. Book 1 - Of the Epidemics (460-370 BCE). In *The Genuine Works of Hippocrates* (Vol. 1, pp. 352–354).

Hsu, A., Granneman, G. R., & Bertz, R. J. 1998. Ritonavir: Clinical pharmacokinetics and interactions with other anti-HIV agents. *Clinical Pharmacokinetics*, *35*, 275–291. https://doi.org/10.2165/00003088-199835040-00002

Hu, Y., Coates, A. R., & Mitchison, D. A. 2006. Sterilising action of pyrazinamide in models of dormant and rifampicin-tolerant *Mycobacterium tuberculosis*. *International Journal of Tuberculosis and Lung Disease*, *10*, 317–322.

Hua, H., Kong, Q., Yin, J., Zhang, J., & Jiang, Y. 2020. Insulin-like growth factor receptor signaling in tumorigenesis and drug resistance: A challenge for cancer therapy. In *Journal of Hematology and Oncology* (Vol. 13, Issue 1). https://doi.org/10.1186/s13045-020-00904-3

Huang, H., Berg, S., Spencer, J. S., Vereecke, D., D'Haeze, W., Holsters, M., & McNeil, M. R. 2008. Identification of amino acids and domains required for catalytic activity of DPPR synthase, a cell wall biosynthetic enzyme of *Mycobacterium tuberculosis*. *Microbiology*, *154*, 736–743. https://doi.org/10.1099/mic.0.2007/013532-0

Huang, H., Scherman, M. S., D'Haeze, W., Vereecke, D., Holsters, M., Crick, D. C., & McNeil, M. R. 2005. Identification and active expression of the *Mycobacterium tuberculosis* gene encoding 5-phospho-α-D-ribose-1-diphosphate: Decaprenyl-phosphate 5-phosphoribosyltransferase, the first enzyme committed to decaprenylphosphoryl- D-arabinose synthesis. *Journal of Biological Chemistry*, *280*, 24539–24543. https://doi.org/10.1074/jbc.M504068200

Hughes, C. S., Foehr, S., Garfield, D. A., Furlong, E. E., Steinmetz, L. M., & Krijgsveld, J. 2014. Ultrasensitive proteome analysis using paramagnetic bead technology. *Molecular Systems Biology*, *10*, 757. https://doi.org/10.15252/msb.20145625

Hussain Bhat, K., & Mukhopadhyay, S. 2015. Macrophage takeover and the host-bacilli interplay during tuberculosis. In *Future Microbiology* (Vol. 10, Issue 5, pp. 853–872). https://doi.org/10.2217/fmb.15.11

Ii, T. C. S., Pullen, K. M., Olson, M. C., McNellis, M. E., Richardson, I., Hu, S., Larkins-Ford, J., Wang, X., Freundlich, J. S., Ando, D. M., & Aldridge, B. B. 2020. Morphological profiling of tubercle bacilli identifies drug pathways of action. *Proceedings of the National Academy of Sciences of the United States of America*, *117*, 18744–18753. https://doi.org/10.1073/pnas.2002738117

Ioerger, T. R., Feng, Y., Ganesula, K., Chen, X., Dobos, K. M., Fortune, S., Jacobs, W. R., Mizrahi, V., Parish, T., Rubin, E., Sassetti, C., & Sacchettini, J. C. 2010. Variation among genome sequences of H37Rv strains of *Mycobacterium tuberculosis* from multiple laboratories. *Journal of Bacteriology*, *192*, 3645–3653. https://doi.org/10.1128/JB.00166-10

Jackson, M., Crick, D. C., & Brennan, P. J. 2000. Phosphatidylinositol is an essential phospholipid of mycobacteria. *Journal of Biological Chemistry*, *275*, 30092–30099. https://doi.org/10.1074/jbc.M004658200

Jackson, M., Raynaud, C., Lanéelle, M. A., Guilhot, C., Laurent-Winter, C., Ensergueix, D., Gicquel, B., & Daffé, M. 1999. Inactivation of the antigen 85C gene profoundly affects the mycolate content and alters the permeability of the *Mycobacterium tuberculosis* cell envelope. *Molecular Microbiology*, *31*, 1573–1587. https://doi.org/10.1046/j.1365-2958.1999.01310.x

Jagtap, P. K. A., Soni, V., Vithani, N., Jhingan, G. D., Bais, V. S., Nandicoori, V. K., & Prakash, B. 2012. Substrate-bound crystal structures reveal features unique to *Mycobacterium tuberculosis* N-Acetyl-glucosamine 1-phosphate uridyltransferase and a catalytic mechanism for acetyl transfer. *Journal of Biological Chemistry*, *287*, 39524–39537. https://doi.org/10.1074/jbc.M112.390765

Jankute, M., Alderwick, L. J., Noack, S., Veerapen, N., Nigou, J., & Besra, G. S. 2017. Disruption of mycobacterial *aftB* results in complete loss of terminal β(1 → 2) arabinofuranose residues of Lipoarabinomannan. *ACS Chemical Biology*, *12*, 183–190. https://doi.org/10.1021/acschembio.6b00898

Jin, Y., Xin, Y., Zhang, W., & Ma, Y. 2010. *Mycobacterium tuberculosis* Rv1302 and *Mycobacterium smegmatis* MSMEG-4947 have WecA function and MSMEG-4947 is required for the growth of M. smegmatis. *FEMS Microbiology Letters*, *310*, 54–61. https://doi.org/10.1111/j.1574-6968.2010.02045.x

Johnston, J. C., Campbell, J. R., & Menzies, D. 2017. Effect of intermittency on treatment outcomes in pulmonary tuberculosis: An updated systematic review and metaanalysis. *Clinical Infectious Diseases*, *64*, 1211–1220. https://doi.org/10.1093/cid/cix121

Jumper, J., Evans, R., Pritzel, A., Green, T., Figurnov, M., Ronneberger, O., Tunyasuvunakool, K., Bates, R., Žídek, A., Potapenko, A., Bridgland, A., Meyer, C., Kohl, S. A. A., Ballard, A. J., Cowie, A., Romera-Paredes, B., Nikolov, S., Jain, R., Adler, J., … Hassabis, D. 2021. Highly accurate protein structure prediction with AlphaFold. *Nature*, *596*, 583–589. https://doi.org/10.1038/s41586-021-03819-2

Kamal, A., Faazil, S., Shaheer Malik, M., Balakrishna, M., Bajee, S., Siddiqui, M. R. H., & Alarifi, A. 2016. Convenient synthesis of substituted pyrroles via a cerium (IV) ammonium nitrate (CAN)-catalyzed Paal-Knorr reaction. *Arabian Journal of Chemistry*, *9*, 542–549. https://doi.org/10.1016/j.arabjc.2013.04.009

Kana, B. D., Karakousis, P. C., Parish, T., & Dick, T. 2014. Future target-based drug discovery for tuberculosis? In *Tuberculosis* (Vol. 94, Issue 6, pp. 551–556). https://doi.org/10.1016/j.tube.2014.10.003

Karamanou, M., & Androutsos, G. 2012. The masterful description of pulmonary tuberculosis by Soranus of Ephesus (c. 98-138 A.D.). In *American Journal of Respiratory and Critical Care Medicine* (Vol. 186, Issue 6, p. 571). https://doi.org/10.1164/ajrccm.186.6.571

Kaur, D., Obregón-Henao, A., Pham, H., Chatterjee, D., Brennan, P. J., & Jackson, M. 2008. Lipoarabinomannan of Mycobacterium: Mannose capping by a multifunctional terminal mannosyltransferase. *Proceedings of the National Academy of Sciences of the United States of America*, *105*, 17973–17977. https://doi.org/10.1073/pnas.0807761105

Kenakin, T. P. 2017. Pharmacokinetics I. In *Pharmacology in Drug Discovery and Development* (pp. 157–191). https://doi.org/10.1016/b978-0-12-803752-2.00007-7

Kendall, S. L., Withers, M., Soffair, C. N., Moreland, N. J., Gurcha, S., Sidders, B., Frita, R., Ten Bokum, A., Besra, G. S., Lott, J. S., & Stoker, N. G. 2007. A highly conserved transcriptional repressor controls a large regulon involved in lipid degradation in *Mycobacterium smegmatis* and *Mycobacterium tuberculosis*. *Molecular Microbiology*, *65*, 684–699. https://doi.org/10.1111/j.1365-2958.2007.05827.x

Kesely, K., Noomuna, P., Vieth, M., Hipskind, P., Haldar, K., Pantaleo, A., Turrini, F., & Low, P. S. 2020. Identification of tyrosine kinase inhibitors that halt *Plasmodium falciparum* parasitemia. *PLoS ONE*, *15*. https://doi.org/10.1371/journal.pone.0242372

Khasnobis, S., Zhang, J., Angala, S. K., Amin, A. G., McNeil, M. R., Crick, D. C., & Chatterjee, D. 2006. Characterization of a Specific Arabinosyltransferase Activity Involved in Mycobacterial Arabinan Biosynthesis. *Chemistry and Biology*, *13*, 787–795. https://doi.org/10.1016/j.chembiol.2006.05.016

Khoo, K. H., Dell, A., Morris, H. R., Breman, P. J., & Chatterjee, D. 1995. Structural definition of acylated phosphatidylinositol mannosides from *Mycobacterium tuberculosis*: Definition of a common anchor for lipomannan and lipoarabinomannan. *Glycobiology*, *5*, 117–127. https://doi.org/10.1093/glycob/5.1.117

Kieser, K. J., Boutte, C. C., Kester, J. C., Baer, C. E., Barczak, A. K., Meniche, X., Chao, M. C., Rego, E. H., Sassetti, C. M., Fortune, S. M., & Rubin, E. J. 2015. Phosphorylation of the Peptidoglycan Synthase PonA1 Governs the Rate of Polar Elongation in Mycobacteria. *PLoS Pathogens*, *11*. https://doi.org/10.1371/journal.ppat.1005010

Kim, C. J., Kim, N. H., Song, K. H., Choe, P. G., Kim, E. S., Park, S. W., Kim, H. Bin, Kim, N. J., Kim, E. C., Park, W. B., & Oh, M. don. 2013. Differentiating rapid- and slow-growing mycobacteria by difference in time to growth detection in liquid media. *Diagnostic Microbiology and Infectious Disease*, *75*, 73–76. https://doi.org/10.1016/j.diagmicrobio.2012.09.019

Kim, M. J., Wainwright, H. C., Locketz, M., Bekker, L. G., Walther, G. B., Dittrich, C., Visser, A., Wang, W., Hsu, F. F., Wiehart, U., Tsenova, L., Kaplan, G., & Russell, D. G. 2010. Caseation of human tuberculosis granulomas correlates with elevated host lipid metabolism. *EMBO Molecular Medicine*, *2*, 258–274. https://doi.org/10.1002/emmm.201000079

Knapp, S. 2018. New opportunities for kinase drug repurposing and target discovery editorial. In *British Journal of Cancer* (Vol. 118, Issue 7, pp. 936–937). https://doi.org/10.1038/s41416-018-0045-6

Knight, M., Braverman, J., Asfaha, K., Gronert, K., & Stanley, S. 2018. Lipid droplet formation in *Mycobacterium tuberculosis* infected macrophages requires IFN-γ/HIF-1α signaling and supports host defense. *PLoS Pathogens*, *14*. https://doi.org/10.1371/journal.ppat.1006874

Korduláková, J., Gilleron, M., Puzo, G., Brennan, P. J., Gicquel, B., Mikušová, K., & Jackson, M. 2003. Identification of the required acyltransferase step in the biosynthesis of the phosphatidylinositol mannosides of Mycobacterium species. *Journal of Biological Chemistry*, *278*, 36285–36295. https://doi.org/10.1074/jbc.M303639200

Kremer, L., & Besra, G. S. 2014. A Waxy Tale, by *Mycobacterium tuberculosis*. In *Tuberculosis and the Tubercle Bacillus* (pp. 287–305). https://doi.org/10.1128/9781555817657.ch19

Kremer, L., De Chastellier, C., Dobson, G., Gibson, K. J. C., Bifani, P., Balor, S., Gorvel, J. P., Locht, C., Minnikin, D. E., & Besra, G. S. 2005. Identification and structural characterization of an unusual mycobacterial monomeromycolyl-diacylglycerol. *Molecular Microbiology*, *57*, 1113–1126. https://doi.org/10.1111/j.1365-2958.2005.04717.x

Kremer, L., Dover, L. G., Carrère, S., Nampoothiri, K. M., Lesjean, S., Brown, A. K., Brennan, P. J., Minnikin, D. E., Locht, C., & Besra, G. S. 2002. Mycolic acid biosynthesis and enzymic characterization of the β-ketoacyl-ACP synthase A-condensing enzyme from *Mycobacterium tuberculosis*. *Biochemical Journal*, *364*, 423–430. https://doi.org/10.1042/BJ20011628

Kremer, L., Dover, L. G., Morehouse, C., Hitchin, P., Everett, M., Morris, H. R., Dell, A., Brennan, P. J., McNeil, M. R., Flaherty, C., Duncan, K., & Besra, G. S. 2001. Galactan biosynthesis in *Mycobacterium tuberculosis*: Identification of a bifunctional UDP-galactofuranosyltransferase. *Journal of Biological Chemistry*, *276*, 26430–26440. https://doi.org/10.1074/jbc.M102022200

Kremer, L., Gurcha, S. S., Bifani, P., Hitchen, P. G., Baulard, A., Morris, H. R., Dell, A., Brennan, P. J., & Besra, G. S. 2002. Characterization of a putative α-mannosyltransferase involved in phosphatidylinositol trimannoside biosynthesis in *Mycobacterium tuberculosis*. *Biochemical Journal*, *363*, 437–447. https://doi.org/10.1042/0264-6021:3630437

Kremer, L., Nampoothiri, K. M., Lesjean, S., Dover, L. G., Graham, S., Betts, J., Brennan, P. J., Minnikin, D. E., Locht, C., & Besra, G. S. 2001. Biochemical Characterization of Acyl Carrier Protein (AcpM) and Malonyl-CoA:AcpM Transacylase (mtFabD), Two Major Components of Mycobacterium tuberculosis Fatty Acid Synthase II. *Journal of Biological Chemistry*, *276*, 27967–27974. https://doi.org/10.1074/jbc.M103687200

Kuk, A. C. Y., Hao, A., Guan, Z., & Lee, S. Y. 2019. Visualizing conformation transitions of the Lipid II flippase MurJ. *Nature Communications*, *10*. https://doi.org/10.1038/s41467-019-09658-0

Kuk, A. C. Y., Mashalidis, E. H., & Lee, S. Y. 2017. Crystal structure of the MOP flippase MurJ in an inward-facing conformation. *Nature Structural and Molecular Biology*, *24*, 171–176. https://doi.org/10.1038/nsmb.3346

Kumar, P., Arora, K., Lloyd, J. R., Lee, I. Y., Nair, V., Fischer, E., Boshoff, H. I. M., & Barry, C. E. 2012. Meropenem inhibits D,D-carboxypeptidase activity in *Mycobacterium tuberculosis*. *Molecular Microbiology*, *86*, 367–381. https://doi.org/10.1111/j.1365-2958.2012.08199.x

Kumar, S., Rubino, F. A., Mendoza, A. G., & Ruiz, N. 2019. The bacterial lipid II flippase MurJ functions by an alternating-access mechanism. *Journal of Biological Chemistry*, *294*, 981–990. https://doi.org/10.1074/jbc.RA118.006099

Kurosu, M., Mahapatra, S., Narayanasamy, P., & Crick, D. C. 2007. Chemoenzymatic synthesis of Park's nucleotide: toward the development of high-throughput screening for MraY inhibitors. *Tetrahedron Letters*, *48*, 799–803. https://doi.org/10.1016/j.tetlet.2006.11.160

Kurz, S. G., & Bonomo, R. A. 2012. Reappraising the use of β-lactams to treat tuberculosis. In *Expert Review of Anti-Infective Therapy* (Vol. 10, Issue 9, pp. 999–1006). https://doi.org/10.1586/eri.12.96

La Rosa, V., Poce, G., Canseco, J. O., Buroni, S., Pasca, M. R., Biava, M., Raju, R. M., Porretta, G. C., Alfonso, S., Battilocchio, C., Javid, B., Sorrentino, F., Ioerger, T. R., Sacchettini, J. C.,

Manetti, F., Botta, M., De Logu, A., Rubin, E. J., & De Rossi, E. 2012. MmpL3 is the cellular target of the antitubercular pyrrole derivative BM212. *Antimicrobial Agents and Chemotherapy*, *56*, 324–331. https://doi.org/10.1128/AAC.05270-11

Laponogov, I., Sohi, M. K., Veselkov, D. A., Pan, X. S., Sawhney, R., Thompson, A. W., McAuley, K. E., Fisher, L. M., & Sanderson, M. R. 2009. Structural insight into the quinolone-DNA cleavage complex of type IIA topoisomerases. *Nature Structural and Molecular Biology*, *16*, 667–669. https://doi.org/10.1038/nsmb.1604

Larson, K. B., Wang, K., Delille, C., Otofokun, I., & Acosta, E. P. 2014. Pharmacokinetic Enhancers in HIV Therapeutics. *Clinical Pharmacokinetics*, *53*, 865–872. https://doi.org/10.1007/s40262-014-0167-9

Lavollay, M., Arthur, M., Fourgeaud, M., Dubost, L., Marie, A., Veziris, N., Blanot, D., Gutmann, L., & Mainardi, J. L. 2008. The peptidoglycan of stationary-phase Mycobacterium tuberculosis predominantly contains cross-links generated by L,D-transpeptidation. *Journal of Bacteriology*, *190*, 4360–4366. https://doi.org/10.1128/JB.00239-08

Lawn, S. D., Bekker, L. G., Middelkoop, K., Myer, L., & Wood, R. 2006. Impact of HIV infection on the epidemiology of tuberculosis in a peri-urban community in South Africa: The need for age-specific interventions. *Clinical Infectious Diseases*, *42*, 1040–1047. https://doi.org/10.1086/501018

Le, P., Kunold, E., Macsics, R., Rox, K., Jennings, M. C., Ugur, I., Reinecke, M., Chaves-Moreno, D., Hackl, M. W., Fetzer, C., Mandl, F. A. M., Lehmann, J., Korotkov, V. S., Hacker, S. M., Kuster, B., Antes, I., Pieper, D. H., Rohde, M., Wuest, W. M., … Sieber, S. A. 2020. Repurposing human kinase inhibitors to create an antibiotic active against drug-resistant Staphylococcus aureus, persisters and biofilms. *Nature Chemistry*, *12*, 145–158. https://doi.org/10.1038/s41557-019-0378-7

Lea-Smith, D. J., Pyke, J. S., Tull, D., McConville, M. J., Coppel, R. L., & Crellin, P. K. 2007. The reductase that catalyzes mycolic motif synthesis is required for efficient attachment of mycolic acids to arabinogalactan. *Journal of Biological Chemistry*, *282*, 11000–11008. https://doi.org/10.1074/jbc.M608686200

Lechevalier, M. P., & Lechevalier, H. 1970. Chemical composition as a criterion in the classification of aerobic actinomycetes. *International Journal of Systematic Bacteriology*, *20*, 435–443. https://doi.org/10.1099/00207713-20-4-435

Leclercq, S., Derouaux, A., Olatunji, S., Fraipont, C., Egan, A. J. F., Vollmer, W., Breukink, E., & Terrak, M. 2017. Interplay between Penicillin-binding proteins and SEDS proteins promotes bacterial cell wall synthesis. *Scientific Reports*, *7*. https://doi.org/10.1038/srep43306

Lee, A., Wu, S. W., Scherman, M. S., Torrelles, J. B., Chatterjee, D., McNeil, M. R., & Khoo, K. H. 2006. Sequencing of oligoarabinosyl units released from mycobacterial arabinogalactan by endogenous arabinanase: Identification of distinctive and novel structural motifs. *Biochemistry*, *45*, 15817–15828. https://doi.org/10.1021/bi060688d

Léger, M., Gavalda, S., Guillet, V., van der Rest, B., Slama, N., Montrozier, H., Mourey, L., Quémard, A., Daffé, M., & Marrakchi, H. 2009. The Dual Function of the *Mycobacterium tuberculosis* FadD32 Required for Mycolic Acid Biosynthesis. *Chemistry and Biology*, *16*, 510–519. https://doi.org/10.1016/j.chembiol.2009.03.012

Li, G., Zhang, J., Guo, Q., Jiang, Y., Wei, J., Zhao, L. L., Zhao, X., Lu, J., & Wan, K. 2015. Efflux pump gene expression in multidrug-resistant *Mycobacterium tuberculosis* clinical isolates. *PLoS ONE*, *10*. https://doi.org/10.1371/journal.pone.0119013

Li, K., Schurig-Briccio, L. A., Feng, X., Upadhyay, A., Pujari, V., Lechartier, B., Fontes, F. L., Yang, H., Rao, G., Zhu, W., Gulati, A., No, J. H., Cintra, G., Bogue, S., Liu, Y. L., Molohon, K., Orlean, P., Mitchell, D. A., Freitas-Junior, L., … Oldfield, E. 2014. Multitarget drug discovery for tuberculosis and other infectious diseases. In *Journal of Medicinal Chemistry* (Vol. 57, Issue 7, pp. 3126–3129). https://doi.org/10.1021/jm500131s

Li, W., Upadhyay, A., Fontes, F. L., North, E. J., Wang, Y., Crans, D. C., Grzegorzewicz, A. E., Jones, V., Franzblau, S. G., Lee, R. E., Crick, D. C., & Jackson, M. 2014. Novel insights into the mechanism of inhibition of MmpL3, a target of multiple pharmacophores in *Mycobacterium tuberculosis*. *Antimicrobial Agents and Chemotherapy*, *58*, 6413–6423. https://doi.org/10.1128/AAC.03229-14

Li, W., Yazidi, A., Pandya, A. N., Hegde, P., Tong, W., de Moura, V. C. N., North, E. J., Sygusch, J., & Jackson, M. 2018. MmpL3 as a target for the treatment of drug-resistant nontuberculous mycobacterial infections. *Frontiers in Microbiology*, *9*. https://doi.org/10.3389/fmicb.2018.01547

Li, X. Z., & Nikaido, H. 2009. Efflux-mediated drug resistance in bacteria: An update. In *Drugs* (Vol. 69, Issue 12, pp. 1555–1623). https://doi.org/10.2165/11317030-000000000-00000

Lightner VA, Larson TJ, Tailleur P, Kantor GD, Raetz CR, Bell RM, Modrich P. 1980. Membrane phospholipid synthesis in *Escherichia coli*. Cloning of a structural gene (plsB) of the sn-glycerol-3-phosphate acyl/transferase. *J Biol Chem.* 255(19):9413-20. PMID: 6251087.

Lillebaek, T., Andersen, Å. B., Dirksen, A., Glynn, J. R., & Kremer, K. 2003. Mycobacterium tuberculosis Beijing Genotype. *Emerging Infectious Diseases*, *9*, 1553–1557. https://doi.org/10.3201/eid0912.030276

Lin, P. L., & Flynn, J. L. 2010. Understanding Latent Tuberculosis: A Moving Target. *The Journal of Immunology*, *185*, 15–22. https://doi.org/10.4049/jimmunol.0903856

Liu, J., Barry, C. E., Besra, G. S., & Nikaido, H. 1996. Mycolic acid structure determines the fluidity of the mycobacterial cell wall. *Journal of Biological Chemistry*, *271*, 29545–29551. https://doi.org/10.1074/jbc.271.47.29545

Liu, Y., Yang, K., Zhang, H., Jia, Y., & Wang, Z. 2020. Combating Antibiotic Tolerance Through Activating Bacterial Metabolism. In *Frontiers in Microbiology* (Vol. 11). https://doi.org/10.3389/fmicb.2020.577564

Lobo, N., Brooks, N. A., Zlotta, A. R., Cirillo, J. D., Boorjian, S., Black, P. C., Meeks, J. J., Bivalacqua, T. J., Gontero, P., Steinberg, G. D., McConkey, D., Babjuk, M., Alfred Witjes, J., & Kamat, A. M. 2021. 100 years of Bacillus Calmette–Guérin immunotherapy: from cattle to COVID-19. In *Nature Reviews Urology* (Vol. 18, Issue 10, pp. 611–622). https://doi.org/10.1038/s41585-021-00481-1

Lorenz, M. C., & Fink, G. R. 2002. Life and death in a macrophage: Role of the glyoxylate cycle in virulence. In *Eukaryotic Cell* (Vol. 1, Issue 5, pp. 657–662). https://doi.org/10.1128/EC.1.5.657-662.2002

Low, K. L., Shui, G., Natter, K., Yeo, W. K., Kohlwein, S. D., Dick, T., Rao, S. P. S., & Wenk, M. R. 2010. Lipid droplet-associated proteins are involved in the biosynthesis and hydrolysis of triacylglycerol in *Mycobacterium bovis* bacillus Calmette-Guérin. *Journal of Biological Chemistry*, *285*, 21662–21670. https://doi.org/10.1074/jbc.M110.135731

Ludwiczak, P., Gilleron, M., Bordat, Y., Martin, C., Gicquel, B., & Puzo, G. 2002. *Mycobacterium tuberculosis phoP* mutant: Lipoarabinomannan molecular structure. *Microbiology*, *148*, 3029–3037. https://doi.org/10.1099/00221287-148-10-3029

Maggi, N., Pallanza, R., & Sensi, P. 1965. New derivatives of rifamycin SV. *Antimicrobial Agents and Chemotherapy*, *5*, 765–769.

Maggi, N., Pasqualucci, C. R., Ballotta, R. & Sensi, P., 1966. Rifampicin: A New Orally Active Rifamycin. *Chemotherapia* 11, 285–292.

Mahairas, G. G., Sabo, P. J., Hickey, M. J., Singh, D. C., & Stover, C. K. 1996. Molecular analysis of genetic differences between *Mycobacterium bovis* BCG and virulent M. bovis. *Journal of Bacteriology*, *178*, 1274–1282. https://doi.org/10.1128/jb.178.5.1274-1282.1996

Mahajan, R. 2013. Bedaquiline: First FDA-approved tuberculosis drug in 40 years. *International Journal of Applied and Basic Medical Research*, *3*, 1. https://doi.org/10.4103/2229-516x.112228

Mahapatra, S., Scherman, H., Brennan, P. J., & Crick, D. C. 2005. N glycolylation of the nucleotide precursors of peptidoglycan biosynthesis of *Mycobacterium* spp. is altered by drug treatment. *Journal of Bacteriology*, *187*, 2341–2347. https://doi.org/10.1128/JB.187.7.2341-2347.2005

Mahapatra, S., Yagi, T., Belisle, J. T., Espinosa, B. J., Hill, P. J., McNeil, M. R., Brennan, P. J., & Crick, D. C. 2005. Mycobacterial lipid II is composed of a complex mixture of modified muramyl and peptide moieties linked to decaprenyl phosphate. *Journal of Bacteriology*, *187*, 2747–2757. https://doi.org/10.1128/JB.187.8.2747-2757.2005

Makobongo, M. O., Einck, L., Peek, R. M., & Merrell, D. S. 2013. In Vitro Characterization of the Anti-Bacterial Activity of SQ109 against Helicobacter pylori. *PLoS ONE*, *8*. https://doi.org/10.1371/journal.pone.0068917

Manning, G., Whyte, D. B., Martinez, R., Hunter, T., & Sudarsanam, S. 2002. The protein kinase complement of the human genome. In *Science* (Vol. 298, Issue 5600, pp. 1912–1934). https://doi.org/10.1126/science.1075762

Marrakchi, H., Ducasse, S., Labesse, G., Montrozier, H., Margeat, E., Emorine, L., Charpentier, X., Daffé, M., & Quémard, A. 2002. MabA (FabG1), a *Mycobacterium tuberculosis* protein involved in the long-chain fatty acid elongation system FAS-II. *Microbiology*, *148*, 951–960. https://doi.org/10.1099/00221287-148-4-951

Marrakchi, H., Lanéelle, G., & Quémard, A. 2000. InhA, a target of the antituberculous drug isoniazid, is involved in a mycobacterial fatty acid elongation system, FAS-II. *Microbiology*, *146*, 289–296. https://doi.org/10.1099/00221287-146-2-289

Matsuhashi, M. 1966. Biosynthesis in the bacterial cell wall. In *Tanpakushitsu kakusan koso. Protein, nucleic acid, enzyme* (Vol. 11, Issue 10, pp. 875–886).

Maurya, R. K., Bharti, S., & Krishnan, M. Y. 2019. Triacylglycerols: Fuelling the hibernating *Mycobacterium tuberculosis*. *Frontiers in Cellular and Infection Microbiology*, *9*.

https://doi.org/10.3389/fcimb.2018.00450

Mawuenyega, K. G., Forst, C. V., Dobos, K. M., Belisle, J. T., Chen, J., Bradbury, E. M., Bradbury, A. R. M., & Chen, X. 2005. *Mycobacterium tuberculosis* functional network analysis by global subcellular protein profiling. *Molecular Biology of the Cell*, *16*, 396–404. https://doi.org/10.1091/mbc.E04-04-0329

McCune, R. M., McDermott, W., & Tompsett, R. 1956. The fate of *Mycobacterium tuberculosis* in mouse tissues as determined by the microbial enumeration technique. II. The conversion of tuberculous infection to the latent state by the administration of pyrazinamide and a companion drug. *The Journal of Experimental Medicine*, *104*, 763–802. https://doi.org/10.1084/jem.104.5.763

McFie, P. J., & Stone, S. J. 2011. A fluorescent assay to quantitatively measure in vitro acyl CoA:diacylglycerol acyltransferase activity. *Journal of Lipid Research*, *52*, 1760–1764. https://doi.org/10.1194/jlr.D016626

McNeil, M., Daffe, M., & Brennan, P. J. 1990. Evidence for the nature of the link between the arabinogalactan and peptidoglycan of mycobacterial cell walls. *Journal of Biological Chemistry*, *265*, 18200–18206. https://doi.org/10.1016/s0021-9258(17)44738-7

McNeil, M., Daffe, M., & Brennan, P. J. 1991. Location of the mycolyl ester substituents in the cell walls of mycobacteria. *Journal of Biological Chemistry*, *266*, 13217–13223. https://doi.org/10.1016/s0021-9258(18)98826-5

McNeil, M., Wallner, S. J., Hunter, S. W., & Brennan, P. J. 1987. Demonstration that the galactosyl and arabinosyl residues in the cell-wall arabinogalactan of *Mycobacterium leprae* and *Mycobacterium tuberculosis* are furanoid. *Carbohydrate Research*, *166*, 299–308. https://doi.org/10.1016/0008-6215(87)80065-4

Mdluli, K., Kaneko, T., & Upton, A. 2015. The tuberculosis drug discovery and development pipeline and emerging drug targets. *Cold Spring Harbor Perspectives in Biology*, *7*, 1–25. https://doi.org/10.1101/cshperspect.a021154

Meehan, C., Barco, R., Loh, Y. W., Cogneau, S., Rigouts, L., 2021. Reconstituting the genus *Mycobacterium. International Journal of Systematic and Evolutionary Microbiology*. 71, 9. https://doi.org/10.1099/ijsem.0.004922

Meeske, A. J., Riley, E. P., Robins, W. P., Uehara, T., Mekalanos, J. J., Kahne, D., Walker, S., Kruse, A. C., Bernhardt, T. G., & Rudner, D. Z. 2016. SEDS proteins are a widespread family of bacterial cell wall polymerases. *Nature*, *537*, 634–638. https://doi.org/10.1038/nature19331

Mengin-Lecreulx, D., Texier, L., Rousseau, M., & Van Heijenoort, J. 1991. The murG gene of Escherichia coli codes for the UDP-N-acetylglucosamine:N-acetylmuramyl-(pentapeptide) pyrophosphoryl-undecaprenol N-acetylglucosamine transferase involved in the membrane steps of peptidoglycan synthesis. *Journal of Bacteriology*, *173*, 4625–4636. https://doi.org/10.1128/jb.173.15.4625-4636.1991

Meroueh, S. O., Bencze, K. Z., Hesek, D., Lee, M., Fisher, J. F., Stemmler, T. L., & Mobashery, S. 2006. Three-dimensional structure of the bacterial cell wall peptidoglycan. *Proceedings of the National Academy of Sciences of the United States of America*, *103*, 4404–4409. https://doi.org/10.1073/pnas.0510182103

Meyers, C. D., Noe, A., Salunke, A., Movva, A., Kulmatycki, K., Neelakantham, S., Crissey, A., Majumdar, T., & Chen, J. 2016. Effect of Pradigastat, a Diacylglycerol Acyltransferase 1 Inhibitor, on the QTcF Interval in Humans. *Clinical Pharmacology in Drug Development*, *5*, 450–459. https://doi.org/10.1002/cpdd.278

Mikušová, K., Beláňová, M., Korduláková, J., Honda, K., McNeil, M. R., Mahapatra, S., Crick, D. C., & Brennan, P. J. 2006. Identification of a novel galactosyl transferase involved in biosynthesis of the mycobacterial cell wall. *Journal of Bacteriology*, *188*, 6592–6598. https://doi.org/10.1128/JB.00489-06

Mikušová, K., Huang, H., Yagi, T., Holsters, M., Vereecke, D., D'Haeze, W., Scherman, M. S., Brennan, P. J., McNeil, M. R., & Crick, D. C. 2005. Decaprenylphosphoryl arabinofuranose, the donor of the D-arabinofuranosyl residues of mycobacterial arabinan, is formed via a two-step epimerization of decaprenylphosphoryl ribose. *Journal of Bacteriology*, *187*, 8020–8025. https://doi.org/10.1128/JB.187.23.8020-8025.2005

Milano, A., Pasca, M. R., Provvedi, R., Lucarelli, A. P., Manina, G., Luisa de Jesus Lopes Ribeiro, A., Manganelli, R., & Riccardi, G. 2009. Azole resistance in *Mycobacterium tuberculosis* is mediated by the MmpS5-MmpL5 efflux system. *Tuberculosis*, *89*, 84–90. https://doi.org/10.1016/j.tube.2008.08.003

Miller, D. J., Surfraz, B. U., Akhtar, M., Gani, D., & Allemann, R. K. 2004. Removal of the phosphate group in mechanism-based inhibitors of inositol monophosphatase leads to unusual inhibitory activity. *Organic and Biomolecular Chemistry*, *2*, 671–688. https://doi.org/10.1039/b312808c

Mills, J. A., Motichka, K., Jucker, M., Wu, H. P., Uhlik, B. C., Stern, R. J., Scherman, M. S., Vissa, V. D., Pan, F., Kundu, M., Yu, F. M., & McNeil, M. 2004. Inactivation of the mycobacterial rhamnosyltransferase, which is needed for the formation of the arabinogalactan-peptidoglycan linker, leads to irreversible loss of viability. *Journal of Biological Chemistry*, *279*, 43540–43546. https://doi.org/10.1074/jbc.M407782200

Minato, Y., Gohl, D. M., Thiede, J. M., Chacón, J. M., Harcombe, W. R., Maruyama, F., & Baughn, A. D. 2019. Genomewide Assessment of *Mycobacterium tuberculosis* Conditionally Essential Metabolic Pathways. *MSystems*, *4*. https://doi.org/10.1128/msystems.00070-19

Minnikin, D. E., Kremer, L., Dover, L. G., & Besra, G. S. 2002. The methyl-branched fortifications of *Mycobacterium tuberculosis*. In *Chemistry and Biology*. https://doi.org/10.1016/S1074-5521(02)00142-4

Minnikin, D. E., Lee, O. Y.-C., Wu, H. H. T., Nataraj, V., Donoghue, H. D., Ridell, M., Watanabe, M., Alderwick, L., Bhatt, A., & Besra, G. S. 2015. Pathophysiological Implications of Cell Envelope Structure in *Mycobacterium tuberculosis* and Related Taxa. In *Tuberculosis - Expanding Knowledge*. https://doi.org/10.5772/59585

Minnikin, D. E., Lee, O. Y. C., Wu, H. H. T., Besra, G. S., Bhatt, A., Nataraj, V., Rothschild, B. M., Spigelman, M., & Donoghue, H. D. 2015. Ancient mycobacterial lipids: Key reference biomarkers in charting the evolution of tuberculosis. *Tuberculosis*, *95*, S133–S139. https://doi.org/10.1016/j.tube.2015.02.009

Mishra, A. K., Alderwick, L. J., Rittmann, D., Tatituri, R. V. V., Nigou, J., Gilleron, M., Eggeling, L., & Besra, G. S. 2007. Identification of an α(1→6) mannopyranosyltransferase (MptA), involved in *Corynebacterium glutamicum* lipomanann biosynthesis, and identification of its orthologue in *Mycobacterium tuberculosis*. *Molecular Microbiology*, *65*, 1503–1517.

https://doi.org/10.1111/j.1365-2958.2007.05884.x

Mishra, A. K., Alderwick, L. J., Rittmann, D., Wang, C., Bhatt, A., Jacobs, W. R., Takayama, K., Eggeling, L., & Besra, G. S. 2008. Identification of a novel α(1→6) mannopyranosyltransferase MptB from *Corynebacterium glutamicum* by deletion of a conserved gene, NCgl1505, affords a lipomannan- and lipoarabinomannan-deficient mutant. *Molecular Microbiology*, *68*, 1595–1613. https://doi.org/10.1111/j.1365-2958.2008.06265.x

Mishra, A. K., Krumbach, K., Rittmann, D., Appelmelk, B., Pathak, V., Pathak, A. K., Nigou, J., Geurtsen, J., Eggeling, L., & Besra, G. S. 2011. Lipoarabinomannan biosynthesis in *Corynebacterineae*: The interplay of two α(1→2)-mannopyranosyltransferases MptC and MptD in mannan branching. *Molecular Microbiology*, *80*, 1241–1259. https://doi.org/10.1111/j.1365-2958.2011.07640.x

Moggridge, S., Sorensen, P. H., Morin, G. B., & Hughes, C. S. 2018. Extending the Compatibility of the SP3 Paramagnetic Bead Processing Approach for Proteomics. *Journal of Proteome Research*, *17*, 1730–1740. https://doi.org/10.1021/acs.jproteome.7b00913

Mohammadi, T., Van Dam, V., Sijbrandi, R., Vernet, T., Zapun, A., Bouhss, A., Diepeveen-De Bruin, M., Nguyen-Distéche, M., De Kruijff, B., & Breukink, E. 2011. Identification of FtsW as a transporter of lipid-linked cell wall precursors across the membrane. *EMBO Journal*, *30*, 1425–1432. https://doi.org/10.1038/emboj.2011.61

Molodtsov, V., Scharf, N. T., Stefan, M. A., Garcia, G. A., & Murakami, K. S. 2017. Structural basis for rifamycin resistance of bacterial RNA polymerase by the three most clinically important RpoB mutations found in *Mycobacterium tuberculosis*. *Molecular Microbiology*, *103*, 1034–1045. https://doi.org/10.1111/mmi.13606

Montalvo-Ortiz, B. L., Castillo-Pichardo, L., Hernández, E., Humphries-Bickley, T., De La Mota-Peynado, A., Cubano, L. A., Vlaar, C. P., & Dharmawardhane, S. 2012. Characterization of EHop-016, novel small molecule inhibitor of Rac GTPase. *Journal of Biological Chemistry*, *287*, 13228–13238. https://doi.org/10.1074/jbc.M111.334524

Moody, D. B., Reinhold, B. B., Guy, M. R., Beckman, E. M., Frederique, D. E., Furlong, S. T., Ye, S., Reinhold, V. N., Sieling, P. A., Modlin, R. L., Besra, G. S., & Porcelli, S. A. 1997. Structural requirements for glycolipid antigen recognition by CD1b- restricted T cells. *Science*, *278*, 283–286. https://doi.org/10.1126/science.278.5336.283

More, N. A., Patil, M. D., Garud, D. R., & Gajbhiye, J. M. 2016. An efficient synthesis of potent anti-tubercular drug candidate BM212. *Rasayan Journal of Chemistry*, *9*, 806–811.

Morita, Y. S., Sena, C. B. C., Waller, R. F., Kurokawa, K., Sernee, M. F., Nakatani, F., Haites, R. E., Billman-Jacobe, H., McConville, M. J., Maeda, Y., & Kinoshita, T. 2006. PimE is a polyprenol-phosphate-mannose-dependent mannosyltransferase that transfers the fifth mannose of phosphatidylinositol mannoside in mycobacteria. *Journal of Biological Chemistry*, *281*, 25143–25155. https://doi.org/10.1074/jbc.M604214200

Morris, K. 2009. Global tuberculosis control amid the world economic crisis. In *The Lancet infectious diseases* (Vol. 9, Issue 3, pp. 144–145). https://doi.org/10.1016/S1473-3099(09)70030-1

Moya, B., Bhagwat, S., Cabot, G., Bou, G., Patel, M., & Oliver, A. 2021. Effective inhibition of PBPs by cefepime and zidebactam in the presence of VIM-1 drives potent bactericidal activity

against MBL-expressing *Pseudomonas aeruginosa*. *Journal of Antimicrobial Chemotherapy*, *75*, 1474–1478. https://doi.org/10.1093/JAC/DKAA036

Müller, S., Chaikuad, A., Gray, N. S., & Knapp, S. 2015. The ins and outs of selective kinase inhibitor development. In *Nature Chemical Biology* (Vol. 11, Issue 11, pp. 818–821). https://doi.org/10.1038/nchembio.1938

Munshi, T., Gupta, A., Evangelopoulos, D., Guzman, J. D., Gibbons, S., Keep, N. H., & Bhakta, S. 2013. Characterisation of ATP-Dependent Mur Ligases Involved in the Biogenesis of Cell Wall Peptidoglycan in *Mycobacterium tuberculosis*. *PLoS ONE*, *8*. https://doi.org/10.1371/journal.pone.0060143

Napier, R. J., Rafi, W., Cheruvu, M., Powell, K. R., Zaunbrecher, M. A., Bornmann, W., Salgame, P., Shinnick, T. M., & Kalman, D. 2011. Imatinib-Sensitive tyrosine kinases regulate mycobacterial pathogenesis and represent therapeutic targets against tuberculosis. *Cell Host and Microbe*, *10*, 475–485. https://doi.org/10.1016/j.chom.2011.09.010

NICE. 2016. NICE Guideline: Tuberculosis. In *National Institute for Health and Care Excellence*. National Institute.

O'Garra, A., Redford, P. S., McNab, F. W., Bloom, C. I., Wilkinson, R. J., & Berry, M. P. R. 2013. The immune response in tuberculosis. In *Annual Review of Immunology*. https://doi.org/10.1146/annurev-immunol-032712-095939

Oelkers, P., Behari, A., Cromley, D., Billheimer, J. T., & Sturleyt, S. L. 1998. Characterization of two human genes encoding acyl coenzyme A: Cholesterol acyltransferase-related enzymes. *Journal of Biological Chemistry*, *273*, 26765–26771. https://doi.org/10.1074/jbc.273.41.26765

Oharan, N. 2012. Current status of tuberculosis and recombinant bacillus Calmette-Guérin vaccines. In *Journal of Oral Biosciences* (Vol. 54, Issue 2, pp. 92–95). https://doi.org/10.1016/j.job.2012.04.002

Onajole, O. K., Pieroni, M., Tipparaju, S. K., Lun, S., Stec, J., Chen, G., Gunosewoyo, H., Guo, H., Ammerman, N. C., Bishai, W. R., & Kozikowski, A. P. 2013. Preliminary structure - Activity relationships and biological evaluation of novel antitubercular indolecarboxamide derivatives against drug-susceptible and drug-resistant *Mycobacterium tuberculosis* strains. *Journal of Medicinal Chemistry*, *56*, 4093–4103. https://doi.org/10.1021/jm4003878

Onwueme, K. C., Vos, C. J., Zurita, J., Ferreras, J. A., & Quadri, L. E. N. 2005. The dimycocerosate ester polyketide virulence factors of mycobacteria. In *Progress in Lipid Research* (Vol. 44, Issue 5, pp. 259–302). https://doi.org/10.1016/j.plipres.2005.07.001

Ortalo-Magné, A., Lemassu, A., Lanéelle, M. A., Bardou, F., Silve, G., Gounon, P., Marchal, G., & Daffé, M. 1996. Identification of the surface-exposed lipids on the cell envelopes of *Mycobacterium tuberculosis* and other mycobacterial species. *Journal of Bacteriology*, *178*, 456–461. https://doi.org/10.1128/jb.178.2.456-461.1996

Pandey, S. D., Pal, S., N, G. K., Bansal, A., Mallick, S., & Ghosh, A. S. 2018. Two DD-carboxypeptidases from *Mycobacterium smegmatis* affect cell surface properties through regulation of peptidoglycan cross-linking and glycopeptidolipids. *Journal of Bacteriology*, *200*. https://doi.org/10.1128/JB.00760-17

Parsons JB, Rock CO. 2013. Bacterial lipids: metabolism and membrane homeostasis. *Prog Lipid Res*. 52(3):249-76. doi: 10.1016/j.plipres.2013.02.002.

Pasca, M. R., Guglierame, P., De Rossi, E., Zara, F., & Riccardi, G. 2005. *mmpL7* gene of *Mycobacterium tuberculosis* is responsible for isoniazid efflux in Mycobacterium smegmatis. *Antimicrobial Agents and Chemotherapy*, *49*, 4775–4777. https://doi.org/10.1128/AAC.49.11.4775-4777.2005

Peng, W., Zou, L., Bhamidi, S., McNeil, M. R., & Lowary, T. L. 2012. The galactosamine residue in mycobacterial arabinogalactan is α-linked. *Journal of Organic Chemistry*, *77*, 9826–9832. https://doi.org/10.1021/jo301393s

Penzo, M., de las Heras-Dueña, L., Mata-Cantero, L., Diaz-Hernandez, B., Vazquez-Muñiz, M. J., Ghidelli-Disse, S., Drewes, G., Fernandez-Alvaro, E., & Baker, D. A. 2019. High-throughput screening of the *Plasmodium falciparum* cGMP-dependent protein kinase identified a thiazole scaffold which kills erythrocytic and sexual stage parasites. *Scientific Reports*, *9*. https://doi.org/10.1038/s41598-019-42801-x

Peterson, D. O., & Bloch, K. 1977. *Mycobacterium smegmatis* fatty acid synthetase. Long chain transacylase chain length specificity. *Journal of Biological Chemistry*, *252*, 5735–5739. https://doi.org/10.1016/s0021-9258(17)40084-6

Petit, J. F., Adam, A., Wietzerbin-Falszpan, J., Lederer, E., & Ghuysen, J. M. 1969. Chemical structure of the cell wall of *Mycobacterium smegmatis*. I - Isolation and partial characterization of the peptidoglycan. *Biochemical and Biophysical Research Communications*, *35*, 478–485. https://doi.org/10.1016/0006-291X(69)90371-4

Petrone, L., Petruccioli, E., Alonzi, T., Vanini, V., Cuzzi, G., Najafi Fard, S., Castilletti, C., Palmieri, F., Gualano, G., Vittozzi, P., Nicastri, E., Lepore, L., Grifoni, A., Antinori, A., Vergori, A., Ippolito, G., Cantini, F., & Goletti, D. 2021. In-vitro evaluation of the immunomodulatory effects of Baricitinib: Implication for COVID-19 therapy. *Journal of Infection*, *82*, 58–66. https://doi.org/10.1016/j.jinf.2021.02.023

Pettersen EF, Goddard TD, Huang CC, Couch GS, Greenblatt DM, Meng EC, Ferrin TE. 2004UCSF Chimera - a visualization system for exploratory research and analysis. *J Comput Chem*. 25(13):1605-12. doi: 10.1002/jcc.20084.

Peyron, P., Vaubourgeix, J., Poquet, Y., Levillain, F., Botanch, C., Bardou, F., Daffé, M., Emile, J. F., Marchou, B., Cardona, P. J., De Chastellier, C., & Altare, F. 2008. Foamy macrophages from tuberculous patients' granulomas constitute a nutrient-rich reservoir for M. tuberculosis persistence. *PLoS Pathogens*, *4*. https://doi.org/10.1371/journal.ppat.1000204

Pezzella, A. T. 2019. History of Pulmonary Tuberculosis. In *Thoracic surgery clinics* (Vol. 29, Issue 1, pp. 1–17). https://doi.org/10.1016/j.thorsurg.2018.09.002

PHE. 2020. Tuberculosis in England: 2019. In *Public Health England, London.* https://assets.publishing.service.gov.uk/government/uploads/system/uploads/attachment_data/file/943356/TB_Annual_Report_2020.pdf

Pitarque, S., Herrmann, J. L., Duteyrat, J. L., Jackson, M., Stewart, G. R., Lecointe, F., Payre, B., Schwartz, O., Young, D. B., Marchal, G., Lagrange, P. H., Puzo, G., Gicquel, B., Nigou, J., & Neyrolles, O. 2005. Deciphering the molecular bases of *Mycobacterium tuberculosis* binding to the lectin DC-SIGN reveals an underestimated complexity. *Biochemical Journal*,

392, 615–624. https://doi.org/10.1042/BJ20050709

Pitarque, S., Larrouy-Maumus, G., Payré, B., Jackson, M., Puzo, G., & Nigou, J. 2008. The immunomodulatory lipoglycans, lipoarabinomannan and lipomannan, are exposed at the mycobacterial cell surface. *Tuberculosis*, *88*, 560–565. https://doi.org/10.1016/j.tube.2008.04.002

Poce, G., Bates, R. H., Alfonso, S., Cocozza, M., Porretta, G. C., Ballell, L., Rullas, J., Ortega, F., De Logu, A., Agus, E., La Rosa, V., Pasca, M. R., De Rossi, E., Wae, B., Franzblau, S. G., Manetti, F., Botta, M., & Biava, M. 2013. Improved BM212 MmpL3 Inhibitor Analogue Shows Efficacy in Acute Murine Model of Tuberculosis Infection. *PLoS ONE*, *8*. https://doi.org/10.1371/journal.pone.0056980

Porter, J. 1992. WHO model prescribing information: Drugs used in mycobacterial diseases. In *Transactions of the Royal Society of Tropical Medicine and Hygiene* (Vol. 86, Issue 4, p. 461). https://doi.org/10.1016/0035-9203(92)90275-h

Portevin, D., De Sousa-D'Auria, C., Houssin, C., Grimaldi, C., Chami, M., Daffé, M., & Guilhot, C. 2004. A polyketide synthase catalyzes the last condensation step of mycolic acid biosynthesis in mycobacteria and related organisms. *Proceedings of the National Academy of Sciences of the United States of America*, *101*, 314–319. https://doi.org/10.1073/pnas.0305439101

Prisic, S., Dankwa, S., Schwartz, D., Chou, M. F., Locasale, J. W., Kang, C. M., Bemis, G., Church, G. M., Steene, H., & Husson, R. N. 2010. Extensive phosphorylation with overlapping specificity by *Mycobacterium tuberculosis* serine/threonine protein kinases. *Proceedings of the National Academy of Sciences of the United States of America*, *107*, 7521–7526. https://doi.org/10.1073/pnas.0913482107

Protopopova, M., Hanrahan, C., Nikonenko, B., Samala, R., Chen, P., Gearhart, J., Einck, L., & Nacy, C. A. 2005. Identification of a new antitubercular drug candidate, SQ109, from a combinatorial library of 1,2-ethylenediamines. *Journal of Antimicrobial Chemotherapy*, *56*, 968–974. https://doi.org/10.1093/jac/dki319

Quemard, A., Laneelle, G., & Lacave, C. 1992. Mycolic acid synthesis: A target for ethionamide in mycobacteria? *Antimicrobial Agents and Chemotherapy*, *36*, 1316–1321. https://doi.org/10.1128/AAC.36.6.1316

Quémard, A., Sacchettini, J. C., Dessen, A., Vilcheze, C., Bittman, R., Jacobs, W. R., & Blanchard, J. S. 1995. Enzymatic Characterization of the Target for Isoniazid in Mycobacterium tuberculosis. *Biochemistry*, *34*, 8235–8241. https://doi.org/10.1021/bi00026a004

Rafidinarivo, E., Lanéelle, M. A., Montrozier, H., Valero-Guillén, P., Astola, J., Luquin, M., Promé, J. C., & Daffé, M. 2009. Trafficking pathways of mycolic acids: Structures, origin, mechanism of formation, and storage form of mycobacteric acids. *Journal of Lipid Research*, *50*, 477–490. https://doi.org/10.1194/jlr.M800384-JLR200

Ramaswamy, S., & Musser, J. M. 1998. Molecular genetic basis of antimicrobial agent resistance in *Mycobacterium tuberculosis*: 1998 update. *Tubercle and Lung Disease*, *79*, 3–29. https://doi.org/10.1054/tuld.1998.0002

Ramón-Garciá, S., González Del Rió, R., Villarejo, A. S., Sweet, G. D., Cunningham, F., Barros, D., Ballell, L., Mendoza-Losana, A., Ferrer-Bazaga, S., & Thompson, C. J. 2016. Repurposing clinically approved cephalosporins for tuberculosis therapy. *Scientific Reports*, *6*.

https://doi.org/10.1038/srep34293

Rao, S. P. S., Lakshminarayana, S. B., Kondreddi, R. R., Herve, M., Camacho, L. R., Bifani, P., Kalapala, S. K., Jiricek, J., Ma, N. L., Tan, B. H., Ng, S. H., Nanjundappa, M., Ravindran, S., Seah, P. G., Thayalan, P., Lim, S. H., Lee, B. H., Goh, A., Barnes, W. S., … Manjunatha, U. H. 2013. Indolcarboxamide is a preclinical candidate for treating multidrug-resistant tuberculosis. *Science Translational Medicine*, *5*. https://doi.org/10.1126/scitranslmed.3007355

Rastogi, N., Hellio, R., & David, H. L. 1991. A New Insight into the Mycobacterial Cell Envelope Architecture by the Localization of Antigens in Ultrathin Sections. *Zentralblatt Fur Bakteriologie*, *275*, 287–302. https://doi.org/10.1016/S0934-8840(11)80292-6

Rawat, R., Whitty, A., & Tonge, P. J. 2003. The isoniazid-NAD adduct is a slow, tight-binding inhibitor of InhA, the *Mycobacterium tuberculosis* enoyl reductase: Adduct affinity and drug resistance. *Proceedings of the National Academy of Sciences of the United States of America*, *100*, 13881–13886. https://doi.org/10.1073/pnas.2235848100

Raymond, J. B., Mahapatra, S., Crick, D. C., & Pavelka, M. S. 2005. Identification of the *namH* gene, encoding the hydroxylase responsible for the N-glycolylation of the mycobacterial peptidoglycan. *Journal of Biological Chemistry*, *280*, 326–333. https://doi.org/10.1074/jbc.M411006200

Reed, M. B., Domenech, P., Manca, C., Su, H., Barczak, A. K., Kreiswirth, B. N., & Kaplan, G. 2004. A glycolipid of hypervirulent tuberculosis strains that inhibits the innate immune response. In *Nature* (Vol. 431, Issue 7004, pp. 84–87). https://doi.org/10.1038/nature02837

Remuiñán, M. J., Pérez-Herrán, E., Rullás, J., Alemparte, C., Martínez-Hoyos, M., Dow, D. J., Afari, J., Mehta, N., Esquivias, J., Jiménez, E., Ortega-Muro, F., Fraile-Gabaldón, M. T., Spivey, V. L., Loman, N. J., Pallen, M. J., Constantinidou, C., Minick, D. J., Cacho, M., Rebollo-López, M. J., … Cammack, N. 2013. Tetrahydropyrazolo[1,5-a]Pyrimidine-3-Carboxamide and N-Benzyl-6',7'-Dihydrospiro[Piperidine-4,4'-Thieno[3,2-c]Pyran] Analogues with Bactericidal Efficacy against *Mycobacterium tuberculosis* Targeting MmpL3. *PLoS ONE*, *8*. https://doi.org/10.1371/journal.pone.0060933

Rene, & Dubos, J. 1953. The White Plague. Tuberculosis, Man and Society. In *Southern Medical Journal* (Vol. 46, Issue 8). Little, Brown, and Company. https://doi.org/10.1097/00007611-195308000-00035

Rengarajan, J., Bloom, B. R., & Rubin, E. J. 2005. Genome-wide requirements for *Mycobacterium tuberculosis* adaptation and survival in macrophages. *Proceedings of the National Academy of Sciences of the United States of America*, *102*, 8327–8332. https://doi.org/10.1073/pnas.0503272102

Robitzek, E. H., Selikoff, I. J., & Ornstein, G. G. 1952. Chemotherapy of human tuberculosis with hydrazine derivatives of isonicotinic acid; preliminary report of representative cases. *Quarterly Bulletin of Sea View Hospital. New York. Sea View Hospital, Staten Island. Clinical Society*, *13*, 27–51.

Rock, J. 2019. Tuberculosis drug discovery in the CRISPR era. *PLoS Pathogens*, *15*. https://doi.org/10.1371/journal.ppat.1007975

Rogers, H. J., Perkins, H. R., & Ward, J. B. 1980. Microbial Cell Walls and Membranes. In *Microbial Cell Walls and Membranes*. https://doi.org/10.1007/978-94-011-6014-8

Rose, N. L., Completo, G. C., Lin, S. J., McNeil, M., Palcic, M. M., & Lowary, T. L. 2006. Expression, purification, and characterization of a galactofuranosyltransferase involved in *Mycobacterium tuberculosis* arabinogalactan biosynthesis. *Journal of the American Chemical Society*, *128*, 6721–6729. https://doi.org/10.1021/ja058254d

Roupie, V., Romano, M., Zhang, L., Korf, H., May, Y. L., Franken, K. L. M. C., Ottenhoff, T. H. M., Klein, M. R., & Huygen, K. 2007. Immunogenicity of eight dormancy regulon-encoded proteins of *Mycobacterium tuberculosis* in DNA-vaccinated and tuberculosis-infected mice. *Infection and Immunity*, *75*, 941–949. https://doi.org/10.1128/IAI.01137-06

Rozwarski, D. A., Grant, G. A., Barton, D. H. R., Jacobs, W. R., & Sacchettini, J. C. 1998. Modification of the NADH of the isoniazid target (InhA) from *Mycobacterium tuberculosis*. *Science*, *279*, 98–102. https://doi.org/10.1126/science.279.5347.98

Rucker, J., Paul, J., Pfeifer, B. A., & Lee, K. 2013. Engineering *E. coli* for triglyceride accumulation through native and heterologous metabolic reactions. *Applied Microbiology and Biotechnology*, *97*, 2753–2759. https://doi.org/10.1007/s00253-013-4714-3

Ruiz, N. 2008. Bioinformatics identification of MurJ (MviN) as the peptidoglycan lipid II flippase in *Escherichia coli*. *Proceedings of the National Academy of Sciences of the United States of America*, *105*, 15553–15557. https://doi.org/10.1073/pnas.0808352105

Ruiz, N. 2015. Lipid flippases for bacterial peptidoglycan biosynthesis. *Lipid Insights*, *2015*, 21–31. https://doi.org/10.4137/Lpi.s31783

Russell, D. G., Cardona, P. J., Kim, M. J., Allain, S., & Altare, F. 2009. Foamy macrophages and the progression of the human tuberculosis granuloma. In *Nature Immunology* (Vol. 10, Issue 9, pp. 943–948). https://doi.org/10.1038/ni.1781

Ryan, N. J., & Lo, J. H. 2014. Delamanid: First global approval. *Drugs*, *74*, 1041–1045. https://doi.org/10.1007/s40265-014-0241-5

Sacco, E., Covarrubias, A. S., O'Hare, H. M., Carroll, P., Eynard, N., Jones, T. A., Parish, T., Daffé, M., Bäckbro, K., & Quémard, A. 2007. The missing piece of the type II fatty acid synthase system from *Mycobacterium tuberculosis*. *Proceedings of the National Academy of Sciences of the United States of America*, *104*, 14628–14633. https://doi.org/10.1073/pnas.0704132104

Safi, H., Fleischmann, R. D., Peterson, S. N., Jones, M. B., Jarrahi, B., & Alland, D. 2010. Allelic exchange and mutant selection demonstrate that common clinical *embCAB* gene mutations only modestly increase resistance to ethambutol in *Mycobacterium tuberculosis*. *Antimicrobial Agents and Chemotherapy*, *54*, 103–108. https://doi.org/10.1128/AAC.01288-09

Safi, H., Sayers, B., Hazbón, M. H., & Alland, D. 2008. Transfer of *embB* codon 306 mutations into clinical *Mycobacterium tuberculosis* strains alters susceptibility to ethambutol, isoniazid, and rifampin. *Antimicrobial Agents and Chemotherapy*, *52*, 2027–2034. https://doi.org/10.1128/AAC.01486-07

Salazar, D. E., & Gormley, G. 2017. Modern Drug Discovery and Development. In *Clinical and Translational Science: Principles of Human Research: Second Edition* (pp. 719–743). https://doi.org/10.1016/B978-0-12-802101-9.00041-7

Samanovic, M. I., Hsu, H. C., Jones, M. B., Jones, V., McNeil, M. R., Becker, S. H., Jordan, A. T., Strnad, M., Xu, C., Jackson, M., Li, H., & Darwin, K. H. 2018. Cytokinin signaling in *Mycobacterium tuberculosis*. *MBio*, *9*. https://doi.org/10.1128/mBio.00989-18

Santucci, P., Johansen, M. D., Point, V., Poncin, I., Viljoen, A., Cavalier, J. F., Kremer, L., & Canaan, S. 2019. Nitrogen deprivation induces triacylglycerol accumulation, drug tolerance and hypervirulence in mycobacteria. *Scientific Reports*, *9*. https://doi.org/10.1038/s41598-019-45164-5

Sassetti, C. M., Boyd, D. H., & Rubin, E. J. 2003. Genes required for mycobacterial growth defined by high density mutagenesis. *Molecular Microbiology*, *48*, 77–84. https://doi.org/10.1046/j.1365-2958.2003.03425.x

Sassetti, C. M., & Rubin, E. J. 2003. Genetic requirements for mycobacterial survival during infection. *Proceedings of the National Academy of Sciences of the United States of America*, *100*, 12989–12994. https://doi.org/10.1073/pnas.2134250100

Sauvage, E., Kerff, F., Terrak, M., Ayala, J. A., & Charlier, P. 2008. The penicillin-binding proteins: Structure and role in peptidoglycan biosynthesis. In *FEMS Microbiology Reviews* (Vol. 32, Issue 2, pp. 234–258). https://doi.org/10.1111/j.1574-6976.2008.00105.x

Schaeffer, M. L., Agnihotri, G., Volker, C., Kallender, H., Brennan, P. J., & Lonsdale, J. T. 2001. Purification and Biochemical Characterization of the *Mycobacterium tuberculosis* B-Ketoacyl-acyl Carrier Protein Synthases KasA and KasB. *Journal of Biological Chemistry*, *276*, 47029–47037. https://doi.org/10.1074/jbc.M108903200

Schatz, A., Bugle, E., & Waksman, S. A. 1944. Streptomycin, a Substance Exhibiting Antibiotic Activity Against Gram-Positive and Gram-Negative Bacteria. *Proceedings of the Society for Experimental Biology and Medicine*, *55*, 66–69. https://doi.org/10.3181/00379727-55-14461

Schlesinger, L. S., Hull, S. R., & Kaufman, T. M. 1994. Binding of the terminal mannosyl units of lipoarabinomannan from a virulent strain of *Mycobacterium tuberculosis* to human macrophages. *Journal of Immunology (Baltimore, Md. : 1950)*, *152*, 4070–4079. http://www.ncbi.nlm.nih.gov/pubmed/8144972

Schubert, H. L., Raux, E., Brindley, A. A., Leech, H. K., Wilson, K. S., Hill, C. P., & Warren, M. J. 2002. The structure of *Saccharomyces cerevisiae* Met8p, a bifunctional dehydrogenase and ferrochelatase. *EMBO Journal*, *21*, 2068–2075. https://doi.org/10.1093/emboj/21.9.2068

Scorpio, A., & Zhang, Y. 1996. Mutations in *pncA*, a gene encoding pyrazinamidase/nicotinamidase, cause resistance to the antituberculous drug pyrazinamide in tubercle bacillus. *Nature Medicine*, *2*, 662–667. https://doi.org/10.1038/nm0696-662

Seidel, M., Alderwick, L. J., Birch, H. L., Sahm, H., Eggeling, L., & Besra, G. S. 2007. Identification of a novel arabinofuranosyltransferase AftB involved in a terminal step of cell wall arabinan biosynthesis in Corynebacterianeae, such as *Corynebacterium glutamicum* and *Mycobacterium tuberculosis*. *Journal of Biological Chemistry*, *282*, 14729–14740. https://doi.org/10.1074/jbc.M700271200

Seidel, M., Alderwick, L. J., Sahm, H., Besra, G. S., & Eggeling, L. 2007. Topology and mutational analysis of the single Emb arabinofuranosyltransferase of *Corynebacterium glutamicum* as a model of Emb proteins of *Mycobacterium tuberculosis*. *Glycobiology*, *17*, 210–219.

https://doi.org/10.1093/glycob/cwl066

Selikoff, I. J., & Robitzek, E. H. 1952. Tuberculosis chemotherapy with hydrazine derivatives of isonicotinic acid. *Diseases of the Chest*, *21*, 385–438. https://doi.org/10.1378/chest.21.4.385

Serafim, L. S., Xavier, A. M. R. B., & Lemos, P. C. 2018. Storage of Hydrophobic Polymers in Bacteria. In *Biogenesis of Fatty Acids, Lipids and Membranes* (pp. 1–25). https://doi.org/10.1007/978-3-319-43676-0_33-1

Severn, W. B., Furneaux, R. H., Falshaw, R., & Atkinson, P. H. 1998. Chemical and spectroscopic characterisation of the phosphatidylinositol manno-oligosaccharides from *Mycobacterium bovis* AN5 and WAg201 and *Mycobacterium smegmatis* mc2 155. *Carbohydrate Research*, *308*, 397–408. https://doi.org/10.1016/S0008-6215(98)00108-6

Sham, L. T., Butler, E. K., Lebar, M. D., Kahne, D., Bernhardt, T. G., & Ruiz, N. 2014. MurJ is the flippase of lipid-linked precursors for peptidoglycan biogenesis. *Science*, *345*, 220–222. https://doi.org/10.1126/science.1254522

Shao, M., McNeil, M., Cook, G. M., & Lu, X. 2020. MmpL3 inhibitors as antituberculosis drugs. *European Journal of Medicinal Chemistry*, *200*. https://doi.org/10.1016/j.ejmech.2020.112390

Shapira, T., Rankine-Wilson, L., Chao, J. D., Pichler, V., Rens, C., Pfeifer, T., & Av-Gay, Y. 2020. High-Content Screening of Eukaryotic Kinase Inhibitors Identify CHK2 Inhibitor Activity Against *Mycobacterium tuberculosis*. *Frontiers in Microbiology*, *11*. https://doi.org/10.3389/fmicb.2020.553962

Sherman, D. R., Mdluli, K., Hickey, M. J., Arain, T. M., Morris, S. L., Barry, C. E., & Stover, C. K. 1996. Compensatory ahpC gene expression in isoniazid-resistant *Mycobacterium tuberculosis*. *Science*, *272*, 1641–1643. https://doi.org/10.1126/science.272.5268.1641

Shi, L., Berg, S., Lee, A., Spencer, J. S., Zhang, J., Vissa, V., McNeil, M. R., Khoo, K. H., & Chatterjee, D. 2006. The carboxy terminus of EmbC from *Mycobacterium smegmatis* mediates chain length extension of the arabinan in lipoarabinomannan. *Journal of Biological Chemistry*, *281*, 19512–19526. https://doi.org/10.1074/jbc.M513846200

Shi, W., Chen, J., Feng, J., Cui, P., Zhang, S., Weng, X., Zhang, W., & Zhang, Y. 2014. Aspartate decarboxylase (PanD) as a new target of pyrazinamide in *Mycobacterium tuberculosis*. *Emerging Microbes & Infections*, *3*, 1–8. https://doi.org/10.1038/emi.2014.61

Shiloh, M. U., & DiGiuseppe Champion, P. A. 2010. To catch a killer. What can mycobacterial models teach us about *Mycobacterium tuberculosis* pathogenesis? In *Current Opinion in Microbiology* (Vol. 13, Issue 1, pp. 86–92). https://doi.org/10.1016/j.mib.2009.11.006

Shim, D., Kim, H., & Shin, S. J. 2020. *Mycobacterium tuberculosis* Infection-Driven Foamy Macrophages and Their Implications in Tuberculosis Control as Targets for Host-Directed Therapy. In *Frontiers in Immunology* (Vol. 11). https://doi.org/10.3389/fimmu.2020.00910

Shukla, S., Richardson, E. T., Drage, M. G., Boom, W. H., & Harding, C. V. 2018. Mycobacterium tuberculosis lipoprotein and lipoglycan binding to toll-like receptor 2 correlates with agonist activity and functional outcomes. *Infection and Immunity*, *86*. https://doi.org/10.1128/IAI.00450-18

Sinha, P., Gupta, A., Prakash, P., Anupurba, S., Tripathi, R., & Srivastava, G. N. 2016. Differentiation of *Mycobacterium tuberculosis* complex from non-tubercular mycobacteria by nested multiplex PCR targeting IS6110, MTP40 and 32kD alpha antigen encoding gene fragments. *BMC Infectious Diseases*, *16*. https://doi.org/10.1186/s12879-016-1450-1

Sinha, S., Kosalai, K., Arora, S., Namane, A., Sharma, P., Gaikwad, A. N., Brodin, P., & Cole, S. T. 2005. Immunogenic membrane-associated proteins of *Mycobacterium tuberculosis* revealed by proteomics. *Microbiology*, *151*, 2411–2419. https://doi.org/10.1099/mic.0.27799-0

Škovierová, H., Larrouy-Maumus, G., Pham, H., Belanová, M., Barilone, N., DasGupta, A., Mikušová, K., Gicquel, B., Gilleron, M., Brennan, P. J., Puzo, G., Nigou, J., & Jackson, M. 2010. Biosynthetic origin of the galactosamine substituent of arabinogalactan in *Mycobacterium tuberculosis*. *Journal of Biological Chemistry*, *285*, 41348–41355. https://doi.org/10.1074/jbc.M110.188110

Škovierová, H., Larrouy-Maumus, G., Zhang, J., Kaur, D., Barilone, N., Korduláková, J., Gilleron, M., Guadagnini, S., Belanová, M., Prevost, M. C., Gicquel, B., Puzo, G., Chatterjee, D., Brennan, P. J., Nigou, J., & Jackson, M. 2009. AftD, a novel essential arabinofuranosyltransferase from mycobacteria. *Glycobiology*, *19*, 1235–1247. https://doi.org/10.1093/glycob/cwp116

Sogi, K. M., Lien, K. A., Johnson, J. R., Krogan, N. J., & Stanley, S. A. 2017. The Tyrosine Kinase Inhibitor Gefitinib Restricts *Mycobacterium tuberculosis* Growth through Increased Lysosomal Biogenesis and Modulation of Cytokine Signaling. *ACS Infectious Diseases*, *3*, 564–574. https://doi.org/10.1021/acsinfecdis.7b00046

Sohlenkamp, C., Geiger, O., Bacterial membrane lipids: diversity in structures and pathways. 2016. *FEMS Microbiology Reviews*, 40,133–159, https://doi.org/10.1093/femsre/fuv008

Spinelli, F. R., Conti, F., & Gadina, M. 2020. HiJAKing SARS-CoV-2? The potential role of JAK inhibitors in the management of COVID-19. *Science Immunology*, *5*. https://doi.org/10.1126/sciimmunol.abc5367

Sridharan, S., Kurzawa, N., Werner, T., Günthner, I., Helm, D., Huber, W., Bantscheff, M., & Savitski, M. M. 2019. Proteome-wide solubility and thermal stability profiling reveals distinct regulatory roles for ATP. *Nature Communications*, *10*. https://doi.org/10.1038/s41467-019-09107-y

Stanley, S. A., Grant, S. S., Kawate, T., Iwase, N., Shimizu, M., Wivagg, C., Silvis, M., Kazyanskaya, E., Aquadro, J., Golas, A., Fitzgerald, M., Dai, H., Zhang, L., & Hung, D. T. 2012. Identification of novel inhibitors of *M. tuberculosis* growth using whole cell based high-throughput screening. *ACS Chemical Biology*, *7*, 1377–1384. https://doi.org/10.1021/cb300151m

Starks, A. M., Gumusboga, A., Plikaytis, B. B., Shinnick, T. M., & Posey, J. E. 2009. Mutations at *embB* codon 306 are an important molecular indicator of ethambutol resistance in *Mycobacterium tuberculosis*. *Antimicrobial Agents and Chemotherapy*, *53*, 1061–1066. https://doi.org/10.1128/AAC.01357-08

Sturgill-Koszycki, S., Schlesinger, P. H., Chakraborty, P., Haddix, P. L., Collins, H. L., Fok, A. K., Allen, R. D., Gluck, S. L., Heuser, J., & Russell, D. G. 1994. Lack of acidification in Mycobacterium phagosomes produced by exclusion of the vesicular proton-ATPase. *Science*, *263*, 678–681. https://doi.org/10.1126/science.8303277

Su, C. C., Klenotic, P. A., Bolla, J. R., Purdy, G. E., Robinson, C. V., & Yu, E. W. 2019. MmpL3 is a lipid transporter that binds trehalose monomycolate and phosphatidylethanolamine. *Proceedings of the National Academy of Sciences of the United States of America*, *166*, 11241–11246. https://doi.org/10.1073/pnas.1901346116

Sugawara, E., & Nikaido, H. 2014. Properties of AdeABC and AdeIJK efflux systems of *Acinetobacter baumannii* compared with those of the AcrAB-TolC system of *Escherichia coli*. In *Antimicrobial Agents and Chemotherapy* (Vol. 58, Issue 12). https://doi.org/10.1128/AAC.03728-14

Sunder, S., Lanotte, P., Godreuil, S., Martin, C., Boschiroli, M. L., & Besnier, J. M. 2009. Human-to-human transmission of tuberculosis caused by *Mycobacterium bovis* in immunocompetent patients. *Journal of Clinical Microbiology*, *47*, 1249–1251. https://doi.org/10.1128/JCM.02042-08

T. Virtanen, A., Haikarainen, T., Raivola, J., & Silvennoinen, O. 2019. Selective JAKinibs: Prospects in Inflammatory and Autoimmune Diseases. In *BioDrugs* (Vol. 33, Issue 1, pp. 15–32). https://doi.org/10.1007/s40259-019-00333-w

Taguchi, A., Welsh, M. A., Marmont, L. S., Lee, W., Sjodt, M., Kruse, A. C., Kahne, D., Bernhardt, T. G., & Walker, S. 2019. FtsW is a peptidoglycan polymerase that is functional only in complex with its cognate penicillin-binding protein. *Nature Microbiology*, *4*, 587–594. https://doi.org/10.1038/s41564-018-0345-x

Tahlan, K., Wilson, R., Kastrinsky, D. B., Arora, K., Nair, V., Fischer, E., Whitney Barnes, S., Walker, J. R., Alland, D., Barry, C. E., & Boshoff, H. I. 2012. SQ109 targets MmpL3, a membrane transporter of trehalose monomycolate involved in mycolic acid donation to the cell wall core of *Mycobacterium tuberculosis*. *Antimicrobial Agents and Chemotherapy*, *56*, 1797–1809. https://doi.org/10.1128/AAC.05708-11

Takayama, K., & Kilburn, J. O. 1989. Inhibition of synthesis of arabinogalactan by ethambutol in *Mycobacterium smegmatis*. *Antimicrobial Agents and Chemotherapy*, *33*, 1493–1499. https://doi.org/10.1128/AAC.33.9.1493

Telenti, A., Imboden, P., Marchesi, F., Matter, L., Schopfer, K., Bodmer, T., Lowrie, D., Colston, M. J., & Cole, S. 1993. Detection of rifampicin-resistance mutations in Mycobacterium tuberculosis. *The Lancet*, *341*, 647–651. https://doi.org/10.1016/0140-6736(93)90417-F

Thoen, C. O., Steele, J. H., & Gilsdorf, M. J. 2008. *Mycobacterium bovis* Infection in Animals and Humans: Second Edition. In *Mycobacterium Bovis Infection in Animals and Humans: Second Edition*. https://doi.org/10.1002/9780470344538

To, K., Cao, R., Yegiazaryan, A., Owens, J., & Venketaraman, V. 2020. General overview of nontuberculous mycobacteria opportunistic pathogens: *Mycobacterium avium* and *Mycobacterium abscessus*. *Journal of Clinical Medicine*, *9*, 1–24. https://doi.org/10.3390/jcm9082541

Tobin, D. M., & Ramakrishnan, L. 2008. Comparative pathogenesis of *Mycobacterium marinum* and *Mycobacterium tuberculosis*. In *Cellular Microbiology* (Vol. 10, Issue 5, pp. 1027–1039). https://doi.org/10.1111/j.1462-5822.2008.01133.x

Torres, J. N., Paul, L. V., Rodwell, T. C., Victor, T. C., Amallraja, A. M., Elghraoui, A., Goodmanson, A. P., Ramirez-Busby, S. M., Chawla, A., Zadorozhny, V., Streicher, E. M., Sirgel, F. A., Catanzaro, D., Rodrigues, C., Gler, M. T., Crudu, V., Catanzaro, A., & Valafar, F. 2015. Novel

katG mutations causing isoniazid resistance in clinical *M. Tuberculosis* isolates. *Emerging Microbes and Infections*, *4*, e42. https://doi.org/10.1038/emi.2015.42

Tortoli, E. 2019. The Taxonomy of the Genus *Mycobacterium*. In *Nontuberculous Mycobacteria (NTM): Microbiological, Clinical and Geographical Distribution* (pp. 1–10). https://doi.org/10.1016/B978-0-12-814692-7.00001-2

Trivedi, O. A., Arora, P., Sridharan, V., Tickoo, R., Mohanty, D., & Gokhale, R. S. 2004. Enzymic activation and transfer of fatty acids as acyl-adenylates in mycobacteria. *Nature*, *428*, 441–445. https://doi.org/10.1038/nature02384

Trott, O., & Olson, A. J. 2010. AutoDock Vina: improving the speed and accuracy of docking with a new scoring function, efficient optimization, and multithreading. *Journal of computational chemistry*, 31(2), 455-461.

Tsolaki, A. G., Hirsh, A. E., DeRiemer, K., Enciso, J. A., Wong, M. Z., Hannan, M., Goguet De La Salmoniere, Y. O. L., Aman, K., Kato-Maeda, M., & Small, P. M. 2004. Functional and evolutionary genomics of *Mycobacterium tuberculosis*: Insights from genomic deletions in 100 strains. *Proceedings of the National Academy of Sciences of the United States of America*, *101*, 4865–4870. https://doi.org/10.1073/pnas.0305634101

Turkish, A., & Sturley, S. L. 2007. Regulation of Triglyceride Metabolism. I. Eukaryotic neutral lipid synthesis: "Many ways to skin ACAT or a DGAT." *American Journal of Physiology - Gastrointestinal and Liver Physiology*, *292*. https://doi.org/10.1152/ajpgi.00509.2006

Turnbull, W. B., Shimizu, K. H., Chatterjee, D., Homans, S. W., & Treumann, A. 2004. Identification of the 5-methylthiopentosyl substituent in *Mycobacterium tuberculosis* lipoarabinomannan. *Angewandte Chemie - International Edition*, *43*, 3918–3922. https://doi.org/10.1002/anie.200454119

Turner, R. D., & Bothamley, G. H. 2015. Cough and the transmission of tuberculosis. In *Journal of Infectious Diseases* (Vol. 211, Issue 9, pp. 1367–1372). https://doi.org/10.1093/infdis/jiu625

Umezawa, H., Mizuno, S., Yamazaki, H., & Nitta, K. 1968. Inhibition of DNA-dependent RNA synthesis by rifamycins. In *Journal of Antibiotics* (Vol. 21, Issue 3, pp. 234–236). https://doi.org/10.7164/antibiotics.21.234

Vannelli, T. A., Dykman, A., & Ortiz De Montellano, P. R. 2002. The antituberculosis drug ethionamide is activated by a flavoprotein monooxygenase. *Journal of Biological Chemistry*, *277*, 12824–12829. https://doi.org/10.1074/jbc.M110751200

Veiga-Santos, P., Li, K., Lameira, L., De Carvalho, T. M. U., Huang, G., Galizzi, M., Shang, N., Li, Q., Gonzalez-Pacanowska, D., Hernandez-Rodriguez, V., Benaim, G., Guo, R. T., Urbina, J. A., Docampo, R., De Souza, W., & Oldfield, E. 2015. SQ109, a new drug lead for chagas disease. *Antimicrobial Agents and Chemotherapy*, *59*, 1950–1961. https://doi.org/10.1128/AAC.03972-14

Ventura, M., Canchaya, C., Tauch, A., Chandra, G., Fitzgerald, G. F., Chater, K. F., & van Sinderen, D. 2007. Genomics of Actinobacteria : Tracing the Evolutionary History of an Ancient Phylum . *Microbiology and Molecular Biology Reviews*, *71*, 495–548. https://doi.org/10.1128/mmbr.00005-07

Viljoen, A., Dubois, V., Girard-Misguich, F., Blaise, M., Herrmann, J. L., & Kremer, L. 2017. The diverse family of MmpL transporters in mycobacteria: from regulation to antimicrobial developments. In *Molecular Microbiology* (Vol. 104, Issue 6, pp. 889–904). https://doi.org/10.1111/mmi.13675

Villeneuve, M., Kawai, M., Horiuchi, K., Watanabe, M., Aoyagi, Y., Hitotsuyanagi, Y., Takeya, K., Gouda, H., Hirono, S., & Minnikin, D. E. 2013. Conformational folding of mycobacterial methoxy- and ketomycolic acids facilitated by α-methyl trans-cyclopropane groups rather than cis-cyclopropane units. *Microbiology (United Kingdom)*, *159*, 2405–2415. https://doi.org/10.1099/mic.0.068866-0

Villeneuve, M., Kawai, M., Kanashima, H., Watanabe, M., Minnikin, D. E., & Nakahara, H. 2005. Temperature dependence of the Langmuir monolayer packing of mycolic acids from *Mycobacterium tuberculosis*. *Biochimica et Biophysica Acta - Biomembranes*, *1715*, 71–80. https://doi.org/10.1016/j.bbamem.2005.07.005

Villeneuve, M., Kawai, M., Watanabe, M., Aoyagi, Y., Hitotsuyanagi, Y., Takeya, K., Gouda, H., Hirono, S., Minnikin, D. E., & Nakahara, H. 2007. Conformational behavior of oxygenated mycobacterial mycolic acids from Mycobacterium bovis BCG. *Biochimica et Biophysica Acta - Biomembranes*, *1768*, 1717–1726. https://doi.org/10.1016/j.bbamem.2007.04.003

Vinet, L., & Zhedanov, A. 2011. A "missing" family of classical orthogonal polynomials. *Journal of Physics A: Mathematical and Theoretical*, *44*. https://doi.org/10.1088/1751-8113/44/8/085201

Vollmer, W., Blanot, D., & De Pedro, M. A. 2008. Peptidoglycan structure and architecture. In *FEMS Microbiology Reviews* (Vol. 32, Issue 2, pp. 149–167). https://doi.org/10.1111/j.1574-6976.2007.00094.x

Vollmer, W., & Höltje, J. V. 2004. The architecture of the murein (peptidoglycan) in gram-negative bacteria: Vertical scaffold or horizontal layer(s)? In *Journal of Bacteriology* (Vol. 186, Issue 18, pp. 5978–5987). https://doi.org/10.1128/JB.186.18.5978-5987.2004

Voskuil, M. I., Schnappinger, D., Visconti, K. C., Harrell, M. I., Dolganov, G. M., Sherman, D. R., & Schoolnik, G. K. 2003. Inhibition of respiration by nitric oxide induces a *Mycobacterium tuberculosis* dormancy program. *Journal of Experimental Medicine*, *198*, 705–713. https://doi.org/10.1084/jem.20030205

Walz, L., Cohen, A. J., Rebaza, A. P., Vanchieri, J., Slade, M. D., Dela Cruz, C. S., & Sharma, L. 2021. JAK-inhibitor and type I interferon ability to produce favorable clinical outcomes in COVID-19 patients: a systematic review and meta-analysis. *BMC Infectious Diseases*, *21*. https://doi.org/10.1186/s12879-020-05730-z

Wanger, A., Chavez, V., Huang, R. S. P., Wahed, A., Actor, J. K., & Dasgupta, A. 2017. Biochemical Tests and Staining Techniques for Microbial Identification. In *Microbiology and Molecular Diagnosis in Pathology* (pp. 61–73). https://doi.org/10.1016/b978-0-12-805351-5.00005-3

Warren, M. J., Gonzalez, M. D., Williams, H. J., Stolowich, N. J., & Ian Scott, A. 1990. Uroporphyrinogen III Methylase Catalyzes the Enzymatic Synthesis of Sirohydrochlorins II and IV by a Clockwise Mechanism. *Journal of the American Chemical Society*, *112*, 5343–5345. https://doi.org/10.1021/ja00169a048

Warren, M. J., Roessner, C. A., Santander, P. J., & Scott, A. I. 1990. The Escherichia coli cysG gene encodes S-adenosylmethionine-dependent uroporphyrinogen III methylase. *Biochemical*

Journal, *265*, 725–729. https://doi.org/10.1042/bj2650725

Wayne, L. G., & Hayes, L. G. 1996. An in vitro model for sequential study of shiftdown of *Mycobacterium tuberculosis* through two stages of nonreplicating persistence. *Infection and Immunity*, *64*, 2062–2069. https://doi.org/10.1128/iai.64.6.2062-2069.1996

Werner, T., Sweetman, G., Savitski, M. F., Mathieson, T., Bantscheff, M., & Savitski, M. M. 2014. Ion coalescence of neutron encoded TMT 10-plex reporter ions. *Analytical Chemistry*, *86*, 3594–3601. https://doi.org/10.1021/ac500140s

WHO. 2014. *Fact Sheet 104 - Tuberculosis*. World Health Organization. http://www.who.int/mediacentre/factsheets/fs104/en/

WHO. 2015. Global Tuberculosis Report. In *World Health Organization* (Issue September). https://doi.org/978 92 4 156450 2

WHO. 2017. Treatment of Tuberculosis: Guidelines for treatment of drug-susceptible tuberculosis and patient care. 2017 update. In *World Health Orgnaization*.

WHO. 2020. Consolidated Guidelines on Tuberculosis Treatment. In *Who*.

WHO. 2021. WHO consolidated guidelines on tuberculosis. Module 1: Prevention. Tuberculosis preventive treatment. In *Tuberculosis, Lung Diseases, HIV Infection* (Issue 2, pp. 86–92). https://doi.org/10.30978/tb2021-2-86

WHO. 2021. Global Tuberculosis Report. *World Health Organization.* ISBN: 9789240037021

Wohlkönig, A., Remaut, H., Moune, M., Tanina, A., Meyer, F., Desroses, M., Steyaert, J., Willand, N., Baulard, A. R., & Wintjens, R. 2017. Structural analysis of the interaction between spiroisoxazoline SMARt-420 and the *Mycobacterium tuberculosis* repressor EthR2. *Biochemical and Biophysical Research Communications*, *487*, 403–408. https://doi.org/10.1016/j.bbrc.2017.04.074

Wolucka, B. A., McNeil, M. R., De Hoffmann, E., Chojnacki, T., & Brennan, P. J. 1994. Recognition of the lipid intermediate for arabinogalactan/arabinomannan biosynthesis and its relation to the mode of action of ethambutol on mycobacteria. *Journal of Biological Chemistry*, *269*, 23328–23335. https://doi.org/10.1016/s0021-9258(17)31657-5

Xie, Z., Yang, X., Duan, Y., Han, J., & Liao, C. 2021. Small-Molecule Kinase Inhibitors for the Treatment of Nononcologic Diseases. In *Journal of Medicinal Chemistry* (Vol. 64, Issue 3, pp. 1283–1345). https://doi.org/10.1021/acs.jmedchem.0c01511

Xiong, Y., Chalmers, M. J., Gao, F. P., Cross, T. A., & Marshall, A. G. 2005. Identification of *Mycobacterium tuberculosis* H37Rv integral membrane proteins by one-dimensional gel electrophoresis and liquid chromatography electrospray ionization tandem mass spectrometry. *Journal of Proteome Research*, *4*, 855–861. https://doi.org/10.1021/pr0500049

Xu, L., Wu, D., Liu, L., Zheng, Q., Song, Y., Ye, L., Sha, S., Kang, J., Xin, Y., & Ma, Y. 2014. Characterization of mycobacterial UDP-N-acetylglucosamine enolpyruvyle transferase (MurA). *Research in Microbiology*, *165*, 91–101. https://doi.org/10.1016/j.resmic.2014.01.004

Yang, Q., Yu, K., Yan, L., Li, Y., Chen, C., & Li, X. 2011. Structural view of the regulatory subunit of aspartate kinase from *Mycobacterium tuberculosis*. *Protein and Cell*, *2*, 745–754.

https://doi.org/10.1007/s13238-011-1094-2

Yang, X., Kui, L., Tang, M., Li, D., Wei, K., Chen, W., Miao, J., & Dong, Y. 2020. High-Throughput Transcriptome Profiling in Drug and Biomarker Discovery. In *Frontiers in Genetics* (Vol. 11). https://doi.org/10.3389/fgene.2020.00019

Yeager, R. L., Munroe, W. G., & Dessau, F. I. 1952. Pyrazinamide (aldinamide) in the treatment of pulmonary tuberculosis. *American Review of Tuberculosis*, *65*, 523–546.

Young, C., Walzl, G., & Du Plessis, N. 2020. Therapeutic host-directed strategies to improve outcome in tuberculosis. In *Mucosal Immunology* (Vol. 13, Issue 2, pp. 190–204). https://doi.org/10.1038/s41385-019-0226-5

Zampieri, M., Szappanos, B., Buchieri, M. V., Trauner, A., Piazza, I., Picotti, P., Gagneux, S., Borrell, S., Gicquel, B., Lelievre, J., Papp, B., & Sauer, U. 2018. High-throughput metabolomic analysis predicts mode of action of uncharacterized antimicrobial compounds. *Science Translational Medicine*, *10*. https://doi.org/10.1126/scitranslmed.aal3973

Zhan, M. M., Hu, X. Q., Liu, X. X., Ruan, B. F., Xu, J., & Liao, C. 2016. From monoclonal antibodies to small molecules: The development of inhibitors targeting the PD-1/PD-L1 pathway. In *Drug Discovery Today* (Vol. 21, Issue 6, pp. 1027–1036). https://doi.org/10.1016/j.drudis.2016.04.011

Zhang, B., Li, J., Yang, X., Wu, L., Zhang, J., Yang, Y., Zhao, Y., Zhang, L., Yang, X., Yang, X., Cheng, X., Liu, Z., Jiang, B., Jiang, H., Guddat, L. W., Yang, H., & Rao, Z. 2019. Crystal Structures of Membrane Transporter MmpL3, an Anti-TB Drug Target. *Cell*, *176*, 636-648.e13. https://doi.org/10.1016/j.cell.2019.01.003

Zhang, L., Zhao, Y., Gao, Y., Wu, L., Gao, R., Zhang, Q., Wang, Y., Wu, C., Wu, F., Gurcha, S. S., Veerapen, N., Batt, S. M., Zhao, W., Qin, L., Yang, X., Wang, M., Zhu, Y., Zhang, B., Bi, L., … Rao, Z. 2020. Structures of cell wall arabinosyltransferases with the anti-tuberculosis drug ethambutol. *Science*, *368*, 1211–1219. https://doi.org/10.1126/science.aba9102

Zhang, S., Chen, J., Shi, W., Cui, P., Zhang, J., Cho, S., Zhang, W., & Zhang, Y. 2017. Mutation in *clpC1* encoding an ATP-dependent ATPase involved in protein degradation is associated with pyrazinamide resistance in *Mycobacterium tuberculosis*. In *Emerging Microbes and Infections* (Vol. 6, Issue 2). https://doi.org/10.1038/emi.2017.1

Zhang, Y., Heym, B., Allen, B., Young, D., & Cole, S. 1992. The catalase - Peroxidase gene and isoniazid resistance of *Mycobacterium tuberculosis*. *Nature*, *358*, 591–593. https://doi.org/10.1038/358591a0

Zhang, Y., Scorpio, A., Nikaido, H., Sun, Z., Unlike, A., & Organi-, W. H. 1999. Role of Acid pH and De cient Ef ux of Pyrazinoic Acid in Unique Susceptibility of. *Microbiology*, *181*, 2044–2049. http://jb.asm.org/content/181/7/2044.full

Zhang, Y., Shi, W., Zhang, W., & Mitchison, D. 2014. Mechanisms of Pyrazinamide Action and Resistance. *Microbiology Spectrum*, *2*. https://doi.org/10.1128/microbiolspec.mgm2-0023-2013

Zhang, Y., Wade, M. M., Scorpio, A., Zhang, H., & Sun, Z. 2003. Mode of action of pyrazinamide: Disruption of *Mycobacterium tuberculosis* membrane transport and energetics by pyrazinoic acid. *Journal of Antimicrobial Chemotherapy*, *52*, 790–795.

https://doi.org/10.1093/jac/dkg446

Zhang, Y., & Yew, W. W. 2009. Mechanisms of drug resistance in *Mycobacterium tuberculosis*. In *International Journal of Tuberculosis and Lung Disease*. 13, 11, 1320–1330.

Zhang, Z., Bulloch, E. M. M., Bunker, R. D., Baker, E. N., & Squire, C. J. 2009. Structure and function of GlmU from *Mycobacterium tuberculosis*. *Acta Crystallographica Section D: Biological Crystallography*, *65*, 275–283. https://doi.org/10.1107/S0907444909001036

Zhao, L. L., Sun, Q., Liu, H. C., Wu, X. C., Xiao, T. Y., Zhao, X. Q., Li, G. L., Jiang, Y., Zeng, C. Y., & Wan, K. L. 2015. Analysis of *embCAB* mutations associated with ethambutol resistance in multidrug-resistant *Mycobacterium tuberculosis* isolates from China. *Antimicrobial Agents and Chemotherapy*, *59*, 2045–2050. https://doi.org/10.1128/AAC.04933-14

Zheng, S., Sham, L. T., Rubino, F. A., Brock, K. P., Robins, W. P., Mekalanos, J. J., Marks, D. S., Bernhardt, T. G., & Kruse, A. C. 2018. Structure and mutagenic analysis of the lipid II flippase MurJ from *Escherichia coli*. *Proceedings of the National Academy of Sciences of the United States of America*, *115*, 6709–6714. https://doi.org/10.1073/pnas.1802192115

Ziskind, B., & Halioua, B. 2007. Tuberculosis in ancient egypt. *Revue Des Maladies Respiratoires*, *24*, 1277–1283. https://doi.org/10.1016/S0761-8425(07)78506-6

Appendix

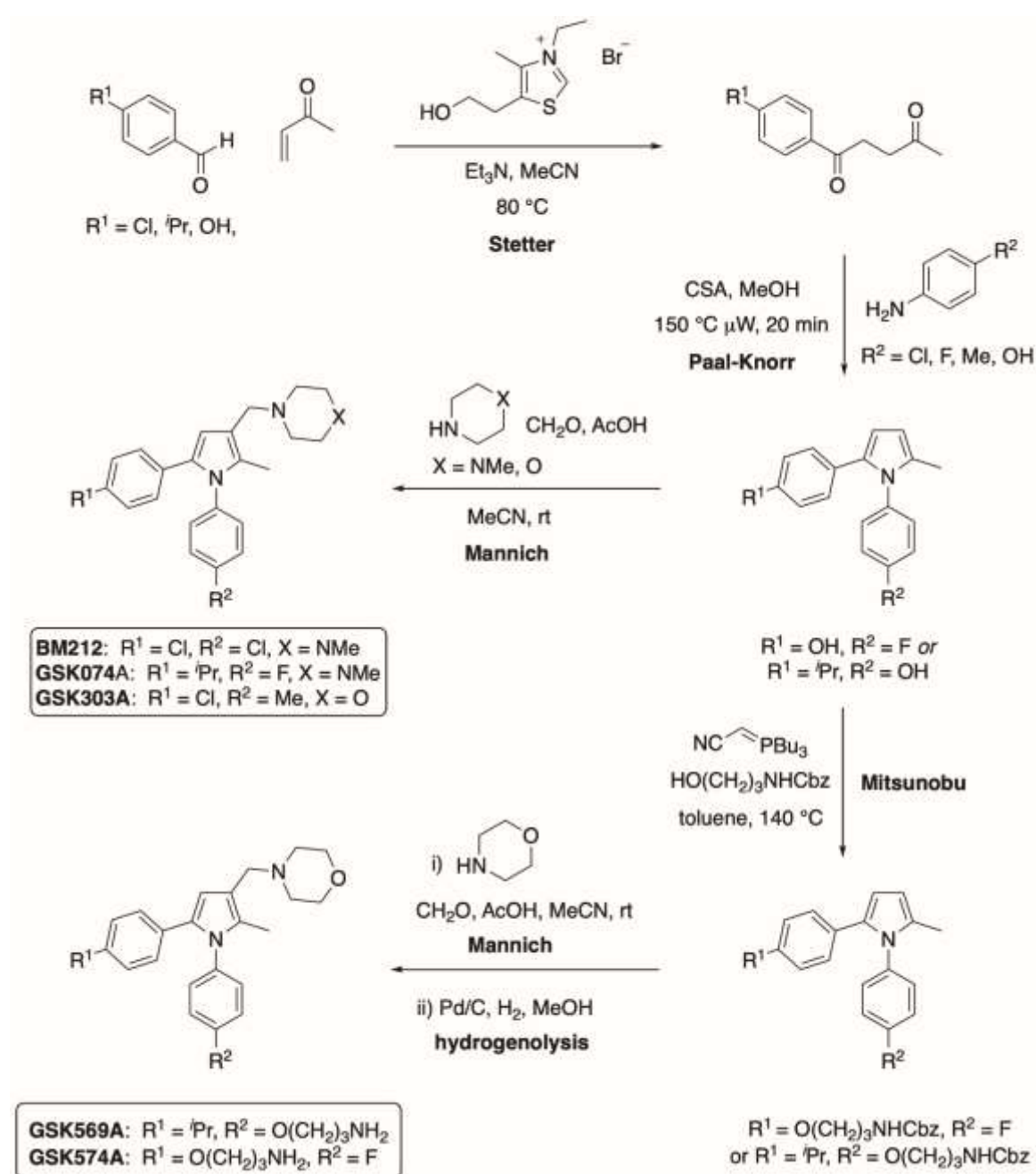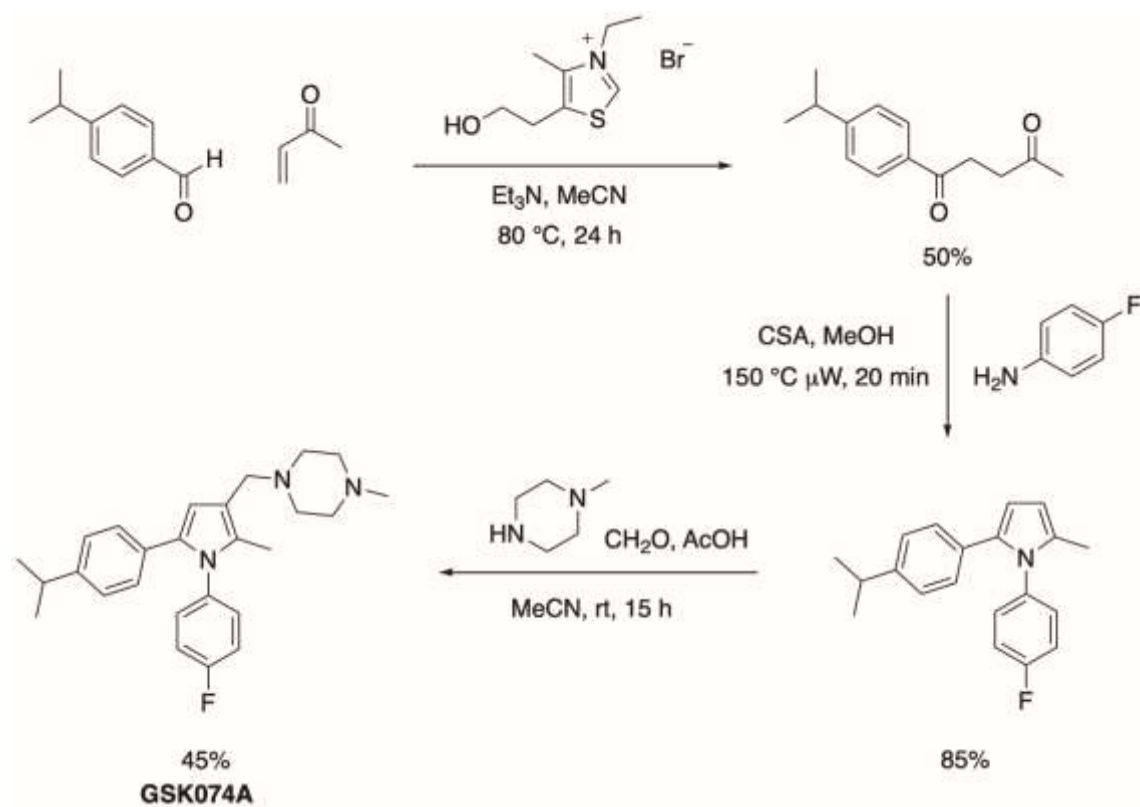**Figure 62. Supplementary Scheme 1 showing the chemical synthesis of BM212**

Figure 63. Supplementary Scheme 2 showing the chemical synthesis of GSK074A
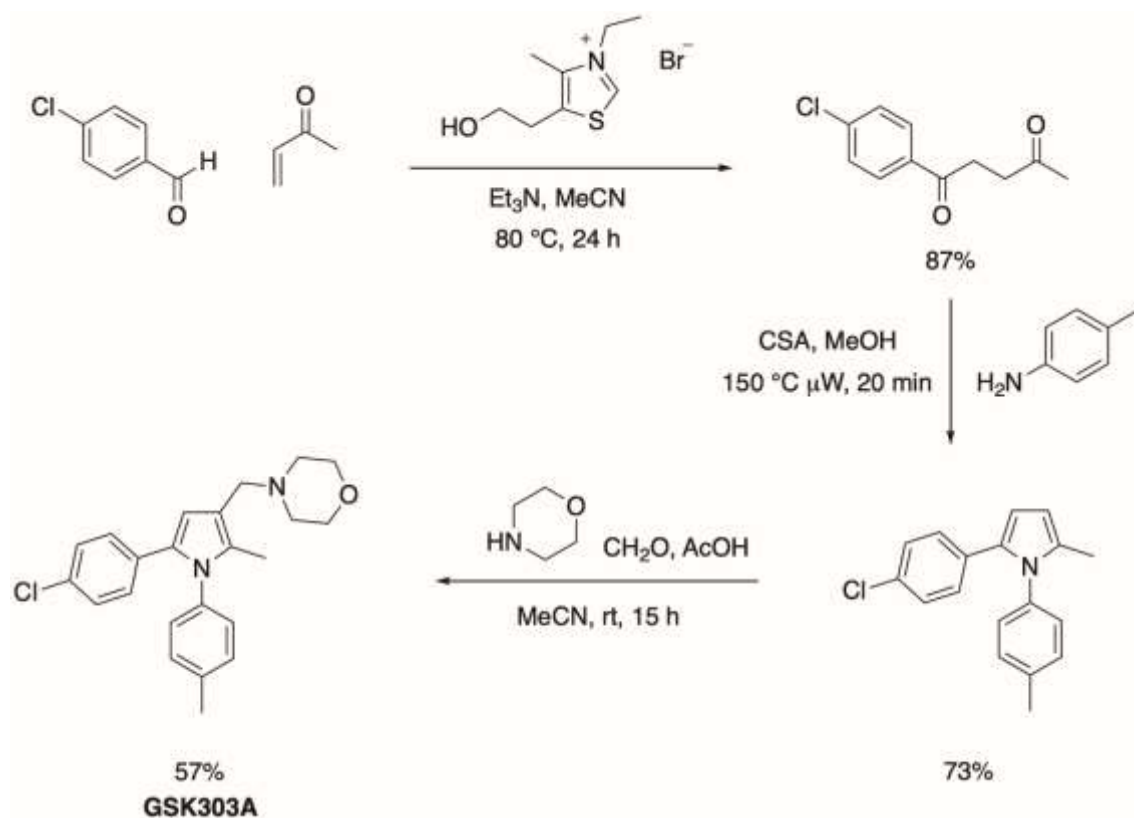
Figure 64. Supplementary Scheme 3 showing the chemical synthesis of GSK303A
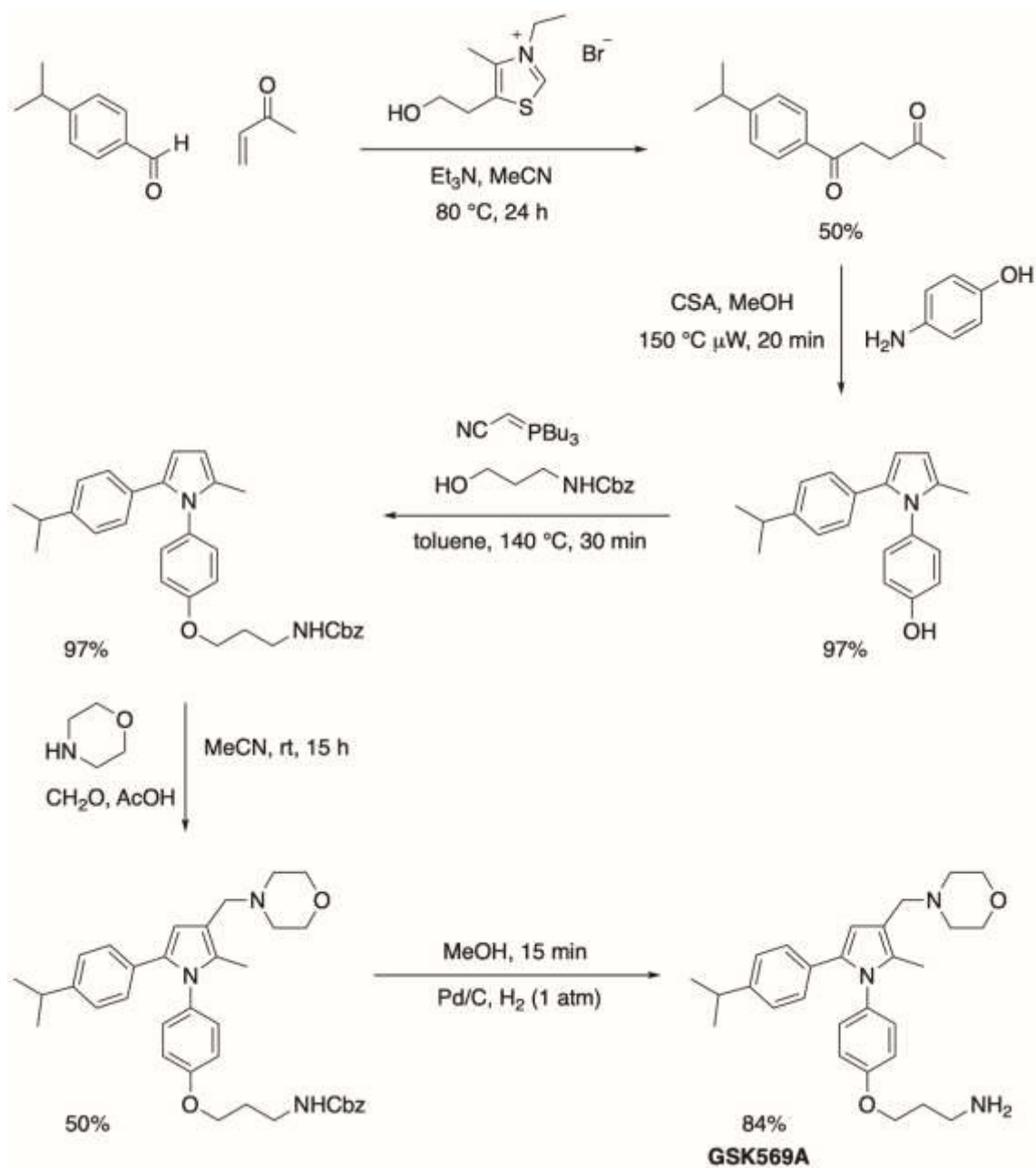
Figure 65. Supplementary Scheme 4 showing the chemical synthesis of GSK569A
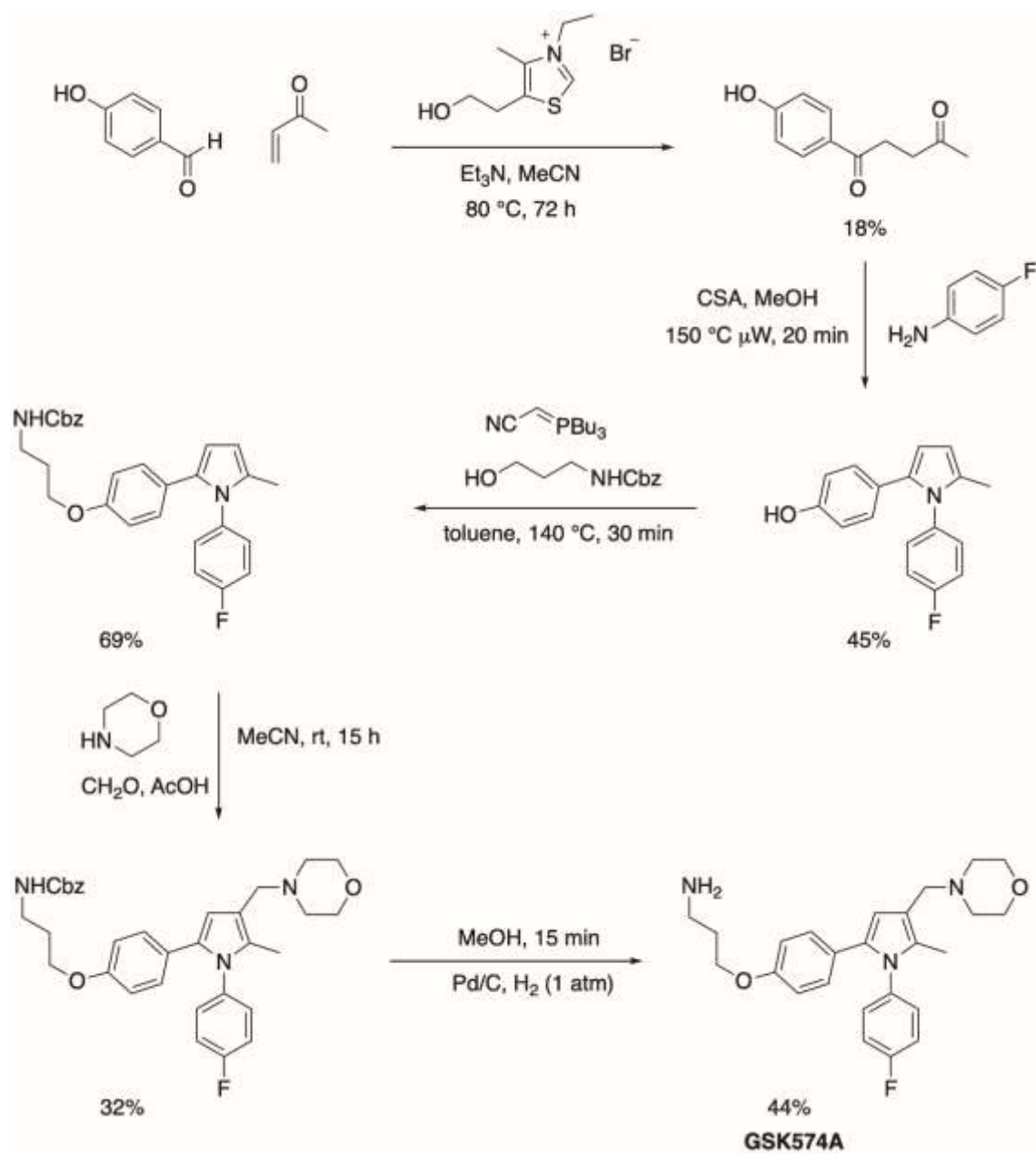
Figure 66. Supplementary Scheme 5 showing the chemical synthesis of GSK574A
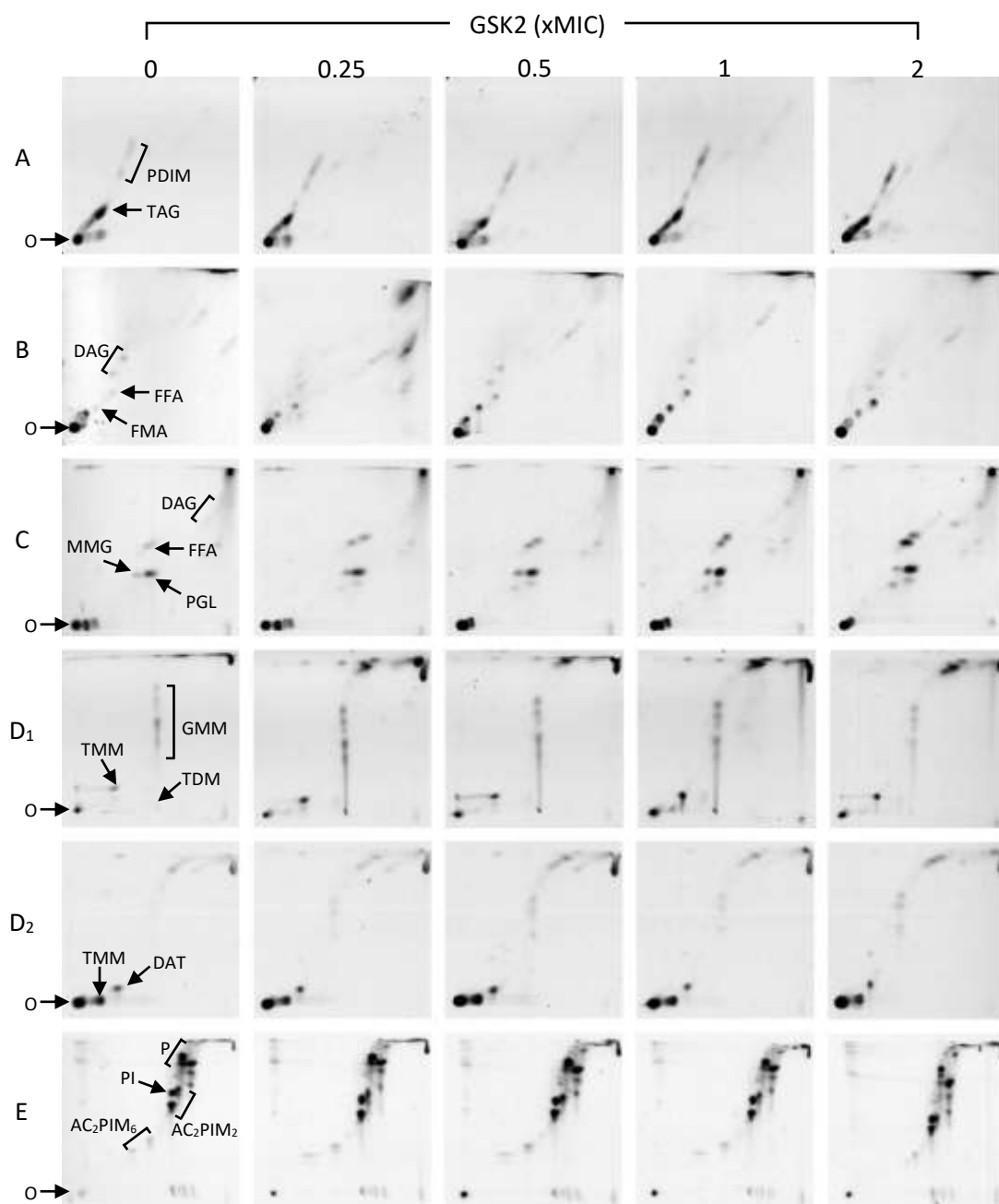
Figure 67. Lipid profile of WT *M. bovis* BCG treated with GSK2. *M. bovis* BCG was cultured in the presence of GSK2 for 24 hours and labelled with [^{14}C] acetic acid. Cells were harvested by centrifugation and polar and apolar lipids were extracted. Aluminium backed silica TLC plates loaded with 10,000 cpm lipids were run in solvent systems A - E. Autoradiograph films were exposed to the TLC plates for 6 days, scanned then transformed to grayscale and cropped using Adobe Photoshop. The contrast of the whole image was adjusted for image clarity. Apolar lipids run in systems A-D_1 reveal a number to the lipids with GSK2 treatment, specifically, an apparent increase in PDIMs, likely indicating a relative reduction in TAG (system A) and an increase in FFA (systems B and C). Polar lipids run in systems D_2 and E do not appear to change with GSK2 treatment. O indicates origin. A - phthiocerol dimycocerosates (PDIM), triacylglycerol (TAG); B – diacylglycerol (DAG), free fatty acid (FFA), free mycolic acid (FMA); C – phenolic glycolipid (PGL), monomycolated glycerol (MMG), DAG, FFA; D_1 – glucose monomycolate (GMM), trehalose monomycolate (TMM), trehalose dimycolate (TDM); D_2 – diacyltrehalose (DAT), TMM; E – phospholipid (P), phosphatidyl inositol (PI), diacylphosphatidylinositol dimannoside (AC$_2$PIM$_2$), diacylphosphatidylinositol hexamannoside (AC$_2$PIM$_6$).

Figure 68. Lipid profile of *M. bovis* BCG overexpressing *tgs1*, treated with GSK2. *M. bovis* BCG pMV261-*tgs1* was cultured in the presence of GSK2 for 24 hours and labelled with [^{14}C] acetic acid. Cells were harvested by centrifugation and polar and apolar lipids were extracted. Aluminium backed silica TLC plates loaded with 10,000 cpm lipids were run in solvent systems A - E. Autoradiograph films were exposed to the TLC plates for 6 days, scanned then transformed to grayscale and cropped using Adobe Photoshop. The contrast of the whole image was adjusted for image clarity. Lipids appear to reflect those of WT *M. bovis* BCG, with an increase in FFA in systems B and C. PGL is considerably reduced in this strain both in the presence and absence of GSK2. O indicates origin. A - phthiocerol dimycocerosates (PDIM), triacylglycerol (TAG); B – diacylglycerol (DAG), free fatty acid (FFA), free mycolic acid (FMA); C – phenolic glycolipid (PGL), monomycolated glycerol (MMG), DAG, FFA; D$_1$ – glucose monomycolate (GMM), trehalose monomycolate (TMM), trehalose dimycolate (TDM); D$_2$ – diacyltrehalose (DAT), TMM; E – phospholipid (P), phosphatidyl inositol (PI), diacylphosphatidylinositol dimannoside (AC$_2$PIM$_2$), diacylphosphatidylinositol hexamannoside (AC$_2$PIM$_6$).

Figure 69. Lipid profile of *M. bovis* BCG overexpressing *tgs2*, treated with GSK2. *M. bovis* BCG pMV261-*tgs2* was cultured in the presence of GSK2 for 24 hours and labelled with [^{14}C] acetic acid. Cells were harvested by centrifugation and polar and apolar lipids were extracted. Aluminium backed silica TLC plates loaded with 10,000 cpm lipids were run in solvent systems A - E. Autoradiograph films were exposed to the TLC plates for 6 days, scanned then transformed to grayscale and cropped using Adobe Photoshop. The contrast of the whole image was adjusted for image clarity. An increase in FFA in systems B and C reflects the lipid profile of WT *M. bovis* BCG. PGL is appears to be absent from this strain both in the presence and absence of GSK2. The crescent shaped marks in panel C2 are caused by damage to autoradiograph film and do not represent lipids. O indicates origin. A - phthiocerol dimycocerosates (PDIM), triacylglycerol (TAG); B – diacylglycerol (DAG), free fatty acid (FFA), free mycolic acid (FMA); C – phenolic glycolipid (PGL), monomycolated glycerol (MMG), DAG, FFA; D$_1$ – glucose monomycolate (GMM), trehalose monomycolate (TMM), trehalose dimycolate (TDM); D$_2$ – diacyltrehalose (DAT), TMM; E – phospholipid (P), phosphatidyl inositol (PI), diacylphosphatidylinositol dimannoside (AC$_2$PIM$_2$), diacylphosphatidylinositol hexamannoside (AC$_2$PIM$_6$).
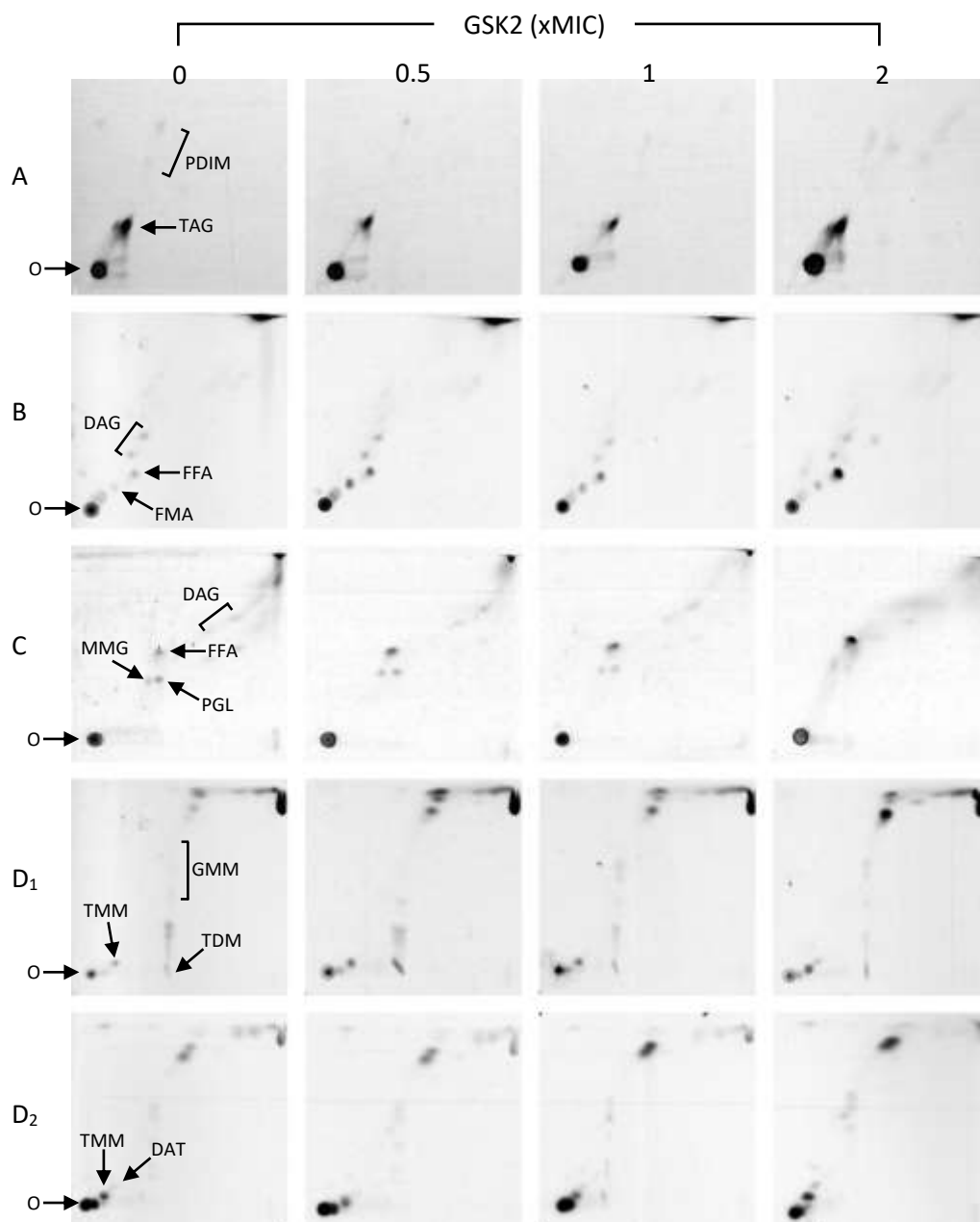
Figure 70. Lipid profile of *M. bovis* BCG overexpressing *tgs3*, treated with GSK2. *M. bovis* BCG pMV261-*tgs3* was cultured in the presence of GSK2 for 24 hours and labelled with [^{14}C] acetic acid. Cells were harvested by centrifugation and polar and apolar lipids were extracted. Aluminium backed silica TLC plates loaded with 10,000 cpm lipids were run in solvent systems A - E. Autoradiograph films were exposed to the TLC plates for 6 days, scanned then transformed to grayscale and cropped using Adobe Photoshop. The contrast of the whole image was adjusted for image clarity. Overexpression of *tgs3* caused a change in lipid profile distinctly different to all other strains tested. The amount of FFA present in systems B and C does not significantly increase with GSK2 treatment. As seen in other overexpression strains, PGL is absent.

O indicates origin. A - phthiocerol dimycocerosates (PDIM), triacylglycerol (TAG); B – diacylglycerol (DAG), free fatty acid (FFA), free mycolic acid (FMA); C – phenolic glycolipid (PGL), monomycolated glycerol (MMG), DAG, FFA; D$_1$ – glucose monomycolate (GMM), trehalose monomycolate (TMM), trehalose dimycolate (TDM); D$_2$ – diacyltrehalose (DAT), TMM; E – phospholipid (P), phosphatidyl inositol (PI), diacylphosphatidylinositol dimannoside (AC$_2$PIM$_2$), diacylphosphatidylinositol hexamannoside (AC$_2$PIM$_6$).
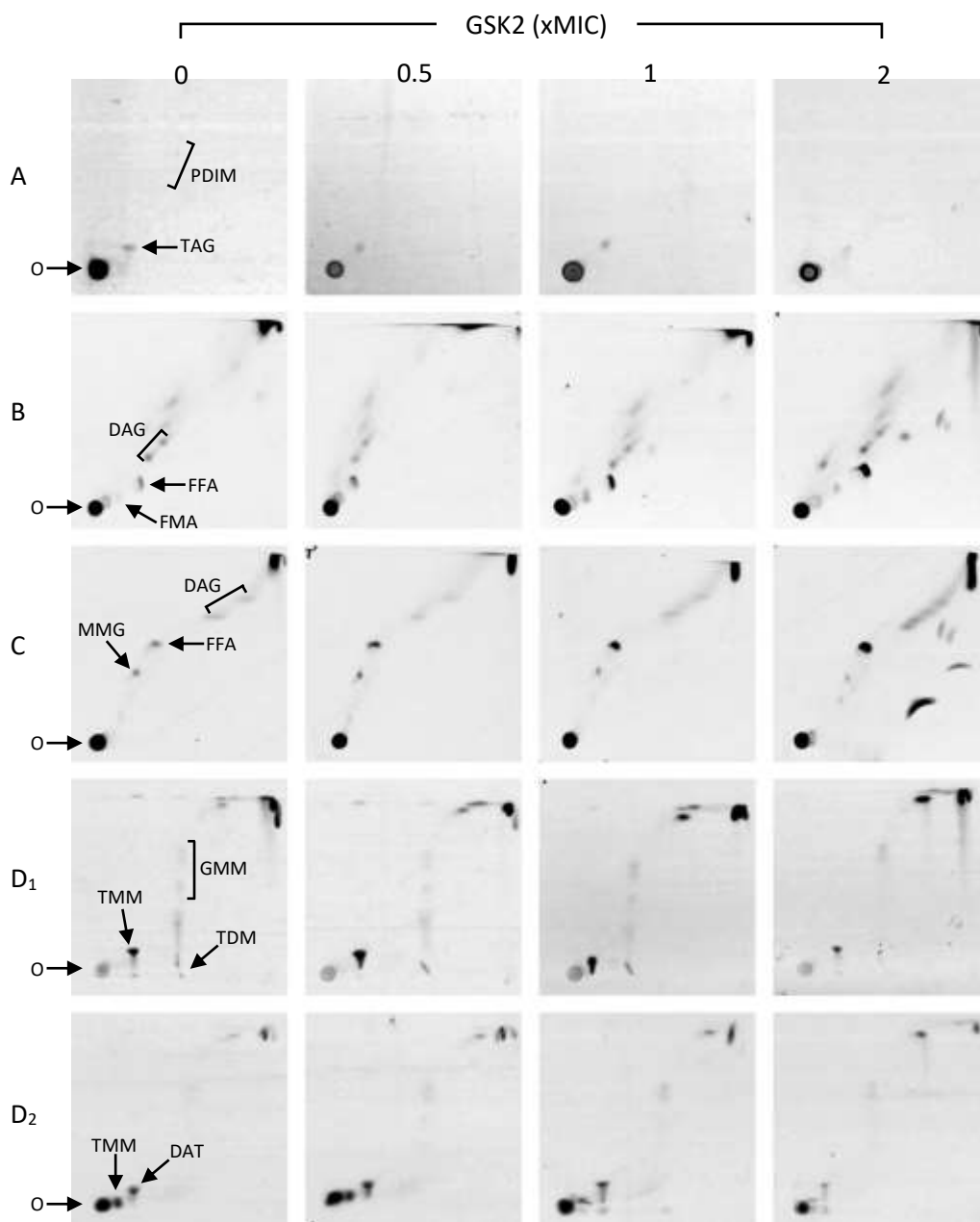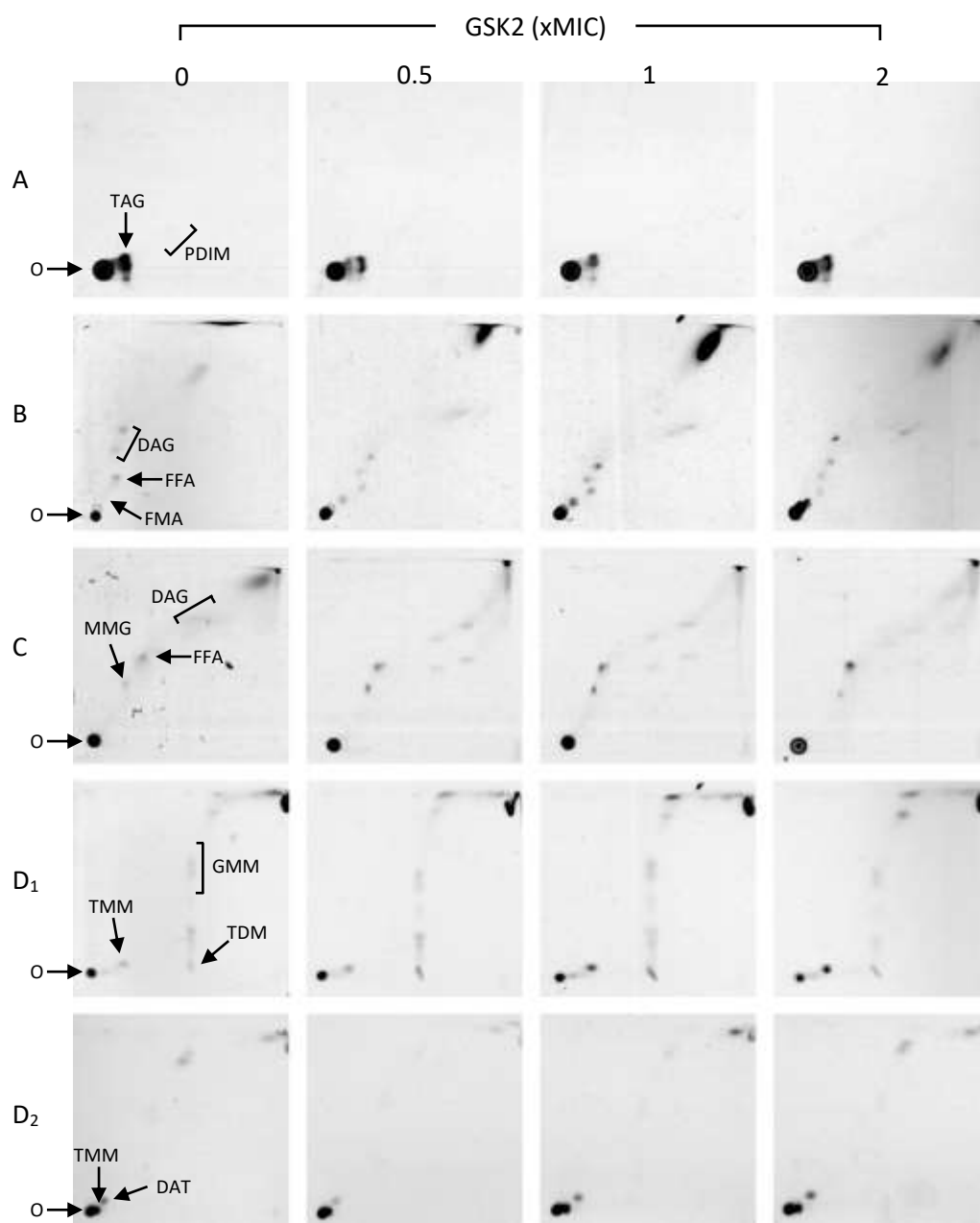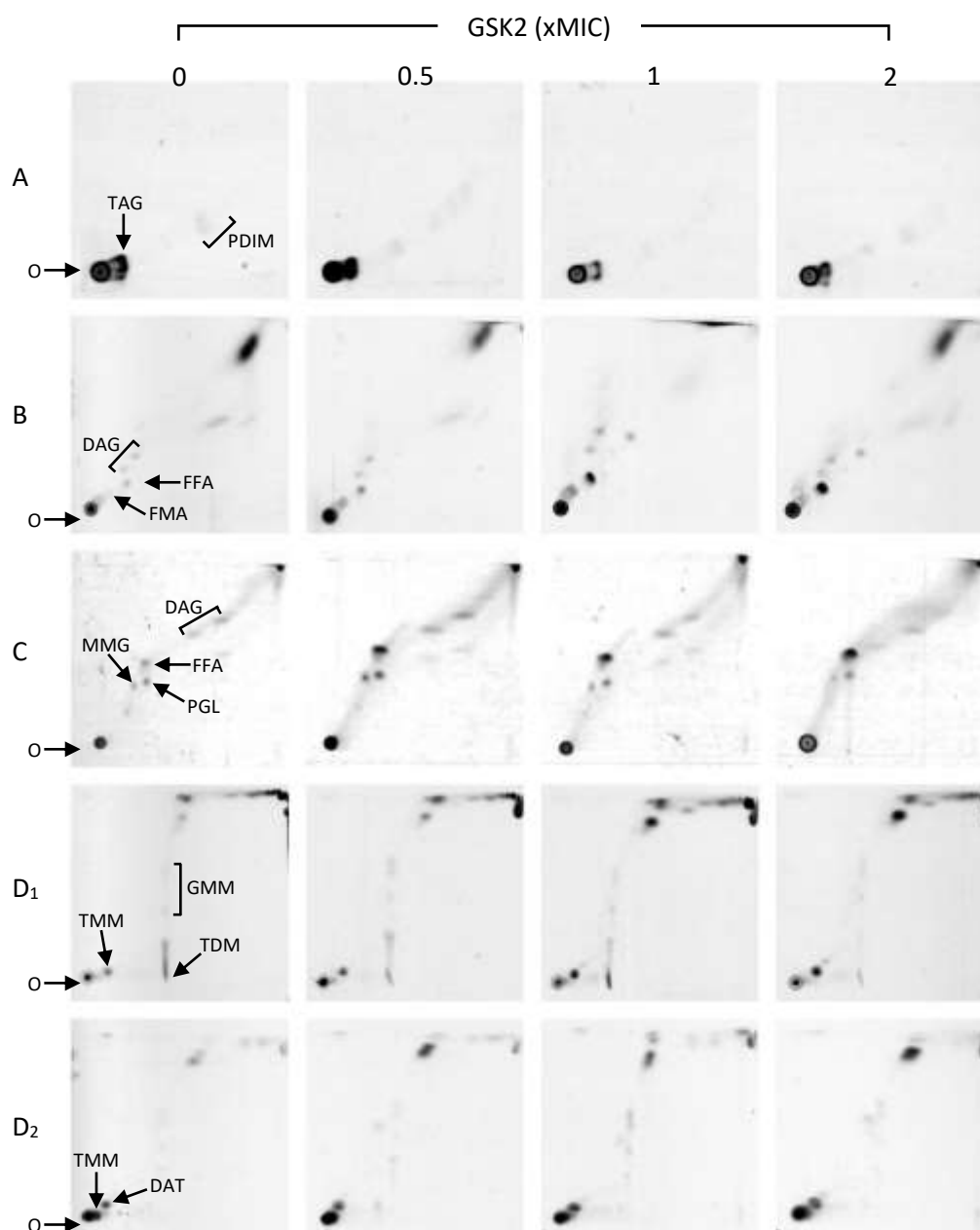
Figure 71. Lipid profile of *M. bovis* BCG overexpressing *tgs4*, treated with GSK2. *M. bovis* BCG pMV261-*tgs4* was cultured in the presence of GSK2 for 24 hours and labelled with [^{14}C] acetic acid. Cells were harvested by centrifugation and polar and apolar lipids were extracted. Aluminium backed silica TLC plates loaded with 10,000 cpm lipids were run in solvent systems A - E. Autoradiograph films were exposed to the TLC plates for 6 days, scanned then transformed to grayscale and cropped using Adobe Photoshop. The contrast of the whole image was adjusted for image clarity. The increase in FFA upon treatment with GSK2, seen also in WT *M. bovis* BCG, and strains overexpressing *tgs1* and *tgs2* is evident here. Unlike all other overexpression strains however, PGL is clearly present. O indicates origin. A - phthiocerol dimycocerosates (PDIM), triacylglycerol (TAG); B – diacylglycerol (DAG), free fatty acid (FFA), free mycolic acid (FMA); C – phenolic glycolipid (PGL), monomycolated glycerol (MMG), DAG, FFA; D$_1$ – glucose monomycolate (GMM), trehalose monomycolate (TMM), trehalose dimycolate (TDM); D$_2$ – diacyltrehalose (DAT), TMM; E – phospholipid (P), phosphatidyl inositol (PI), diacylphosphatidylinositol dimannoside (AC$_2$PIM$_2$), diacylphosphatidylinositol hexamannoside (AC$_2$PIM$_6$).
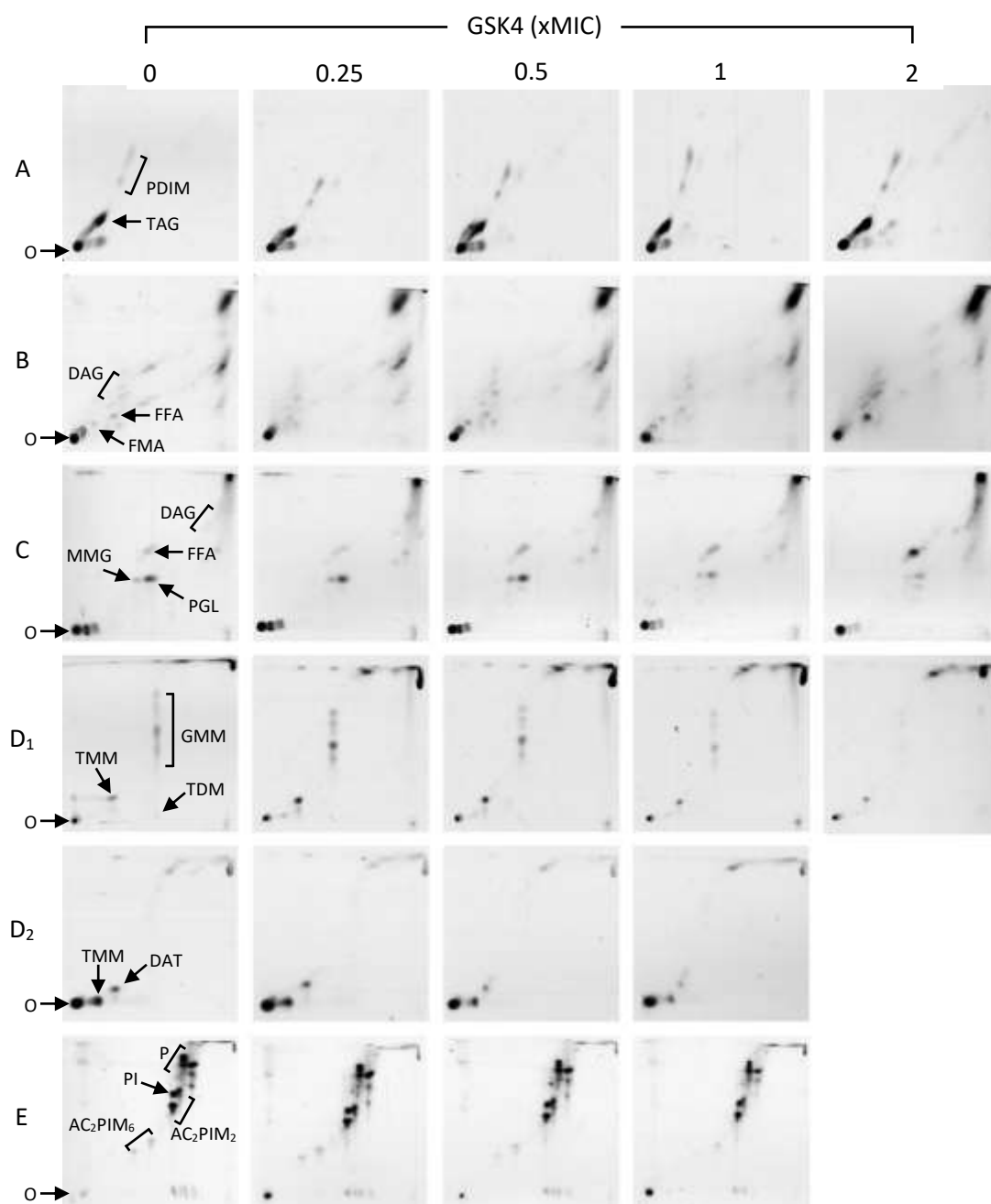
Figure 72. Lipid profile of WT *M. bovis* BCG treated with GSK4. *M. bovis* BCG was cultured in the presence of GSK2 for 24 hours and labelled with [^{14}C] acetic acid. Cells were harvested by centrifugation and polar and apolar lipids were extracted. Aluminium backed silica TLC plates loaded with 10,000 cpm lipids were run in solvent systems A - E. Autoradiograph films were exposed to the TLC plates for 6 days, scanned then transformed to grayscale and cropped using Adobe Photoshop. The contrast of the whole image was adjusted for image clarity. Treatment with GSK4 induced changes to the apolar lipids of *M. bovis* BCG. In system A, PDIMs appear stronger in relation to TAG. In systems B and C, FFA increases. O indicates origin. A - phthiocerol dimycocerosates (PDIM), triacylglycerol (TAG); B – diacylglycerol (DAG), free fatty acid (FFA), free mycolic acid (FMA); C – phenolic glycolipid (PGL), monomycolated glycerol (MMG), DAG, FFA; D$_1$ – glucose monomycolate (GMM), trehalose monomycolate (TMM), trehalose dimycolate (TDM); D$_2$ – diacyltrehalose (DAT), TMM; E – phospholipid (P), phosphatidyl inositol (PI), diacylphosphatidylinositol dimannoside (AC$_2$PIM$_2$), diacylphosphatidylinositol hexamannoside (AC$_2$PIM$_6$).

Table 18 Molecular Dimensions MIDAS screen. Plate plan for MIDAS crystal screen, detailing the concentrations of precipitants, salts/additives and buffers used in different conditions.

Well		% conc	Precipitant	% conc	Salt/Additive	pH	% conc	Buffer
A	1	50%v/v	polypropylene glycol 400	5 %	dimethyl sulfoxide	6	0.1 M	HEPES-NaOH
A	2	12%w/	v polyvinyl pyrrolidone K15			5.5	0.1 M	MES- NaOH
A	3	45%w/v	polyacrylate 2100, sodium salt			6.5	0.1 M	HEPES-NaOH
A	4	14%v/v	acrylic acid/maleic acid copolymer (50:50), sodium salt					
A	5	12.5 % w/v	polyacrylate 2100, sodium salt	0.5 M	ammonium phosphate			
A	6	19%v/v	acrylic acid/maleic acid copolymer (50:50), sodium salt			8.5	0.1 M	Tris-HCl
A	7	10%v/v	polypropylene glycol 400					
A	8	5%w/v	polyacrylate 2100, sodium salt					
A	9	25%v/v	pentaerythritol propoxylate (5/4 PO/OH)			6	0.1 M	MES- NaOH
A	10	24 % w/v	polyvinyl pyrrolidone K15	0.1 M	sodium sulfate			
A	11	35 % v/v	pentaerythritol ethoxylate (15/4 EO/OH)	0.2 M	calcium chloride	6.5	0.1 M	HEPES-NaOH
A	12	35 % v/v	polypropylene glycol 400			7	0.1 M	K/Na Phosphate
B	1	20% v/v	Jeffamine D2000	0.2 M	sodium chloride	5.5	0.1 M	MES- NaOH
		10 %v/v	Jeffamine M2005					
B	2	15 % v/v	pentaerythritol propoxylate (5/4 PO/OH	0.2 M	sodium thiocyanate	7	0.1 M	HEPES-NaOH
B	3	5 % w/v	polyvinyl alcohol type II	0.2 M	potassium acetate	7	0.1 M	HEPES-NaOH
		10 % v/v	Jeffamine T403					
B	4	45% v/v	pentaerythritol propoxylate (5/4 PO/OH)	0.2 M	sodium chloride	6	0.1 M	MES- NaOH
B	5	8 % w/v	polyvinyl alcohol type II	10 % v/v	1- propanol	7	0.1 M	HEPES-NaOH
B	6	30 % w/v	polyvinyl pyrrolidone K15	0.1 M	lithium sulfate	7	0.1 M	HEPES-NaOH

						pH		
B	7	40 % v/v	polypropylene glycol 400	0.2 M	imidazole	7		
B	8	8 % w/v	acrylic acid/maleic acid copolymer (50:50), sodium salt	0.06 M	lithium sulfate	7.5	0.1 M	HEPES-NaOH
		3 % v/v	pentaerythritol ethoxylate (3/4 EO/OH)					
B	9	35 % v/v	Jeffamine SD2001	0.1 M	sodium chloride	8	0.1 M	Tris-HCl
B	10	30 % v/v	Jeffamine M600	10 % v/v	dimethyl sulfoxide			
B	11	20 % v/v	polypropylene glycol 400	10 % v/v	1-propanol			
B	12	28 % w/v	acrylic acid/maleic acid copolymer (50:50), sodium salt			6.5	0.1 M	HEPES-NaOH
C	1	15 % w/v	Jeffamine ED2003	10 % v/v	ethanol			
C	2	30 % w/v	Jeffamine ED2003	0.2 M	sodium chloride	6	0.1 M	MES- NaOH
C	3	25 % v/v	Jeffamine SD2001	0.1 M	sodium malonate	5.5	0.1 M	MES- NaOH
C	4	15 % v/v	pentaerythritol propoxylate(5/4 PO/OH)	0.2 M	sodium chloride	6	0.1 M	MES- NaOH
C	5	35 % v/v	pentaerythritol ethoxylate (3/4 EO/OH)	0.2 M	Magnesium chloride			
C	6	40 % v/v	pentaerythritol propoxylate (5/4 PO/OH)	15 % v/v	ethanol			
C	7	50 % v/v	pentaerythritol propoxylate (5/4 PO/OH)			8	0.1 M	Tris-HCl
C	8	12.5 % w/v	polyvinyl pyrrolidone K15	0.2 M	sodium chloride	8	0.1 M	Tris-HCl
		10 % w/v	PEG 4000					
C	9	25 % v/v	pentaerythritol propoxylate (5/4 PO/OH)	0.1 M	sodium chloride			
		10 % v/v	dimethyl sulfoxide					
C	10	35 % w/v	polyacrylate 2100, sodium salt	0.2 M	ammonium sulfate	7.5	0.1 M	HEPES-NaOH
C	11	30 % v/v	pentaerythritol ethoxylate (15/4 EO/OH)	0.1 M	magnesium formate	8.5	0.1 M	Tris-HCl
C	12	20 % v/v	Glascol W13	0.2 M	sodium sulfate	7.5	0.1 M	HEPES-NaOH
D	1	60 % v/v	polypropylene glycol 400			8	0.1 M	Tris-HCl

D	2	30 % v/v	pentaerythritol ethoxylate (15/4 EO/OH)			7.5	0.1 M	HEPES-NaOH
		6 % w/v	polyvinyl pyrrolidone K15					
D	3	45 % v/v	polypropylene glycol 400	10 % v/v	ethanol			
D	4	10 % v/v	pentaerythritol ethoxylate (3/4 EO/OH)	10 % v/v	1-butanol			
D	5	12.5 % w/v	polyacrylate 2100, sodium salt			7	0.1 M	HEPES-NaOH
		6 % v/v	Jeffamine SD2001					
D	6	6 % w/v	polyvinyl pyrrolidone K15			6.5	0.1 M	HEPES-NaOH
D	7	20 % w/v	Jeffamine ED2003			6.5	0.1 M	HEPES-NaOH
D	8	20 % v/v	glycerol ethoxylate	10% v/v	tetrahydrofuran	8	0.1 M	Tris-HCL
D	9	25 % v/v	Jeffamine D2000	0.2 M	imidazole	7		
D	10	30 % v/v	Jeffamine SD2001	0.2 M	potassium chloride	6.5	0.1 M	HEPES-NaOH
D	11	30 % v/v	Polypropylene glycol 400	0.1 M	Sodium chloride			
D	12	20 % v/v	Jeffamine SD2001	15% v/v	1-propanol			
E	1	25 % v/v	Jeffamine T403	0.2 M	lithium sulfate	8	0.1 M	Tris-HCl
E	2	35 % v/v	pentaerythritol propoxylate (5/4 PO/OH)	0.2 M	potassium acetate			
E	3	20 % v/v	pentaerythritol ethoxylate (15/4 EO/OH)	0.2 M	potassium chloride	9.5	0.1 M	Glycine
E	4	40 % v/v	pentaerythritol propoxylate (5/4 PO/OH)	0.2 M	sodium thiocyanate	7	0.1 M	HEPES-NaOH
E	5	15 % v/v	Jeffamine T403	0.2 M	potassium chloride	6.5	0.1 M	HEPES-NaOH
		15 % v/v	Jeffamine ED2003					
E	6	15 % v/v	pentaerythritol ethoxylate (15/4 EO/OH),	0.2 M	potassium acetate	6	0.1 M	MES- NaOH
		3 % v/v	Jeffamine T403					
E	7	30 % w/v	polyacrylate 2100, sodium salt	0.1 M	sodium malonate	7	0.1 M	HEPES-NaOH

E	8	10 % v/v	JeffamineD2000	10 % v/v	ethanol			
		10 % v/v	Jeffamine M2005					
E	9	25 % w/v	Jeffamine ED2003	0.1 M	lithium sulfate	8	0.1 M	Tris-HCl
E	10	10 % v/v	Jeffamine T403			8	0.1 M	Tris-HCl
		10 % w/v	Jeffamine ED2003					
E	11	25 % w/v	polyacrylate 2100, sodium salt	0.1 M	lithium sulfate	6.5	0.1 M	HEPES-NaOH
E	12	15 % w/v	polyacrylate 2100, sodium salt	0.2 M	magnesium chloride	7.5	0.1 M	HEPES-NaOH
F	1	40 % v/v	Jeffamine D2000			6.5	0.1 M	HEPES-NaOH
F	2	10 % w/v	polyacrylate 2100, sodium salt	0.5M	sodium chloride	8	0.1 M	Tris-HCl
F	3	14 % v/v	Jeffamine ED900			7	0.1 M	K/Na Phosphate
		11 % v/v	Jeffamine SD2001					
F	4	20 % w/v	polyacrylate 2100, sodium salt	0.2 M	sodium chloride	9	0.1 M	Bicine
F	5	20 % v/v	Jeffamine D2000	0.2 M	sodium malonate	5.5	0.1 M	MES- NaOH
F	6	30 % v/v	Jeffamine M2070	0.2 M	potassium chloride	8	0.1 M	Tris-HCl
F	7	20 % v/v	Jeffamine M2070	20 % v/v	dimethyl sulfoxide			
F	8	40 % w/v	pentaerythritol propoxylate (17/8 PO/OH)	0.2 M	magnesium chloride	5.5	0.1 M	MES- NaOH
F	9	20 % w/v	polyacrylate 5100, sodium salt			8	0.1 M	Tris-HCl
F	10	28 % v/v	poly(ethylene imine) branched			7	0.1 M	HEPES-NaOH
F	11	20 % v/v	Sokalan® CP 7	0.1 M	ammonium formate	7	0.1 M	HEPES-NaOH
F	12	20 % w/v	Sokalan® HP 56	0.2 M	sodium sulfate	8	0.1 M	Tris-HCl
G	1	25 % v/v	Sokalan® CP 7	0.1 M	potassium chloride	7	0.1 M	HEPES-NaOH
G	2	20 % v/v	Sokalan® CP 5	0.3 M	ammonium formate	7	0.1 M	HEPES-NaOH

G	3	40 % v/v	glycerol ethoxylate					
G	4	30 % v/v	glycerol ethoxylate			8.5	0.1 M	Tris-HCl
G	5	15 % v/v	Sokalan® HP 66 K			7	0.1 M	HEPES-NaOH
		3 % v/v	poly(ethylene imine)					
G	6	35% v/v	glycerol ethoxylate	0.2 M	lithium citrate			
G	7	30 % v/v	glycerol ethoxylate	0.2 M	ammonium acetate	6.5	0.1 M	MES- NaOH
G	8	20 % v/v	Sokalan® CP 42	5% v/v	methanol	8	0.1 M	Tris-HCl
G	9	25 % v/v	Sokalan® CP 42	10 % v/v	tetrahydrofuran	7	0.1 M	Tris-HCl
G	10	20 % v/v	Sokalan® CP 42	0.1 M	lithium acetate	6	0.1 M	Bis-Tris- NaOH
G	11	15 % v/v	Sokalan® CP 12 S	0.1 M	lithium citrate	5.5	0.1 M	Bis-Tris- NaOH
G	12	15 % v/v	Sokalan® CP 5			6	0.1 M	Bis-Tris- NaOH
H	1	25 % v/v	Sokalan® CP 42			6	0.1 M	Bis-Tris- NaOH
H	2	25 % v/v	Sokalan® HP 66 K	0.2 M	ammonium acetate	7	0.1 M	HEPES-NaOH
H	3	20 % v/v	glycerol ethoxylate			8.5	0.1 M	Tris-HCl
		3 % v/v	poly(ethylene imine)					
H	4	25 % v/v	glycerol ethoxylate	0.2 M	ammonium chloride	7.5	0.1 M	HEPES-NaOH
H	5	40% v/v	Glascol® W13	0.2 M	Potassium citrate			
H	6	30% w/v	Polyacrylate 5100, sodium salt	10% v/v	ethanol	6	0.1 M	MES-NaOH
H	7	40 % v/v	Sokalan® CP 42	0.2 M	potassium citrate			
H	8	30 % v/v	Sokalan® CP 42			8.5	0.1 M	Tris-HCl
H	9	25 % w/v	Sokalan® HP 56	0.2 M	ammonium acetate	7	0.1 M	HEPES-NaOH
H	10	25 % v/v	Sokalan® CP 5			8.5	0.1 M	Tris-HCl

H	11	10 % w/v	Poly(vinyl pyrrolidone) K 15				
		20 % w/v	PEG 4000	0.2 M	ammonium formate		
H	12	15 % w/v	Poly(vinyl pyrrolidone) K 15			8	0.1 M	Tris-HCl
		25 % w/v	PEG MME 5000				